

Table of Contents

Abstract.....	ii
Acknowledgements.....	iv
List of Figures.....	ix
List of Tables.....	xiv
Abbreviations.....	15
Introduction.....	18
1.1. Polyaniline and Intrinsically Conducting Polymers.....	18
1.1.1. Electrical Conductivity in Conducting Polymers.....	19
1.1.2. Introduction to Polyaniline.....	21
1.1.3. Synthesis of PANI.....	22
1.1.3.1. Chemical Oxidation Polymerization.....	23
1.1.3.2. Electrochemical Polymerization.....	26
1.1.3.3. Mechanism of Aniline Polymerization.....	26
1.1.4. Polyaniline Films.....	27
1.1.5. The Antimicrobial Ability of PANI.....	28
1.1.6. Applications of PANI.....	29
1.2. Click Chemistry and its Applications to Polymers.....	30
1.2.1. The Copper Azide-Alkyne Click Reaction.....	31
1.2.2. The Thiol-ene Hydrothiolation Click Reaction.....	32
1.3. Silver Nanoparticles and Their Antimicrobial Properties.....	34
1.4. Interaction of Conducting Polymers with Lectins and Bacterial Cells.....	36
1.4.1. Concanavalin A.....	36
1.4.2. Bacterial Interaction with Carbohydrates.....	37
1.5. Objectives.....	38
1.6. Thesis structure.....	39
Chapter 2. Methodology.....	41
2.1. Introduction.....	41
2.2. Characterisation.....	41
2.2.1. Nuclear Magnetic Resonance (NMR) Spectroscopy.....	41
2.2.2. High Resolution Mass Spectroscopy (HRMS).....	41
2.2.3. Fourier Transform Infrared (FTIR) Spectroscopy.....	41
2.2.4. UV-Visible (UV-Vis) Spectroscopy.....	42

2.2.5. Gel Permeation Chromatography (GPC).....	42
2.2.6. Cyclic Voltammetry	42
2.2.7. Elemental Analysis.....	42
2.2.8. Scanning Electron Microscopy (SEM) and Energy Dispersive X-ray (EDX) Spectroscopy.....	43
2.2.9. X-ray Photoelectron Spectroscopy (XPS).....	43
2.2.10. Biological Studies.....	43
2.2.10.1. Concanavalin A binding assay of modified PANI's.....	43
2.2.10.2. Biocidal efficacy of modified PANI powders – Analysis of the Minimum Lethal Concentration (MLC)	44
2.2.10.3. Biocidal efficacy of modified PANI films – Analysis of the Minimum Bactericidal Concentration	45
Chapter 3. Synthesis and Polymerization of a Modified Aniline Monomer	47
3.1. Introduction.....	47
3.2. Experimental	47
3.2.1. Chemicals	47
3.2.2. Synthesis of 1,2,3,4,6-penta-O-acetyl- α -D-mannopyranoside	48
3.2.3. Synthesis of 2-Bromoethyl 2,3,4,6-tetra-O-acetyl- α -D-mannopyranoside.....	48
3.2.4. Synthesis of 2-azidoethyl 2,3,4,6-tetra-O-acetyl- α -D-mannopyranoside (1)	49
3.2.5. Synthesis of 2-aminophenyl 1,2,3-triazole-N-2,3,4,6-O-acetyl- α -D-mannopyranoside (2).....	49
3.2.6. Synthesis of acetyl protected mannose functionalized PANI (3).....	49
3.2.7. Synthesis of α -D-mannose functionalized PANI (4).....	50
3.3. Results and Discussion.....	50
3.3.1. NMR spectroscopy	52
3.3.2. Cyclic Voltammetry	55
3.3.3. FTIR spectroscopy.....	59
3.3.4. UV-Vis Spectroscopy	63
3.3.5. Gel-permeation Chromatography/Size Exclusion Chromatography.....	66
3.3.6. Elemental Analysis.....	67
3.3.7. Chemical Synthesis Characterization Conclusion.....	69
3.3.8. Interaction of mannose functionalized PANI 4 with <i>Concanavalin A</i>	69
3.3.9. Determination of the Minimum Lethal Concentration of Mannose Functionalized PANI 4.....	72
3.4. Conclusion	74

Chapter 4. The Synthesis of a Thiolated PANI by Sulfonation and Reduction and the Subsequent Click reaction with Allyl Mannose	75
4.1. Introduction	75
4.2. Experimental	75
4.2.1. Chemicals	75
4.2.2. Synthesis of Polyaniline Emeraldine Base Powder (5)	75
4.2.3. Synthesis of Leucoemeraldine (6)	76
4.2.4. Synthesis of Sulfonated Polyaniline (7)	76
4.2.5. Reduction of PANI-sulfonic acid to Thiolated PANI (8).....	76
4.2.6. Synthesis of Allyl- α -D-mannopyranoside (9)	77
4.2.7. Synthesis of Mannose Functionalized PANI (10)	77
4.3. Results and Discussion.....	77
4.3.1. FTIR	79
4.3.2. UV-Vis	81
4.3.3. X-ray Photoelectron Spectroscopy	83
4.3.4. Characterization Conclusion	88
4.3.5. Minimum Lethal Concentration (MLC) of Mannose Functionalized PANI 10.....	89
4.4. Conclusion	91
Chapter 5. The Solvent Casting of PANI films and Surface Modification with Glucose for the Preparation of a PANI Glycopolymer	92
5.1. Introduction	92
5.2. Experimental	95
5.2.1. Chemicals	95
5.2.2. Synthesis of PANI EB freestanding films (11)	95
5.2.3. Synthesis of 1-thio- β -D-Glucose tetraacetate functionalized PANI (12).....	95
5.2.4. Synthesis of glucose functionalized PANI film (13).....	95
5.3. Results and Discussion.....	96
5.3.1. Parent PANI film synthesis	96
5.3.2. FTIR spectroscopy.....	97
5.3.3. Scanning Electron Microscopy and EDX.....	100
5.3.4. X-ray Photoelectron Spectroscopy	100
5.3.5. Characterization Conclusion	105
5.3.6. Concanavalin A adhesion study	106
5.3.7. MBC of synthesized glucose functionalized PANI films.....	110
5.4. Conclusion	113

Chapter 6. Polyaniline thin films incorporating Silver nanoparticles and Glucose.....	114
6.1. Introduction	114
6.2. Experimental	114
6.2.1. Chemicals	114
6.2.2. Synthesis of PANI EB film 11	115
6.2.3. Synthetic Route 1	115
6.2.3.1. Synthesis of PANI EB powder containing silver nanoparticles	115
6.2.3.2. Synthesis of PANI films with surface bound silver nanoparticles (14).....	115
6.2.3.3. Synthesis of 1-thio- β -D-glucose tetraacetate modified PANI films containing silver nanoparticles (15).....	115
6.2.3.4. Synthesis of glucose modified PANI films containing silver nanoparticles (16)	116
6.2.4. Synthetic Route 2	116
6.2.4.1. Synthesis of surface bound silver nanoparticles on acetyl protected glucose modified PANI films (17).....	116
6.2.4.2. Synthesis of surface bound silver nanoparticles on glucose modified PANI films (18).....	116
6.3. Results and Discussion.....	116
6.3.1. Scanning Electron Microscopy (SEM).....	118
6.3.2. Energy Dispersive X-ray Spectroscopy (EDX).....	120
6.3.3. X-ray Photoelectron Spectroscopy	123
6.3.4. Conclusion on the Characterization of PANI containing silver nanoparticles and glucose	128
6.3.5. Antimicrobial Ability of the Silver Nanoparticle Functionalized PANI Powders and Films	132
6.3.5.1. Minimum Lethal Concentration of Silver Nanoparticle Functionalized Powders	132
6.3.5.2. Minimum Bactericidal Concentration of PANI/Ag NP/Glucose Functionalized Films	134
6.4. Conclusion	137
Chapter 7. Conclusion.....	139
7.1. Future Work	141

List of Figures

Figure 1.1: Chemical structures of a few common organic conducting polymers.

Figure 1.2: Diagram of band structures for an insulator, semiconductor and metal with the valence band (blue) and conduction band (red).

Figure 1.3: The three redox forms of polyaniline.

Figure 1.4: Reaction mechanism of the polymerization of PANI.

Figure 1.5: Formation of PANI film on a surface depicting parallel chain growth and lateral progression of the adsorption and nucleation.

Figure 1.6: General scheme for the Copper azide alkyne click reaction.

Figure 1.7: Reaction mechanism for the radical initiated thiol-ene click reaction.

Figure 3.1: Chemical reaction scheme for the synthesis of 2-azidoethyl 2,3,4,6-tetra-O-acetyl- α -D-mannopyranoside starting material **1**.

Figure 3.2: Chemical reaction scheme for the polymerization of mannose functionalized PANI **4**.

Figure 3.3: ^1H NMR spectrum of mannose functionalized aniline monomer **2** (400 MHz, CDCl_3).

Figure 3.4: ^{13}C NMR spectrum of mannose functionalized aniline monomer **2** (400 MHz, CDCl_3).

Figure 3.5: Cyclic voltammogram of aniline and the resulting PANI film at a GCE in 0.5 M H_2SO_4 .

Figure 3.6: Cyclic Voltammogram of mannose functionalized aniline **2** and the resulting polymer **3** at a GCE in 0.5 M H_2SO_4 .

Figure 3.7: FTIR spectrum of leucoemeraldine (A) and PANI EB (B).

Figure 3.8: FTIR spectrum of acetyl protected mannose functionalized PANI **3** and mannose functionalized PANI **4**.

Figure 3.9: Structure of phenazine.

Figure 3.10: Proposed structure of byproduct formed in the synthesis of **4**.

Figure 3.11: UV-vis spectrum displaying PANI EB, mannose functionalized aniline monomer **2**, acetyl protected mannose functionalized PANI **3** and mannose functionalized PANI **4** in NMP.

Figure 3.13: Schematic representation of ConA-polymer binding and de-binding. Images shown are of the precipitate formed by interaction of mannose functionalized PANI **4** with ConA (A) and the clear solution after addition of methyl- α -D-mannopyranoside (B). Both solutions were left for 1 hour after addition and centrifuged.

Figure 3.14: ConA analysis of binding to mannose functionalized PANI **4** at 280 nm in both the resulting precipitate and supernatant.

Figure 4.1: Proposed synthetic route to mannose functionalized PANI **10**.

Figure 4.2: FTIR spectrum of PANI EB **5**, leucoemeraldine **6**, sulfonated PANI **7** and thiolated PANI **8**.

Figure 4.3: FTIR spectrum of mannose functionalized PANI **10**.

Figure 4.4: UV-Vis spectra of PANI EB **5**, sulfonated PANI **7** and thiolated PANI **8**.

Figure 4.5: UV-Vis spectrum of mannose functionalized PANI **10**.

Figure 4.6: Carbon 1s core level scan of PANI EB **5**, thiolated PANI **8** and mannose functionalized PANI **10**.

Figure 4.7: Nitrogen 1s core level scan of PANI EB **5**, thiolated PANI **8** and mannose functionalized PANI **10**.

Figure 4.8: Self-doping mechanism of PANI by attached sulfonic acid moieties as described by Yue et al..

Figure 4.9: O 1s core level scan of PANI EB **5**, thiolated PANI **8** and mannose functionalized PANI **10**.

Figure 4.10: S 2p core level scan of PANI EB **5**, thiolated PANI **8** and mannose functionalized PANI **10**.

Figure 4.11: Synthetic pathway for the synthesis of glucose modified PANI **13**.

Figure 4.12: Plated sample concentrations of *Staphylococcus aureus* on an agar plate after incubation.

Figure 5.1: Reaction scheme for the thiol-ene reaction between PANI and a thiol as suggested by the literature.

Figure 5.2: Proposed reaction mechanism for the thiol-ene reaction between PANI EB and xxx as hypothesised by Halliwell et al..

Figure 5.3: Proposed synthetic procedure for the synthesis of **13**.

Figure 5.4: FTIR-ATR of PANI EB film **11** dried at 100 °C and 200 °C overnight.

Figure 5.5: FTIR spectrum of PANI EB film **11**, **12**, and **13** conducted on a diamond crystal ATR attachment.

Figure 5.6: SEM scan of **12** with the EDX spectrum inset.

Figure 5.7: XPS survey scan of **12**.

Figure 5.8: C 1s core level scans of **12**.

Figure 5.9: N 1s core level scans for **12**.

Figure 5.10: O 1s core level scans of **12**.

Figure 5.11: S 2p core level scan of **12**.

Figure 5.12: The reaction scheme resulting in the formation of **13** from empirical evidence.

Figure 5.13: Diagram depicting the process for the attachment of Texas Red labelled ConA to glucose functionalized PANI film **13**.

Figure 5.14: Control samples with no wash (top), 1 wash (middle top), 3 washes (middle bottom) and after methyl- α -D-mannopyranoside wash (bottom).

Figure 5.15: PANI EB samples with no wash (top), 1 wash (middle top), 3 washes (middle bottom) and after methyl- α -D-mannoside wash (bottom).

Figure 5.16: **9** with no wash (top), 1 wash (middle top), 3 washes (middle bottom) and after methyl- α -D-mannopyranoside wash (bottom).

Figure 5.17: Difference in OD₆₀₀ after rescue of *Staphylococcus aureus* and 16 hour incubation on control, **11** and **13** surfaces.

Figure 5.18: Difference in OD₆₀₀ after rescue of *Escherichia coli* and 16 hour incubation on control, **11** and **13** surfaces.

Figure 6.1: Proposed synthetic procedure of synthetic route 1 for the synthesis of a glucose functionalized PANI bearing silver nanoparticles.

Figure 6.2: Proposed synthetic procedure of synthetic route 2 for the synthesis of a glucose functionalized PANI bearing silver nanoparticles.

Figure 6.4: SEM scans of silver nanoparticle modified PANI film **14** at 0.1 (top left), 0.5 (top right), 1.0 (bottom left) and 5.0 (bottom right) mmol silver nitrate concentrations

Figure 6.5: Attachment of silver nanoparticles with 0.1 mmol/L AgNO₃ on silver nanoparticle modified glucose functionalized PANI film **16**.

Figure 6.6: Attachment of silver nanoparticles with 0.5 mmol/L AgNO₃ on silver nanoparticle modified glucose functionalized PANI film **16**.

Figure 6.7: Attachment of silver nanoparticles with 1.0 mmol/L AgNO₃ on silver nanoparticle modified glucose functionalized PANI film **16**.

Figure 6.8: Attachment of silver nanoparticles with 5.0 mmol/L AgNO₃ on silver nanoparticle modified glucose functionalized PANI film **16**.

Figure 6.9: Survey scan of silver nanoparticle modified glucose functionalized PANI film **16**.

Figure 6.10: C 1s core level scan of silver nanoparticle modified glucose functionalized PANI film **16**.

Figure 6.11: N 1s core level scan of silver nanoparticle modified glucose functionalized PANI film **16** (left) and silver nanoparticle modified glucose functionalized PANI film **18** (right).

Figure 6.12: O 1s core level scan of silver nanoparticle modified glucose functionalized PANI film **16** (left) and silver nanoparticle modified glucose functionalized PANI film **18** (right).

Figure 6.13: S 2p core level scan of silver nanoparticle modified glucose functionalized PANI film **16** (left) and silver nanoparticle modified glucose functionalized PANI film **18** (right).

Figure 6.14: Ag 3d core level scan of silver nanoparticle modified glucose functionalized PANI film **164** (left) and silver nanoparticle modified glucose functionalized PANI film **18** (right).

Figure 6.15: Photograph depicting the formation of silver particles on the surface of silver nanoparticle modified PANI **14** (powder).

Figure 6.16: Photograph of a PANI film with metallic silver film after reaction of silver nitrate for >6 hours.

Figure 6.17: Empirical reaction pathway deduced for route 1, the synthesis of silver nanoparticle modified glucose functionalized PANI film **16**

Figure 6.18: Empirical reaction pathway deduced for route 1, the synthesis of PANI EB films with pendant glucose and silver nanoparticles **18**.

Figure 6.18: Photographs showing the results of the MLC analysis of silver nanoparticle modified PANI **14** (powder) against *S aureus* (left) and *E coli* (right).

Figure 6.20: MLC of silver nanoparticle modified PANI **14** (powder) against both *Staphylococcus aureus* and *Escherichia coli* after 4 and 24 hours. Note that the maximum polymer concentration analysed was 2 wt % and 4 wt % indicates that the powder was inactive up to 2 wt % concentrations tested.

Figure 6.21: Rescue of *Escherichia coli* after a 16 hour challenge on control, PANI EB film **11**, silver nanoparticle modified glucose functionalized PANI film **16** and silver nanoparticle modified glucose functionalized PANI film **18** surfaces.

Figure 6.22: Rescue of *Staphylococcus aureus* after a 16 hour challenge on control, PANI EB film **11**, silver nanoparticle modified glucose functionalized PANI film **16** and silver nanoparticle modified glucose functionalized PANI film **18** surfaces.

List of Tables

Table 3.1: ^1H NMR assignments for **1**.

Table 3.2: C^{13} NMR assignments of **1**.

Table 3.3: Elemental Analysis of PANI and **2**.

Table 3.4: MLC of poly(3-aminobenzoic acid) and **3** against *E coli* and *S aureus*.

Table 4.1: MLC of mannose modified PANI **10** against *Staphylococcus aureus* and *Escherichia coli* after inoculation for 4 and 24 hours. Note that the maximum polymer concentration analysed was 2 wt % and 4 wt % indicates that the powder was inactive up to 2 wt %.

Abbreviations

2,2-Dimethoxy-2-acetylphenone	DMPA
Ammonium persulfate	APS
Attenuated total reflectance	ATR
Concanavalin A	ConA
Copper azide-alkyne click reaction	CuAAC
Cyclic voltammetry	CV
Emeraldine base	EB
Emeraldine salt	ES
Energy dispersive x-ray spectroscopy	EDX
<i>Escherichia coli</i>	E coli
Fourier transform infrared spectroscopy	FTIR
Full width at half maximum	FWHM
Gel permeation chromatography	GPC
Glassy carbon electrode	GCE
High resolution mass spectroscopy	HRMS
Intrinsically conducting polymer	ICP
Minimum bactericidal concentration	MBC
Tryptic soy agar	TSA
Minimum lethal concentration	MLC
<i>N</i> -methylpyrrolidone	NMP
Nuclear magnetic resonance	NMR
Optical density at 600 nm	OD ₆₀₀
Parts per million	ppm
Poly(3-aminobenzoic acid)	P3ABA
<i>p</i> -aminodiphenylamine	PADPA
Polyaniline	PANI
<i>Pseudomonas aeruginosa</i>	P aeruginosa
Scanning electron microscopy	SEM
<i>Staphylococcus aureus</i>	S aureus
Sulfonated PANI	SPANI
Thin-layer chromatography	TLC
Tryptic soy broth	TSB

Uropathogenic *Escherichia coli*
UV-Visible spectroscopy
X-ray photoelectron spectroscopy

UPEC
UV-Vis
XPS

Co-Authorship Form

This form is to accompany the submission of any PhD that contains published or unpublished co-authored work. **Please include one copy of this form for each co-authored work.** Completed forms should be included in all copies of your thesis submitted for examination and library deposit (including digital deposit), following your thesis Acknowledgements. Co-authored works may be included in a thesis if the candidate has written all or the majority of the text and had their contribution confirmed by all co-authors as not less than 65%.

Please indicate the chapter/section/pages of this thesis that are extracted from a co-authored work and give the title and publication details or details of submission of the co-authored work.	
Chapter 3 Synthesis and Polymerization of a Modified Aniline Monomer. Synthesis of the monomer	
Nature of contribution by PhD candidate	Aided in monomer synthesis. Completed polymerization and characterisation of monomer/products. Interpreted data and wrote up results.
Extent of contribution by PhD candidate (%)	85 %


CO-AUTHORS

Name	Nature of Contribution
Hayley Charville	Completed monomer synthesis with help of author.
Jianyong Jin	Chemical synthesis discussion.
Simon Swift	Microbiology testing discussion.
Other Authors	Discussion.

Certification by Co-Authors

The undersigned hereby certify that:

- ❖ the above statement correctly reflects the nature and extent of the PhD candidate's contribution to this work, and the nature of the contribution of each of the co-authors; and
- ❖ that the candidate wrote all or the majority of the text.

(1) Author signature		Print name	Chris Wilcox	Date	05/09/13
(2) Author signature		Print name	Jianyong Jin	Date	3 Sep 2013
(3) Author signature		Print name	Hayley Charville	Date	11 Sep 2013
(4) Author signature		Print name	Simon Swift	Date	5 SEP 2013
(5) Author signature		Print name	Teresa To	Date	03 Sep 2013
(6) Author signature		Print name	Paul Kilmartin	Date	5 Sept. 2013
(7) Author signature		Print name	Clive Evans	Date	9 Sept 2013
(8) Author signature		Print name	Ralph Cooney	Date	27/9/13
(9) Author signature		Print name	Margaret Brimble	Date	9/9/13

Introduction

1.1. Polyaniline and Intrinsically Conducting Polymers

Prior to 1977, organic polymers were thought to be insulators, unable to conduct electricity leaving metallic elements to pick up the brunt of the electronic world. However, in this year a paradigm shift occurred as Hideki Shirakawa, Alan Heeger and Alan MacDiarmid discovered the ability of polyacetylene, an organic polymer, to conduct electricity. This property was imparted to the polymer upon doping with halogen atoms, which resulted in a massive increase in the electrical conductivity.¹ For their work in the discovery of this new class of material, coined a “synthetic metal”, they were awarded the Nobel Prize in Chemistry in 2000. The focus of the research was on polyacetylene doped with different halogens, namely chlorine, bromine and iodine, the effect that the halogens had on the conductivity of the polymer and the charge transfer complexes they believed formed.

This ground-breaking paper by Shirakawa et al. showed that the semi-conducting *trans*-polyacetylene could have its electrical conductivity increased by several orders of magnitude with the simple doping of halogen ions. They reported polyacetylene to have an undoped conductivity of $4.4 \times 10^{-5} \Omega^{-1} \text{ cm}^{-1}$ and they managed to increase this conductivity to $0.5 \Omega^{-1} \text{ cm}^{-1}$ after doping for 10 minutes with bromine (1 Torr, room temperature). A further increase could be gained by doping with iodine to $38 \Omega^{-1} \text{ cm}^{-1}$, a 10^5 increase in conductivity. These materials were stable for several hours in air. It was concluded that upon doping, free radicals formed along the polymer chain and became delocalized which allowed the movement of charge and therefore conduction of electricity, much like the delocalisation of electrons in metals and hence the term given to conducting polymers as synthetic metals.

Scheme 1 shows the structure of a few of the more common intrinsically conducting polymers including polyacetylene, polyaniline (PANI) and polypyrrole. Observable from scheme 1 is that intrinsically conducting polymers all have their conjugation, or alternating single-double bonds, in common.² This extended conjugation of conducting polymers provides a “highway” for delocalised charges on their chains to move and therefore conduct electricity. Due to their unique and useful conducting properties, as well as their interesting chemical and physical properties conducting polymers have found uses in conductive inks, antistatic textiles, gas sensors, biosensors, membranes for separation, energy storage devices, artificial muscles, solar cells and light emitting diodes to name a few applications.³⁻⁸

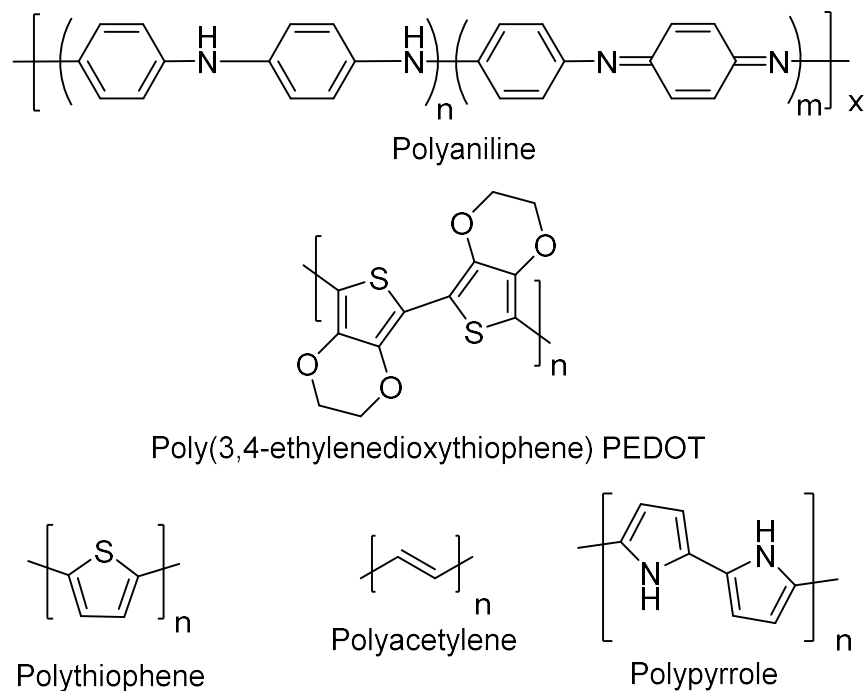


Figure 1.1: Chemical structures of a few common organic conducting polymers.

1.1.1. Electrical Conductivity in Conducting Polymers

The theory for the electrical conductivity in the above organic polymers is rooted in band theory. Band theory denotes three possible denominations for materials, they can be either electrically insulating, semi-conducting or conducting. Materials fall into one of these groupings depending on how their electronic structures are presented.⁹ Bands are formed in solid materials from the overlap of all the molecular orbitals from the atoms in the bulk of the material. The overlap of these molecular orbitals which have similar energies form a continuous band as shown in Figure 1.2. The valence band of the solid material is where all the highest occupied molecular orbital electrons reside whereas the conduction band contains the unoccupied orbitals in the solid, with the two molecular orbitals being separated by the Fermi level. The group a material falls into, insulator, semi-conductor and conductor and whether the material can conduct electricity comes from the interaction of the valence and conduction bands, and the size of the band gap between them.

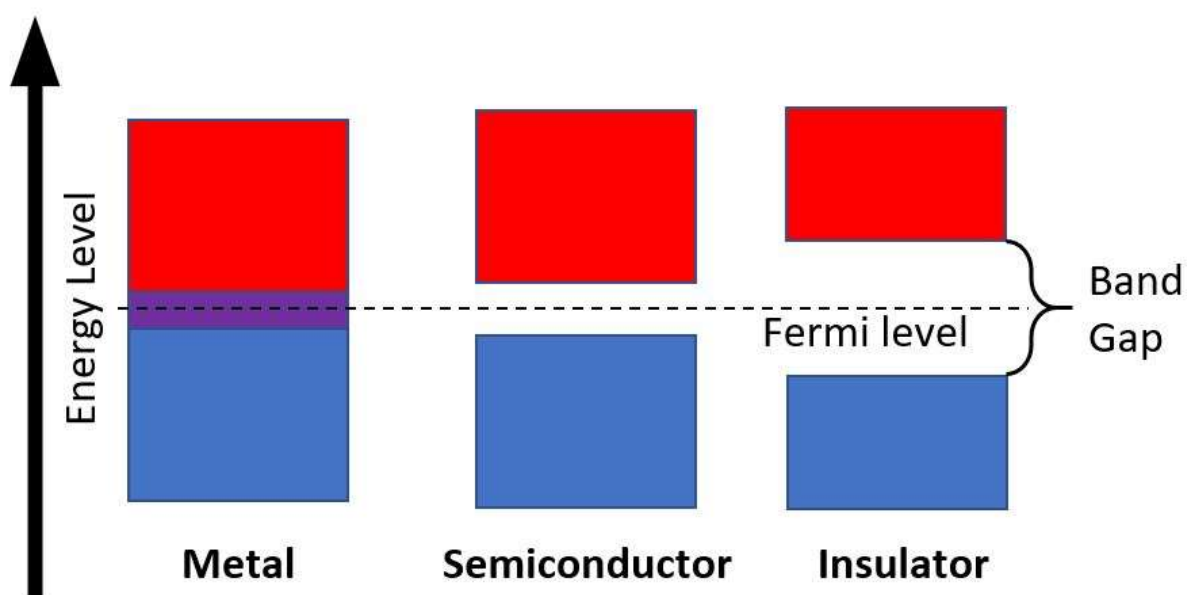


Figure 1.2: Diagram of the band structure for an insulator, semiconductor and metal with the valence band (blue) and conduction band (red).

A large band gap results in electrons being unable to migrate from the valence to the conduction band and hence are trapped completely in the valence band. An insulating material is the result, as charge carriers are unable to migrate through the conduction band. However, when the band gap is small, and the valence and conduction bands are close together, electrons can move through the conduction band and carry charge resulting in a conductive material. The final type of material is known as a semi-conductor, of which PANI and other organic conducting polymers fall under. Semi-conductors, like insulators, have a relatively large band gap compared to conductive materials preventing easy promotion of the electrons from the valence to the conduction band. The two bands are, however, much closer together when compared to a pure insulator, close enough that a sufficient input of energy can promote an electron from one band to the other and thus produce an electrical current. To further increase the conductivity of these materials, and lower the energy input requirement, doping is used. Doping refers to the deliberate inclusion of impurities into a semi-conducting material which results in either an excess of electrons or “holes”. In conducting polymers like PANI, doping refers to the process of adding or removing an electron from the polymer backbone creating an excess of electrons or inclusion of vacancies with the presence of a suitable counter ion which allows charge carriers to migrate the length of the polymer chain or protonation of the polymer backbone with no change in the number of electrons associated with the polymer.¹⁰

1.1.2. Introduction to Polyaniline

After the success of polyacetylene as the first intrinsically conducting polymer (ICP) scientists considered other materials that had the potential to be organic conducting polymers. As already alluded, the polymer of aniline was one of the most promising candidates. The first reported evidence of PANI dates back to 1862 when Henry Letheby was investigating a number of deaths which was believed to be caused by aniline.¹¹ His paper notes the electrochemical reaction of aniline in sulfuric acid on a platinum electrode producing a green colour and describes the blue colouration that forms when dipped in ammonia. These are now commonly known as the base (blue) and salt (green) forms of PANI. Its electrical properties were not well understood at this stage and further research into this material was sporadic until the 1980's and 1990's when the structure of PANI and the usefulness of conducting polymers was fully realised via the Shirakawa's research presented.¹² Research exploded for these new materials, with PANI being one of the foremost due to its useful properties including its facile synthesis, environmental and thermal stability, price of the precursors and simple redox chemistry providing electrical conductivity.¹³

As shown in Figure 1.3 PANI exists in three main redox forms. The aromatic rings and nitrogen atoms can be altered via oxidation and reduction reactions to and from benzoidal and quinoidal type rings, and their respective amine, -NH-, and imine, -N=, type nitrogen's, which denotes the form of the PANI. Other than the most stable emeraldine form, which exists in a 50:50 ratio of amine to imine nitrogen's, PANI can also exist as leucoemeraldine, for the most reduced form, and pernigraniline for the most oxidised form. Partially oxidised and reduced forms can also exist, with the material being more leucoemeraldine in character and vice versa. The emeraldine form is the most stable PANI structure and is the only redox form that becomes electrically conducting when doped, with the other two forms being insulators.¹⁴

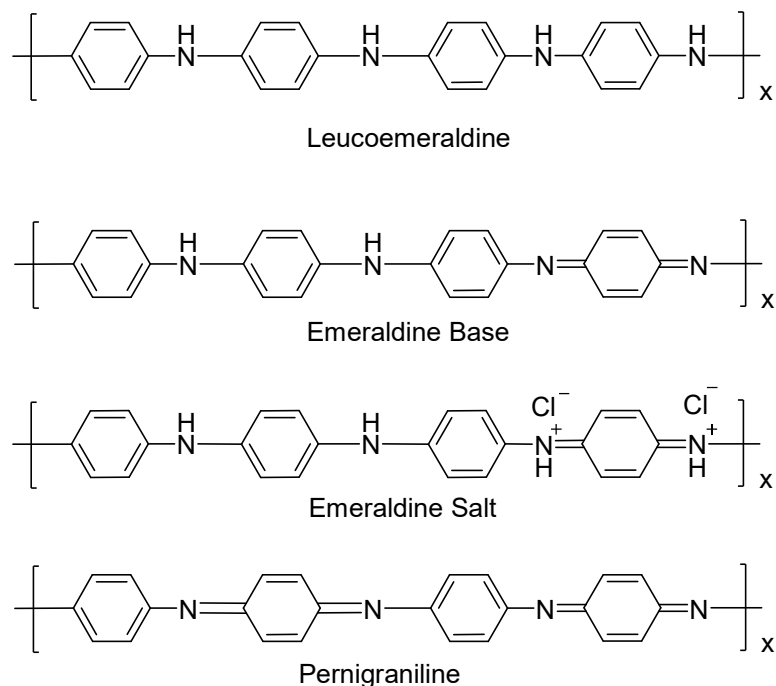


Figure 1.3: The three redox forms of polyaniline and the salt form.

PANI emeraldine salt (ES) is formed by doping of the emeraldine base (EB) with a protonic acid such as hydrochloric acid or sulfuric acid, which makes PANI unique in that it involves no change in the number of electrons associated with the polymer chain when doped.¹⁵ This doping process, known as protonation, is reversible via both chemical and electrochemical means such as reaction with a strong base (ammonium hydroxide, sodium hydroxide etc) to transform the ES form to the EB form. Doping and dedoping are both important reactions because even though the ES form is highly conductive, it is very insoluble making it difficult to process. Upon dedoping PANI is an insulator, however, becomes more processable because of increased solubility in certain solvents. The ease at which PANI can be transformed from insoluble conductive salt to soluble insulator allows synthetic procedures to be undertaken on the more processable form and then treatment to provide the more electrically conductive form.

1.1.3. Synthesis of PANI

PANI is generally prepared via either chemical or electrochemical methodology. The chemical synthesis involves the oxidation of aniline with an oxidant and is useful for the ability to prepare copious amounts of product. One of the drawbacks of this procedure is that it can produce unwanted by-products and presents a lack of control over the polymerization. The electrochemical method allows very controlled preparation of a polymer film, however, at a much smaller scale. Because of this it is less suited for upscaling syntheses but is useful for the ability to study PANI under almost pristine conditions. In comparing the polymerization

conditions of aniline to other common polymers of commercial significance there is a lack of control exerted over the reaction which is common in high end polymer production. In polymerizations such as the synthesis of high density polyethylene, addition of reagents such as the Ziegler-Natta catalyst allow control of the branching of the polymer and therefore control of the molecular weight and morphology of the product.¹⁶ This massively affects its end properties such as increasing the impact strength of high density polyethylene in comparison to low density polyethylene. While there are template directed methods for the synthesis of PANI, these templates are normally used to control the morphology of the resultant PANI, rather than the molecular weight or molecular weight dispersity.¹² Stejskal and MacDiarmid, both authorities on PANI and its synthesis, made similar statements, “there are as many PANIs as the number of people who prepare them”.^{17,18} The chemical synthesis of PANI has several variables which are important to control due to the effect they have on the end products properties such as oxidant concentration, ratio of aniline to oxidant, solvent, stirring/agitation and temperature.¹⁹ However, even though this polymerization isn't as finely controlled as the synthesis of commercial plastics, it is very robust and even with changes in the reaction conditions a workable PANI is still produced most of the time. Electrochemical polymerization allows synthesis of a purer polymer to be formed as it doesn't require the addition, and therefore the contamination from, an added oxidant to initiate the reaction.²⁰

1.1.3.1. Chemical Oxidation Polymerization

There are a wide variety of methods to synthesise PANI, however, a general synthetic procedure for preparing PANI utilises a chemical oxidation procedure as described by Stejskal et al., which is the oxidation of aniline using a chemical oxidant in an acidic medium.¹⁷ By carrying out the reaction in an acidic solution, aniline becomes protonated to the anilinium cation, $C_6H_5NH_3^+$, which due to the increased polarity of the molecule becomes more soluble in aqueous solutions.²¹ In terms of the oxidant a variety of oxidising agents have been applied in this synthesis ranging from the most common, ammonium persulfate (APS), but also potassium dichromate, hydrogen peroxide and potassium persulfate have been reported.²² A very brief description of a typical aniline polymerization follows: aniline is dissolved in an aqueous acidic solution and a solution of oxidant is added and the mixture left for a predetermined amount of time. An initial induction period occurs followed by formation of a dark precipitate as PANI forms and precipitates. This induction period can be followed by monitoring the temperature as this reaction is exothermic and increases in temperature as further PANI chains are formed. The resultant solid polymer precipitate is then collected via vacuum filtration on filter paper and washed to remove unreacted products and small chain oligomers. The remaining solvent is

removed by oven drying the PANI to a constant weight. Once polymerised utilising the above method, the PANI product is in the ES form because of doping via the acid solvent and becomes almost completely insoluble.

Pron et al. studied the effects of four different oxidant reagents, ammonium persulfate, potassium dichromate, potassium iodate and hydrogen peroxide and found that other than hydrogen peroxide they all produced similar products and thus concluded that the redox potential had a weak effect on the properties of the synthesised polymer for chemical polymerizations.²³ Blinova et al. showed that the polymerization of aniline with APS only had a major effect when the ratio of monomer:oxidant was very low or very high. It was most effective in terms of yield and conductivity to keep the molar ratio of monomer to oxidant at 1.25.²⁴ Reactivity in the *para* position (i.e. head-to-tail attachment) is favoured for this reaction and results in the polymeric PANI rather than by-products such as phenazine that form from interactions in *ortho* or *meta* positioning.¹² Wudl et al. attempted to prove the favourable reaction through the *para* position by utilising reactive analogues of aniline that forced the reaction to proceed only via the *para* position. The work found that the formed product was poly(*p*-phenyleneamineimine) which had several properties the same as a synthesised PANI.²⁵ Stejskal et al. concluded that the *para* configuration is favourable due to the charge delocalization along the formed polymer chains, which cannot occur when side reactions occur as they are not electrically conducting however also note that while *para* positioning is favourable at low pH formation of some *ortho* linked molecules also occurs and is more likely at higher pH.²⁶ Some variations of this polymerization have been coined a “falling pH” method as the use of certain oxidants results in a more acidic solution as the reaction progresses, such as the formation of sulfuric acid when utilising APS from the release of protons, over the course of the reaction.²⁷ The general reaction scheme for the synthesis of PANI ES is given in Figure 1.4.

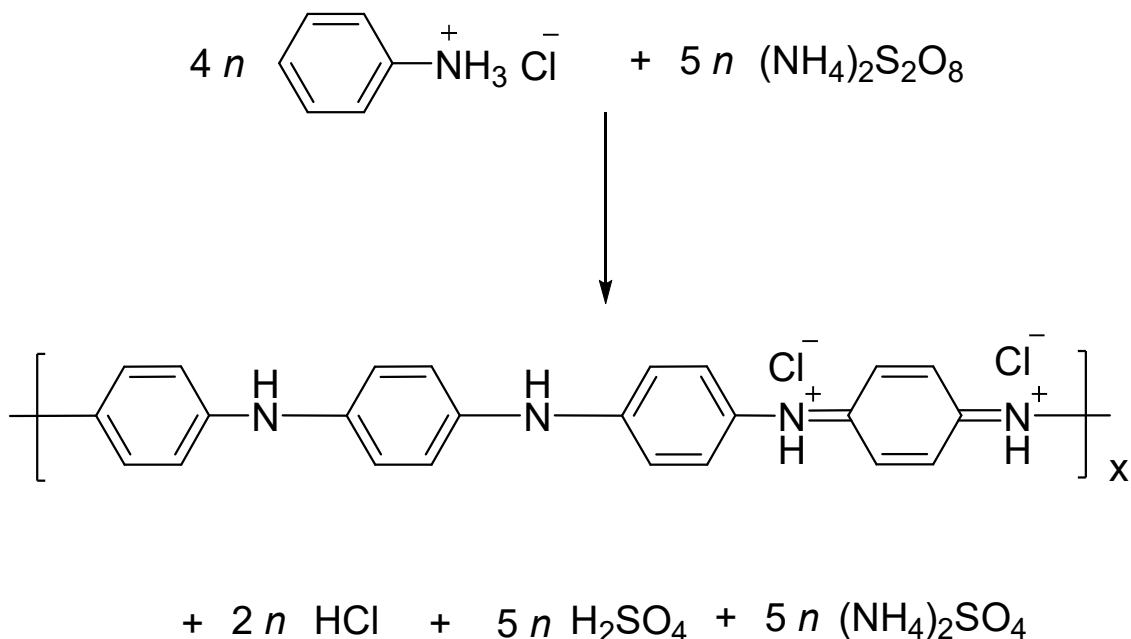


Figure 1.4: Reaction mechanism for the polymerization of PANI using APS as the oxidant.

The electrically conducting form of PANI is the ES form and is produced when EB is treated with a suitable dopant, which as mentioned previously are reagents such as hydrochloric acid. In the early case of Shirakawa et al. investigating polyacetylene, the first dopants used were halogens such as iodine, probably due to its high electronegativity which promoted hole formation resulting in charge transfer complexes. The oxidant may also offer up usable counter ions and must therefore be considered in the overall reaction scheme, such is the case with APS. An example of this would be the formation of sulfonic groups as dopants anions, observed by the presence of sulfur found in PANI samples when APS is used as the oxidant.²⁸ The existence of sulfur is due to the formation of sulfuric acid after reaction of the APS oxidant with aniline as shown in Figure 1.4, which can dope the PANI repeat units that subsequently form.²⁹

The choice of dopant is important because it affects the structure, morphology, thermal stabilities and electrical conductivity of PANI.³⁰ Examples of common protonic acids used as dopants include the previously mentioned hydrochloric acid and sulfuric acid but also other organic based acids such as camphorsulfonic acid, methanesulfonic acid, toluenesulfonic acid (TSA) and dodecylbenzenesulfonic acid.³¹⁻³³ The addition of large counter ions in the case of the organic acids was expected to alter the properties of PANI to be more favourable for processing and solubility.

1.1.3.2. Electrochemical Polymerization

The electrochemical polymerization of PANI allows the synthesis of a pristine product and the ability to easily change between the redox forms of PANI by applying varying voltages.³ However, with the electrochemical route you are limited by the size of the electrodes on which the PANI is grown which can affect the scalability of the process. Potentially the earliest recorded evidence of the PANI was found via electropolymerization and was mentioned previously. Letheby was investigating fatal poisonings resulting from nitrobenzol, which is transformed in the stomach to aniline. By preparing a solution of aniline in sulfuric acid on a platinum strip and placing the strip across the terminals of a Grove's battery, a powder was formed. Immersion of the powder in ammonia gives the expected deep blue EB product. Cyclic voltammetry (CV) is a common electrochemical method of synthesising PANI and can also be used to probe the structure of the PANI formed as the reversible redox reactions can be tracked via an applied voltage.

1.1.3.3. Mechanism of Aniline Polymerization

While both chemical and electrochemical polymerizations have been intensely studied, the actual mechanism of the polymerization of aniline is still debated. Genies et al. conducted an early historical review which included a discussion on the polymerization mechanisms.²² The first step in the oxidation of aniline is the formation of a radical cation via oxidation of aniline. This molecule has several resonance forms resulting from interaction of the radical with the benzene ring. Formation of the dimer *p*-aminodiphenylamine (PAPDA) results from a head-to-tail reaction of the amine centred radical with a *para* carbon centred radical on a neighbouring aniline molecule. Some by-products may form here such as benzidine and *N-N'*-diphenylhydrazine which result from head-to-head and tail-to-tail reactions along with *ortho* substituted products however *para* substitution, and the formation of PANI, is favoured in these conditions.^{34,35} The oxidation potential of PADPA and other dimers/oligomers is lower than that of aniline and as such increasing chain length reactions dominate. The rate limiting step is therefore the oxidation of aniline which may be the reason behind the typical induction period observed in aniline polymerizations.

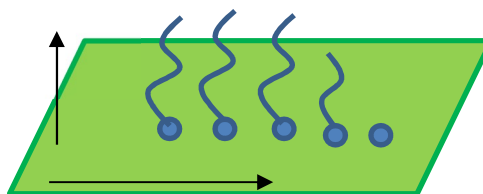
Substitution on the aromatic ring of aniline massively affects the polymerization of the monomer including the rate of polymerization and resulting PANI formed. Affecting the charge density of the benzene ring by inclusion of electron withdrawing or donating groups also affects the polymerization reaction while steric effects can also come into play.³⁶ By studying the polymerization of a number of substituted anilines (poly(*m*-nitroaniline), poly(*m*-aminophenol)

and poly(*o*-ethylaniline)) Bhadra et al. showed that the resulting polymers were far inferior in yield and conductivity which resulted from the electronic and steric effects imparted by the substituent groups.

1.1.4. Polyaniline Films

Various morphologies exist for PANI such as the already discussed forms including powder and films formed on electrodes. When the polymerization of aniline is conducted in a vessel containing a solid substrate, the substrate acts as a point of nucleation and becomes coated in a film of PANI. Growth of the PANI occurs perpendicular to the surface of the substrate and ongoing adsorption and nucleation occurs laterally resulting in growth of the PANI film as shown in Figure 1.5.³⁷ PANI films have been grown on many supports including glass, plastics, carbon nanotubes, metals, cotton fabrics and membranes while also being synthesised as freestanding films.³⁸⁻⁴¹

Polymer chain growth direction



Lateral progression of film growth

Figure 1.5: Formation of PANI film on a surface depicting parallel chain growth and lateral progression of the adsorption and nucleation.

Mehdizadeh et al. synthesised PANI films on an ABS plastic substrate. Their goal was to metallize plastics, which result in materials containing properties that benefit from both their plastic and metal components. Majority of plastics are metallized using a palladium-based activator to form conductive sites on the insulating plastic surface. However, the reaction is very sensitive and complex, and palladium is environmentally hazardous and expensive. By utilising a conducting polymer such as PANI they hoped to avoid the use of palladium-based surface chemistry resulting in an electrically conductive surface that was successfully metallized with, in this case, nickel.⁴²

Chen et al. showed that noble metals such as palladium and platinum can spontaneously cause the polymerization of aniline from acidic solution, resulting in a film of PANI on the surface with no added oxidant. They noted that this reaction did not proceed significantly in either

hydrochloric acid or in the absence of oxygen, leading one to believe that the oxygen is being utilised as an oxidant after formation of the protonated aniline cation on the metals surface.⁴³

1.1.5. The Antimicrobial Ability of PANI

On top of all the promising properties of PANI that have already been discussed previously (facile synthesis, high thermal stability, non-leaching properties and electrical conductivity) it was shown in the early 2000's that PANI also possesses antimicrobial properties. One of the first reports of the antimicrobial ability of PANI was released by Shi et al. who analysed the biocidal ability of TSA doped PANI embedded polyvinyl alcohol films against *Escherichia coli* (*E coli*) and *Staphylococcus aureus* (*S aureus*) in both light and dark conditions.⁴⁴ They reported 100 % bacterial knockdown against both the above bacterial strains for their blended films with 0 % reported for the blank samples. Due to the report by Shi et al., PANI was quickly examined as a potential powerful antimicrobial agent and research was heavily invested on trying to deduce its mechanism of action and improve its antimicrobial ability by the formation of PANI blends and alternative functionalized PANI's.

The antimicrobial ability of PANI is expected to be a result of electrostatic interaction between the positively charged nitrogen sites on PANI and the negatively charged cell wall of the target organism. The negatively charged groups in the outer membranes of cell envelopes are found in phospholipid and lipopolysaccharide molecules (gram negative) and teichoic acid molecules (gram positive) and provide interaction points for the polymer to react with and bind to. After successful attachment the polymer inserts into the cell wall, disrupting the membrane, increasing membrane permeability and resulting in leakage of the cells contents and cell lysis.

To further elucidate the mechanism of the antimicrobial ability of PANI, Robertson et al. conducted an involved analysis into the interaction of poly(3-aminobenzoic acid) P3ABA against single-gene deletion mutants. Robertson concluded that the antimicrobial ability of PANI in rich media was a result of increasing H₂O₂ levels which led to oxidative stress characterised by the disruption of iron homeostasis. The increase in H₂O₂ and its interaction with iron results in the increase in hydroxyl radical formation through the Fenton reaction.⁴⁵

On the topic of functionalized PANI's, Gizdavic-Nikolaidis has deeply researched into the antimicrobial ability of functionalized PANI's such as P3ABA which were shown to be broad spectrum antimicrobial agents and effective against *E coli*, *Pseudomonas aeruginosa* (*P aeruginosa*) and *S aureus* along with extended spectrum β -lactamase positive, multidrug resistant *E coli*, metallo β -lactamase positive, multidrug resistant *P aeruginosa* and methicillin/oxacillin resistant, multidrug resistant *S aureus*.⁴⁶ It was shown that PANI and

functionalized PANI were more effective against these strains in their conducting salt forms as opposed to the base forms (typical minimum inhibitory concentration (MIC) in the range of 1.25-10 mg/mL). Analysis into the mechanism of action of P3ABA revealed that P3ABA interacts with cell membranes and induces the expression of oxidative damage responsive genes while also affecting genes whose products are used in energy metabolism and transport and cell wall synthesis.

Therefore, based on the above studies into the effect of antimicrobial polymers and conducting polymers like PANI along with the literature reports into their effectiveness it shows that the EB form of PANI is less active than the ES form. The reasoning for this would be due to the lack of electrostatic interaction between the polymer and the bacterial cell wall for the EB polymer due to the absence of charged nitrogen sites which are formed upon doping. As per Figure 1.3 upon doping the dopant provides a suitable counter ion which produces the charged nitrogen atoms and allows the interaction between the polymer chain and the cell wall. Therefore, in the comparison of the antimicrobial efficacy of PANI EB and ES it would be expected that the salt form is much more active.

1.1.6. Applications of PANI

Because of some of PANI's more useful properties including its electrical conductivity, thermal stability, ease of synthesis, and cheapness of its reagents, it has found several useful applications. The ease of which a conducting polymer can be grown on a substrate has resulted in significant volumes of research into coating substrates with PANI. By placing a cotton or fabric support in the reaction vessel, a coating of PANI can be formed on the surface resulting in materials with unique conductive properties. Marakova et al. utilised cotton as a support to load PANI and silver nanoparticles resulting in an antimicrobial fabric which was slightly more effective against *E coli* than *S aureus*.⁴¹ Guo et al. covered stretchy spandex with PANI with the aim to synthesise a stretchable humidity sensor. Because of the unique configuration of the fibres, their product maintained a stable electrical conductivity up to strains of 200 %, allowing the material to maintain its humidity sensing properties at high levels of stress.⁴⁷ PANI is also very useful as a sensing material due to its highly conductive nature and can be designed to measure many different interactions. For example, Zhang et al. synthesised a PANI electrode in camphorsulfonic acid for the determination of ascorbic acid, due to the important role it plays in biological systems.⁴⁸ Their sensor showed a linearly dependent anodic peak current that was dependent on the ascorbic acid concentration in the range of 5-50 mM while showing very high correlation coefficient (0.998). Liu et al. also synthesised a PANI electrode for the determination of ascorbic acid but utilised carbon nanotubes as an intermediate between the sensor surface and

PANI. The carbon nanotubes are used to increase the surface area on which the PANI can be formed, improving the sensing ability of the sensor. Their sensor measured linearly down to 20 μM and showed good reproducibility.⁴⁹ The use of PANI as an antimicrobial compound has also been shown previously and is another interesting application for these materials.

Because of PANI's unique properties it has found useful niches in a wide range of potential applications with only a very small selection shown above. An important area of research is in increasing PANI's already useful properties such as attaining a higher conductivity, making it more processable or deadlier to bacteria. Because of the difficulty in processing of PANI a large area of research is into the chemical reactions of PANI and how various functionality can be introduced while retaining the desired properties of the polymer.

1.2. Click Chemistry and its Applications to Polymers

The term "click reaction" was coined by Sharpless, Kolb and Finn in 2001 and was used to describe a chemical reaction that is simple to perform, gives rise to the intended product in very high yields with little to no by-products, are robust enough to handle alterations to the reaction conditions and work for a large number of molecules.^{50,51} The paramount click reaction is the copper azide-alkyne click reaction (CuAAC) which produces a triazole ring after the reaction of azide and alkyne functional groups. Its considerable success paved the way for a surge of interest into this field after the discovery of the catalytic effect of copper (I) allowed almost completely regioselective reactions to be carried out, resulting in only 1,4-disubstituted 1,2,3-triazoles in very mild reaction conditions.^{52,53} For a reaction to be considered "click" it must fill several select criteria, as described by Sharpless et al.; it must be modular, wide in scope, give very high yields, be stereospecific, generate only inoffensive by-products which can be removed by non-chromatographic methods, be conducted in simple reaction conditions (insensitive to oxygen and water preferred), have readily available starting materials, require no solvent or use a solvent that is benign and easily removed, have simple product isolation and purification (if required) which is non-chromatographic, and finally the product must be stable under physiological conditions. Finn et al. describes it more simply, the "click" term signifies that the joining of two molecules should be as simple as closing a buckle. The buckle works no matter what is attached to it, as long as its two pieces can reach each other, and they can only connect with each other.⁵⁰ With such stringent conditions only a handful of reactions can be classified as a click reaction with examples such as cycloadditions of unsaturated products which includes 1,3-dipolar cycloadditions, Diels-Alder cycloadditions, nucleophilic substitution reactions including ring opening reactions of strained heterocyclic electrophiles (epoxides, aziridines, aziridinium ions,

episulfonium ions), carbonyl chemistry of the non-aldol type such as formation of urea's, thioureas, aromatic heterocycles, oxime ethers, hydrazone's and amides and additions to carbon-carbon multiple bonds, especially oxidative ones such as epoxidation, dihydroxylation, aziridination, sulfonyl halide addition and Michael Additions of Nu-H reactants.⁵⁰

1.2.1. The Copper Azide-Alkyne Click Reaction

The CuAAC reaction was described by Sharpless as the “cream of the crop” of click reactions. This reaction is a cycloaddition reaction whereby two unsaturated reactants, an azide 1,3 dipole and alkyne dipolarophile, react together to form a five-membered heterocyclic triazole ring. The azide alkyne reaction has been known for more than 100 years, with early reports of 1,2,3 triazoles being formed from phenyl azide and diethyl acetylene-dicarboxylate being made by Arthur Michael in 1893.⁵⁴ Historically the reaction was used without the copper catalyst resulting in a mixture of the 1,3 and 1,4 disubstituted triazole products which required increased temperatures to form. However, with discovery of the catalytic ability of Cu(I) in this reaction the 1,4 regioisomer forms in large majority with a lower energy input required. The exact mechanistic pathway for the copper catalysed reaction is still debated, however, it is believed that the reaction occurs in a stepwise mechanism as opposed to a concerted one with the formation of a Cu(I) acetylide.⁵⁵ Interaction of the alkyne with the Cu(I) acetylide results in a copper acetylide-alkyne complex with subsequent cyclisation. Contraction of the ring then occurs with protonation resulting in the formation of the click product and regeneration of the catalyst.

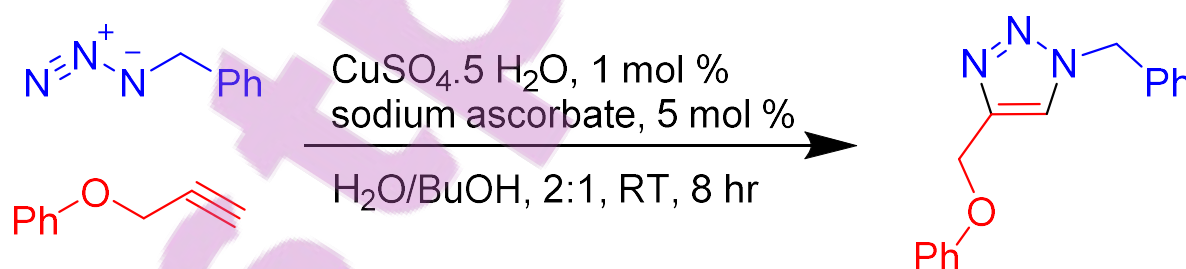


Figure 1.6: General scheme for the copper azide alkyne click reaction.

While there are many different 1,3-dipoles that can take part in the CuAAC, special attention has been given to azides. It is very useful for the ability to carry the functionality through several chemical steps invisibly, is stable to a wide range of reaction conditions such as hydrolysis, dimerization and standard organic synthesis conditions, so long as a dipolarophile (such as an alkene or alkyne that is not part of the synthetic procedure) is not present.⁵⁰ Sharpless pondered that perhaps the reason the reaction had not been given its dues was because of the tendency of

azides to be explosive, meaning many synthetic chemists may have shied away from the potential of the reaction. Alkynes also show similar stability as azides in the above synthesis conditions and are therefore perfect dipolarophiles be carried through their respective reactive steps until merging is required.

1.2.2. The Thiol-ene Hydrothiolation Click Reaction.

The thiol-ene click reaction is the hydrothiolation of an unsaturated carbon-carbon bond and has been known for over 100 years.⁵⁶ Thiol-ene reactions achieve nearly quantitative yields, have rapid reaction rates, proceed in benign solvents over a large concentration range, are insensitive to moisture and air, are regiospecific and react quickly and efficiently, proving they are worthy of being considered a click reaction.⁵⁷ Interestingly, Lowe depicted a graph in his 2014 review showing the increase in publications based on the search parameters “thiol-ene” in SciFinder, with less than 10 papers being published a year in the early 2000’s to their being more than 400 as of 23rd December 2013 (for the year 2013).⁵⁸ Note that Sharpless et al. published their click chemistry paper in 2001. The thiol-ene reaction has been shown to react using two different mechanistic pathways, a radical process and a nucleophilic mediated catalytic route.

The radical initiated thiol-ene reaction is a typical chain process reaction and as such has three main steps: initiation, propagation and termination. Initiation of this reaction occurs upon cleavage of the S-H bond, resulting in a thiyl radical due to abstraction of the hydrogen atom, which then reacts with the alkene via anti-Markovnikov addition as shown in Figure 1.7.⁵⁹ Initiation of the reaction can occur solely by UV-irradiation, however, chemical initiation with photo- or thermal initiators is often used.⁶⁰ It is the relatively weak S-H bond that allows the thiol-ene reaction to proceed under such favourable conditions with a high thermodynamic driving force. The bond energy is affected by its environment and the surrounding elements of the molecule and as such some variations of thiols and alkenes are more susceptible to this reaction than others. There are two steps during this propagation reaction, the first step is the addition of the thiyl radical across the unsaturated carbon-carbon double bond of an alkene, which transfers the radical to the carbon atom of the previously unsaturated alkene. Secondly abstraction of a hydrogen atom from a neighbouring unreacted thiol molecule allows propagation of the radical to a new thiol molecule, allowing the reaction to continue.⁶¹ The thiol-ene reaction is also possible allowing the addition of two thiyl radicals to one unsaturated bond in some cases.⁶² The addition across the unsaturated bond follows anti-Markovnikov addition where the hydrogen atom adds to the carbon with the least amount of hydrogen atoms, or more non-hydrogen substituents. There are several termination reactions that led to the destruction of the reacting radical species without formation of the desired product which all occur via radical-

radical coupling. Two thiyl radicals can react together forming a disulfide bond, a functional group with the general structure of R-S-S'-R', where the initial thiyl radical has propagated through a non-reacted thiol terminating the reaction. Termination can also occur when a thiyl radical reacts with a carbon centred radical (which occurs after propagation of thiyl radical to carbon but prior to abstracting another hydrogen) or when two carbon centred radicals react together.

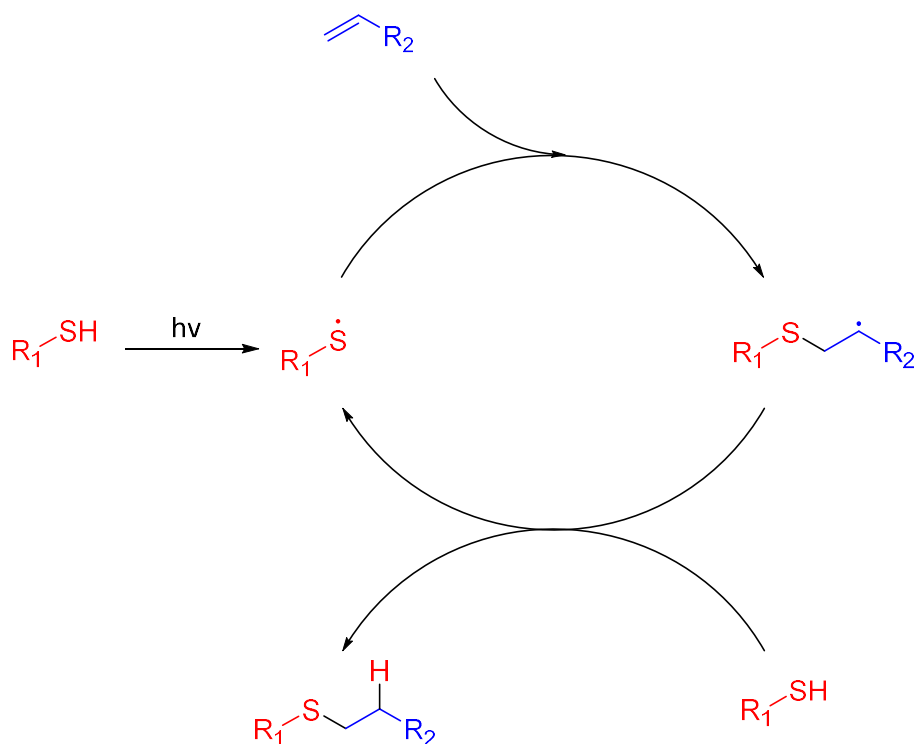


Figure 1.7: Reaction mechanism for the radical initiated thiol-ene click reaction.

As well as the radical initiated process, the thiol-ene reaction can be catalysed by a nucleophile or base in a Michael conjugate addition reaction. This, however, limits the number of unsaturated compounds and thiols that can take part in this reaction because slight activation is required in most cases. To proceed with the highest chance of succeeding using this mechanism the unsaturated compound will have a strong electron withdrawing group which pulls electron density away from the unsaturated bond, making it as nucleophilic as possible. On the other hand, the thiol needs to pull electron density away from the hydrogen atom, making it as acidic as possible, to be able to be abstracted by the base to initiate the reaction. The pKa of the thiol must therefore be as low/strongly acidic as possible. The general reaction method is as follows, firstly the acidic proton is removed by reaction with a base giving the sulfur atom a negative charge and thereby making the thiol more nucleophilic. The activated alkene double bond then attacks the charged sulfur, because the alkene is electrophilic, to form a similar product to that found during the propagation step of the radical initiated reaction, however, here we have a

negative charge rather than the radical centred on the carbon. Finally, the hydrogen extracted by the base is attacked by the carbon centred negative charge leading to the final product.⁵⁸ These two mechanisms allow a wide variety of thiols and unsaturated bonds to come together.

Click reactions have been used in various industries throughout the world because of their very useful reaction properties and the push towards greener chemistry with industries such as pharmaceuticals, chemical engineering, natural product synthesis, polymer and biopolymer synthesis utilising these reactions.

1.3. Silver Nanoparticles and Their Antimicrobial Properties

Silver has been used since ancient times with recordings of its use as early as 4000 BC as a powerful antibacterial agent with low toxicity that fell into disuse with the rise of antibiotics.⁶³ Antibiotics led to a golden age of human health, however, recent discoveries of the evolution of antibiotic resistant pathogens due to their overuse has resulted in the need for exploration of alternative treatment methods for containing the spread of infectious diseases.^{64,65} Silver has therefore received renewed interest as it is active against a wide variety of microbes. The advent of nanotechnology and the discovery of silver nanoparticles have also helped this resurgence as nanoparticles offer greater surface area to volume ratios in comparison to metallic silver, promoting enhanced interaction with the targets and increased antimicrobial efficacy.⁶⁶

Different forms of silver offer antimicrobial properties to varying degrees of potency. While the theory may not have been completely understood, antimicrobial wound dressings containing silver foil were widely used prior to the 20th century to promote healing and prevent infection.⁶⁷ Silver nitrate and other compounds containing silver ions, also showed wide spread use and enhanced control of bacterial infections as the silver already existed in the antimicrobial ionized form.

Generally, the antimicrobial efficacy of silver and silver-based salts is closely related to the rate of release of free silver ions.⁶⁸ Therefore, silver nanoparticles which have high surface area to volume ratios promote the release of greater concentrations of silver ions due to increased surface interaction with the target. Silver nanoparticles are widely researched due to the lower potential for bacteria to develop resistance. This is because silver attacks a broad swathe of bacterial mechanisms resulting in many different routes to shut down the target cell.^{68,69} Contact with bacterial cell envelopes due to electrostatic interactions between the Ag⁺ ion and the negatively charged cell wall resulting in structural changes and increasing cell permeability have been reported by many studies. Also suggested was the formation of reactive oxygen species

and free radicals which both induce membrane damage resulting in cell death.⁷⁰ Finally, interaction of silver with various functional groups found within cell envelopes also results in the potent biocidal ability of silver nanoparticles. Silver has been shown to react with the phosphorus bases in DNA and RNA, interfering with their ability to replicate and ultimately affecting the ability of the cell to divide, leading to cell death. Silver also has a high affinity to sulfur, resulting in the interaction of the antimicrobial silver with thiol groups found in enzymes within the target cells. Their ease of synthesis makes attachment of silver nanoparticles to various substrates a highly viable way to make an antimicrobial material. Reduction of silver (I), such as the commonly used silver nitrate, is an easily accomplished method to metallic ground state silver nanoparticles.

As shown in the literature silver nanoparticles can be easily introduced to PANI, as the unique redox properties of PANI allows it to efficiently reduce silver (I) ions in solution to form metallic silver (0) nanoparticles on its surface.⁷¹⁻⁷⁴ Salem et al. showed that silver nanoparticles could be simply applied to PANI surface by firstly preparing a PANI ES. Dedoping of the PANI ES to EB with sodium hydroxide was subsequently completed. Silver nanoparticles were then applied by reduction of silver nitrate with a suspension of the PANI in distilled water. The formed silver nanoparticles were of the size range of 6.92-12.4 nm as elucidated by transmission electron microscopy. These samples were used to analyze their ability to remove brilliant green dye from solution as the release of dyes to the aquatic environment is a significant pollutant issue.⁷⁵ Marakova et al. synthesized PANI and polypyrrole coatings on cotton fabric and successfully attached silver nanoparticles to these products producing a unique antimicrobial fabric. Nanoparticles in the range of 50-500 nm of non-uniform size were produced. The fabrics produced were effective against both *S aureus* and *E coli* with the silver coated fabrics offering enhanced antimicrobial efficacy. They also noted that polypyrrole exhibited decent antimicrobial ability by itself while attachment of silver nanoparticles enhanced this effect whereas PANI by itself was quite innocuous against both bacterial strains but exhibited biocidal ability at increased silver nanoparticle concentrations.⁴¹

Other routes have also been displayed, Khesuoe et al. showed that electropolymerizing aniline in the presence of preproduced silver nanoparticles successfully incorporated the particles into the formed PANI matrix while Das et al. completed a one-pot synthesis for the purposes of energy storage by dissolving aniline, folic acid, silver nitrate, sodium bicarbonate and sulfuric acid and with the subsequent addition of APS produced a series of hydrogels.^{76,77}

Synergistic effects of PANI coated with silver nanoparticles may therefore offer increased antimicrobial efficacy with either reduced dose rates required or a more broad-spectrum

compound being produced. As such it is an interesting avenue to explore in the search for more potent antimicrobial agents.

1.4. Interaction of Conducting Polymers with Lectins and Bacterial Cells

1.4.1. Concanavalin A

Lectins are carbohydrate binding proteins which are found throughout nature and are utilized for their ability to bind to carbohydrates for important biological events. Goldstein et al. defined lectins as “sugar-binding proteins or glycoprotein of non-immune origin which agglutinates cells and/or precipitates glycoconjugates”.⁷⁸ The research and study of lectins took off in the 1960’s when researchers first began to understand their importance, the influenza virus as an example binds to *N*-acetyl neuraminic acid residues on the host cells surface via hemagglutinin structures which act as a lectin.⁷⁹ This initial binding step is the first major step in the virus’s life cycle and by preventing this the researchers hoped to therefore prevent the continuation of the virus’ lifecycle and stop the virus replicating. Similarly, in 1979 it was demonstrated that urinary tract infections in mice caused by the binding of mannose specific *E coli* to the mannosylated walls in the urinary tract could be prevented by the administering of methyl- α -D-mannoside, a glycoside that can block the mannose binding sites that *E coli* uses to attach to the cell wall.⁸⁰ Lectins were first described as “hemagglutinins” because their initial discovery was due to their ability to agglutinate blood. This was noticed by Peter Hermann Stillmark in 1888 for his doctoral thesis where he was studying the toxicity of beans of the castor tree which arose from the presence of the Ricin toxin. After identifying these abilities arising from a protein, he incorrectly assigned the agglutination properties of the bean to the same compound, the “Ricin” protein. Half a century later, researchers finally noted that the agglutination properties were not due to the ricin toxin, but to the non-toxic protein *Ricinus communis* agglutinin which was also found in the castor beans. *Concanavalin A* was first isolated in 1919 by James Sumner at Cornell University from *Canavalia ensiformis*, commonly known as the jack bean, and was the first pure hemagglutinin. Nearly 20 years later they showed that ConA agglutinated erythrocytes and yeasts and demonstrated how adding glycogen caused precipitation. They also demonstrated the competition in binding strengths of different carbohydrates, as it was observed that the addition of sucrose inhibited the hemagglutination. This led them to deduce that the hemagglutination of ConA is most likely due to the carbohydrates located on the erythrocytes surface.⁸¹

The use of ConA in this thesis will be to observe and measure the ability of synthesized glycopolymers to interact with a biological moiety. This is especially useful due to the

carbohydrates chosen for attachment in this thesis are D-+-mannose and D-+-glucose which both show specific binding to ConA.⁸²

1.4.2. Bacterial Interaction with Carbohydrates

The initial step for pathogenic bacterial infections is interaction or attachment of the organism cell to the target. A primary example of this are urinary tract infections, which result from the binding and colonization of uropathogenic *E coli* (UPEC) cells to the urinary tract.⁸³ The attachment of UPEC results from type 1 pili which are filamentous organelles used for binding.^{84,85} These structures are found on UPEC and are tipped with the FimH adhesin, a protein that binds specifically to mannose containing glycoprotein receptors. These infectious pathogens bind to the many mannosylated receptors that are found within the urinary tract on mammalian epithelial cells.

The prevention and treatment of these infections have been shown to be possible with inhibition of the initial binding event of the uropathogenic bacteria. This can be done with FimH inhibitors, as the FimH protein is responsible for the binding of these cells to the urinary tract.⁸⁶ This is effective in preventing urinary tract infections, however, for the treatment of established infections the first line of defense is still antibiotics. By using antibiotics there is the risk of further exacerbating the existence of antibiotic resistant pathogens, so alternatives such as orally applicable treatments with low potential for bacterial resistance are constantly sought after.⁸⁷ In particular, broad spectrum antimicrobials which are not specifically targeted to the antagonist, negatively affect the natural fauna and increase the chances of antimicrobial resistant strains persisting and evolving. An example of the latter is infections resulting from *Clostridium difficile* where the treatment is the reduction in the frequency and duration of antimicrobial therapy and the number of antimicrobial agents prescribed. A majority of patients who had infections resulting from *Clostridium difficile* had prior exposure to antimicrobial agents. Treatment has been recommended by using specific antibiotics targeting *Clostridium difficile* such as Vancomycin.⁸⁸

Glycopolymers that contain mannoside groups may offer unique applications to the treatment of infections resulting from cells which require binding to or interaction with mannosylated compounds. This narrow spectrum targeting of the antimicrobial polymer will alleviate the issues raised previously surrounding broad-spectrum antimicrobial compounds. Synergistic effects by the antagonistic mannoside along with the antimicrobial potency of the polymeric structure may offer new and unique ways to not only treat urinary tract infections but other infections resulting in similar binding events.

1.5. Objectives

PANI has been shown to be antimicrobial, with effectiveness documented against both gram positive and gram negative bacteria. The hypothesis to be tested throughout this thesis is that attachment of biologically active molecules to PANI will result in increased interaction with specific proteins and cells and therefore increase the biocidal activity against them. The major objectives of this thesis were therefore to observe biological interaction with synthesised PANI glycopolymers and to increase the antimicrobial efficacy of PANI. The antimicrobial efficacy of PANI is believed to be due to electrostatic interaction of the positively charged polymer chain which binds to the negatively charged cell envelope of the target bacteria causing cell lysis. It was therefore hypothesised that by increasing the binding strength to the bacterial cell wall by adding functional groups that were specific to target bacteria that the bacterial efficacy could be improved.

Initially compounds such as penicillin's, carbapenems, and carbohydrates were all hypothesised as useful candidates to improve the interaction and/or the biocidal action of PANI and target bacteria, however, the focus was narrowed to be primarily on carbohydrates as they are simple, cheap, readily available and are an important class of compounds in the life cycles of bacteria. The aim was to synthesise a PANI glycopolymer and to observe if enhanced interaction between PANI and bacterium increased improved the biocidal properties.

The method to achieve the goals mentioned previously was to initially investigate the synthesis of a PANI glycopolymer from a modified aniline monomer containing D-mannose. Click chemistry has been shown as a powerful tool to link two molecules together and can be utilised to quickly and efficiently form the bond between aniline and carbohydrate. Polymerization of the monomer would provide a PANI glycopolymer with a high concentration of pendant carbohydrate groups to maximise the biological interaction. This glycopolymer would be tested against ConA, gram positive and gram negative bacteria to analyse their interaction and if there was any enhanced bactericidal efficacy in comparison to a control.

Functionalisation of PANI is an interesting undertaking due to the difficulty posed in its processing resulting from its very low solubility. If PANI can be successfully functionalized in such a way that allows it to take part in click chemistry, such as attachment of a thiol or alkyne, then a library of various PANI materials can be synthesised and analysed quickly and efficiently. The sulfonation of benzene is a common electrophilic aromatic substitution reaction in organic chemistry utilising sulfuric acid to form sulfonic acid groups on the aromatic ring and is also applicable to the aromatic rings found in PANI. Reduction of these sulfonic acid groups will

allow the synthesis of a thiolated PANI, PANI-SH. This thiol functionalized PANI can then be used in a thiol-ene click reaction with an alkene functionalized carbohydrate to form a PANI glycopolymer.

An alternative strategy in the processing of PANI has been shown to be the polymerization of aniline in solutions containing a substrate material, resulting in a coating of the substrate and formation of a PANI film on the surface. Freestanding PANI films are also possible. The synthesis and evaluation of a PANI film surface functionalized with a carbohydrate through click chemistry and its comparison against native PANI can be used to show the positive effects the carbohydrate can impart on the material. The previous goal was to form a thiolated PANI but it may also be possible to utilize the unsaturated ring and therefore react a thiol with PANI.

While surface functionalized of PANI thin films with glucose were shown in a previous chapter, silver nanoparticles were shown to be easily and efficiently added to PANI samples. The ability of PANI to reduce silver nitrate is a simple method to attach highly biocidal silver nanoparticles to the film, opening further avenues of attack for the PANI glycopolymer. The objective for this final chapter was to investigate the increased biocidal ability of the films by attachment of silver nanoparticles.

1.6. Thesis structure

Chapter 1 of this thesis will focus on an introduction to the history, relevant theory and processes that are applied throughout this thesis.

Chapter 2 will introduce the methodology to be employed to characterise the synthesised novel polymeric materials and the biological experiments for determining binding and antimicrobial activity.

Chapter 3's aim will be to investigate the feasibility of synthesising a mannose functionalized aniline monomer. This functionalized monomer will then be chemically polymerised and the effect of the carbohydrate on the polymerization process will be investigated. The final product will be characterised, and its biological interactions will be investigated.

In chapter 4 the functionalization of PANI will be introduced. PANI will be sulfonated with sulfuric acid to introduce a sulfonic acid moiety which will then be reduced to produce a thiol functional group which can partake in the thiol-ene click reaction. Mannose will then need to be functionalized with an alkene group, so it can be the "ene" part of the reaction. The thiol-ene reaction will then allow the click of these two products to form a PANI-mannose glycopolymer.

Chapter 5 will investigate PANI films as potential surfaces for functionalisation with carbohydrates. The ability of PANI to directly take part in the thiol-ene reaction as the “ene” with no added side chains will be investigated by a thiol-ene click reaction with a thiolated glucose. The product will be tested to investigate its ability to interact and bind fluorescently labelled ConA and its antimicrobial properties against gram positive and negative bacteria.

Chapter 6 will build on chapter 5 and utilise PANI films functionalised with thiolated glucose. PANI films with and without added glucose will be utilised in the reduction of silver nitrate, resulting in the formation of highly antimicrobial silver nanoparticles on the films surface. The effect of the glucose on the silver nanoparticle formation will be explored and the films antimicrobial ability against both gram positive and gram negative bacteria will be elucidated.

Chapter 7 will give a brief summarisation of the thesis and tie in all that was found and possible directions for future work in this field of study.

Chapter 2. Methodology

2.1. Introduction

This chapter describes both the chemical and biological characterisation methods used throughout this thesis along with the reagents, parameters and instruments utilised.

2.2. Characterisation

2.2.1. Nuclear Magnetic Resonance (NMR) Spectroscopy

^1H -NMR spectra were recorded on 400 MHz Bruker spectrometer and are reported in parts per million (ppm) on the δ scale relative to CDCl_3 (δ 7.26). ^{13}C -NMR spectra were recorded on a 100 MHz Bruker spectrometer and are reported in parts per million (ppm) on the δ scale relative to CDCl_3 (δ 77.16). The multiplicities of ^1H signals are designated by the following abbreviations: s = singlet; d = doublet; t = triplet; q = quartet; m = multiplet; br = broad; dd doublet of doublets; dt = doublet of triplets; dm = doublet of multiplets. All coupling constants J are reported in hertz.

2.2.2. High Resolution Mass Spectroscopy (HRMS)

HRMS was conducted by the University of Auckland's Mass Spectroscopy Centre. It was conducted on a Bruker micrOFOT-Q mass spectrometer using electrospray ionization mass spectroscopy.

2.2.3. Fourier Transform Infrared (FTIR) Spectroscopy

FTIR spectroscopy was conducted by utilizing two different analysis methods on a Thermo Nicolet 8700 FTIR spectrophotometer. The KBr disk method was utilized for all PANI powders. The KBr was firstly dried in an oven at 110°C before use. 150-200 mg of KBr was weighed into a mortar and 1 mg of sample was subsequently added. The mixture was ground together with a pestle and then pressed under 5 tons of pressure for 5 minutes in a pellet press. Measurements were taken immediately following pellet preparation. A blank KBr disk was also produced and used as a background to account for any moisture absorption. Absorbance spectra were taken as an average over 32 scans over a wavelength range of $550\text{-}4000\text{ cm}^{-1}$ with a resolution of 4 cm^{-1} .

PANI films mounted on glass slides were analyzed using an attenuated total reflectance (ATR) attachment with diamond crystal on the same spectrometer. Absorbance spectra were taken as

an average over 32 scans over a wavelength range of 550-4000 cm^{-1} with a resolution of 4 cm^{-1} .

2.2.4. UV-Visible (UV-Vis) Spectroscopy

UV-Vis spectra were collected on a Shimadzu UV-2101PC UV-Vis Scanning Spectrophotometer between 250 and 800 nm with a 1 cm quartz cuvette. N-methylpyrrolidone (NMP) was used as the solvent and the samples were filtered through a 0.45 μm PTFE syringe filter prior to analysis.

2.2.5. Gel Permeation Chromatography (GPC)

GPC was conducted on a system consisting of a Waters 515 HPLC pump, a Degassex DG-4400 on-line degasser connected to a TSK Gel Super AWM-H column (9 μm , 6 x 150 mm) with column guard, 0.5 μm in-line filters, a Rheodyne manual injector, and a Waters column oven. The eluent was NMP and the flow rate was 0.12 mL/min. Sample concentrations were 10 mg/mL and the injection volume was 200 μL . The solution was filtered through 0.45 μm PTFE syringe filters before injection. Polystyrene standards used were Agilent Easical GPC/SEC calibration standards. Data acquisition and processing were performed using the ASTRA 4 software (Wyatt Technologies Corporation). The detector was a Shimadzu RID-10A Differential Refractive Index detector. The columns and RI detector were maintained at 35 $^{\circ}\text{C}$.

2.2.6. Cyclic Voltammetry

Cyclic voltammetry was conducted using a three-electrode setup with a glassy carbon working electrode (GCE), platinum counter electrode and Ag/AgCl reference on a BAS100B electrochemical analyser. The experiments started at -200 mV vs Ag/AgCl and increased to 1000 mV vs Ag/AgCl at a scan rate of 100 mV/s with 10 $\mu\text{A/V}$ sensitivity. The solutions for the electrochemical polymerization were 0.1 M of sample in 0.5 M aqueous H_2SO_4 supporting electrolyte. All electropolymerization solutions were deaerated with oxygen-free nitrogen for at least 15 minutes prior to beginning.

2.2.7. Elemental Analysis

The elemental analysis results provided in this thesis were all conducted by the Campbell Microanalytical Laboratory, the University of Otago, Dunedin, New Zealand. CHNX analysis was the method used which determines the mass fractions of elements such as carbon, hydrogen, nitrogen and certain heteroatoms (halogens, sulfur etc). Oxygen concentration is calculated by difference.

2.2.8. Scanning Electron Microscopy (SEM) and Energy Dispersive X-ray (EDX) Spectroscopy

SEM scans were taken using a Phillips XL30S field emission gun with an accelerating voltage of 20 kV and a back scattered electron detector. Samples were sputter coated with platinum prior to characterization to prevent charging and increase the conductivity of the samples. The EDX detector was a SiLi (Lithium drifted) super ultra-thin window.

2.2.9. X-ray Photoelectron Spectroscopy (XPS)

The XPS data were collected on a Kratos Axis UltraDLD X-ray Photoelectron Spectrometer (Kratos Analytical, Manchester, UK) equipped with a hemispherical electron energy analyser. Spectra were excited using monochromatic Al K α X-rays (1486.69 eV) with the X-ray source operating at 150W. In this case the analysis area was a 300 by 700 micron spot obtained using the hybrid magnetic and electrostatic lens and the slot aperture. Samples were secured to the sample bar using indium wire. Charge neutralisation was used to alleviate surface charge build-up, resulting in a shift of approximately 3 eV to lower binding energy. Survey scans were collected with a 160 eV pass energy, whilst core level scans were collected with a pass energy of 20 eV. The analysis chamber was at pressures in the 10⁻⁹ torr range throughout the data collection.

Data analysis was performed using CasaXPS (www.casaXPS.com). Shirley backgrounds were used in the peak fitting. Quantification of survey scans utilised relative sensitivity factors supplied with the instrument. Core level data were fitted using Gaussian-Lorentzian peaks (30% Lorentzian). During curve fitting the C 1s binding energy of the adventitious hydrocarbon on the surface was used to correct for this shift, with the saturated hydrocarbon peak set to 285 eV. The spin orbit doublets of the S 2p 1/2 peak area was constrained to be exactly half the S 2p 3/2 and due to the core hole lifetime being the same the full width half maximum (FWHM) of the two peaks were constrained to be the same.

2.2.10. Biological Studies

2.2.10.1. Concanavalin A binding assay of modified PANI's

ConA is a useful, easily sourced carbohydrate binding lectin that has a strong interaction with mannose-like carbohydrate groups and a weaker interaction with glucose-like carbohydrate groups.⁸² There were two different ConA assays used in this thesis to measure the binding efficacy of glycopolymers.

The first ConA assay is a spectroscopic method employing UV-Vis spectroscopy as described by Cairo et al.⁸⁹ A buffer solution (0.1 M tris-HCl pH 7.2, 0.9 M NaCl, 1 mM CaCl₂, 1 mM MnCl₂) was prepared and used to dissolve all solids including ConA and the sample. The sample (4 mg) was dissolved in the above buffer solution (400 µL) and vortexed (5 minutes) to prepare a polymer stock solution. This polymer stock solution was further diluted with buffer to make the following polymer concentrations 800, 700, 600, 500, 400, 300, 200, 100, 50, and 0 µg/mL. A separate ConA stock solution was prepared by dissolving ConA (30.42 mg, 90 µM, assuming ConA tetramer with a molecular weight of 104,000 Da.) in buffer (1.63 mL) and vortexing. Each polymer sample (125 µL) was mixed with ConA solution (125 µL) and left overnight (16 hours). The next day the solution was centrifuged (5000 rpm, 60 seconds), and the supernatant removed by pipette. The precipitate cake was then dissolved in methyl α-D-mannopyranoside (1 mol/L, 1 mL). Both the supernatant and pellet were measured by UV-Vis at 280 nm in a quartz cuvette over an average of 2 scans.

ConA Texas Red conjugate (10 mg) was dissolved in a buffer prepared with milli-q water and the following salts: MnCl₂ (10 mM), CaCl₂ (10 mM) and NaCl (0.9 M). The solution was vortexed to fully dissolve the ConA and the salts, centrifuged and decanted to remove any particulates. The films were measured using fluorescent microscopy prior to the assay to get a background reading. ConA buffer solution (5 µL) was dropped onto each film and left sitting for ten minutes. The films were then washed with clean buffer (100 µL) by pipetting the solution onto the surface and using the pipette to draw the washing solution up and down multiple times to remove any unbound ConA. The films were then measured under the fluorescent microscope. The washing step was repeated five times with measurement of the fluorescence after 0, 1 and 3 washes. After the repeat washes the films were rinsed with a solution of methyl-α-D-mannopyranoside (1 mol/L, 5 µL) using the same method as the washing step and the fluorescence measured.

2.2.10.2. Biocidal efficacy of modified PANI powders – Analysis of the Minimum Lethal Concentration (MLC)

E coli ATCC[®] 25922[™] (referred to as *E coli* and *E coli* 25922) and *S aureus subsp. aureus* ATCC[®] 6538[™] (referred to as *S aureus* and *S aureus* 6538) were the strains utilised in the antimicrobial testing throughout this thesis as they are standard antibiotic strains.⁹⁰⁻⁹² They are routinely used as control organisms to verify that antibiotic susceptibility results are accurate.^{90,93}

The MLC of the powders produced in this thesis were analyzed using a method described by Jorgensen et al. and Robertson.^{94,95} A stock solution of sample to be tested (2 wt %) was prepared in aqueous tryptic soy broth (TSB, 30 g/L) and vortexed to suspend. Sample mixtures were ultrasonicated using a QSonica Q700 sonicator from Alphatech for 10 seconds four times. To a 96 well plate 50 μ L of the stock solution was added to the top row of wells. TSB (25 μ L) was added to the remaining wells in a column. 25 μ L of the top well was then pipetted into the next well down creating a series of doubling dilutions. This was repeated for all the wells in the column to prepare a concentration series of polymer along with a blank containing no agent. The final 25 μ L was discarded to waste. These preparations were carried out in triplicate for each sample being tested. Overnight cultures of *S aureus* 6538 and *E coli* 25922 were diluted 1:1000 in TSB and vortexed to suspend. 25 μ L of each culture was added to the sample wells prepared previously. These samples were incubated for 1, 4 and 24 hours. Each well was analyzed for bactericidal activity by pipetting 5 μ L to a tryptic soy agar (TSA) plate. A count of <5 colonies was taken as a lethal concentration. Determination of MLC was conducted by observing the lowest concentration required to give no growth or <5 colonies after an incubation period and a non-active concentration was considered when there was confluent growth or >5 colonies of bacterial colonies.

The MLC of silver nanoparticle functionalized PANI powder **14** was assessed using the same method presented above, however, the experimental inoculum was prepared in sodium bicarbonate buffer (0.2 mmol) rather than TSB.

2.2.10.3. Biocidal efficacy of modified PANI films – Analysis of the Minimum Bactericidal Concentration

The biocidal activity of modified PANI films was assayed using a method developed in house based on the Japanese Industry Standard Z-2801. An overnight culture of the desired bacterial strain (*E coli* 25922 or *S aureus* 6538) was prepared in TSB and incubated overnight at 37 °C with 200 rpm shaking. Films to be tested were sterilized aseptically in a biosafety cabinet using successive ethanol washes, 5 minutes with 70 % ethanol and 3 minutes with 100 % ethanol. They were left in the cabinet overnight to dry fully. An ethanol sterilized hole punch was used to punch out films of 6 mm diameter in triplicate for each sample to be tested. Agarose (0.5 %) in milli-q water was prepared and heated in a microwave to liquefy. 5 μ L of agarose was pipetted into the bottom of the well plate and each film section was placed on top so that it adhered to the well plate. A sterilized polypropylene film was also punched out of a stomacher bag and used as a non-biocidal cover film to sandwich the culture and prevent the culture from drying

out. The experimental inoculum was prepared to a concentration of 10^6 CFU/mL in sodium bicarbonate buffer (0.2 mmol). 10 μ L of inoculum was pipetted onto each film to be tested including into empty wells to serve as a control. This gave 10^4 CFU of bacteria on each film. The films were placed in a sealed box with moist tissue and incubated at 37 °C for 24 hours. For each film 190 μ L of TSB was added to each drop of inoculum and pipette mixed well. The 200 μ L culture was added to a sterile 96 well plate and the optical density is measured at 600 nm (OD_{600}) was measured and taken as time point 0. The well plates were then incubated for 16 hours at 37 °C and the OD_{600} remeasured.

The results of the surface biocide test were statistically analysed using a Kruskal-Wallis test between treated and untreated cells. The Kruskal-Wallis test was followed up with Dunn's multiple comparison test if a significant difference is found between the treated and control samples after 16 hours of incubation.

Chapter 3. Synthesis and Polymerization of a Modified Aniline Monomer

3.1. Introduction

The chemical transformation of PANI to add new functionality can be difficult, due to its processability, as it has a very low solubility in most common solvents.²² The difficulty in forming a PANI solution means that general chemical techniques cannot be employed optimally which deters post synthesis processing. To form a functionalized PANI with the highest rate of attachment of the carbohydrate, synthesis of a novel aniline monomer and subsequent polymerization was considered as one of the optimal synthetic pathways to achieve this goal. The major advantage of this method is that it allows the initial reactions to be completed using wet chemistry, so both the purity of the final product and attachment rate of the desired side group is optimised. The purity and rate of attachment of the carbohydrate is important in synthesising powerful glycopolymers because increased binding with biological cells is found with increased carbohydrate concentration due to the glycoside cluster effect.⁹⁶ The theory of the glycoside cluster effect is that enhanced binding activity occurs due to a multivalent display of carbohydrates compared with the binding of an individual carbohydrate.

Unless otherwise stated the results are from the products synthesised from the chemical oxidation of aniline and not the electrochemical synthesis.

3.2. Experimental

3.2.1. Chemicals

Unless otherwise stated all chemicals were used as received from commercial sources. All moisture sensitive reactions were performed in an inert, dry atmosphere of nitrogen in oven dried glassware. Analytical thin-layer chromatography (TLC) was performed using Kieselgel F254 0.2 mm (Merck) silica plates with visualization by ultraviolet radiation and/or staining with vanillin. Flash chromatography was performed using Kieselgel S 63-100 μm (Riedel-de-Hahn) silica gel. The solvent compositions reported for all chromatographic separations are on a volume/volume (v/v) basis. Dialysis tubing was Spectra/Por Dialysis Membrane Molecular Weight Cut-off 1000. PANI in both emeraldine salt and emeraldine base forms were prepared in house to standard syntheses.¹⁷

Synthesis of 2-aminophenyl 1,2,3-triazole-N-2,3,4,6-O-acetyl- α -D-mannopyranoside was generously completed and donated by Dr Hayley Charville.

3.2.2. Synthesis of 1,2,3,4,6-penta-O-acetyl- α -D-mannopyranoside

D-mannose (7 g, 38.9 mmol) was added (in five portions) to a stirred solution of iodine (0.4 g, 1.55 mmol) in acetic anhydride (40 mL, 432 mmol) at 0 °C. The reaction mixture was stirred at this temperature for 30 minutes and then allowed to warm up to room temperature. After 1 h at room temperature, methanol (20 mL) was added and the mixture was stirred for a further 30 minutes, followed by evaporation of the solvent *in vacuo*. The residue was dissolved in DCM (50 mL) and washed with Na₂S₂O₅ solution (2 × 50 mL). The layers were separated, and the resulting colourless organic phase was washed with NaHCO₃ solution (4 × 50 mL), dried (MgSO₄) and concentrated under reduced pressure to afford a pale-yellow oil (12.9 g, 85%) as an anomeric mixture (α : β , 4:1) as determined by ¹H NMR. This was used in the next step without any further purification. δ_{H} (400 MHz, CDCl₃): 1.97 (s, 3H, OC(O)CH₃), 2.02 (s, 3H, OC(O)CH₃), 2.06 (s, 3H, OC(O)CH₃), 2.14(s, 3H, OC(O)CH₃), 2.15 (s, 3H, OC(O)CH₃), 4.01-4.13 (m, 2H, CH₂OAc), 4.23-4.29 (m, 1H, CH), 5.22-5.32 (m, 3H 3 × CH), 6.05 (d, *J* 1.9, 1H, CH). Resonances for minor β anomer: δ_{H} (400 MHz, CDCl₃): 2.00 (s, 3H, OC(O)CH₃), 2.07 (s, 3H, OC(O)CH₃), 2.18 (s, 3H, OC(O)CH₃), 3.77-3.81 (m, 1H, CH), 5.10 (dd, *J* 6.6, 3.4, 1H, CH), 5.43-5.46 (m, 1H, CH), 5.83 (d, *J* 1.2, 1H, CH). Data was consistent with that reported in the literature.⁹⁷

3.2.3. Synthesis of 2-Bromoethyl 2,3,4,6-tetra-O-acetyl- α -D-mannopyranoside

BF₃·Et₂O (7.9 mL, 64.05 mmol) was added dropwise to a solution of 1,2,3,4,6-penta-O-acetyl- α -D-mannopyranoside (5 g, 12.81 mmol) and 2-bromoethanol (1.82 mL, 25.62 mmol) in dry DCM (80 mL) at 0°C. After 1 h the ice bath was removed, and the reaction continued at room temperature overnight. The reaction mixture was then slowly added to cold water (80 mL) and the organic layer was separated. The aqueous layer was extracted with DCM (50 mL) and the organic layers combined and washed successively with water (100 mL), sat. NaHCO₃ (2 × 100 mL), water (100 mL). The solution was dried over MgSO₄ and concentrated under reduced pressure to afford a yellow oil. The product was precipitated from diethyl ether to produce a white powdery solid which was filtered, washed with diethyl ether and dried under high vacuum. (4.03 g, 65%). δ_{H} (400 MHz, CDCl₃): 1.99 (s, 3H, OC(O)CH₃), 2.05 (s, 3H, OC(O)CH₃), 2.11 (s, 3H, OC(O)CH₃), 2.16 (s, 3H, OC(O)CH₃), 3.50-3.53 (m, 2H, CH₂Br), 3.79-3.91 (m, 2H, OCH₂), 4.10-4.15 (m, 2H, CH₂OAc), 4.24-4.29 (m, 1H, CH), 4.87 (d, *J* 1.7, 1H, CH), 5.26-5.33 (m, 3H, 3 × CH). δ_{C} (100 MHz, CDCl₃): 20.6, 20.7, 20.8, 20.9 (CH₃), 29.6 (CH₂Br), 62.4 (CH₂OAc), 66.0, 68.5, 68.9 (CH), 69.0 (OCH₂CH₂Br), 69.4 (CH), 97.8 (CH), 169.7, 169.8, 170.0, 170.6 (OC(O)CH₃). Data is consistent with that reported in the literature.⁹⁸

3.2.4. Synthesis of 2-azidoethyl 2,3,4,6-tetra-O-acetyl- α -D-mannopyranoside (1)

2-bromoethyl 2,3,4,6-tetra-O-acetyl- α -D-mannopyranoside (2 g, 4.4 mmol) and sodium azide (2.28 g, 35.12 mmol) were dissolved in dry DMF (60 mL) and the reaction was stirred under N₂ at 60°C for 6 h before cooling to room temperature and stirring overnight. The following day the reaction mixture was poured into ethyl acetate (150 mL) and washed with water (3 × 100 mL) and brine (2 × 100 mL). The organic layer was dried (MgSO₄), filtered and concentrated under vacuum. The crude product was purified by silica gel column chromatography (ethyl acetate : hexane, 2 : 1) to afford the title compound as white crystals (1.59 g, 87%). δ_{H} (400 MHz, CDCl₃): 1.99 (s, 3H, OC(O)CH₃), 2.05 (s, 3H, OC(O)CH₃), 2.12 (s, 3H, OC(O)CH₃), 2.16 (s, 3H, OC(O)CH₃), 3.46-3.49 (m, 2H, OCH₂CH₂N₃), 3.65-3.70 (m, 1H, OCH₂CH₂N₃), 3.85-3.89 (m, 1H, OCH₂CH₂N₃), 4.02-4.15 (m, 2H, CH₂OAc), 4.27-4.31 (dd, *J* 5.4, 12.1, 1H, CH), 4.87 (d, *J* 1.5, 1H, CH), 5.27-5.35 (m, 3H, 3 × CH). δ_{C} (100 MHz, CDCl₃): 20.6, 20.7, 20.7, 20.9 (CH₃), 50.5, (OCH₂CH₂N₃), 62.5 (OCH₂CH₂N₃), 66.0 (CH), 67.0 (CH₂OAc), 68.9 (CH), 69.4 (CH), 97.8 (CH), 169.8, 169.9, 170.2, 170.8 (OC(O)CH₃). Data is consistent with that already in the literature.⁹⁹

3.2.5. Synthesis of 2-aminophenyl 1,2,3-triazole-N-2,3,4,6-O-acetyl- α -D-mannopyranoside (2)

Copper (II) sulfate pentahydrate (23 mg, 0.0935 mmol), sodium ascorbate (37 mg, 0.187 mmol) and 2-ethynylaniline (0.26 mL, 2.25 mmol) were dissolved in water (20 mL) and heated to 50°C under a N₂ atmosphere for 10 minutes. 2'-Azidoethyl 2,3,4,6-tetra-O-acetyl- α -D-mannopyranoside (1.00 g, 1.87 mmol) as a solution in DMSO (40 mL) was then added and the mixture left to stir at 50 °C for 3 h. The reaction mixture was diluted with DCM (50 mL) and washed with brine (4 × 50 mL), dried (MgSO₄), filtered and concentrated under vacuum. The crude product was purified by silica gel column chromatography (ethyl acetate : hexane, 6 : 1) to afford the title compound as a white solid which was dried under high vacuum. (973 mg, 97%). Melting point 54-57°C. $[\alpha]_{\text{D}}^{20}$ 40.7 (c=0.26 g/100 mL, MeOH). Mass spec: *m/z* (ES⁺): 535.2 [M + H⁺]. HRMS (ES⁺): C₂₄H₃₀N₄O₁₀ requires 557.1854 [M + Na], found 557.1849 [M + Na].

3.2.6. Synthesis of acetyl protected mannose functionalized PANI (3)

Polymerization was conducted using a slightly altered general oxidative polymerization procedure for aniline as outlined in 4.1.2. Monomer 2 (100 mg, 0.187 mmol) was weighed into a beaker and HCl (0.05 M, 5 mL) was added. The solution was stirred until complete dissolution

was achieved. APS (64.07 mg, 0.281 mmol) was weighed into a separate beaker and completely dissolved in HCl (0.05 M, 0.5 mL). The APS solution was then added all at once to the monomer **2** containing solution, briefly stirred then left at room temperature. After 24 hours a dark green/black precipitate had formed. The precipitate and remaining solution were poured into a 50 mL centrifuge tube and distilled water was used to ensure quantitative transfer. The sample was then centrifuged at 4000 rpm for 15 minutes. The supernatant was decanted off and distilled water (20 mL) was added. The precipitate cake was vortexed to resuspend the material. This washing was repeated three times. The precipitate was then dried in a vacuum oven at 40°C overnight to afford a dark powdery solid (average yield 20%).

3.2.7. Synthesis of α -D-mannose functionalized PANI (**4**)

The resulting polymer **3** was deprotected using sodium methoxide (NaOMe). A solution containing NaOMe (0.1 mol/L) in MeOH was prepared and 0.2 mL of this solution was added to 10 mg of polymer **3** that was dissolved in DMF (1 mL). This reaction was left for 24 hours and was added drop wise to cold diethyl ether (30 mL). A brown precipitate formed. This mixture was centrifuged (4000rpm, 5 minutes) and the ether decanted off. The ether wash was repeated three times. The final product was dialyzed using dialysis tubing with a molecular weight cutoff of 1000 against distilled water for two days. The product was finally freeze dried to afford a brown powder (yield 92%).

3.3. Results and Discussion

The application of the CuAAC reaction in this procedure showed great merit as an effective way to promote the joining of the PANI polymer backbone and the pendant carbohydrate while taking advantage of the strengths of click chemistry. Similar reactions have already been reported for a number of glycopolymeric syntheses which utilised glycosyl azides being clicked onto alkyne functionalized polymers.¹⁰⁰ The choice of carbohydrate was rigorously discussed however a simple sugar, D+-mannose, was finally chosen due to its strong binding interactions with many bacteria and biological entities including ConA and UPEC.¹⁰¹ Strong selective binding interactions of mannose with ConA is observed making it a useful biological lectin for studying the model binding of the glycopolymer. Yu et al. has already demonstrated a robust reaction synthesis of azide functionalized carbohydrates allowing the easy synthesis of azide mannose 2-azidoethyl 2,3,4,6-tetra-O-acetyl- α -D-mannopyranoside.⁹⁹ While the azide containing aniline could be purchased, the synthetic procedure towards the azide containing starting material **1** is shown in Figure 3.1.

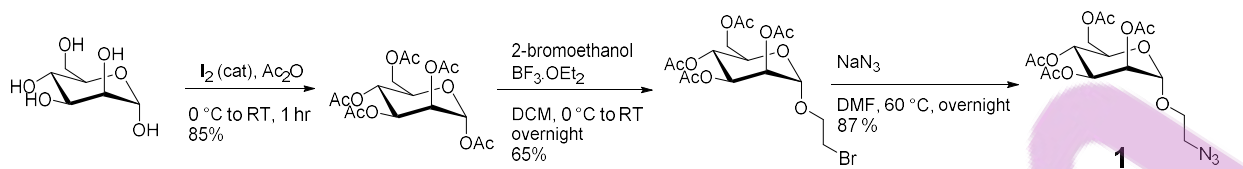


Figure 3.1: Chemical reaction scheme for the synthesis of 2-azidoethyl 2,3,4,6-tetra-O-acetyl- α -D-mannopyranoside starting material **1**.

The polymerization of novel monomer **2**, which was successfully formed from the reaction of monomer **1** with an azide containing aniline initially used general reaction conditions consistent with the polymerization of native aniline as described in section 3.1.1. Aniline is historically polymerised in mineral acids; 1 M HCl being used regularly for its dual effects of both increasing the solubility of aniline in aqueous solution and acting as a chloride dopant *in situ* resulting in the formation of the highly conductive ES form. The stability of the monomer towards acids is therefore important if these concentrations are to be used. Mannose functionalised aniline **2** dissolved completely to form an initially colourless solution in the acidic solvent at a concentration of 0.2 mol/L. After a brief delay a black substance was observed in the reaction vessel prior to addition of the oxidant. This was believed to be elemental carbon and it was hypothesised that the acid led to destruction of the mannose structure, as the polymerization had not yet been initiated. A much weaker acid concentration was therefore used to circumvent this and to keep the carbohydrate functionality intact. Unlike aniline, **2** showed increased aqueous solubility, most likely due to the ability to both hydrogen bond with water and an increase in polarity due to the attached carbohydrate group. Upon decreasing the HCl concentration to 0.05 M it was found that a brown dusty powder **3** could be produced with an average yield of 20 %. Deprotection of **3** resulted in the regeneration of the hydroxyls located on the carbohydrate molecule leading to **4** as shown in Figure 3.2.

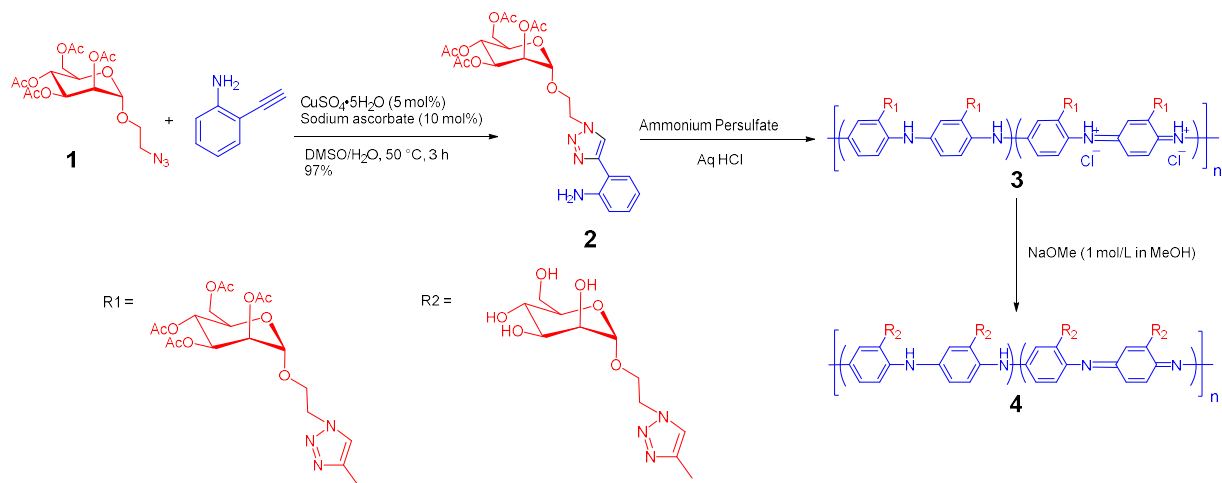


Figure 3.2: Chemical reaction scheme for the polymerization of mannose functionalized PANI **4**.

3.3.1. NMR spectroscopy

Figure 3.3 shows the ^1H NMR spectrum of monomer **2** in deuterated chloroform with the peak assignments being found in table 3.1. The theoretical chemical formula of **2** is $\text{C}_{24}\text{H}_{30}\text{N}_4\text{O}_{10}$. The presence of the aniline molecule is shown by the peaks corresponding to the aromatic rings found at the higher chemical shift of 6.70–7.42 ppm. The shifts that result from the mannose moiety are all found from 1.50–2.505 ppm. Finally, the 1,2,3-triazole proton is found at 7.93 ppm due to the deshielding of the proton by the neighbouring nitrogen atom. The ^1H NMR spectrum confirms the successful formation of monomer **2** with peaks resulting from the theoretical structure shown in Figure 3.2 being observed.

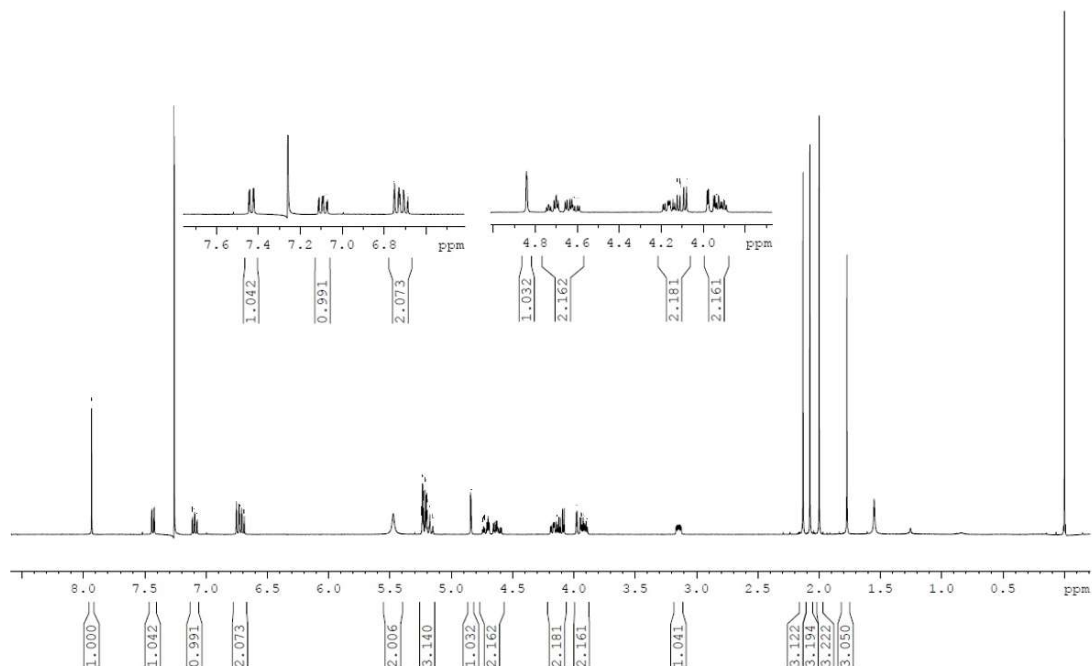


Figure 3.3: ^1H NMR spectrum of mannose functionalized aniline monomer **2** (400 MHz, CDCl_3).

Shift	Multiplicity	Integral	Assignment
1.77	s	3	$\text{CO}(\text{O})\underline{\text{C}}\text{H}_3$
1.99	s	3	$\text{CO}(\text{O})\underline{\text{C}}\text{H}_3$
2.07	s	3	$\text{CO}(\text{O})\underline{\text{C}}\text{H}_3$
2.13	s	3	$\text{CO}(\text{O})\underline{\text{C}}\text{H}_3$
3.14	m	1	$\underline{\text{C}}\text{H}$
3.90	m	2	$\text{CH}_2\underline{\text{C}}\text{H}_2\text{N}$
4.10	m	2	$\underline{\text{C}}\text{H}_2\text{CH}_2\text{N}$
4.60	m	2	$\underline{\text{C}}\text{H}_2\text{OAc}$
4.82	d	1	$\underline{\text{C}}\text{H}$
5.15	m	3	3x $\underline{\text{C}}\text{H}$
5.47	s	2	$\underline{\text{N}}\text{H}_2$
6.70	m	2	2x $\text{Ar}\underline{\text{H}}$
7.10	m	1	$\text{Ar}\underline{\text{H}}$
7.42	dd	1	$\text{Ar}\underline{\text{H}}$
7.93	s	1	Triazole $\underline{\text{H}}$

Table 3.1: ^1H NMR assignments for mannose functionalized aniline monomer **2**.

^{13}C NMR spectroscopy was also conducted on monomer **2** to confirm the environments for the carbon atoms and is shown in Figure 3.4, with their specific assignments found in table 3.2. The carbon atoms in the aromatic ring from PANI are found at chemical shifts >100 ppm. The peaks at lower chemical shifts show the presence of mannose and the $2\times \text{CH}_2$ groups show the alkyl chain between the triazole and carbohydrate. Finally, the triazole group itself has two carbon atoms found with similar chemical shifts to the aromatic carbons. Again, the ^{13}C NMR confirms the presence of the expected molecule which agrees with the theoretical chemical formula of **2**.

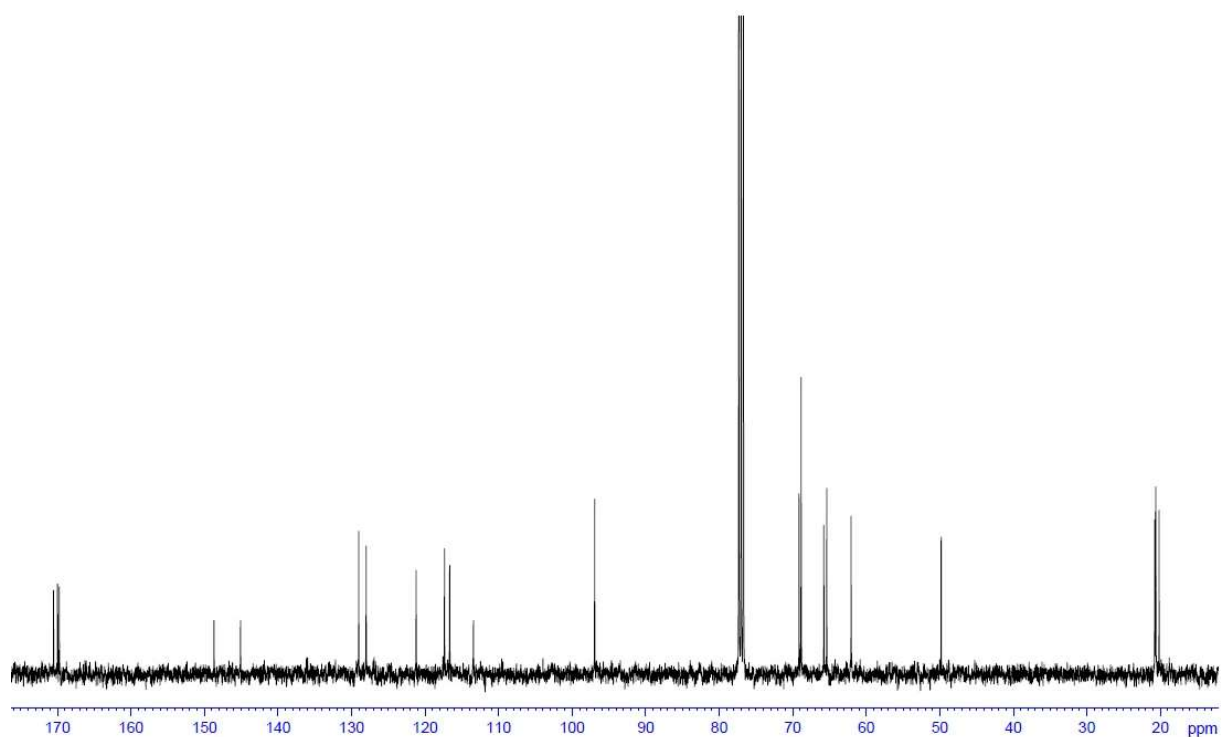


Figure 3.4: ^{13}C NMR spectrum of mannose functionalized aniline monomer **2** (400 MHz, CDCl_3).

Chemical Shift	Assignment
20.2-20.8	$\underline{\text{C}}\text{H}_3$
49.8	$\text{CH}_2\underline{\text{C}}\text{H}_2\text{N}$
62.1	$\underline{\text{C}}\text{H}_2\text{CH}_2\text{N}$
65.4	$\underline{\text{C}}\text{H}$
65.8	$\underline{\text{C}}\text{H}_2\text{OAc}$
68.9	2x $\underline{\text{C}}\text{H}$
69.2	$\underline{\text{C}}\text{H}$
96.9	$\underline{\text{C}}\text{H}$
113.4	$\text{Ar}\underline{\text{C}}$
116.7	$\text{Ar}\underline{\text{C}}$
117.4	$\text{Ar}\underline{\text{C}}$
121.2	Triazole $\underline{\text{C}}\text{H}$
128.0	$\text{Ar}\underline{\text{C}}$
129.0	$\text{Ar}\underline{\text{C}}$
145.1	$\text{Ar}\underline{\text{C}}\text{NH}_2$
148.7	Triazole $\underline{\text{C}}$
169.7 – 170.5	$\text{O}\underline{\text{C}}(\text{O})\text{CH}_3$

Table 3.2: C^{13} NMR assignments of mannose functionalized aniline monomer **2**.

3.3.2. Cyclic Voltammetry

CV is a useful electroanalytical technique that can be utilised to both study the synthesis of conducting polymers from their respective monomers but also investigate the redox properties of the formed electroactive polymers themselves. A three-electrode cell set up is typically used in redox reaction analyses due to its increased accuracy which consists of a working, counter and reference electrode, however, two electrodes can also be utilised which are commonly used for the electrochemical synthesis of conducting polymers. In electrochemical cells a potential is applied at the working electrode and charge transfer from electrochemical reactions of the molecules in solution occur. The counter electrode is used to balance the charge produced at the working electrode and is used in three electrode set ups. In two electrode setups the role of the counter electrode is undertaken by the reference electrode which is why it is less accurate than three electrode setups.

The electrochemical synthesis of PANI requires dissolution of aniline in a suitable solvent. A suitable solvent must meet several criteria such as sufficient solvation power for the solute of

interest, be unreactive towards the solute and any redox products produced, be able to dissolve sufficient concentrations of electrolytes and provide a potential range wide enough so that no interference occurs with the solutes redox processes being analysed.¹⁰² Solvents such as mineral and inorganic acids (hydrochloric, sulfuric, perchloric etc) and organic solvents have all been shown to be suitable for the electrochemical synthesis of PANI.^{20,103-105} Upon application of the dynamic potential aniline molecules begin oxidizing, forming PANI precursors similar to the chemical synthesis. These PANI precursors form on the surface of the working electrode, and as their molecular weight increases, their solubility decreases resulting in precipitation. Due to the electrical properties on PANI charge transfer can occur resulting in increased polymer film thickness as the polymer grows.

The cyclic voltammograms for the electropolymerization of pure aniline and of mannose functionalized aniline **2** at a glassy carbon electrode (GCE) against Ag/AgCl are shown in Figures 3.5 and 3.6. The voltammograms were obtained at a 100 mV/s scan rate over the potential range of -200 to 1000 mV. At the high potential end of the scan from the first cycle both aniline and **2** exhibited a similar large rise in anodic current for potentials greater than 900 mV, which corresponds to two processes, oxidation of the PANI film and oxidation of the monomer with both processes resulting in electron transfer.¹⁰⁵ For aniline, at the low potential end of the scan the first pair of redox peaks is found at 228 (oxidation) and 144 (reduction) eV and corresponds to electron transfer between the fully reduced leucoemeraldine and partially oxidized emeraldine forms of the electrodeposited PANI film along with corresponding doping and dedoping to balance the change in charge. Baba et al. showed via both the cyclic voltammograms and a recorded increase in mass on a quartz crystal microbalance the effect of doping on PANI thin films corresponding to this process.¹⁰⁵ The first oxidation peak for mannose functionalized PANI **3**, formed via electropolymerization of **2**, occurred at 272 mV while an associated broad cathodic peak for this process was seen at 260 mV. These peaks had higher current flow than the peaks assumed to be the same process observed for pure polyaniline ,however, no successive film formation was observed.

The peak found for neat PANI situated at 490 mV is termed as the so-called “middle peak” and does not corresponding to any PANI redox process involving the different redox forms of leucoemeraldine - emeraldine - pernigraniline. Possible reasons for the formation of this peak include: 1) the presence of ortho-coupled reaction products which may include dimers, oligomers or polymers 2) degradation of the PANI chain via soluble quinone type compounds incorporated into the polymer film 3) film degradation via side reactions including polymer crosslinking and/or branching during synthesis resulting in reduced conductivity 4) film

degradation due to hydrolysis and cycling in a monomer free solution (chain scission etc).^{20,106,107} All the above possible reasons for the middle peak are due to unwanted side reactions and degradation of the polymer chain, which all result in lower molecular weights products with reduced conductivities and differing properties to PANI.

The final redox peak pair for PANI is located at 709/661 mV which is attributed to oxidation of the polymer chain from emeraldine to pernigraniline. A significant increase in current is observed at the high potential (>800 eV) side of the scan as a first cycle effect. This peak found in the first cycle is attributed to oxidation of monomeric aniline and **1**, which is a result of the initial stages of polymer formation on the electrode as mentioned previously.¹⁰⁸

While PANI being a highly conductive polymer showed successive film layer formation in its CV observed by the increasing current for the peaks after each subsequent cycle, this was not seen with **2**, where more limited polymer film growth was observed. This possibly indicates that the resulting electrochemically deposited **3** is poorly conductive in nature and forms an insulating layer preventing further film formation. Initial oxidation of the monomer forms the film on the surface, however, due to its potentially insulating nature it prevents further film growth via blocking of the transfer of charge. This results in no further layer formation and no increase in current measured. If this is a result of an insulating layer forming the difference in conductivity between PANI, which shows increased current for each cycle, and **3** is likely caused by a loss of planarity in the polyaniline due to the large D-mannose substituent and an electronic inductive effect of the triazole group.³⁶ This loss in planarity results in a decrease in conductivity most likely via hindrance of π electron delocalization along the polymer backbone and as such an more insulating polymer forms.

Mannose functionalized PANI **3** had fewer redox processes in comparison with neat PANI, with shifts in the redox peaks that were found and assumed to be like that of PANI. The assignment of the oxidative peak for **2** situated at 531 mV (corresponding reductive peak at 477 mV) has been assigned to the “middle peak” which has been shifted to a higher potential compared to neat PANI. While a raft of potential reasons for the formation of this peak was explained earlier, Genies et al. proposed that the appearance of this middle peak is related to the formation and existence of phenazine type rings in the PANI structure.¹⁰⁷

The absence of a peak around 600-800 eV for **3** indicates that there is no further oxidation of the formed polymer chain. Inzelt et al. studied the electrochemical reduction of phenazine and found a similar voltammogram occurred with two redox processes being detected.¹⁰⁹ They assigned these peaks to 1) the first electron transfer resulting in a phenazylium cation (PhH_2^+)

and 2) the second electron transfer process resulting in 5,10-dihydrophenazine (PhH₂). They also noted that successive film formation was limited by redissolution of the charged phenazine back into the solution. Based on this it could indicate that rather than being insulating, monomer **2** is simply forming an initial film layer and then dissolving into solution due to the solubility of **3**.

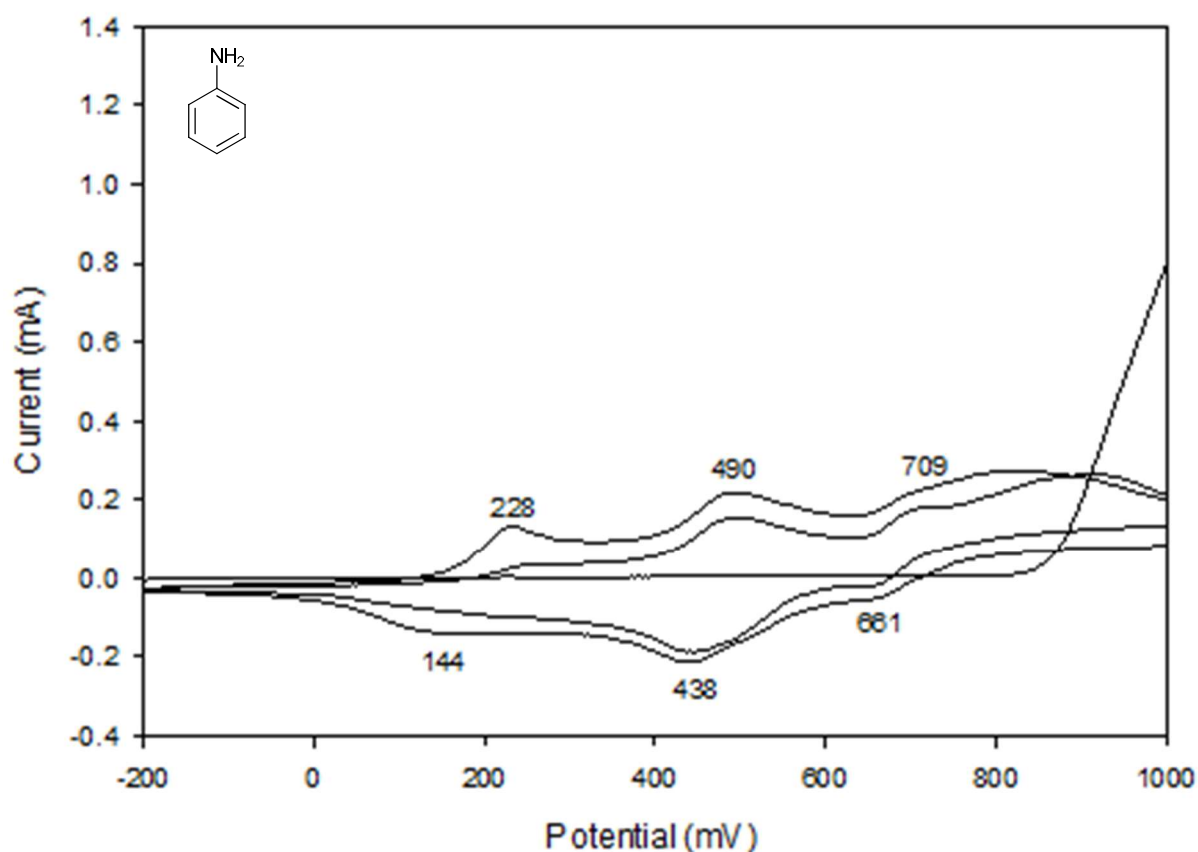


Figure 3.5 Cyclic voltammogram of aniline and the resulting PANI film at a GCE in 0.5 M H₂SO₄ against an Ag/AgCl reference electrode. The initial sweep direction was positive.

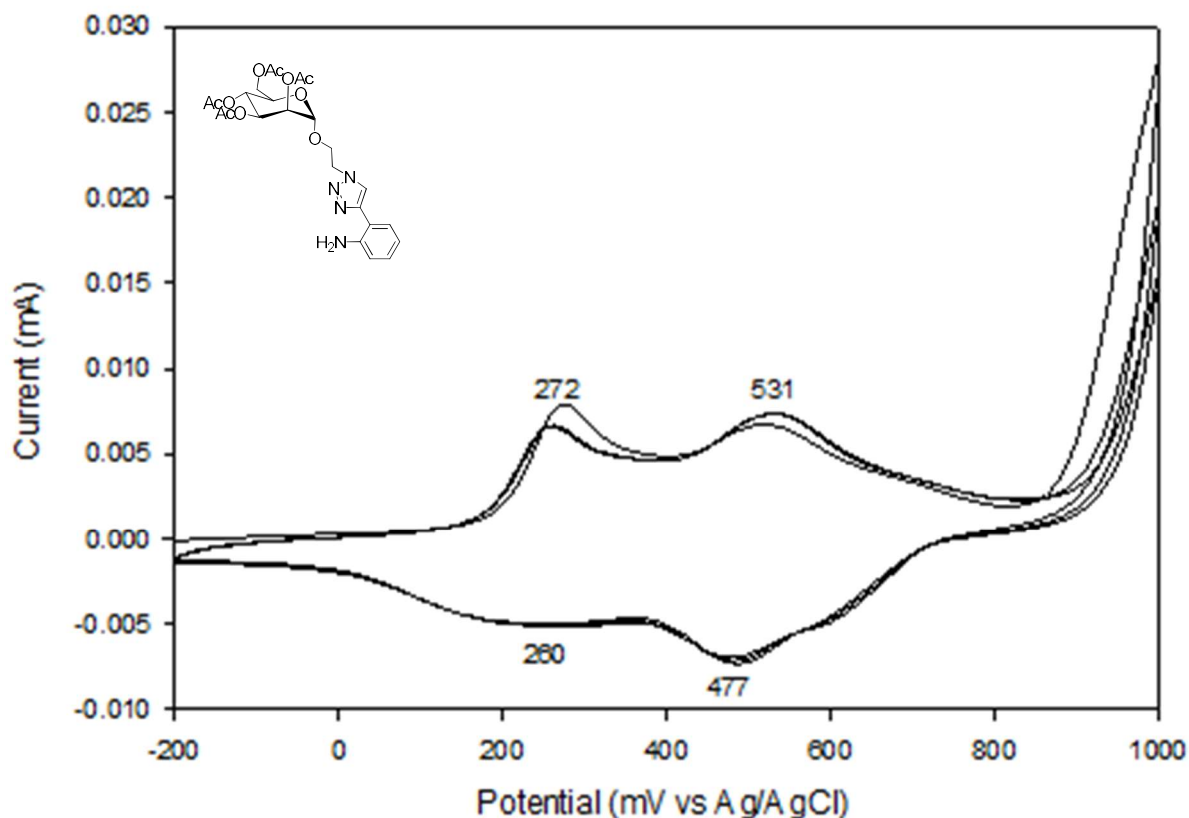


Figure 3.6: Cyclic Voltammogram of mannose functionalized aniline **2** and the resulting polymer **3** at a GCE in 0.5 M H₂SO₄ against an Ag/AgCl reference electrode. The initial sweep direction was positive.

3.3.3. FTIR spectroscopy

FTIR, both transmission and ATR, is one of the most useful techniques for the characterization of PANI and derivatives of PANI due to its simple methodology, fast analysis times and ability to analyze a wide range of polymer types in the solid state. The FTIR of PANI EB and leucoemeraldine conducted as a KBr disk is shown in Figure 3.7 as background information towards the analysis of functionalized PANI's.

Two peaks are found at 1583 and 1504 cm⁻¹ are indicative of PANI as they correspond to the C=N quinoid and C-N benzoid aromatic ring stretch absorptions respectively. These peaks can be used to investigate both the redox form of PANI as well as any new chemical bonds to the aromatic ring by changes in the intensity and position of the peaks. For example, PANI with a quinoid peak larger than the benzoid peak is pernigraniline whereas PANI has more leucoemeraldine character when the benzoid absorbance is stronger than the quinoid. The emeraldine form is where benzoid and quinoid are approximately equal in intensity indicating

50:50 C-N:C=N. The PANI spectrum shown in Figure 3.7 shows a similar peak height between the quinoid and benzoid peaks which indicate an emeraldine backbone which is expected as it is the most stable PANI form. The leucoemeraldine spectrum shows an increased C-N benzoid peak relative to the C=N quinoid peak as the PANI chain has been reduced resulting in an increase in benzoid ring concentration. The absorption at 1308 cm^{-1} has been assigned as the C-N stretch of a secondary aromatic amine which is indicative of the formation of a PANI via C-N-C linkage.¹¹⁰ The peak at 1163 cm^{-1} is a result of N=Q=N bending and C-NH-C bending vibrations with the lower wavenumber absorption possibly being the shoulder on the peak centered at 1163 cm^{-1} , which are both expected in emeraldine PANI. The final significant peak found at 837 cm^{-1} is a result of C-H out-of-plane bending of a 1,4-disubstituted benzene ring and is indicative of *para* coupling of the PANI chain.²⁸

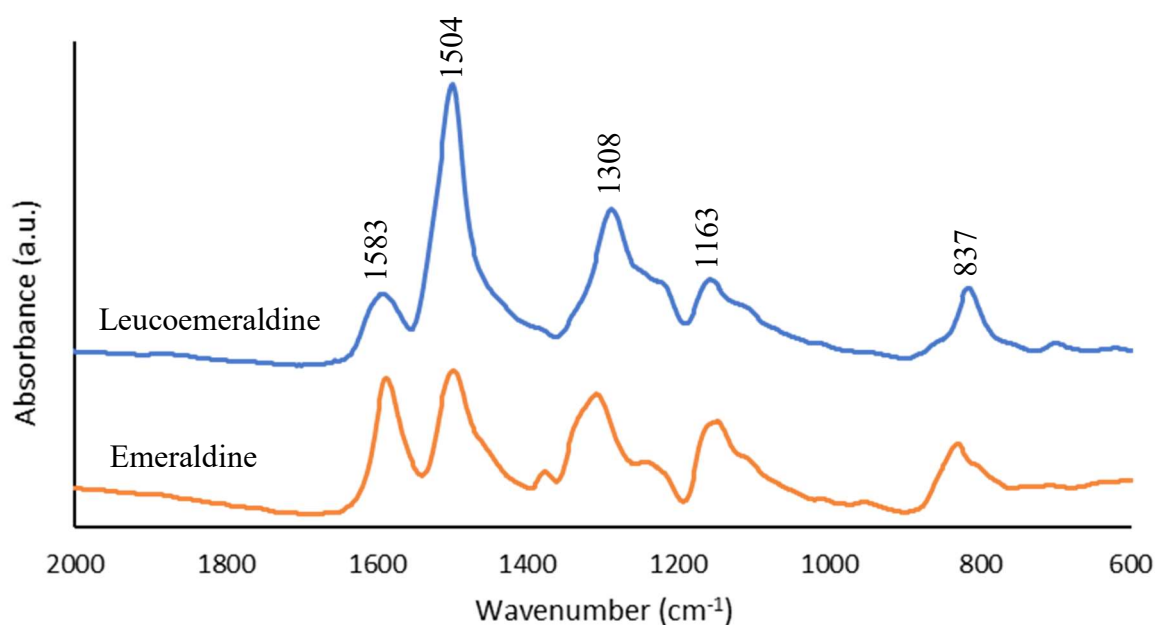


Figure 3.7: FTIR spectrum of leucoemeraldine and PANI EB as KBr disks.

The spectra for acetyl protected mannose functionalized PANI **3** and mannose functionalized PANI **4** are shown in Figure 3.8. **3** is dominated by two large peaks which are not observed in the spectrum for neat PANI are found at 1751 and 1227 cm^{-1} . These peaks show strong intensities and are assigned as C=O and C-O respectively. These functional groups are a result of the presence of carbohydrate acetyl groups, $-\text{O}-\text{C}(\text{CH}_3)=\text{O}$ and give obvious evidence for the presence of the mannose functionality. The benzoid and quinoid peaks are found at 1581 and 1504 cm^{-1} , which are at similar locations to that found in the model PANI EB spectrum. Their heights, while relatively minor compared to the very strong C=O and C-O absorbances, are roughly 1:1 indicating an emeraldine backbone. The broadness of the quinoid peak could indicate several quinoid type structures in the resulting polymer formed rather than a single

distinct environment for C=N. The large cluster of peaks in the region of 1150-1050 cm^{-1} are representative of carbohydrates as they correspond to C-O, C-C, C-OH stretching peaks with the peak centered at 1150 cm^{-1} characteristic of pyranose sugars.^{111,112} Finally the weak peak at 3140 cm^{-1} is assigned as the 1,2,3-triazole linker.^{113,114} The spectrum below confirms the presence of both the PANI backbone and the mannose moiety along with the triazole showing promising results for the theoretical structure presented earlier and agreeing with the NMR results. There is also a relatively large peak observed at 1377 cm^{-1} which has been assigned as C-N stretching in a phenazine type ring.

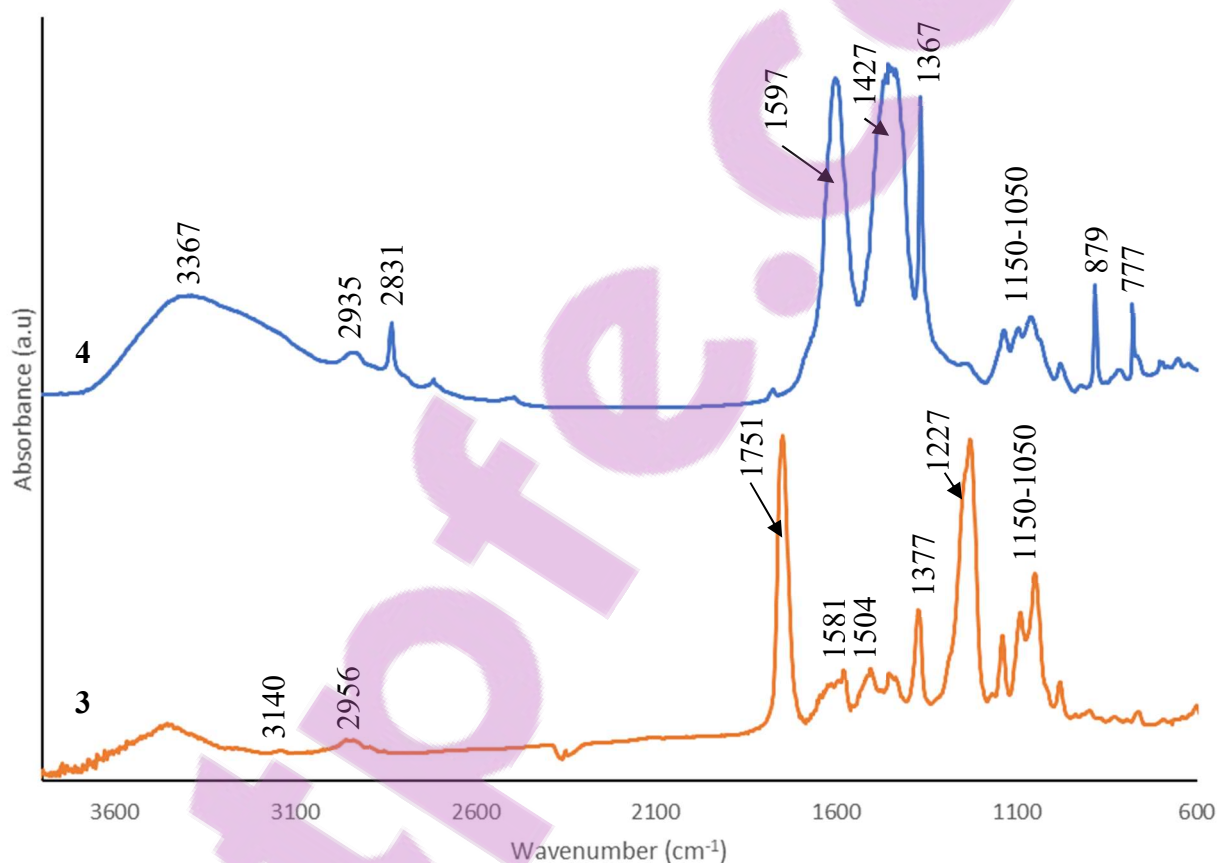


Figure 3.8: FTIR spectrum of acetyl protected mannose functionalized PANI **3** and mannose functionalized PANI **4**.

The deprotection of acetyl protected mannose functionalized PANI **3** to mannose functionalized PANI **4** results in removal of the acetyl groups and therefore disappearance of the C=O and C-O absorbances which is reflected in the spectrum. The loss of the C=O and C-O peaks shows almost but not quite complete deprotection of **3**, as a very small residual peak was observed for the C=O and C-O absorbances. The mannose peaks remain after the deprotection with the same configuration between 1150 and 1050 cm^{-1} . The increased absorbance of the -OH peak at 3400

cm⁻¹ due to reformation of the hydroxyl groups after the deprotection results in the 1,2,3-triazole peak existing as a small shoulder at the lower wavelength end of its peak.^{113,114}

The peak found at 1367 cm⁻¹ in the spectra for both **3** and **4** (1377 cm⁻¹ for **3**) has already been assigned as a result of C-N ring stretching arising from phenazine-like rings and is normally found as a minor impurity in PANI polymerization reactions. However, in the current synthesis it is observed in relatively large concentrations for **3** and **4** compared to native PANI. The phenazine molecule is shown in Figure 3.9:

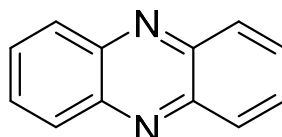


Figure 3.9: Structure of phenazine.

In the formation of PANI, the polymerization of aniline occurs in a head-to-tail fashion, via *p*-semidine, which allows the propagation of the radical and formation of the linear polymer with the nitrogen atom attacking the carbon at the para position of the neighboring aniline molecule.²⁸ Phenazine is an unwanted side reaction which occurs when the aniline groups form in a head-to-head fashion through *o*-semidine, terminating the propagation and resulting in formation of short chain oligomers. The reaction pathway to neat PANI in the general PANI synthesis through a *p*-semidine could be favored due to the steric hindrance presented via the amino group on the neighboring aniline molecule preventing formation of the *o*-semidine in large concentrations.

Therefore, formation of a phenazine type byproduct is observed in the synthetic procedure. Because phenazine forms from a head-to-head polymerization mechanism, the steric hindrance caused by the carbohydrate group must be greater than the steric hindrance of the nitrogen group, directing the propagation of the radical towards the ortho position rather than the para position resulting in an increased amount of the byproduct. The result minimizes the steric strain by keeping the carbohydrate groups at opposing sides of the molecule and is the driving force for the polymerization reaction proceeding via the *o*-semidine molecule, resulting in the dimer. The hypothesized by-product for this reaction is shown in Figure 3.10.

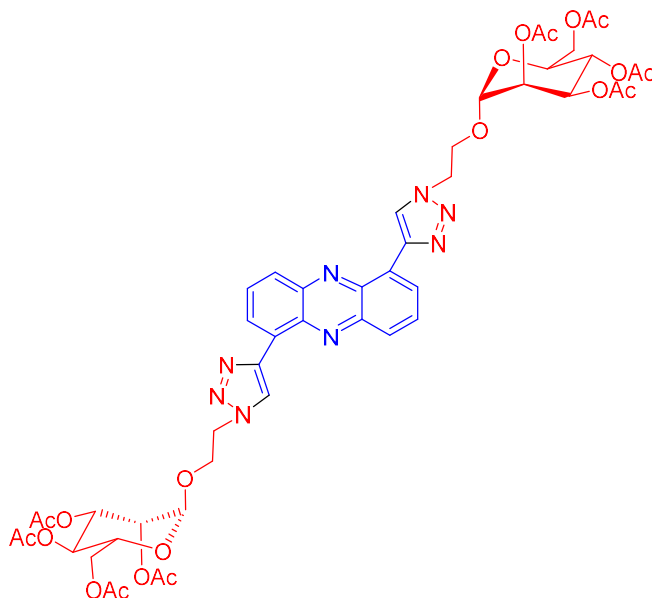


Figure 3.10: Proposed structure of the phenazine byproduct formed during the synthesis of mannose functionalized PANI **4**.

3.3.4. UV-Vis Spectroscopy

Because organic conducting polymers all show high levels of conjugation and π bonding (resulting in their strong colouration), UV-Vis is a very useful characterisation technique with typical absorptions for PANI occurring in the UV region corresponding to π transitions in the aromatic rings, and at higher wavelengths resulting from protonation and polaron formation.¹¹⁵ The position, strength and number of the excitations of the absorptions allow one to approximate the oxidation state, conjugation length and extent of doping of the conjugated polymers. Figure 3.11 compares the UV-Vis spectra of PANI EB, monomer **2**, acetyl protected mannose functionalised PANI **3** and mannose functionalised PANI **4**.

The PANI EB spectrum shows two excitation peaks at 325 and 630 nm. The first peak at 325 nm corresponds to the π - π^* transition of the aromatic ring and is a common feature observed across all the above spectra as they all contain these π bonds in their aromaticity. The second peak for PANI EB is centred at 630 nm and is assigned as a charge transfer complex between the quinoid and benzoid units.⁷¹ This peak is highly pH dependent and shifts to a higher wavelength as the PANI chain becomes protonated due to formation of a benzoid/quinoid intermediate with increased conjugation, which also results in increased conductivity.¹¹⁵

The UV-Vis spectrum of mannose functionalized aniline monomer **2** shows two excitations, both below 350 nm. The peak at 325 nm is assigned to the π - π^* excitations and is in the same position as that for PANI EB which result from the aromatic ring. A series of 1,2,3-triazoles

with differing ligands were synthesised and analysed by Schweinfurth et al. and found the peak at 260 nm, the same wavelength for the second absorbance found in the present work, common to all the triazole containing products and assigned this peak to a π - π^* excitation arising from the 1,2,3-triazole ring.¹¹⁶ Therefore, this peak found for **2** is assigned as a result of the π - π^* excitation of the 1,2,3-triazole ring.

After the attempted polymerization procedure several new absorptions arise, resulting in five total absorptions for acetyl protected mannose functionalized PANI **3** occurring at 260, 300, 325, 400 and 580 nm. The transitions at 260 and 325 nm are assigned to the π - π^* absorptions in both the triazole and benzoid aromatic rings respectively as shown previously for monomer **2** with no shift in peak position. The peak at 300 nm occurs in the spectrum of **3**, however, it is absent in the spectrum of mannose functionalized PANI **4**. Removal of the acetyl groups to hydroxyl groups is the only reaction that takes place between **3** and **4**, therefore this absorption is assigned to a π - π^* excitation from the acetyl groups.^{117,118}

The absorption at 400 nm is present in the spectra for both **3** and **4** and has been assigned to excitation of π - π^* of phenazine type ring structures. This is consistent with the interpretation of the FTIR and CV analyses which shows the formation of a phenazine by-product. This excitation is noted in the UV-Vis of short chain oligomers studied by Stejskal et al..²⁸

The final absorption in the spectrum of **3** and **4** is found at 580 nm and is relatively small in intensity. This peak has been assigned the same as PANI EB, however, a blue shift has occurred which indicates reduced polymer chain length in comparison to neat PANI.¹¹⁹ The result of a reduced polymer molecular weight is the diminished conjugation of the polymer chain and a shift of the absorption to higher energy.¹²⁰

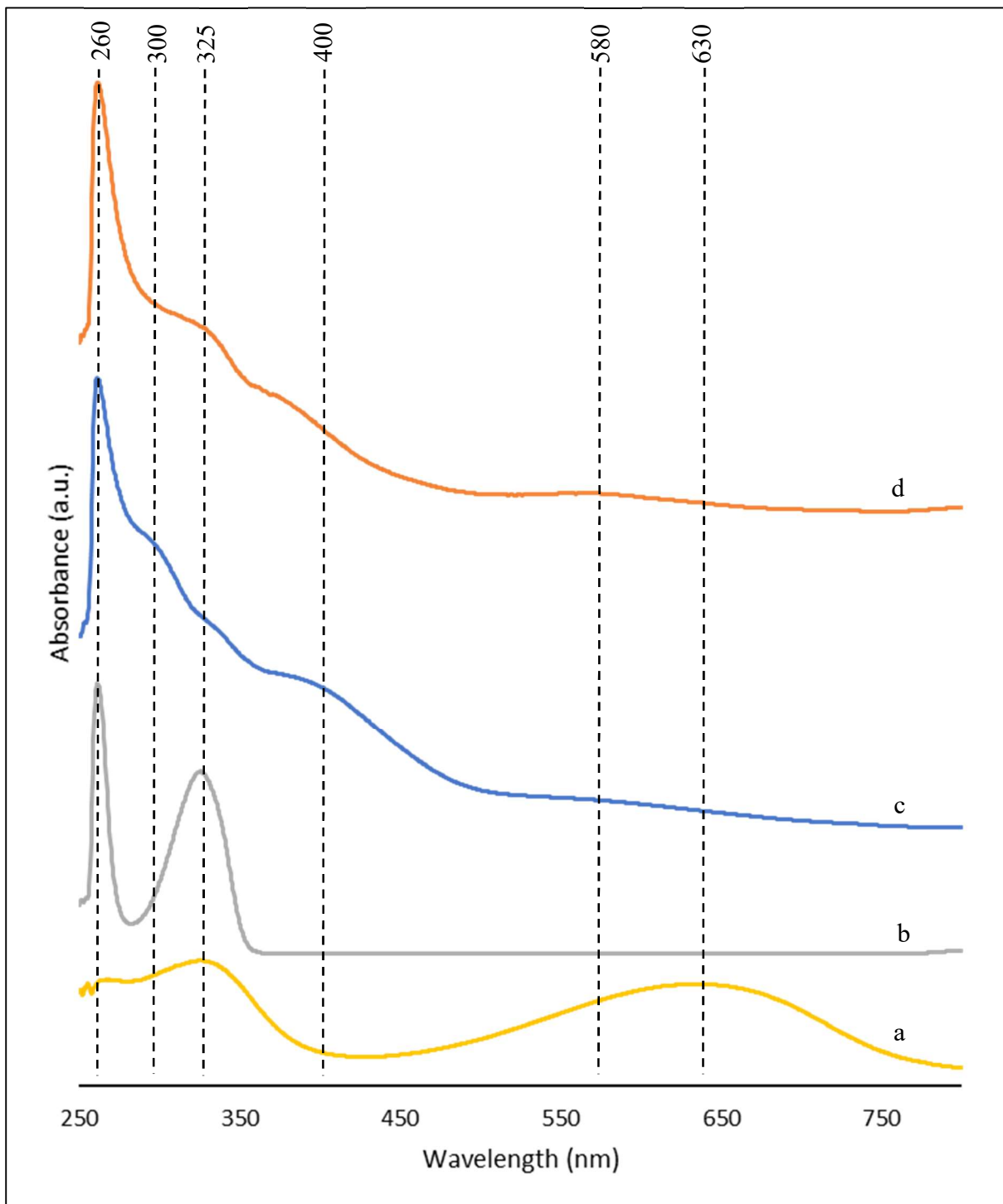


Figure 3.11: UV-vis spectrum displaying PANI EB (a), mannose functionalized aniline monomer **2** (b), acetyl protected mannose functionalized PANI **3** (c) and mannose functionalized PANI **4** (d) in NMP.

3.3.5. Gel-permeation Chromatography/Size Exclusion Chromatography

GPC is a means of measuring the molecular weight of a polymer and is one of the most useful characterisation techniques for a polymer chemist, as it can have profound effects on the products end properties. The measurement of the molecular weight of conducting polymers such as PANI can be quite difficult, as the measurement technique requires complete dissolution of the polymer in a suitable solvent. It has already been mentioned that PANI is insoluble in many solvents, making the processing of it difficult. NMP, a powerful dipolar aprotic solvent, is the primary solvent used in the literature for preparing PANI solutions, sometimes with an added lithium salt to decrease aggregation of PANI particles which can result in distorted peak shapes.¹²¹ The molecular weight of acetyl protected mannose functionalized PANI **3** was measured using this technique with pure NMP being used as the solvent.

In GPC larger polymers elute first, due to being unable to enter the stationary phase and progress straight through the column. Small molecules can spend longer periods of time being retained in the pores of the stationary phase and therefore take longer to elute. Molecular weights of the peaks were ascertained by comparison of the GPC trace to that of five polystyrene standards. The elution volumes for the polystyrene peaks allow determination of the molecular weight via interpolation.

The GPC trace shows two peaks at retention volumes of 3.2 ml and 2.8 mL. The molecular weights at the middle of the elution peaks are determined as an average over two runs as approximately 1000 and 23000 g/mol with an 80:20 ratio split respectively. The molecular weight of the theoretical monomer repeat unit, $C_{24}H_{29}N_4O_{10}$, is 533.57 g/mol as confirmed by mass spectroscopy. The larger molecular weight therefore has approximately 43 repeat monomeric units in its polymer chain. The lower molecular weight product is approximately twice that of the repeat monomeric unit indicating two repeat units. As previously hypothesised the reaction has possibly resulted in the formation of a dimeric by-product and according to the previous results has a phenazine type structure.²⁸ The results from the GPC analysis therefore agree with the conclusions drawn from the CV, FTIR and UV-Vis spectra that two products have formed. The formation of a lower molecular weight polymer was eluded to previously as the UV-Vis spectra shown in Figure 3.11 exhibited a peak, which reflects longer chain PANI conjugation, that was blue shifted (630 \rightarrow 580 nm) but is absent in the spectra of aniline oligomers.

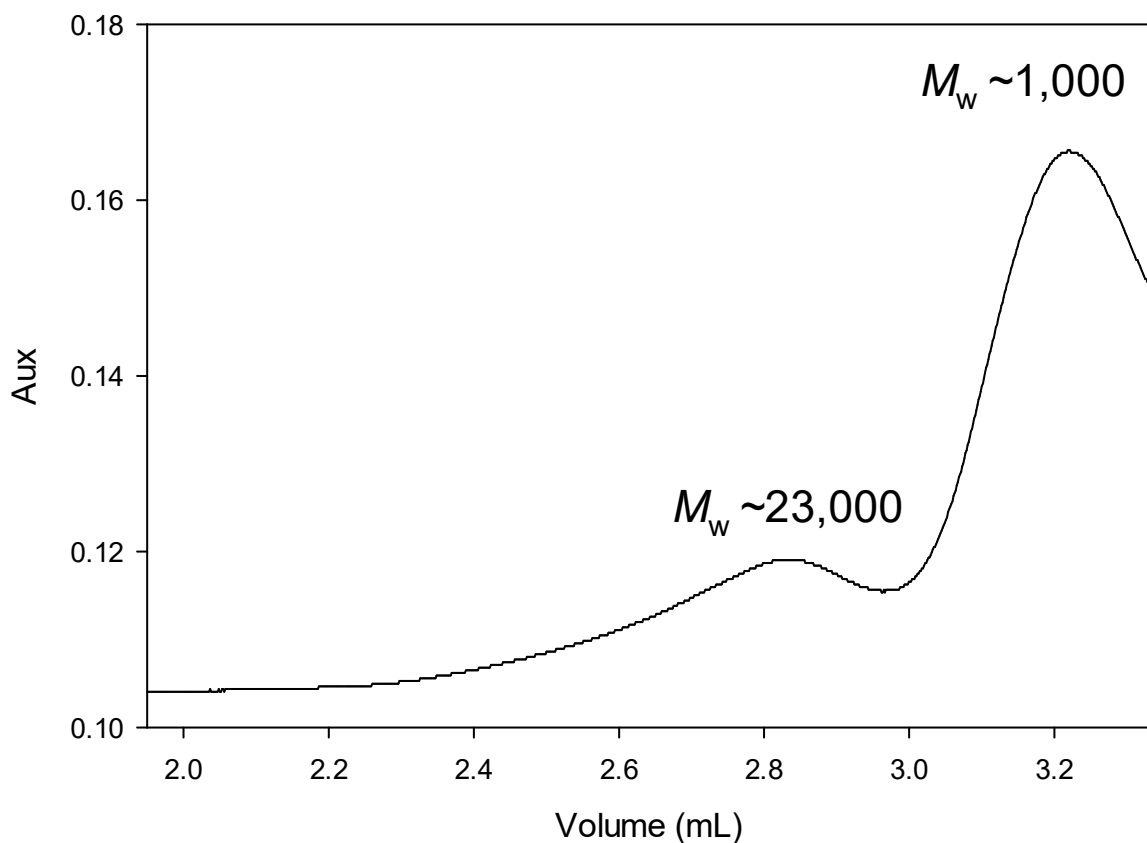


Figure 3.12: GPC trace of a 200 μ L injection volume of acetyl protected mannose functionalized PANI **3** in NMP with a concentration of 10 mg/mL and a flow rate of 0.12 mL/min.

3.3.6. Elemental Analysis

Elemental analysis is a technique that measures the concentration of elements in a sample and gives their relative compositions, normally as a percentage. Elemental analysis is useful for analysing PANI and functionalized PANI, as any changes when new atoms, molecules or functional groups are attached are easily identified. It can be used qualitatively to show the presence of the unique elements in a sample or quantitatively when comparing multiple elements against a reference.

Pure PANI and acetyl protected mannose functionalized PANI **3** had their elemental compositions measured via elemental analysis which is useful in exploring the atomic ratios of the components of materials as well as qualitatively confirming the presence of certain important atoms. Percent oxygen is calculated by difference.

For comparison purposes, PANI ES was used to explore the similarities and differences in the elemental composition of acetyl protected mannose functionalized PANI **3**. Theoretically PANI is expected to show a C:N ratio of 6:1, as the six aromatic carbon atoms are found with one

nitrogen atom per aniline repeat molecule. PANI ES prepared in house has a C:N ratio of 6.02:1, showing very good correlation between the theoretical and empirical results. After inclusion of the carbohydrate and triazole, there is a significant increase in the molecular weight for **3** compared to PANI. However, the theoretical C:N ratio remains at 6:1. The C:N ratio found for **3** is 6.25:1, which still conforms to the proposed structure presented in previously.

The concentration of oxygen in PANI ES is relatively high and could potentially be a result of oxidation that may occur to the PANI chain along with any moisture that results from exposure to the atmosphere.^{122,123} Potential adventitious impurities could also result in an increased oxygen concentration, which are found on samples exposed to the atmosphere.¹²⁴ The oxygen concentration for **3**, however, is increased compared to the PANI ES analysed, which is expected due to the attached mannose moiety. Here it is assumed that similar levels of oxygen due to impurities would be found between the two samples and that the higher concentration of oxygen for **3** is therefore due to the attached mannose.

There was no sulfur observed in the elemental composition of PANI ES. Sulfur can often be found in the PANI chain as an impurity due to doping of the polymer chain from sulfuric acid. Sulfuric acid forms when APS oxidises aniline during the formation of PANI, which is then able to dope the newly formed PANI chain.²⁶ Sometimes these sulfur impurities are due to dopant ions, which can be removed by addition of a base, however, they may also be found as defect like structures which still remain after extensive purification.¹²⁵ It is quite common for sulfur to be found therefore in the elemental analyses of PANI EB and PANI ES. The sulfur found for **3** is expected to be a potential result of the APS by-product sulfuric acid undergoing low levels of doping of the polymer chain.

Sample	%C (atom)	%H	%N (atom)	%S (atom)	%Cl (atom)	C:N	N:S	%O
PANI ES	56.70 (4.72)	5.36	10.99 (0.78)	0 (0)	11.86 (0.33)	6.02	-	15.09 (0.94)
3	58.01 (4.83)	5.09	10.83 (0.77)	4.11 (0.13)	0	6.25	6.03	21.96 (1.37)

Table 3.3: Elemental analysis of PANI and acetyl protected mannose functionalized PANI **3**.

3.3.7. Chemical Synthesis Characterization Conclusion

The synthesis of an aniline monomer functionalized with D-+-mannose was successfully carried out utilizing a CuAAC reaction with high yield. Use of general acid concentrations, typical of PANI syntheses, resulted in degradation of the finalized monomer. The structure of the monomer was determined via ^1H and ^{13}C NMR, high-resolution mass spectroscopy, cyclic voltammetry, UV-Vis and FTIR. The NMR and HRMS studies confirmed that the theoretical monomer was indeed synthesized as expected with an atomic formula of $\text{C}_{24}\text{H}_{30}\text{N}_4\text{O}_{10}$. Cyclic voltammetry showed mannose functionalized aniline monomer **2** had some similarity with aniline, however, only showed two redox pairs as opposed to the three for PANI. Polymerization at lower acid concentrations using APS as the oxidant resulted in a brown powder. The resulting products were characterized by elemental analysis, FTIR, UV-Vis and GPC. The FTIR and GPC both showed the formation of a dimeric by-product, which was hypothesized to be a phenazine type molecule. The hypothesis for the dimerization reaction was that the carbohydrate group exhibited a large steric hindrance on the molecule preventing head-to-tail polymerization and forcing a head-to-head polymerization via attachment to the *ortho* carbon resulting in termination.

3.3.8. Interaction of mannose functionalized PANI **4** with *Concanavalin A*

The binding of ConA to mannose and mannose-like carbohydrates is well documented and has been commonly used as a model study to show the interaction of glycopolymers with biological entities.^{89,126} ConA binds specifically with mannose and glucose type carbohydrates which form what is known as the Man/Glc specificity group, as opposed to other carbohydrates, and was therefore an excellent option to investigate the binding of ConA with the synthesized glycopolymer.¹²⁷

This experiment utilizes UV-Vis absorption intensities to measure the concentration of ConA that has precipitated due to binding with a glycopolymer and comparing it with the ConA remaining in the supernatant solution, of which there should be a proportional decrease. When there is no carbohydrate present the ConA remains in solution, resulting in a high absorbance in the supernatant with no precipitate. As a carbohydrate containing glycopolymer is added to the solution, interaction between the glycopolymer and ConA occurs and the polymer-ConA agglutinates to form a crosslinked precipitate. The result is an increase in absorbance for the precipitate with a proportional decrease in the absorbance of the supernatant as the ConA is removed.¹²⁸ The precipitate can then be dissolved by addition of methyl- α -D-mannopyranoside

which allows analysis via UV-Vis spectroscopy for the concentration of ConA in the precipitate cake. This process is depicted in Figure 3.13.

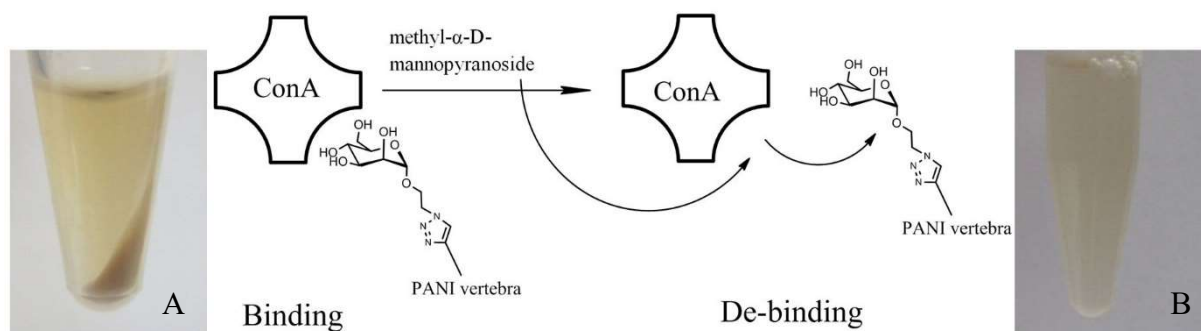


Figure 3.13: Schematic representation of ConA-polymer binding and de-binding. Images shown are of the precipitate formed by interaction of mannose functionalized PANI **4** with ConA (A) and the clear solution after addition of methyl- α -D-mannopyranoside (B). Both solutions were left for 1 hour after addition and centrifuged.

Figure 3.14 shows the results for the experiment involving mannose functionalized PANI **4** with absorptions for both the precipitate and supernatant displayed. When no glycopolymer has been added to the solution there is no carbohydrate to bind to, therefore there is no agglutination and precipitation resulting in the full concentration of ConA remaining in the starting solution. When the glycopolymer concentration is increased to 50 $\mu\text{g/mL}$ precipitation occurs. The formation of a pellet is readily discernable and can be removed and measured separately with approximately 50 % of the ConA being removed by the glycopolymer at this concentration. This gave a concentration of ConA in the pellet at 0.5 mg/mL. As the polymer concentration is further increased an increase in the absorbance is noted for the ConA concentration found in the pellet and an approximately proportional decrease in the concentration of ConA in the supernatant. The peaks plateau around a polymer concentration of approximately 100 $\mu\text{g/ml}$ indicating complete removal of ConA from the solution which is also noted due to an absorbance reading of nearly 0 in the supernatant at this concentration. The exact concentration for complete removal is difficult to ascertain due to interference from the polymer which will be explained further in the chapter. Charville et al. functionalized a range of poly(hydroxyethylmethacrylate) hydrogel glycopolymers and copolymers containing α -D-mannose at varying concentrations (100, 80, 60, 40 and 20 %).¹²⁸ These were tested with the same method utilized above. It was found that the 100 % mannose containing polymer synthesized by Charville et al. showed the greatest binding to ConA, as it required a lower concentration of polymer to fully remove the dissolved ConA from solution. Full removal of the ConA by Charville et al. 100 % mannose

functionalized polymer was found at *ca* 300 $\mu\text{g/mL}$, three times higher than the required concentration of **3** with the same concentration of ConA.

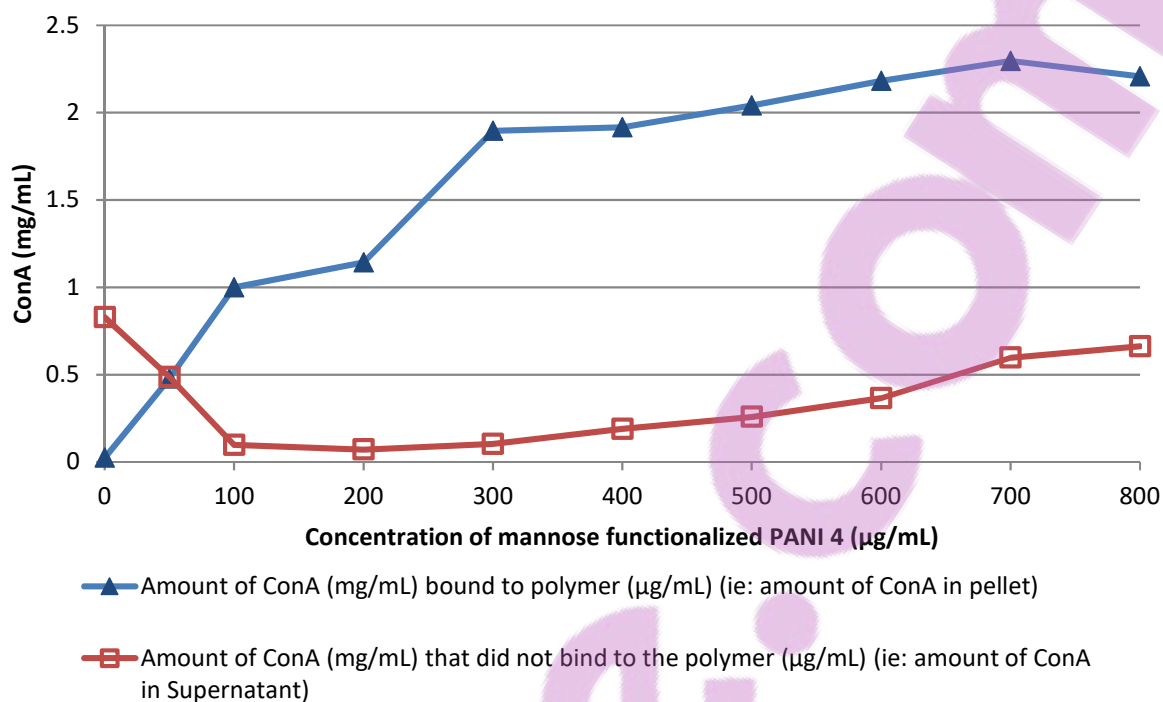


Figure 3.14: ConA analysis of binding to mannose functionalized PANI **4** at 280 nm in both the resulting precipitate and supernatant. The blue line depicts concentration of ConA which is bound by the polymer and removed from the solution whereas the red line shows the concentration of the ConA that remains in the solution and therefore was not bound by **4**.

The absorbance found at concentrations above that required for the complete removal of ConA continues to increase for both the supernatant and precipitate. This has been attributed to absorbance resulting from the glycopolymer itself. ConA absorbs at 280 nm in the UV-Vis spectrum. However, as noted in the UV-Vis spectrum in section 3.2.4, mannose functionalized PANI **4** also showed strong absorbance in the range of 260-300 nm. This interference results in increasing absorbances found as the glycopolymer concentration is increased even after removal of the ConA.

The results of this study show that **4** successfully interacted with the biological lectin ConA. Precise quantitative results are difficult using this method due to absorbance from **4** resulting in increasing intensity from the precipitate reading, however, the general trend in UV absorption and the formation of the precipitate is noted allowing the conclusion that **4** has successfully bound ConA.

3.3.9. Determination of the Minimum Lethal Concentration of Mannose Functionalized PANI 4

The antimicrobial ability of PANI's and functionalized PANI's has been well documented by various groups.^{41,44,46} It is known that the cell envelopes of bacteria are negatively charged so most polymers that display antimicrobial properties are positively charged to promote electrostatic interaction between the polymer and the cell wall, such as with quaternary ammonium salts.¹²⁹ Therefore, salt forms of PANI are generally more potent than their corresponding base forms due to the formation of a positive charge upon doping. The mode of action for PANI, and other conducting polymers, has been explained via electrostatic interaction of the positively charged conducting polymer with the negatively charged cell wall of bacteria. The electrostatic attachment of the conducting polymer then allows it to insert in the cell wall of the bacteria, allowing leakage of the internal cell components leading to cell death.¹³⁰ Gram positive bacteria are generally more susceptible to the action of conducting polymers, however, PANI has also shown potential to kill gram negative bacteria.^{131,132} It is speculated that the enhanced resistance of gram negative bacteria is due to the structure of the bacteria cell envelope. Gram positive bacteria have a very thick peptidoglycan cell wall and contain teichoic acid molecules which provide a net negative charge. Gram negative bacteria contain lipopolysaccharides and phospholipids which provide the bacteria with a negative charge. Gram negative bacteria have a much thinner peptidoglycan wall protecting it, but it is the outer membrane containing the lipopolysaccharides and phospholipids which provide the enhanced protection.

The antimicrobial activity of mannose functionalized PANI 4 and P3ABA were both tested to ascertain their MLC. The samples were tested up to a concentration of 1 wt %. Table 3.4 shows the results of the growth on agar plates after 24 hours averaged across triplicate experiments.

Bacterial Strain	Minimum Lethal Concentration (wt %)		
	PANI EB (powder)	Poly(3-aminobenzoic acid) (ES)	Mannose functionalized PANI 4
<i>Staphylococcus aureus</i> 6538	> 1	0.5	> 1
<i>Escherichia coli</i> 25922	> 1	1.0	> 1

Table 3.4: MLC of poly(3-aminobenzoic acid) and mannose functionalized PANI 4 against *E coli* and *S aureus*. Values are the mean of 3 technical replicates.

P3ABA required a concentration of 0.5 % to treat *S aureus*, a commonly used model gram positive bacterium while against the model gram-negative bacteria *E coli* it required a dose rate of 1.0 %. These results are comparable to that found by Gizdavic-Nikolaidis et al. who studied P3ABA, P2ABA and PANI in both the salt and base forms.⁴⁶ Their results found that of 1.25-5 mg/mL was effective for both P2ABA and P3ABA against a wide range of bacteria but neat PANI required dose rates were >10 mg/mL. The base forms were less effective in all cases as expected. Mannose functionalized PANI **4**, however, showed confluent bacterial growth at all concentrations after 24 hours indicating it was not active against either of the chosen bacterial strains.

There are several factors which may result in the lack of activity of mannose functionalized PANI **4** against either bacterial strain up to 1 wt %. Potentially the formation of the phenzine byproduct as mentioned previously may have influenced the MLC of **4**. The effect of molecular weight on antimicrobial polymers has been shown to be important as an increase in polymer chain length generally results in better biocidal activity because of the increased charge.¹³³ Ikeda et al. showed that the antimicrobial activity of polycations having biguanide units or quaternary ammonium salts are much more biocidal than their monomeric equivalents.¹³⁴ Due to a significant fraction of the product containing the lower molecular weight product, this may result in an increased MLC to achieve the correct concentration of **4**. To test this hypothesis in the future, dialysis of the product solution in membrane tubing with a greater molecular weight cut-off could be applied to enable separation of the two fractions for analysis.

It was believed that the acetyl deprotection step, the deprotection of acetyl protected mannose functionalized PANI **3** to mannose functionalized PANI **4** may have resulted in deprotonation of the PANI backbone resulting in the base form of the polymer. It has been described extensively previously that the base form of PANI is generally less active than the salt form. It was also believed that due to the inclusion of the mannose moiety, and the promising interaction results with ConA, that potentially the electrostatic interaction would be superseded by the interaction of the bacterial cells with ConA rather than the polymer backbone and that perhaps this would be enough to show improved bactericidal effects. Boomi et al. showed that the antibacterial activity of PANI is due to factors such as surface hydrophilicity, electrostatic adsorption between PANI and bacteria, higher molecular weight and direct contact between polymer material and bacterial cells.¹³¹

3.4. Conclusion

Interaction between mannose functionalized PANI **4** and ConA were analyzed using a ConA binding assay. The characterization of the resultant products all showed presence of the D-+-mannose structure in the polymer chain. Approximately 100 $\mu\text{g/mL}$ of the product fully crosslinked and removing 1 mg/mL of ConA from solution. It did not, however, show any ability to inhibit or kill either of the tested bacterial strains *S aureus* or *E coli*.

The ability of mannose functionalized PANI **4** to interact and bind to a mannose specific lectin, ConA, was promising. However, by addition of the large carbohydrate molecule, polymerization was inhibited and the antimicrobial ability in comparison with native PANI ES was lost. Therefore, to retain the useful biological binding ability of the PANI glycopolymer and alleviate the issues surrounding the polymerization, chapter 4 investigates the attachment of a carbohydrate to a PANI post-polymerization (as opposed to aniline pre-polymerization).

Chapter 4. The Synthesis of a Thiolated PANI by Sulfonation and Reduction and the Subsequent Click reaction with Allyl Mannose

4.1. Introduction

The previous chapter explored the potential of synthesizing a novel aniline monomer bearing a carbohydrate moiety. Polymerization of this monomer would then form a unique glycopolymer, which would be able to show increased interaction with target bacteria and therefore display increased biocidal action in comparison with native PANI. Difficulty arose during the polymerization due to the increased steric strain of the relatively large carbohydrate. The scalability of the reaction was also an issue with low yields after the polymerization which made complete biological testing difficult. To alleviate these issues the ability to directly functionalize PANI was explored. The chemical preparation of PANI allows substantial amounts of the polymer to be formed, so if a method to form glycopolymers directly from PANI is successful then more extensive testing can be conducted on the material. It has been shown that reaction of PANI with sulfuric acid is a reasonably simple method for the introduction of sulfonic acid groups onto the polymer chain through an electrophilic aromatic substitution reaction. Subsequent reduction of these groups will theoretically allow the formation of a thiol, which can take part in the thiol-ene reaction. Therefore, a carbohydrate bearing alkene functionality must also be prepared for this reaction to proceed.

4.2. Experimental

4.2.1. Chemicals

Aniline, ammonium persulfate, phenylhydrazine, fuming sulfuric acid, ethyl ether, ammonium hydroxide, allyl alcohol, D+-mannose and 2,2-dimethoxy-2-phenylacetophenone (DMPA) were all purchased from Sigma Aldrich and used as received. Hydrochloric acid was purchased from Macron.

4.2.2. Synthesis of Polyaniline Emeraldine Base Powder (5)

PANI emeraldine base was synthesized via a general oxidative procedure similar to that given by Stejskal et al.¹⁷ Aniline hydrochloride (5.18 g, 0.2 mol/L) was dissolved in a solution of aqueous hydrochloric acid (100 mL, 1 mol/L) and stirred to fully dissolve. To a separate vessel ammonium persulfate (13.69 g, 0.25 mol/L) was dissolved in hydrochloric acid (100 mL, 1 mol/L) and fully dissolved. The solution containing ammonium persulfate was then added all at

once to the solution containing aniline hydrochloride and briefly stirred to form a homogenous solution. It was then left for 12 hours to polymerize. A rapidly darkening solution can be observed after approximately 5 minutes. After 12 hours the mixture was collected on a vacuum filter. It was then washed with distilled water (200 mL x 3) and acetone (100 mL x 3) and allowed to air dry for 30 minutes. The bright green PANI was then dried in a vacuum oven at 50 °C for at least 12 hours. This afforded a bright green powder. Dedoping to the PANI emeraldine base was completed by adding the powder to a solution of ammonium hydroxide (100 mL, 1 mol/L) and stirred overnight. This was then collected on a vacuum filter and washed with distilled water (200 mL x 3) and dried overnight in a vacuum oven at 50 °C. A dark blue powder was thus formed.

4.2.3. Synthesis of Leucoemeraldine (6)

The PANI EB prepared in 4.1.2 is sulfonated using fuming sulfuric acid as suggested by Epstein et al.¹³⁵ PANI EB (0.5 g) is added to a mortar and ground to a fine powder. To this powder phenylhydrazine (5 mL) is added to reduce the powder to the leucoemeraldine form. The mixture effervesced and was left for 1 hour. Ethyl ether (75 mL) was added to the reaction and stirred for 15 minutes. The powder was then collected via vacuum filtration and washed with ethyl ether (50 mL x 3) and suction dried for 30 minutes. The leucoemeraldine form of PANI was a light grey colour.

4.2.4. Synthesis of Sulfonated Polyaniline (7)

Leucoemeraldine (0.5 g) was finely ground in a mortar and added to a beaker. To this powder fuming sulfuric acid (10 mL) was added carefully. This reacted for 1 hour while stirring. The mixture was quenched very carefully in a solution of water (1000 mL) by adding it dropwise to keep control of the temperature. Sulfonated PANI (SPANI) was then again collected via vacuum filtration and fully dried to a green powder in a vacuum oven at 50 °C overnight. Yield 68%.

4.2.5. Reduction of PANI-sulfonic acid to Thiolated PANI (8)

This reaction was done following a method outlined by Fujimori et al.¹³⁶ Triphenylphosphine (PPh₃) (0.75 g, 3 mmol, 10 mol equivalents) was dissolved in benzene (10 mL) in a round bottom flask with stirring. To this iodine (0.035 g, 0.3 mmol, 1 mol equivalent) was added and fully dissolved with stirring. Upon addition of the iodine the solution turned a vivid yellow colour. SPANI prepared in 4.1.3 (0.1 g, 0.6 mmol, 2 mol equivalent) was added and the resulting mixture stirred under reflux at 85 °C for 4 days. After about 10 minutes the solution changed to an off-white colour. After 4 days the solution was clear with the solid PANI still floating in the

solution. The solid was vacuum filtered and washed with benzene (20 mL x 3) and then acetone (20 mL x 3). The PANI solid was a light grey colour, similar to that of the leucoemeraldine prepared in 4.1.2.

4.2.6. Synthesis of Allyl- α -D-mannopyranoside (9)

Allyl alcohol (30 mL, 0.441 mol) was precooled to 0 °C in an ice bath. Acetyl chloride (2.75 g, 0.0350 mol) was added dropwise and the solution stirred for 1 hour. It was then allowed to warm to room temperature. D-+-Mannose (2.5 g, 0.0139 mol) was added and the mixture heated to 70 °C and left for 4 hours under stirring and reflux. The D-+-mannose fully dissolved after 10 minutes. NaHCO₃ was used to neutralize the reaction mixture. The resulting mixture was filtered over a celite pad and the solvent removed under reduced pressure. The product was purified using silica gel column chromatography (ethyl acetate:methanol, 17:3) to afford the final product which was a thick yellow syrup. Yield 42.4%. ¹H NMR (X MHz, D₂O): δ = 5.98 (m, 1H, OCH₂CH=CH₂), 5.33 (m, 2H, OCH₂CH=CH₂), 4.92 (s, 1H, H-1), 4.17 (m, 2H, OCH₂CH=CH₂), 3.95-3.88 (m, 2H, H-2, H-6A), 3.80-3.72 (m, 2H, H-3, H-6B) 3.67 (m, 2H, H-4, H-5). C₉H₁₆O₆ requires 243.0845 [M + Na], found 243.0846.

4.2.7. Synthesis of Mannose Functionalized PANI (10)

Thiolated PANI **8** (0.093 g, 0.76 mmol, 10 mol eq.) was weighed out and ground to a fine powder in a mortar and pestle. Allyl- α -D-mannopyranoside **9** (0.009 g, 0.076 mmol, 1 mol eq.) and DMPA (0.0001 g, 0.00379 mmol, 0.05 mol eq.) were fully dissolved in MeOH (2.5 mL) in a separate beaker. To this beaker the ground thiolated PANI **8** was added, stirred and irradiated with UV light (365 nm). The mixture was then dialysed against methanol (500 mL) for two days and milli-q water (500 mL) for one and collected under reduced pressure. The final product was vacuum dried at 50 °C to a constant weight.

4.3. Results and Discussion

The synthesis of the building blocks allyl- α -D-mannopyranoside **9** and thiolated PANI **8** is the first step in the attachment of functionality to perform a thiol-ene click with the goal to achieve a PANI glycopolymer. The reaction pathway utilized reduction of a sulfonic acid moiety on the PANI chain to achieve the thiol functionality is shown in Figure 4.1.

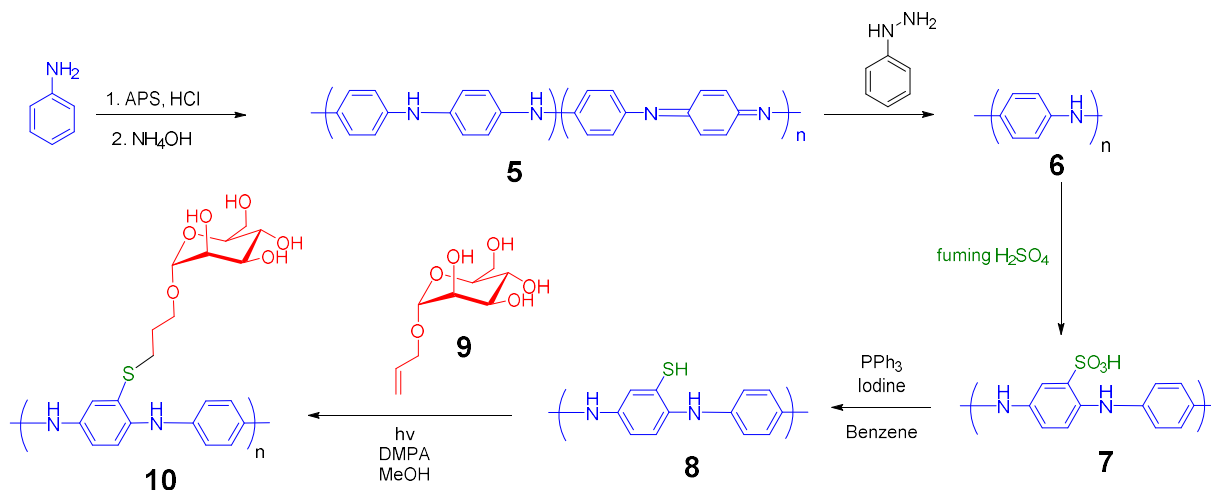


Figure 4.1: Proposed synthetic route to mannose functionalized PANI **10**.

The characterization of pure PANI has been briefly described in the previous chapter, however, due to the requirement to prepare pure PANI in this chapter, it will be explored further here. Aniline is a hydrophobic organic molecule with low solubility in aqueous solvents. Its solubility can be increased, however, by dissolution in an acidic medium due to the formation of a cationic form, known as the anilinium cation, and therefore gaining increased solubility in polar solvents. APS on the other hand is readily soluble in aqueous environments, being a salt. When solutions of these chemicals are brought together, after a brief delay, a colour change is observed as PANI starts forming. This can also be monitored by measuring the temperature as the reaction is exothermic. The darkening also indicates that the insoluble PANI is forming in the solution. After collection via vacuum filtration the clumps of powder appear black, however, after fully drying it is a bright green, demonstrating formation of the emeraldine salt. After dedoping with ammonium hydroxide, or another suitable base, it forms a deep blue color. The reactions that transform ES to EB is reversible, and the ES form can be regenerated by adding the EB powder to an acidic solution.

Allyl- α -D-mannopyranoside **9** was prepared following a method outlined by Hartmann et al.¹³⁷ One of the criteria to be considered a click reaction is the mild reaction conditions required. Due to this it was decided that protection of the hydroxyl groups on the carbohydrate as per chapter 3 with acetyl group chemistry was unwarranted. In chapter 3 the mannose was required to survive the polymerization reaction which uses low concentrations of strong acids. However, here it only needs to endure through the click reaction, which is expected to be milder. The characterisation of allyl- α -D-mannopyranoside **9** involved ^1H NMR and mass spectroscopy to confirm formation against literature results. The ^1H NMR spectroscopy results agreed with the theoretical structure of **9**. The major peak found in the high-resolution mass spectroscopy found

a molecular weight of 243.08 g/mol which is $C_9H_{16}O_6 + Na$. The second largest peak in the mass spectrum was found at 463.18 g/mol which has been assumed to be a dimerised form of **9**.

The thiol-ene click reaction between allyl- α -D-mannopyranoside **9** and mannose functionalized PANI **10** was conducted utilizing similar molar equivalent concentrations as Huynh et al. (thiol:alkene:initiator 10:1:0.05).⁶² Thiol-ene reactions have been shown to proceed with no added initiator and no added UV light. However, for this reaction DMPA was used as a photoinitiator with a UV lamp at 365 nm to ensure that the highest rates of conversion were achieved.

4.3.1. FTIR

The FTIR of PANI EB **5** was taken as a KBr disk. If ATR is to be utilized for PANI powders, typically a germanium crystal will be utilized as it has a higher refractive index than diamond. The FTIR of pure PANI EB (**5**), PANI leucoemeraldine (**6**), sulfonated PANI (**7**) and thiolated PANI (**8**) are shown in Figure 4.2. The common indicative peaks of PANI, as shown by **5** and observed in previous chapters, are the two large peaks centered around 1583 and 1490 cm^{-1} .¹³ These are both aromatic peaks corresponding to the quinoid and benzoid ring stretches respectively. As can be seen for **6**, the reduced form of PANI leucoemeraldine has a much higher concentration of benzoid rings resulting in a higher response for the peak at 1490 cm^{-1} relative to 1583 cm^{-1} . The peak found at 1300 cm^{-1} in all the spectra is determined to be the C-N stretch of a secondary aromatic amine and is indicative of PANI polymers due to transformation of the amine from primary to secondary in the polymerization reaction.¹¹⁰ Wei et al. described an increased degree of sulfonation resulting in the use of leucoemeraldine base as opposed to emeraldine or pernigraniline. The expected reaction pathway is via electrophilic aromatic substitution, so an increase in electron density of the aromatic ring upon reduction would therefore enhance the rate of sulfonation. The spectrum of **8** indicates an increase in the benzoid peak which as mentioned indicates an increase in the concentration of the reduced benzoid segments. This means that the reduction of the sulfonic acid to thiol has also resulted in the reduction of the PANI chain. The peak at 1147 cm^{-1} is found in all the spectra and is attributed to the C-H stretching in B-NH-B fragments of the PANI chain. The formation of peaks at 1066, 1020 and 700 for **7** and **8** are absent in the spectra of **5** and **6**. These peaks are assigned as aromatic ring – S vibrational bands which arise from the aromatic sulfonation of the PANI rings.¹³⁵

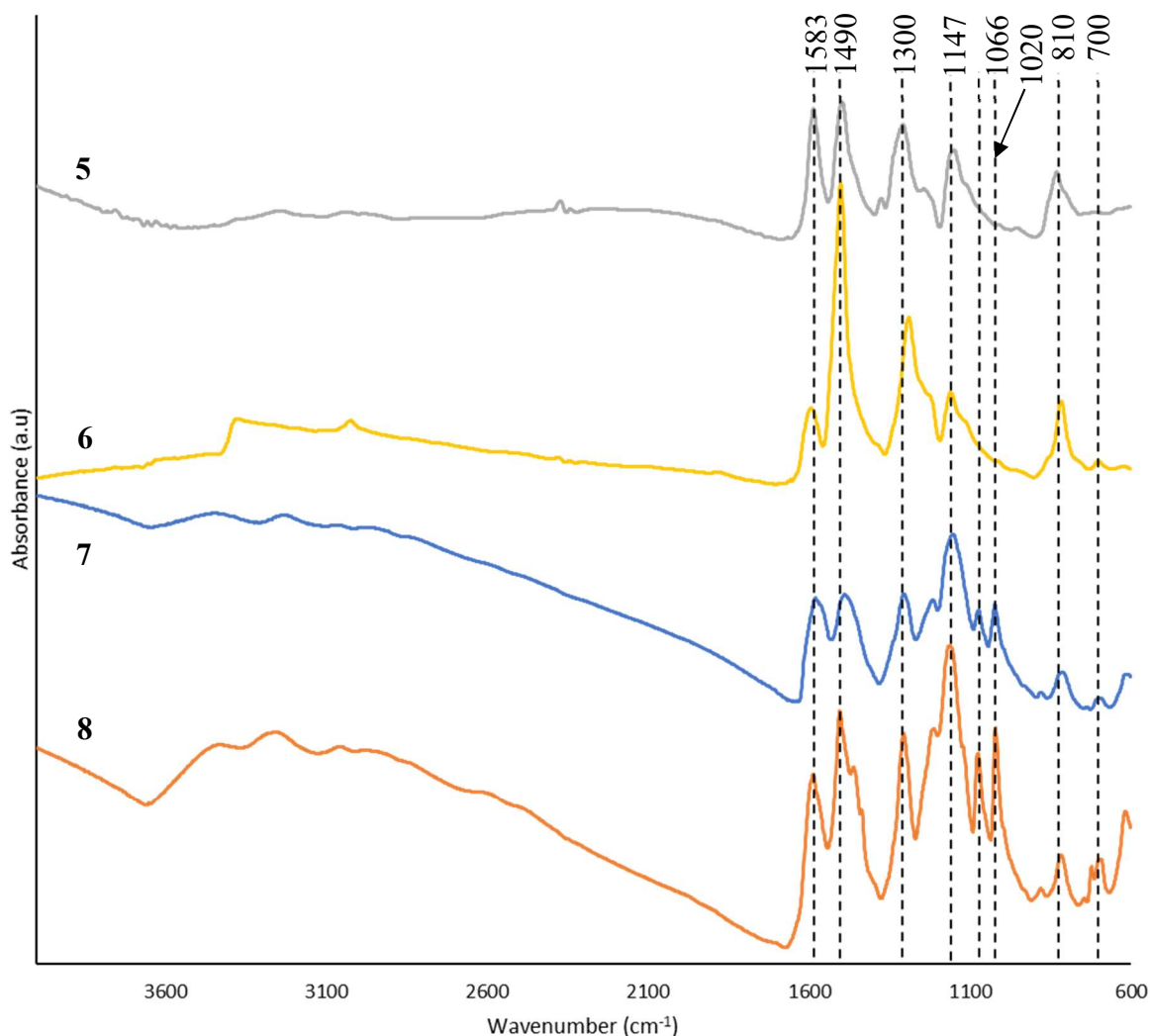


Figure 4.2: FTIR spectrum of PANI EB **5**, leucoemeraldine **6**, sulfonated PANI **7** and thiolated PANI **8**.

The FTIR spectrum of mannose functionalized PANI **10** shown in Figure 4.3 shows similarity with the spectra of **7** and **8** found in Figure 4.2. Analysis of the structure after attachment of allyl mannose **9** to thiolated PANI **8**, via thiol-ene click reaction, shows a strong broad -OH stretch at 3437 cm^{-1} for **10** but not for either PANI EB or SPANI, which has been assigned as the -OH stretch from the hydroxyl groups found on the mannose moiety. C-O stretches also resulting from the mannoside structure normally occur in the region of $1050\text{-}1150\text{ cm}^{-1}$, however, the presence of peaks already in this region which were found in the previous spectra. Thiol and sulfide bonds are typically weak in the IR region and are quite often looked over or are no greater than the noise of the spectrometer. The sulfide bond, C-S, has been experimentally observed in the region of $1400\text{-}1430\text{ cm}^{-1}$, however, the benzoid peak above masks any observation of this

peak.^{138,139} The FTIR spectrum is therefore unable to explicitly confirm the completion of the click reaction but nevertheless the presence of mannose has been detected.

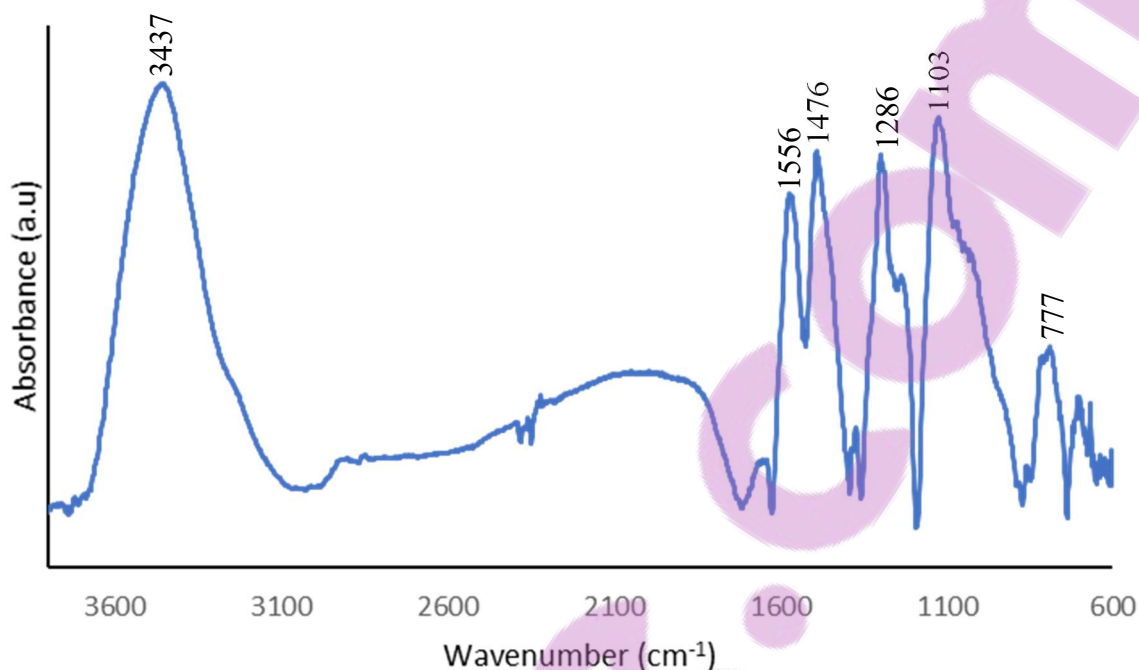


Figure 4.3: FTIR spectrum of mannose functionalized PANI **10**.

4.3.2. UV-Vis

The UV-Vis spectra of PANI **EB 5**, sulfonated PANI **7** and thiolated PANI **8** are shown in Figure 4.4. The shape and position of the two absorbances for each polymer are very similar with the spectra found in chapter 3 previously showing absorption maxima at ~ 320 and ~ 620 nm. The lower wavelength absorption is the π - π^* absorption, as has been previously discussed, and there is very little shift in the peak maximum between the two spectra. The higher wavelength absorption, which is described as a charge transfer process between the benzoid and quinoid rings of the PANI chain, is blue shifted for sulfonated PANI **7** and thiolated PANI **8** in comparison with PANI **EB 5**.¹⁴⁰ This slight blue shifted peak could indicate a lower molecular weight product as reduced conjugation and therefore chain length often attributes to a blue shift of this absorbance. This could result from the use of fuming sulfuric acid which can hydrolyze the PANI chain resulting in chain scission and a reduced molecular weight for sulfonated PANI **7** and thiolated PANI **8**.¹³⁵ Furthermore, the absence of peaks at *ca* 400 and 800 nm indicates that no polaron has formed for PANI **EB 5**, sulfonated PANI **7** or thiolated PANI **8**.

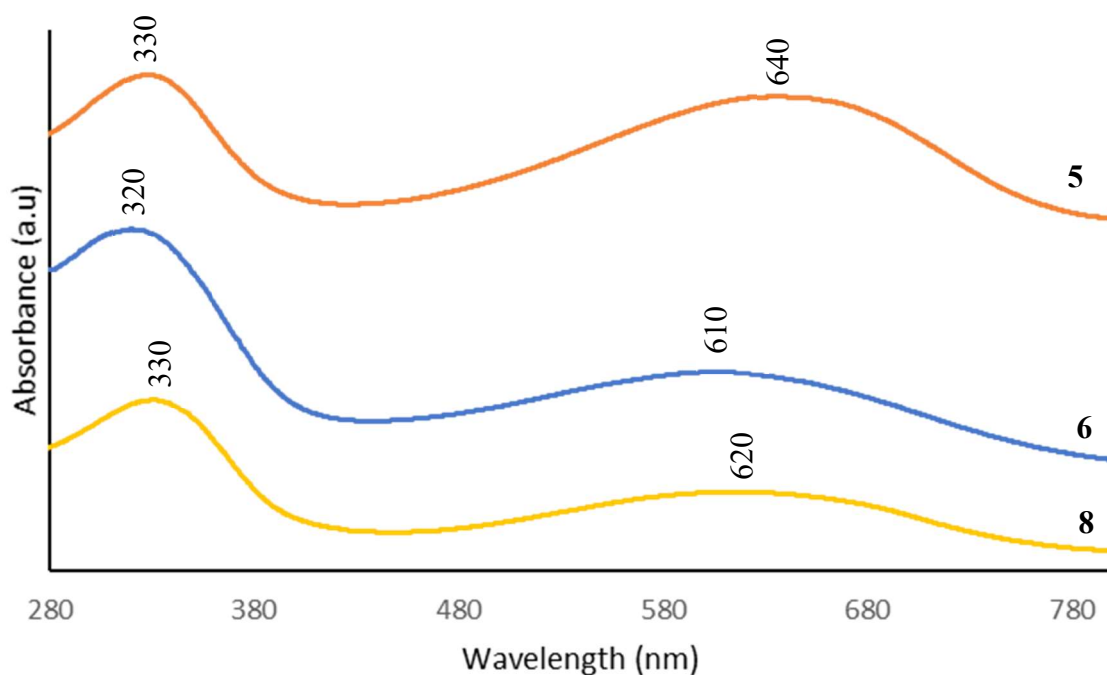


Figure 4.4: UV-Vis spectra of PANI EB **5**, sulfonated PANI **7** and thiolated PANI **8**.

The UV-Vis spectrum of mannose functionalized PANI **10** is similar to the spectra shown in Figure 4.4, however, with one notable exception, an extra peak is observed at 261 nm. The two peaks at higher binding energy are in the same positions previously shown for PANI and are therefore assigned to the PANI transitions already described. In chapter 3 a similar peak was observed at 260 nm, however, this was assigned to the 1,2,3-triazole ring which was corroborated with the literature. This reaction did not result in the formation of a triazole ring, however, and therefore must result from a different excitation. However, because there is no triazole ring formed in this synthetic procedure it is possibly due to the lone pairs found on the sulfur and oxygen atoms of the attached mannoside and click linkage.

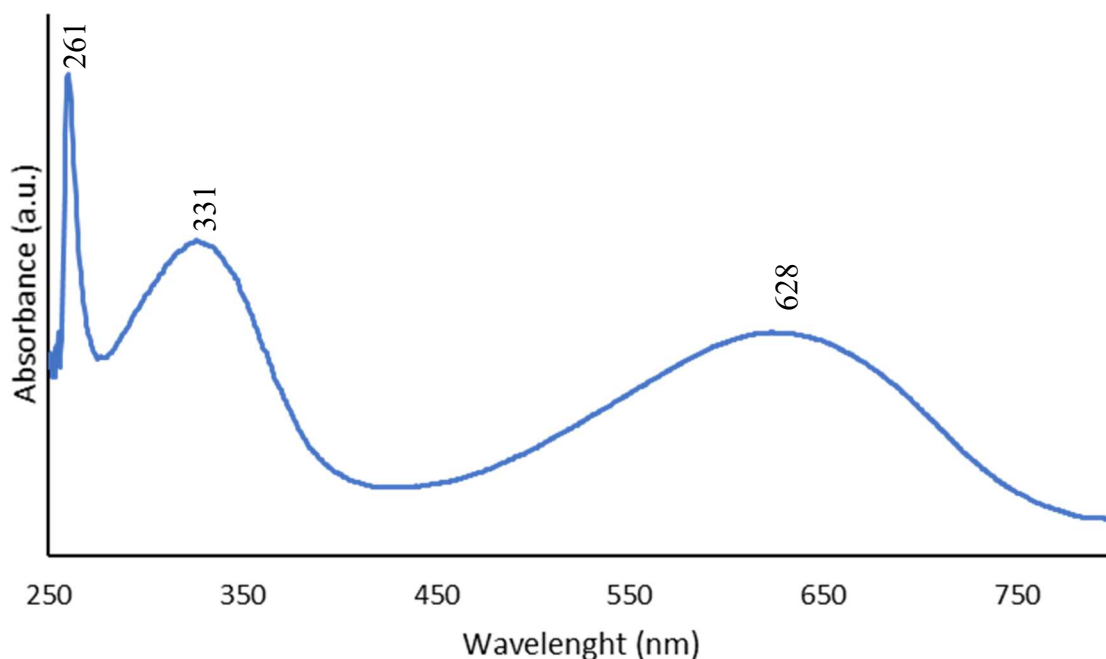


Figure 4.5: UV-Vis spectrum of mannose functionalized PANI **10**.

4.3.3. X-ray Photoelectron Spectroscopy

XPS is a very useful tool for probing the environments of each element in a polymer sample. It is possible to distinguish between different environments for each element such as amine and imine type nitrogen and therefore is very powerful for exploring PANI samples. The survey scan is a useful tool for exploring the existence of these elements, however, it is not sensitive enough to deconvolute the peaks into separate environments. To successfully explore the different elemental environments sensitive core level scans of the desired elements is required with mathematical deconvolution to separate the parent peak into its components. The binding energy of each deconvoluted peak therefore represents the types of each atom found. The binding energy position is affected primarily by electron density around the element with higher binding energy resulting from increased electron density around the atom, shielding the electrons from being removed.

The C 1s core level scan for PANI EB **5**, thiolated PANI **8** and mannose functionalized PANI **10** are shown in Figure 4.6. For PANI EB **5** the C 1s peak can be deconvoluted into two peaks while thiolated PANI **8** and mannose functionalized PANI **10** were deconvoluted into three with the extra peak found at a higher binding energy. The lower energy peak (285.0 eV) has been assigned to C-C, C-H of the PANI backbone and also commonly results from adventitious hydrocarbon species. Adventitious carbon is a generally unavoidable surface contamination by various hydrocarbon species upon exposure to the atmosphere, where nearly instantaneous

formation of a film of these materials forms.¹²³ Because all analyzed samples contained these carbon species and are exposed to the atmosphere resulting in this adventitious carbon, this peak can be used as an internal reference standard and is used to calibrate the spectra to 285.0 eV.^{141,142} The peak centered at 285.9 eV arises from the C-N and C=N bonds from the PANI chain and is found approximately 0.6-0.8 eV higher than the C-H,C-C peak.^{123,143} The peak at 287.1 eV is from carbon-oxygen species which for thiolated PANI **8** may result from oxidation of the PANI chain when reacted in the strongly oxidizing fuming sulfuric acid. For mannose functionalized PANI **10** this peak would obviously be expected to be a result of the attached allyl- α -D-mannopyranoside **9** which will account for its slightly increased concentration.

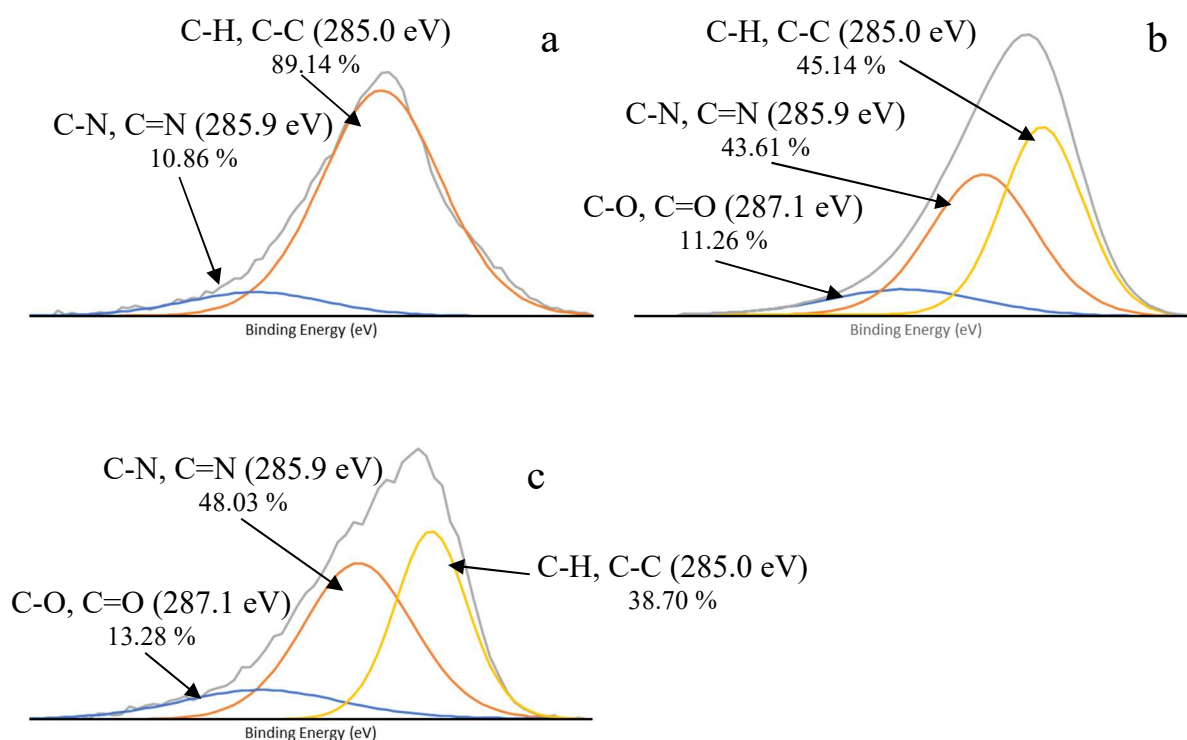


Figure 4.6: C 1s core level scan of PANI EB **5** (a), thiolated PANI **8** (b) and mannose functionalized PANI **10** (c).

Figure 4.7 shows the N 1s core level scan for PANI EB **5**, thiolated PANI **8** and mannose functionalized PANI **10** and has been deconvoluted into two distinct peak shapes for all three samples. The scan of PANI EB **5** follows the theoretically expected deconvoluted peak positions and ratios of nitrogen with the imine nitrogen appearing at a lower binding energy compared to the amine nitrogen. Therefore, assignment is -N= for the peak at lower binding energy (398.6 eV) and -NH- for the peak at the higher binding energy (399.9 eV). Their peak areas are approximately 55 % for the imine and 45 % amine nitrogen which can be used to describe the oxidation state of PANI. The roughly 1:1 area of the peaks represents approximately equal

concentrations of the imine and amine nitrogen which corresponds to an emeraldine backbone, as is also shown by the FTIR previously. Absence of a peak at higher binding energy than the amine nitrogen also is indicative of an undoped PANI backbone, as charged nitrogen species (N^+) have less shielding of the nucleus resulting in higher binding energy (>400 eV), displaying that PANI EB **5** is undoped. These results for the synthesis of PANI EB are in good agreement with the binding energy peaks for the N 1s peaks found by several other authors.^{123,144,145}

Thiolated PANI **8** and mannose functionalized PANI **10** have also been deconvoluted into two distinct peaks but are found at a higher binding energy in comparison with PANI EB **5**. The peaks found at approximately 399.9-400.0 eV are assigned as the amine nitrogen, -NH-, which is the same as PANI EB **5**, however, the absence of a peak at *ca* 398.5 eV shows that there are no uncharged -N= atoms in the sample.

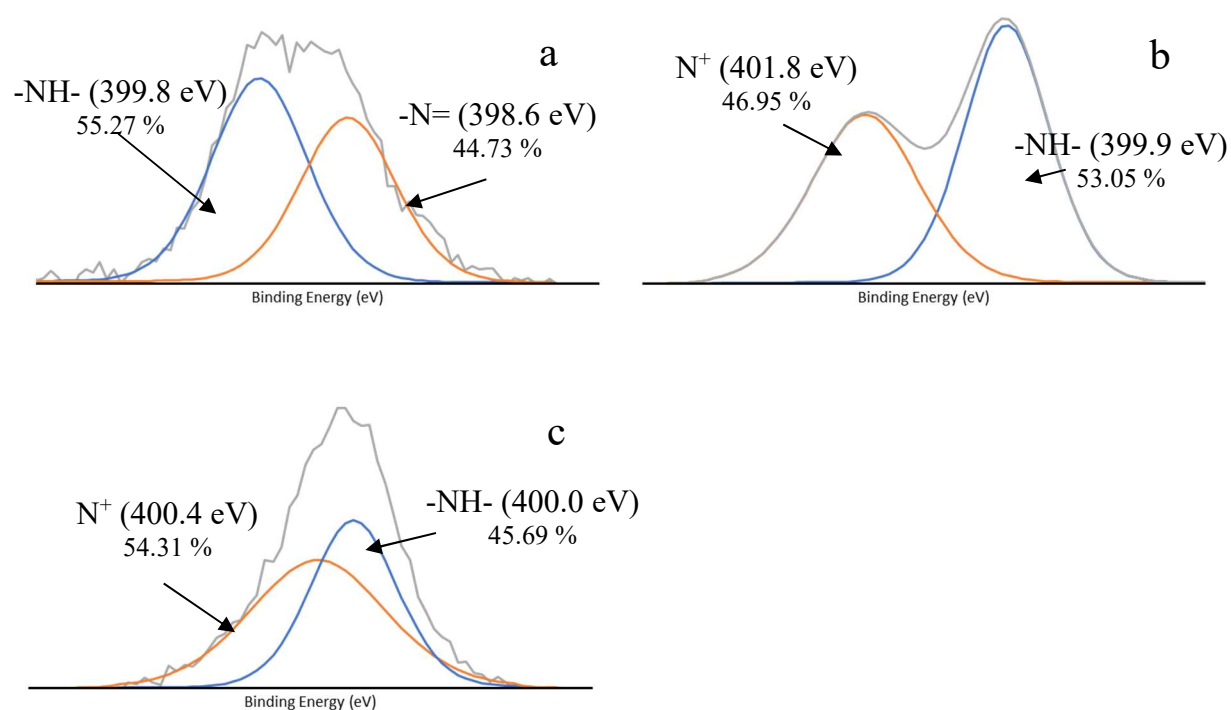


Figure 4.7: N 1s core level scan of PANI EB **5** (a), thiolated PANI **8** (b) and mannose functionalized PANI **10** (c).

The peak at the higher binding energy (401.8 eV for thiolated PANI **8** and 400.4 eV for mannose functionalized PANI **10**) is indicative of a charged nitrogen species (N^+) which occurs when the nitrogen atoms have been doped.¹²³ The doping of nitrogen atoms is found when the base form of PANI is transformed to the salt form, typically via reaction of the PANI chain with an acid such as hydrochloric, methanesulfonic or toluenesulfonic which has been described in previous chapters. In the present case, however, doping of the nitrogen atoms in this experiment are most

likely doped with sulfonic acid groups which result from the use of fuming sulfuric acid. Yue and Epstein utilized the same procedure reacting PANI with fuming sulfuric acid and concluded that the disappearance of the imine nitrogen peak along with the appearance of the charged nitrogen peak is a result of the sulfonic acid groups protonating the imine nitrogen's as shown in Figure 4.8 in a “self-doping” process, as the sulfonic acids are formed via electrophilic aromatic substitution of the aromatic rings and not via a doping mechanism. The formation of this peak in the N 1s scan of **8** and **10** perhaps displays that not all of the sulfonic acid groups have been reduced.

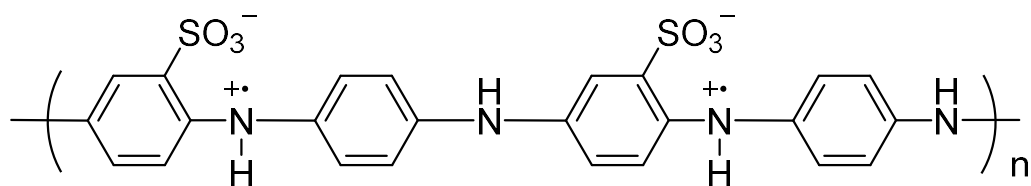


Figure 4.8: Self-doping mechanism of PANI by attached sulfonic acid moieties as described by Yue et al..¹⁴⁴

It can difficult to draw concrete conclusions from the O 1s spectrum due to the complex nature of oxygen in these samples along with their exposure to the atmosphere and the variety of impurities that are formed. However, based on the fitting parameters used two peaks have been deconvoluted for PANI EB **5** and three peaks for thiolated PANI **8** and mannose functionalized PANI **10** from the O 1s parent peak shown in Figure 4.9. The lowest binding energy peak is loosely attributed to the C-O bonds found from the inclusion of allyl mannose **9**, however, is also present for PANI EB **5** which may be a result of H₂O. The peak at 532.5 eV is described as C=O bonding which is found in the XPS of thiolated PANI **8** and mannose functionalized PANI **10**. A peak at approximately 533.6 eV is found for thiolated PANI **8** and mannose functionalized PANI **10** but is not found in the spectra of PANI EB **5** and is therefore assigned to the S-O bonding found in the sulfonic acid moiety.

b

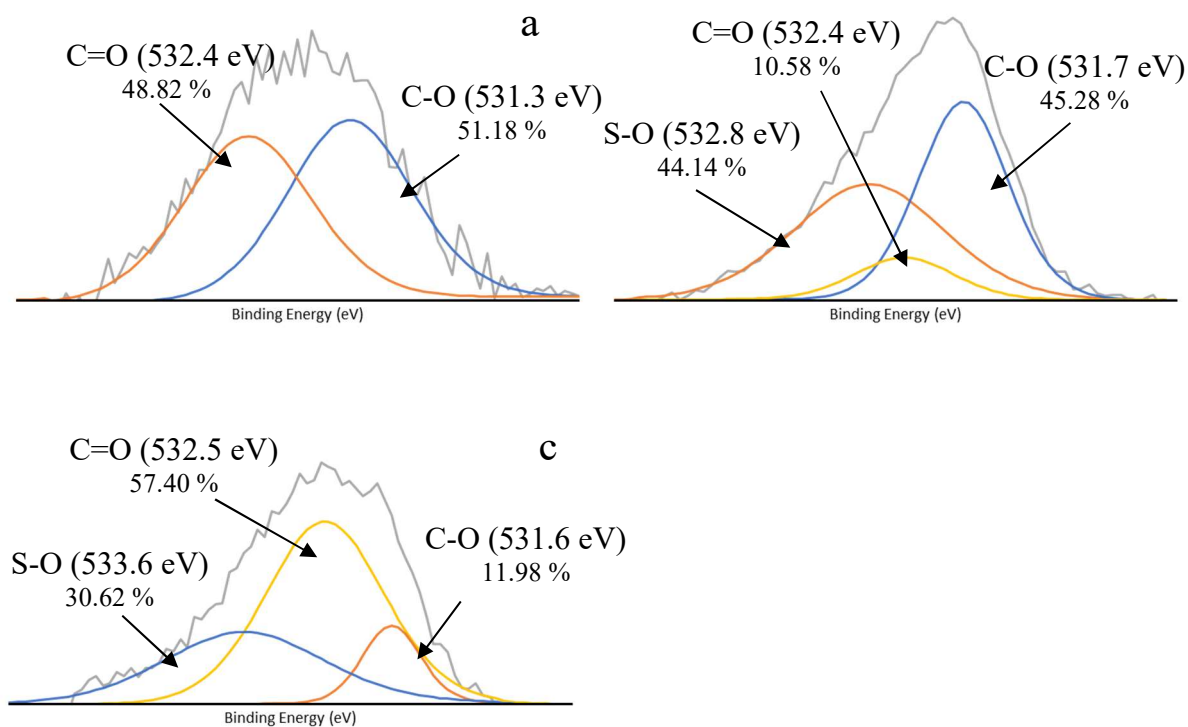


Figure 4.9: O 1s core level scan of PANI EB **5** (a), thiolated PANI **8** (b) and mannose functionalized PANI **10** (c).

The S 2p core level scans are shown in Figure 4.10. S 2p peaks are found in pairs due to spin-orbit splitting resulting in a 3/2 and 1/2 peak. These peaks are closely spaced with an energy difference between the 3/2 and 1/2 of approximately 1.18 eV and an area ratio of 2:1.¹⁴⁶ Sulfur is found in one environment for PANI EB **5** and two for thiolated PANI **8** and mannose functionalized PANI **10** with the 3/2 peaks centered at approximately 168.6 eV for PANI EB **5** and 164.3 and 168.5 eV for thiolated PANI **8** and mannose functionalized PANI **10**. The sulfur in the sulfonic acid is surrounded by highly electronegative oxygen groups, which pull the electron density away from the sulfur resulting in less shielding and therefore a higher binding energy. Based on this reasoning the S 2p 3/2 peak centered at 168.5 eV is assigned as the sulfonic acid.¹⁴⁷ This agrees with the N 1s scans which show the formation of charged nitrogen species, suspected to be via a self-doping process of the sulfonic acid moieties. Gonzalez et al. synthesized sulfonic acid functionalized aerogels and found a single S 2p 3/2 peak corresponding for their sulfonic acid at 168-169 eV which agrees with the current analysis.¹⁴⁸ Brunetti et al. modified glassy carbon electrodes with 8-hydroxyquinoline-5-sulfonic acid and found an S 2p 3/2 peak at higher binding energy (167.6 eV), however, their calibration utilized Cu 2p 3/2 and Au 4f 7/2 agreeing with the position found by both Gonzalez and the current work.¹⁴⁹ PANI EB **5** shows a very low concentration of this peak which is commonly found in PANI due to the use of APS as the oxidant resulting in the attachment of some sulfonic acid

groups. Thiolated PANI **8** showed a very small peak centered at 164.2 eV which was not found for PANI EB **5** and has been attributed to the -SH functional group showing successful reduction of the sulfonic acid. Only low concentrations of the thiol were found with a large concentration of sulfonic acid remaining. The presence of the peak at 168.5 eV in the spectrum of thiolated PANI **8**, however, shows that this reaction was not 100 % effective as some sulfonic acid molecules remains. Mannose functionalized PANI **10** shows the same peaks as thiolated PANI **8** situated at 164.3 and 168.5 eV. The inability to remove allyl mannose **9** with common solvents from **10** alludes to strong binding between the PANI surface and the carbohydrate and therefore the peak at 164.3 eV may also represent a thioether linkage.

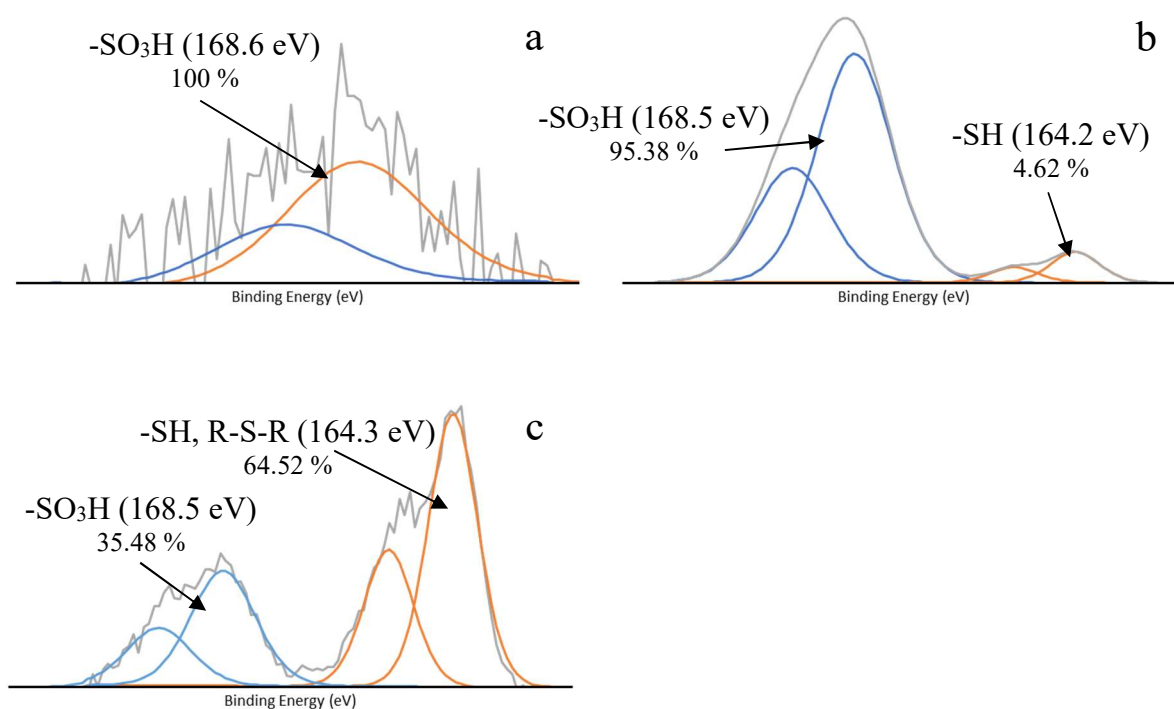


Figure 4.10: S 2p core level scan of PANI EB **5** (a), thiolated PANI **8** (b) and mannose functionalized PANI **10** (c).

4.3.4. Characterization Conclusion

The synthesis of a sulfonated PANI that can be reduced to a thiol was attempted and proven possible. The synthesis and characterization of PANI EB **5** and sulfonated PANI **7** followed the results already reported in the literature. The FTIR of the sulfur containing compounds **7**, **8** and **10** all showed new absorbances due to ring-S stretches in the FTIR spectra while the XPS further differentiated the sulfonic acid and thiol peaks due to the very different binding energies. The N 1s core level scan of PANI EB **5** showed that it was in the EB due to the presence of two deconvoluted peaks with 50:50 ratios at binding energies that agreed with the literature for

amino and imino nitrogen groups.. The sulfur binding peak of **8** and **10** showed that while the reaction did result in a peak corresponding to a thiol/thioether, a large percentage of the total S 2p core level peak resulted from unreacted sulfonic acid moieties indicating the reaction did not go to completion. Upon sulfonation and reduction the deconvoluted peaks shifted with the formation of charged nitrogen's and the disappearance of the imine nitrogen peak. The experimentally determined synthetic mechanism is thus shown in Figure 4.11.

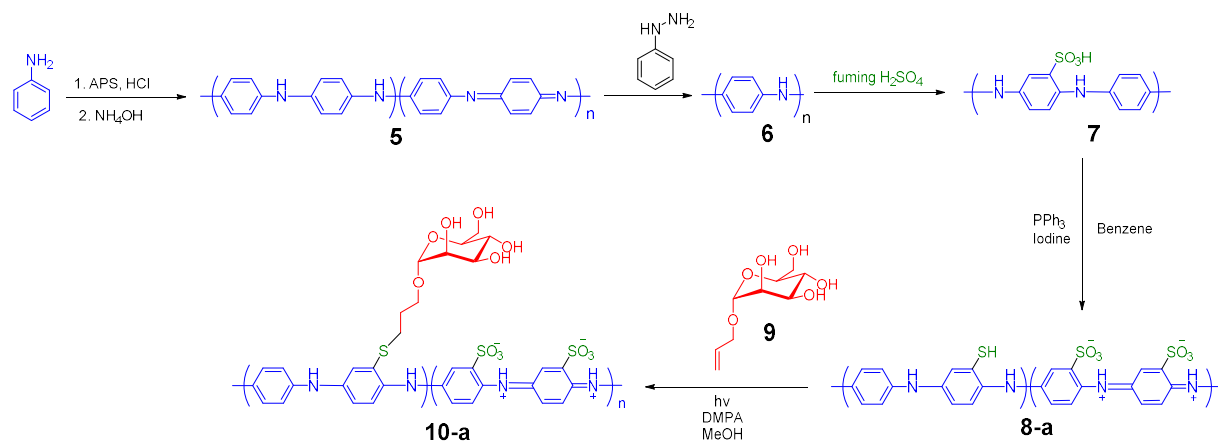


Figure 4.11: Synthetic pathway for the synthesis of mannosylated PANI **10-a** from experimental evidence.

Future work into this synthetic procedure would first investigate simple adjustments in reagent ratios and methodology to try providing a higher concentration of reduced thiol and also potentially a stronger reducing agent or reducing system may be required to achieve improved conversion. If the reduction of sulfonic acid to thiol moiety can be improved, it opens the possibility to synthesize various functionalized PANI's by utilizing thiol-ene reactions, not only for the synthesis of a glycopolymer but by attaching other unsaturated molecules for other applications.

4.3.5. Minimum Lethal Concentration (MLC) of Mannose Functionalized PANI **10**

The MLC of mannosylated PANI **10** was studied utilizing the same procedure that was used for the determination of MLC of mannosylated PANI **4**. This analysis involves suspending the polymer in TSB and producing a doubling dilution series which is inoculated with bacteria. After inoculation the samples are incubated and the lowest concentration to show non-confluent growth is determined as the MLC. Figure 4.12 shows the results of an experiment (the samples are run in triplicate to minimize variations) showing that the sample tested was not effective up to 1 wt % as confluent growth of the colonies is seen in all the wedges.

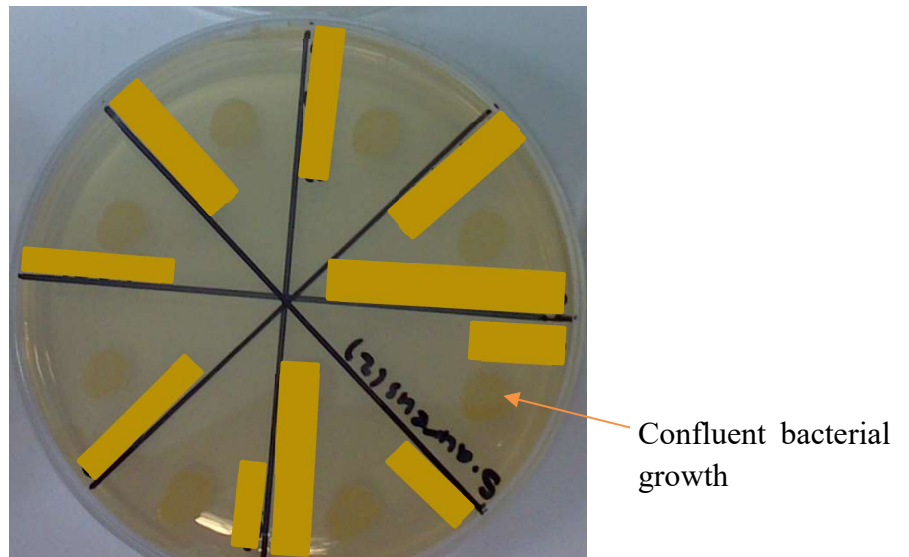


Figure 4.12: Plated sample of *S aureus* on an agar plate with varying concentrations of mannose modified PANI **10** after 24 hours incubation.

Figure 4.13 shows the final results of the experiment to determine the MLC of mannose modified PANI **10** against both a gram positive bacteria, *S aureus*, and gram negative bacteria, *E coli*, after inoculating for 4 and 24 hour time periods up to a maximum polymer concentration of 1 wt %. It is observable that up to 1 wt % mannose modified PANI **10** is ineffective against both bacterial strains analyzed as confluent growth was detected after both the 4 and 24 hour time points at all concentrations for the triplicates. **4** was discussed as potentially being ineffective due to the resultant product being a mixture of very low molecular weight products with a dimeric by-product.

	Minimum Lethal Concentration (wt %)			
	4 hour inoculation		24 hour inoculation	
Bacterial Strain	PANI EB (powder)	Mannose modified PANI 10	PANI EB (powder)	Mannose modified PANI 10
<i>Staphylococcus aureus</i> 6538	> 1	> 1	> 1	> 1
<i>Escherichia coli</i> 25922	> 1	> 1	> 1	> 1

Table 4.1: Mean MLC of PANI EB powder, PANI ES powder and mannose modified PANI **10** over three technical replicates against *S aureus* and *E coli* after inoculation for 4 and 24 hours. Note that the maximum polymer concentration analysed was 1 wt %.

The inability of **10** to successfully eradicate the bacterial cultures could be a result of several factors. Firstly, even though the salt form of PANI was formed via a self-doping process of the sulfonic acid moieties as described in chapter 4.3.3, the effect of the self-doping process on the antimicrobial properties of PANI may result in lowered efficacy in comparison to doping through typical processes such as via an acid such as HCl. Potentially the counter ion may influence the overall antimicrobial ability and as investigation of the different doping regimes and the effect they play on the carbohydrate warrants exploration.

4.4. Conclusion

Explored throughout this chapter was the reaction synthesis of a sulfonic acid functionalized PANI **7**, and subsequent reduction of the sulfonic acid for the formation of thiolated PANI **8**. The FTIR and XPS of **7** was typical for the sulfonation of PANI as per the literature with the N 1s core level XPS scan of this product showing doping of the imine nitrogen atoms via a self-doping process. Synthesis of allylic mannose **9** was also successfully conducted as per the literature which formed the two starting reagents for the thiol-ene click reaction. The click reaction between **8** and **9** was hypothesized to form mannose modified PANI **10**. While there wasn't 100 % conversion of the sulfonic acid moieties, the presence of the mannose was deduced from FTIR, UV-Vis and XPS measurements. The inability for the mannose groups to be removed indicated that covalently bonding had occurred as the mannose was still detected after dialysis in both methanol and water, which would be expected to completely remove the presence of the mannose. The MLC of mannose modified PANI **10** against *S aureus* and *E coli* after inoculation for 4 and 24 hours showed no lethality up to 1 wt %.

For this reaction to be considered further, the reaction methodology needs to be explored to improve the efficiency of the sulfonic acid reduction to maximize the click-ability of the PANI. If the formation of the thiol can be improved this will provide a useful polymer system not only for the formation of glycopolymers but also various PANI's that can be functionalized via the thiol-ene reaction.

The results here show that reduction of sulfonic acids on PANI to thiols is inefficient but possible, however, the thiol-ene reaction should not be dismissed at this stage. While the attachment of a thiol to PANI proved challenging, PANI already has the potential functionality to take part in this reaction. The next chapter will investigate the potential of utilizing the aromatic structure of the PANI as the alkene in the thiol-ene reaction.

Chapter 5. The Solvent Casting of PANI films and Surface Modification with Glucose for the Preparation of a PANI Glycopolymer

5.1. Introduction

The previous chapter showed the synthesis of PANI functionalized with a thiol, however, the reduction of the sulfonic acid was not as efficient as hoped and a large proportion of the sulfur groups remained as the sulfonic acid. Many publications have shown the interesting ability of PANI to take part in the thiol-ene reaction as the unsaturated ene structure, therefore potentially removing the need for chemical alteration of the PANI prior to the click reaction.¹⁵⁰⁻¹⁵³ Su et al. has provided a number of examples of this reaction. 2,5-dimercapto-1,3,4-thiadiazole was chemically bound through the thiol-ene reaction to multiwalled carbon nanotube modified PANI for the determination of Cd^{2+} and Pb^{2+} via stripping voltammetry.¹⁵¹ Su et al. also showed the potential of this reaction for other conducting polymers such as polypyrrole, which as mentioned previously can react in a similar manner to PANI due to similar conjugated structures.¹⁵⁴ Bergman and Hanks showed the thiol-ene reaction occurring on conducting polymers via the treatment of PANI, polypyrrole, polythiophene and poly(ethylenedioxythiophene) with alkanethiols and fluoroalkane thiols.¹⁵³ Molino et al. also showed the ability of polypyrrole and poly(3,4-ethylenedioxythiophene) to partake in the thiol-ene reaction when fluorinated thiols in the gas phase and in solution.¹⁵² Typically thiol-ene reactions are most favorable when the unsaturated bond is unconjugated as represented by the reactivity series by Hoyle et al. which is corroborated with the original experimental observations of Morgan et al..^{59,61} The aromatic structure of PANI would be expected to have high stability towards the thiol-ene reaction because of this and the reaction would be very unique and unusual. Therefore, the exploration of the synthesis of a PANI glycopolymer by thiol-ene reaction with a thiolated carbohydrate is a unique and interesting reaction pathway compared to the previous chapter which required the initial transformation of PANI into a thiol-ene reaction receptive polymer.

The synthesis of a PANI film presents several unique applications. PANI, being an electrical conductor, is heavily researched as a useful sensor material as it can be chemically attached or formed on the electrode surface allowing further functionalisation without hindering the electrical conductivity.^{155,156} A PANI backbone can offer ease of sample preparation, cheap synthesis for large scale, as well as the ability to conduct charge and can therefore be utilised as an intermediate material between the electrode and sensing reagent. In previous chapters PANI was functionalized with a bioactive molecule and was therefore able to interact with lectins. Continuing with this theme, PANI glycopolymers were still the primary objective. PANI

glycopolymer films are unique, surface functionalized materials that can potentially be utilised for bioactive surfaces. In this chapter D-mannose has been substituted for D-glucose, which while shown to be less specific towards lectins such as ConA is still part of the Man/Glc specificity group.⁸²

The thiol-ene click has been shown in the literature to be capable of being performed with the unsaturated component coming directly from the conducting polymers (PANI, polypyrrole) unsaturated π structure and allows direct connection of desired thiols onto the polymer backbone. Several researchers have hypothesised that this reaction occurs via interaction of the sulfur atom with an unsaturated bond in a quinoidal ring, resulting in reduction of the ring to a benzoidal ring. Liu et al. constructed a glassy carbon electrode modified with multiwalled carbon nanotubes, PANI and mercaptosuccinic acid for the amperometric determination of ascorbic acid. They reported a hypothesised reaction synthesis to involve interaction of the mercaptosuccinic acid thiol with the quinoidal ring structure resulting in reduction of the ring to the benzoidal ring resulting in greater leucoemeraldine character of the PANI backbone.⁴⁹ Reoxidation allows the reformation of the stable emeraldine form and further potential for the reaction to proceed by the increase in quinoidal ring concentration. The hypothesised reaction scheme is validated by the reports of Su et al., Han et al. and Bergman et al. whose publications have been described previously.

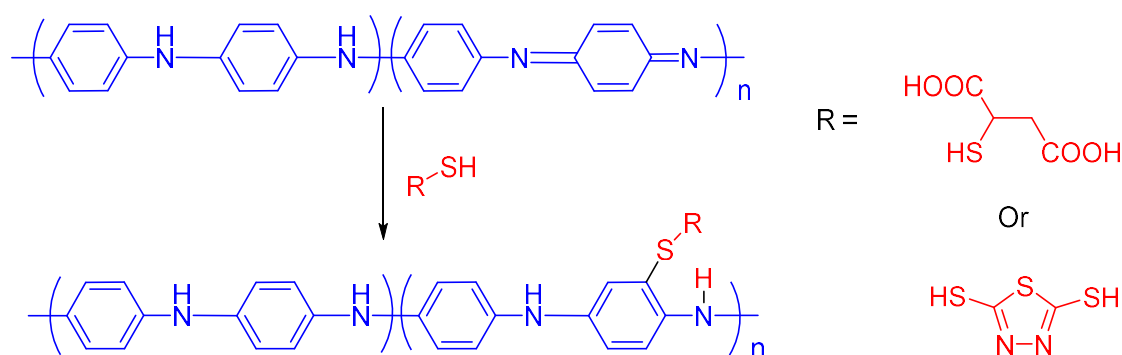


Figure 5.1: Reaction scheme for the thiol-ene reaction between PANI and a thiol as suggested by the literature.

Halliwell et al. went one step further in their proposal for the mechanism of the thiol-ene reaction of thiols with PANI. In their research into lactate biosensors by the immobilisation of lactate dehydrogenase on PANI-poly(acrylate) and PANI-poly(vinyl sulfonate) films they hypothesised that the mechanism, including electron movements is as per Figure 5.2.¹⁵⁷ This could potentially be due to the acidic nature of the thiol hydrogen which is typically much more acidic than alcohol hydrogens. The acidic nature of the hydrogen in the thiol is typically utilised

in the base catalysed thiol-ene reaction, as the more acidic the hydrogen the easier it is for the base abstraction to occur which is explained previously in chapter 1.

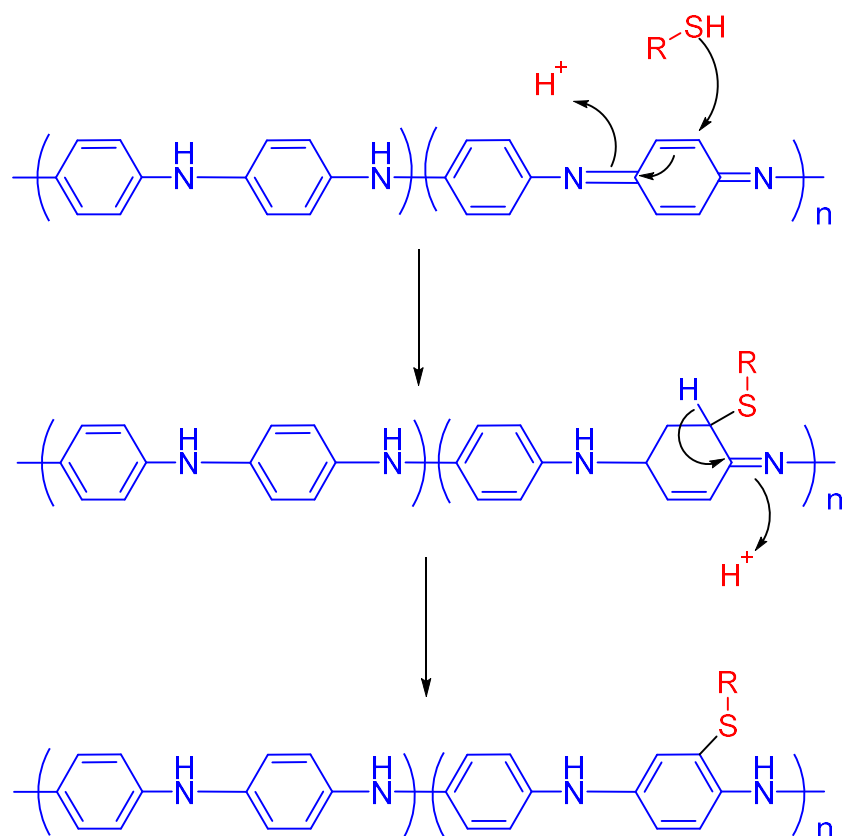


Figure 5.2: Proposed reaction mechanism for the thiol-ene reaction between PANI EB and a thiol as hypothesised by Halliwell et al.¹⁵⁷

The overall mechanism is the same as that previously cited with the thiol sulfur atom interacting with the quinoidal ring on PANI and resulting attachment of the thiol to the PANI backbone.

5.2. Experimental

5.2.1. Chemicals

Aniline, ammonium persulfate, 1-thio- β -D-glucose tetraacetate, NaOMe and NMP were purchased from Sigma Aldrich and used as received. Concentrated HCl was purchased from Macron and used as received. Teflon strips were donated by the Centre for Advanced Composite Materials from the University of Auckland.

ConA Texas Red Conjugate was purchased from ThermoFisher Scientific.

5.2.2. Synthesis of PANI EB freestanding films (11)

PANI films were prepared utilizing PANI EB, which was prepared using the same preparation method as per Chapter 4. PANI EB (1.0 g) was first ground to a fine powder using a mortar and pestle. This powder was then dissolved in NMP (20.0 g) to prepare a 5 wt % solution. This was stirred for 6 hours until the PANI completely dissolved. The dark blue solution was then vacuum filtered to remove any undissolved material or aggregates. Teflon strips were first wiped with methanol to remove any dust or alien material. PANI-NMP solution was then dropped using a glass pipette onto the Teflon strip covering 75 % of it. The strip was placed in an oven at 100 °C for twelve hours. Finally, the temperature in the oven was increased to 210 °C for 6 hours to fully remove the solvent. After complete drying the films delaminated from the Teflon and could be removed with tweezers.

5.2.3. Synthesis of 1-thio- β -D-Glucose tetraacetate functionalized PANI (12)

1-thio- β -D-Glucose tetraacetate (0.200 g, 0.550 mmol) was fully dissolved in DMF (1 mL). Just prior to reaction DMPA (0.015 g, 0.055 mmol) was added. To this solution PANI EB film was immersed and UV light (365 nm) was used to illuminate the sample for the entirety of the reaction. The reaction was left for 24 hours. After the reaction was completed the film was removed from the solution and washed with DMF (3 mL x 3) and methanol (5 mL x 3) and then air dried.

5.2.4. Synthesis of glucose functionalized PANI film (13)

A solution of NaOMe (1 mol/L) in MeOH was prepared. To this solution 1-thio- β -D-glucose tetraacetate functionalized PANI films were added. After an hour the films were washed using methanol (100 mL x 3). The films were left to dry in the fumehood.

5.3. Results and Discussion

Based on the cited literature provided in chapter 5.1, the hypothesised hydrothiolation reaction mechanism between PANI EB film **11** and 1-thio- β -D-glucose tetraacetate is shown in Figure 5.3 to form glucose functionalized PANI film **13**.

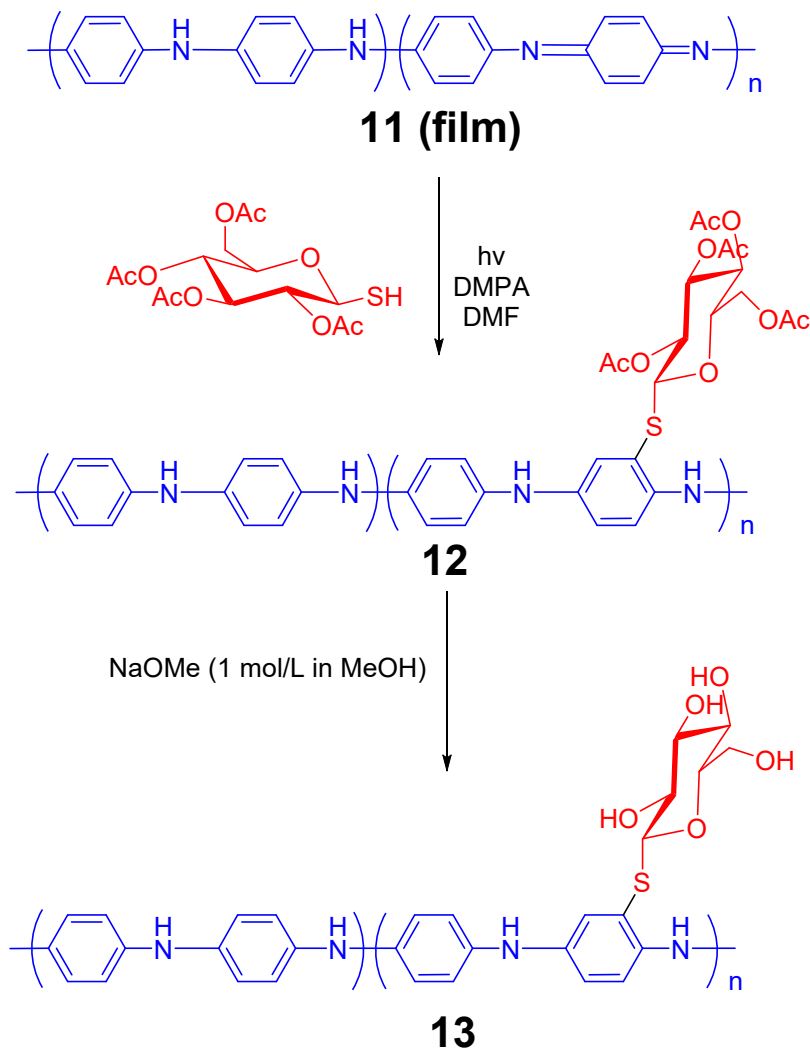


Figure 5.3: Proposed synthetic procedure for the synthesis of glucose functionalized PANI film **13**.

5.3.1. Parent PANI film synthesis

PANI films have been described by several authors who all successfully prepared films while utilising a number of different synthetic procedures.^{105,123,158,159} One of the most common ways to form a PANI film is to complete the polymerization aniline in a vessel containing the target substrate. Stejskal et al. completed an IUPAC technical report on the synthesis of PANI films and utilised this method.³⁷ The substrate acts as a nucleation site for the reacting monomer resulting in the growth of PANI chains perpendicular to the substrate surface. A second method

for film preparation uses a “solvent evaporation” casting method. As the solvent evaporates a film is formed as the polymer chains align with the surface of the substrate. Both solubility of the polymer in the solvent along with its boiling point affect the film formation, as the polymer must be soluble to form a solution and the boiling point low enough that the solvent can be removed. As mentioned numerous times throughout this thesis, the difficulty in the processability of PANI is because it is a highly insoluble material. The most effective solvent for PANI is NMP, which is more effective on the base form of PANI in comparison with the salt form. NMP is a dipolar aprotic solvent which has very strong solvation properties. Polymer films were successfully cast after drying at 100 °C and were pliable and lustrous, able to be bent and displaying enough elasticity to reform their original shape. However the presence of NMP was still found after casting films at this temperature, possibly trapped within the film matrix. Casting at 100 °C then further heating above the boiling point of NMP did remove majority of the NMP remaining in the sample. After heating to a higher temperature (>200 °C) the polymer film became very brittle. NMP is therefore acting as a plasticisation agent for the NMP film, and its removal leads to an increase in the brittleness of the film.

Because of the insolubility of the salt form of PANI, the base form was utilised in preparing workable PANI solutions for film casting. This meant, however, that to achieve the more potent salt form of PANI the film would require redoing with a suitable dopant. Hydrochloric, methanesulfonic and toluenesulfonic acid (1.0 mol/L) were all briefly explored as potential solutions for the doping of the PANI EB films. It was found that during the attempted reaction at these concentrations that the films lost their cohesion, resulting in severely degraded film structures. Therefore, similar to chapter 3 alteration of the concentrations of the doping acids is required to successfully dope the PANI film without adversely affecting the morphology.

5.3.2. FTIR spectroscopy

Pure PANI films were analysed prior to chemical reaction to inspect the chemical structure and its similarity to the parent PANI powder. Initial confirmation of the synthesis of a pure PANI film **11** by way of FTIR is shown in Figure 5.4. Characteristic of all PANI's, the peaks located at 1589 and 1492 cm^{-1} correspond to the quinoid and benzoid stretching modes respectively. The presence of NMP solvent which is used in the casting is present, even after extensive drying and proved to be difficult to remove completely. As explained earlier NMP is a very strong solvent and is used in many polymer industries for the dissolution of polymers and plastics. However, even though it's very useful in this regard it can be difficult to remove due to its very high boiling point. The presence of NMP is confirmed by the peak at 1650 cm^{-1} which is the carbonyl stretching region and results from the C=O bond of NMP. Lamouri et al., who also chemically

prepared PANI films in a very similar method to that described here, also showed the presence of NMP solvent and attributed its difficult removal to hydrogen bonding between the amine on PANI and the carbonyl on NMP but also the fact that NMP is a high boiling point solvent with a boiling point of 202 °C.¹⁵⁹ Complete removal of the solvent was achieved by Lamouri only after doping of the film with sulfanilic acid, which they hypothesised occurred due to interaction between sulfanilic acid and NMP preventing the previously mentioned hydrogen bonding from occurring. Further removal of the NMP in this research was found when the heating temperature was increased to 200 °C, however, low concentrations remained even after drying for 24 hours at this temperature.

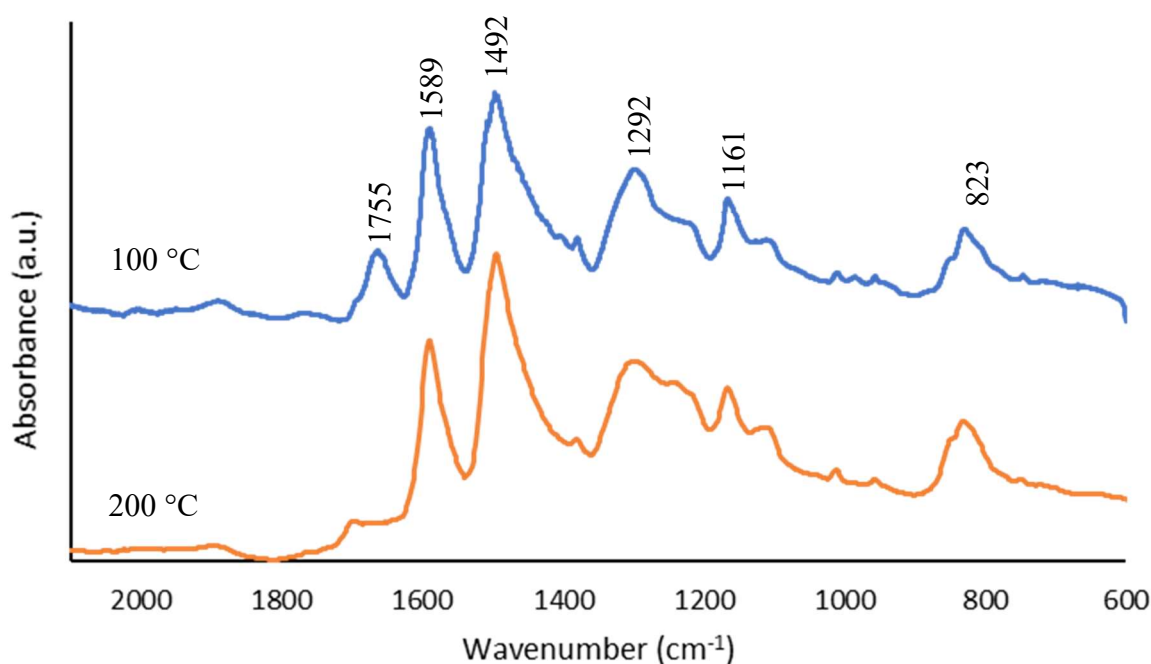


Figure 5.4: FTIR-ATR of PANI EB film **11** dried at 100 °C and 200 °C overnight.

Attachment of 1-thio- β -D-glucose tetraacetate to the PANI EB film surface, forming acetyl protected glucose functionalized PANI film **12**, was also characterised via FTIR to confirm the carbohydrates presence and investigate the mechanism of attachment of the carbohydrate to the PANI substrate is shown in Figure 5.5. The presence of the glucose moiety was observed by the peaks arising at 1741 and 1228 cm⁻¹ which correspond to carbonyl C=O and C-O stretches respectively from the acetyl group, which were much greater in absorbance in comparison with the C=O bond from the NMP shown in Figure 5.4. While the C=O peak may contain absorbance from NMP, the peak at 1228 cm⁻¹ is conclusive evidence for the attachment of glucose. Even after multiple washes with THF and water these peaks remained, displaying strong covalent binding between the carbohydrate and PANI.

Deprotection of the glucose is completed by the addition of NaOMe, which removes the acetyl protecting groups and reintroduces the -OH functionality and forms glucose functionalized PANI film **13**. This is observed in the FTIR spectrum shown in Figure 5.5 where the peaks for C=O and C-O which arise from the acetyl groups mentioned earlier are completely removed after the reaction. Due to the removal of the C=O stretch with NaOMe it was confirmed that these peaks obviously arose from the 1-thio- β -D-glucose tetraacetate and not NMP, as they disappeared after the reaction. The formation of the -OH functionality after deprotection is shown by the increased absorbance for the broad peak found at 3600 cm^{-1} which is the O-H stretching vibration.

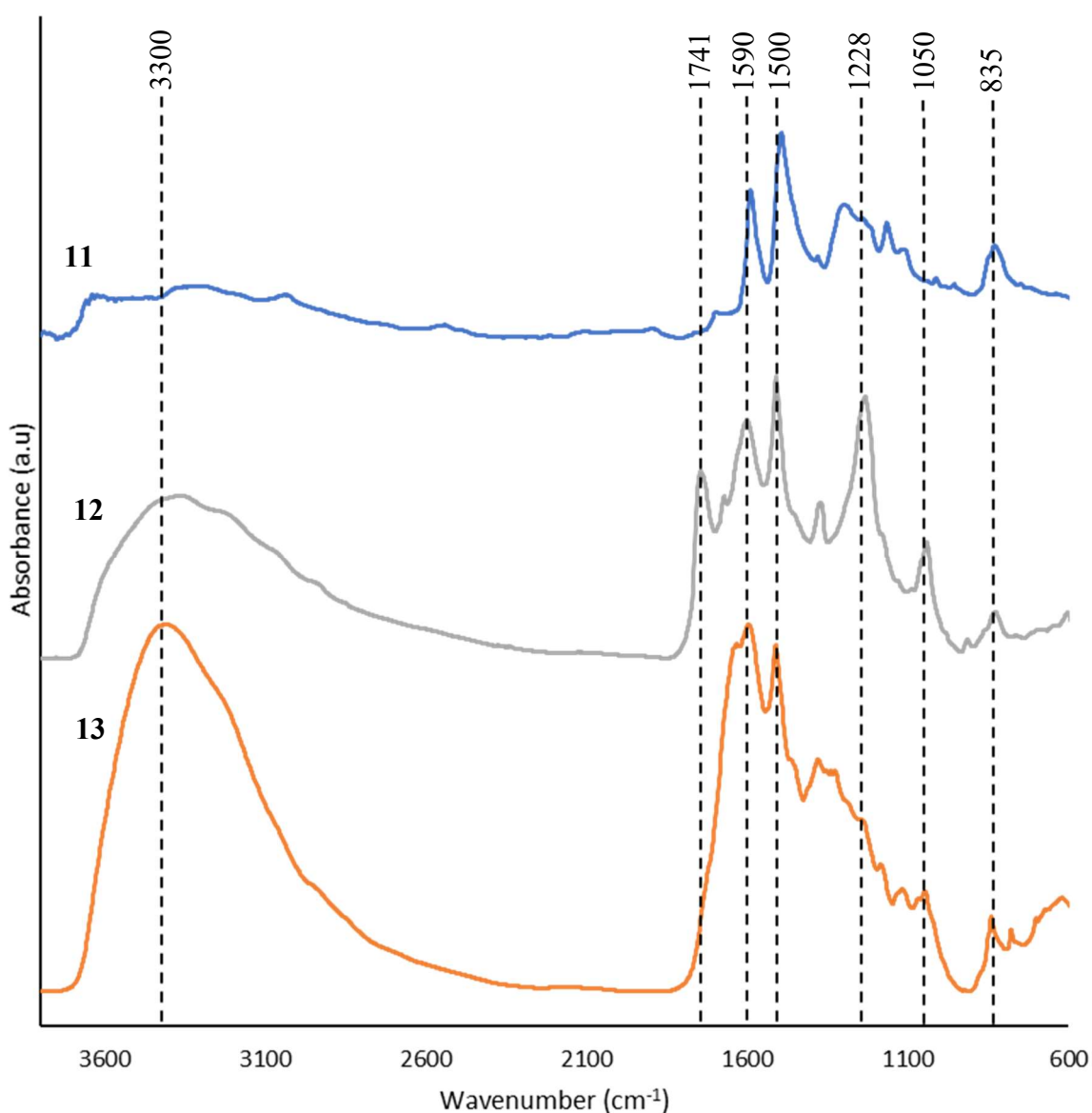


Figure 5.5: FTIR spectrum of PANI EB film **11**, acetyl protected glucose functionalized PANI film **12**, and glucose functionalized PANI film **13** conducted on a diamond crystal ATR attachment.

5.3.3. Scanning Electron Microscopy and EDX

The EDX spectrum of acetyl protected glucose functionalized PANI film **12** is shown in Figure 5.6 and shows high concentrations of carbon, oxygen and sulfur resulting from the incorporation of 1-thio- β -D-glucose tetraacetate onto the PANI film. The EDX spectrum agrees with the FTIR, showing the presence of the glucose moiety via observation of the sulfur and oxygen peaks.

Even though it appears blank, the SEM scan below displays how homogenous and smooth the surface of the film is, even after interaction with the glucose molecules.

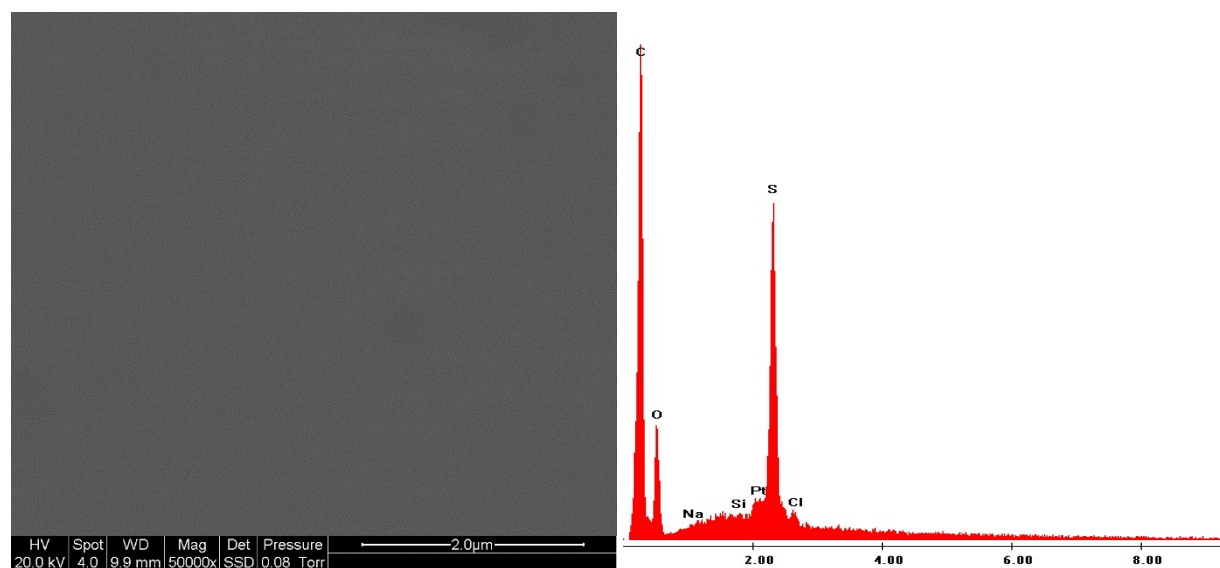


Figure 5.6: SEM scan and EDX spectrum of acetyl protected glucose functionalized PANI film **12**.

5.3.4. X-ray Photoelectron Spectroscopy

The survey spectrum of glucose functionalized PANI film **13** in Figure 5.7 shows the definitive presence of four elements, carbon, nitrogen, oxygen and sulfur. Elements resulting from both the starting reagents are found, nitrogen occurring only from PANI and sulfur only from the thiol-glucose. Both the 2 s and 2 p orbital excitations are observed for sulfur.

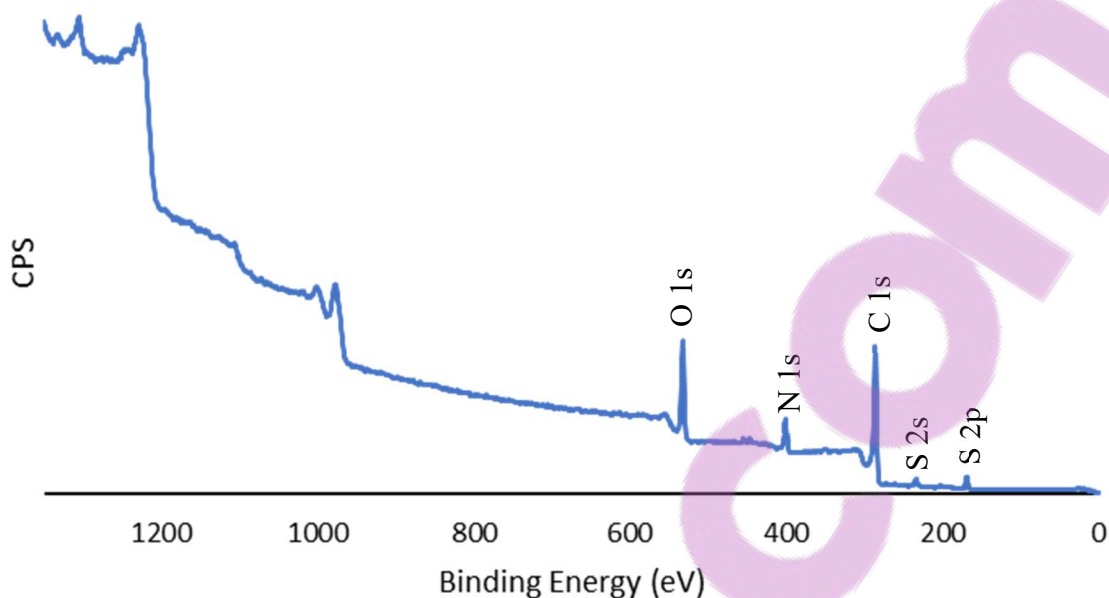


Figure 5.7: XPS survey scan of glucose functionalized PANI film 13.

The C 1s core level scan shown in Figure 5.8 has been deconvoluted into four separate peaks which indicate that there are four different environments found for carbon.

The peak at the lowest binding energy has been assigned as the C-C, C-H peak. This peak arises from both the PANI backbone and the glucose moiety in the sample but also due to contamination from adventitious hydrocarbon species. As mentioned in chapter 4 the saturated carbon peak is used as the charge reference. The peak found at 285.6 eV is attributed to the C-N and C=N species in the PANI chain but may also contain the C-S bond due to similar deshielding effects. The high electronegativity of oxygen results in a higher binding energy peak than the two previous and as such is assigned to the peak at 286.4 eV. The oxygen exists as C-O and C=O from the glucose moiety along with hydrocarbon impurities resulting from adventitious carbon. At the high binding energy side of the C 1s peak is an asymmetric tail which is deconvoluted into a very broad peak found at 288.6 eV. Peaks found in the carbon core level scan at high binding energies have been shown to be a result of π - π^* satellite structures due to PANI's extended conjugation. In this sample this is a result of the extended conjugation resulting from the aromatic rings of the PANI backbone.^{160,161}

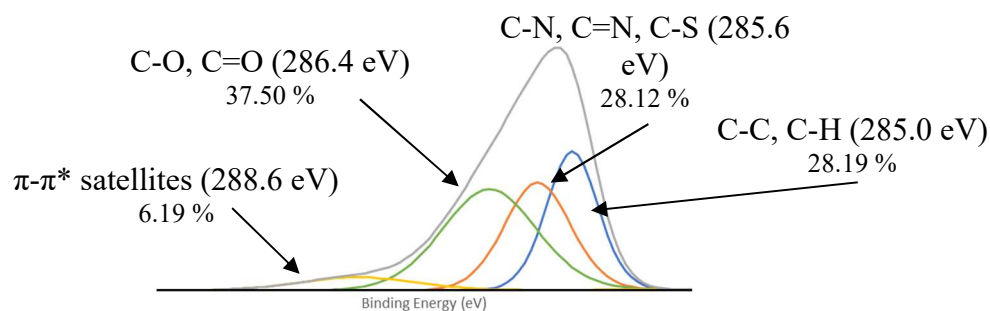


Figure 5.8: C 1s core level scans of glucose functionalized PANI film **13**.

The N 1s core level scan shown in Figure 5.9 shows a large peak centred at approximately 400.1 eV. This peak has been deconvoluted into two peaks at 400.0 and 401.2 eV, indicating two unique chemical environments for nitrogen. Similar to the results found for thiolated PANI **8** and mannose functionalized PANI **10** in chapter 4 the peak found at 400.0 eV is a result of amine nitrogen's (-NH-) and is 52.5 % of the total peak area. The peak situated at 401.2 eV is therefore assigned as charged nitrogen species, N^+ and has the remaining 47.5 % of the peak area. PANI found in the base form also displays two nitrogen deconvoluted peaks, however, as shown in chapter 4 in the XPS of PANI EB powder **5** these peaks are found at lower binding energies, typically approximately 398 and 399 eV. Therefore, doping of the nitrogen's in glucose functionalized PANI **13** has occurred.

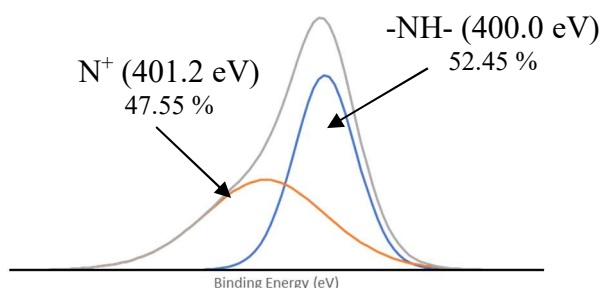


Figure 5.9: N 1s core level scans of glucose functionalized PANI film **13**.

The O 1s core level scan is shown in Figure 5.10. The lower energy binding peaks represent the C-O and C=O bonds. These arise from the both the deprotected glucose (C-O) and adventitious hydrocarbon species and oxidation (C-O and C=O). As shown in the FTIR low concentrations of NMP remains after drying of the PANI EB film which can also be a component of the C-O peak. The higher binding energy peak at 532.5 eV is assigned as S=O, which is also concluded from and is described in the S 2p spectrum below.

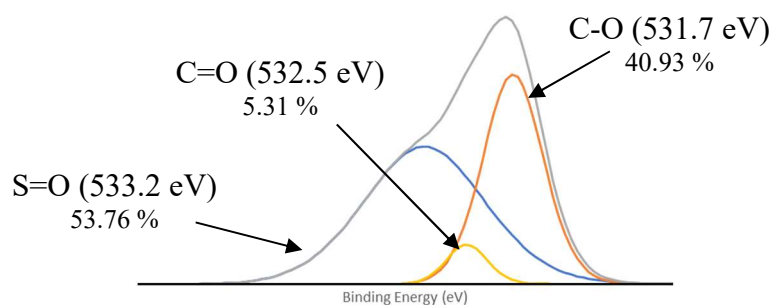


Figure 5.10: O 1s core level scans of glucose functionalized PANI film **13**.

The S 2p core level has been deconvoluted into two peaks which result from a single transition and is shown in Figure 5.11. The larger peak at lower binding energy is a result of the S 2p 3/2 orbital excitation whereas the smaller higher binding energy peak is a result of S 2p 1/2 orbital excitation. The S 2p 3/2 peak is centred at 168.4 eV. Thiol groups are found in the region of 162-164 eV so a large shift to higher binding energy has occurred during the reaction with the PANI thin film. The higher binding energy is generally found for sulfur atoms that are bound to strongly electronegative elements such as oxygen which significantly remove electron density from the sulfur nucleus resulting in the higher binding energy. Yue et al., who synthesised PANI doped with sulfuric acid resulting in sulfonic acid groups found an S 2p binding peak at 167.5 eV, while the sulfonic acid functionalized aerogels synthesised by Gonzalez et al. had a single S 2p peak at 168-169 eV.^{144,148} The sulfonic acid doped PANI synthesised in chapter 4 also showed a peak resulting from the sulfonic acid moiety at approximately 168 eV. However, in the current work this peak is not expected to be as a result of sulfonic acid moiety and is more likely to be due to oxidation of the sulfur on the thiol to either a sulfoxide or sulfone. Sulfuric acid is not utilised in this reaction procedure, so the generation of sulfonic acid molecules is not anticipated. Oxidation of thiols can result in sulfoxides, R-S(=O)-R', however, overoxidation results in sulfones, R-S(=O₂)-R'. In terms of the S 2p core level scans, sulfones would be expected to be found at a higher binding energy (*ca* 168 eV) than the sulfoxide (*ca* 165 eV), because the effect of two oxygen atoms further reducing the electron density at the sulfur atom whereas the sulfide has been shown to be found at much lower binding energy (*ca* 163 eV).^{162,163}

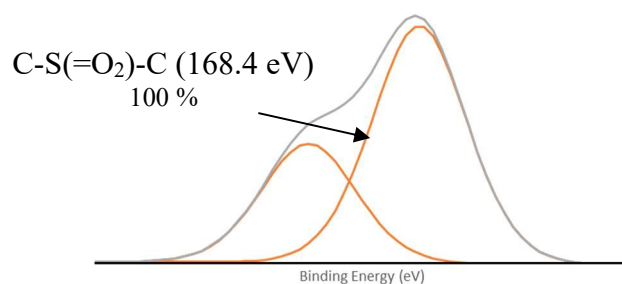


Figure 5.11: S 2p core level scan of glucose functionalized PANI film **13**.

The hypothesised reaction mechanism shown in Figure 5.1 shows the most general reaction pathway for the thiol-ene reaction which results in a thioether linkage, R-S-R' which is the typical product from thiol-ene reactions and was shown in a number of cited references. However, the typical thiol-ene reaction does not utilise unsaturated aromatic bonds, which make the use of this reaction in the synthesis of functionalized PANI's unique. Guerrero-Corella et al. showed the reaction of styrene and phenylmethanethiol resulted in a mixture of the thioether and sulfoxide, with one set of reaction conditions resulting in 99 % of the sulfoxide and 0% of the thioether (1 % being a different by-product).¹⁶⁴ Their reaction conditions for the above result was Eosin Y as the photocatalyst with green irradiating light (~500 nm) and DCM as the solvent. The result found from the S 2p XPS scan leads one to conclude that the thiol-ene reaction has resulted in oxidation of the thiol, leading to a sulfone (-C-S(=O₂)-C-) type bridge as opposed to the thioether -C-S-C-, due to the increased binding energy which occurs from the surrounding electronegative oxygen atoms. 100 % of the converted 1-thio-β-D-glucose tetraacetate has resulted in the sulfone link with no thioether being found in the expected region of the S 2p spectrum above (approximately 162-164 eV).

The inability to remove the surface bound glucose through use of a solvent also indicates that covalent binding has occurred. Li et al. synthesised a graphite-graphite dual ion battery by utilising *N*-butyl-*N*-methyl-piperidinium bis(trifluoromethyl sulfonyl)imide (PP₁₄NTF₂) as the ionic liquid electrolyte and found from the S 2p 3/2 XPS results that a single peak, assigned as the sulfone, was observed at 168.7 eV.¹⁶⁵ Schick et al. immobilized benzenesulfonyl chloride onto aminosilane modified silica surfaces and observed a peak at 168.8 eV, which they concluded was a result of the formed N-SO₂-C structure.¹⁶⁶ Finally, Lee et al. investigated the stability of lithium metal in a Li-O₂ cell with an electrolyte consisting of DMSO. Interestingly they found peaks resulting from both sulfoxide (165.5 eV) and sulfone/sulfonyl (167.0 eV) which they concluded agreed with their O 1s spectra.¹⁶⁷ These authors all found the sulfone groups binding energy in very close agreement with the results from the S 2p spectrum.

5.3.5. Characterization Conclusion

The synthesis of PANI EB films were successfully conducted, producing lustrous, opaque, dark blue freestanding films. After nearly complete removal of the casting solvent, NMP, the film could be easily delaminated from the substrate.

FTIR of PANI EB film **11** showed that drying at 100 °C was insufficient to completely remove the NMP solvent, which has a boiling point of approximately 205 °C. By increasing the temperature to 200 °C nearly complete removal of the NMP was observed. After attachment of 1-thio-β-D-glucose tetraacetate, confirmation was observed by strong presence of both the C=O and C-O absorption bands in the FTIR. After deprotection of acetyl protected glucose functionalized PANI film **12** to glucose functionalized PANI film **16**, the -OH binding peak showed increased absorbance. EDX also confirmed the presence of certain elements with distinct peaks for carbon, oxygen and sulfur being observed. XPS showed that the attachment of 1-thio-β-D-glucose tetraacetate through a thiol-ene reaction resulted not in a R-S-R' bond as hypothesised but due to oxidation of the thiol, as a R-S(=O₂)-R' due to the very high binding energy of the sulfur atoms.

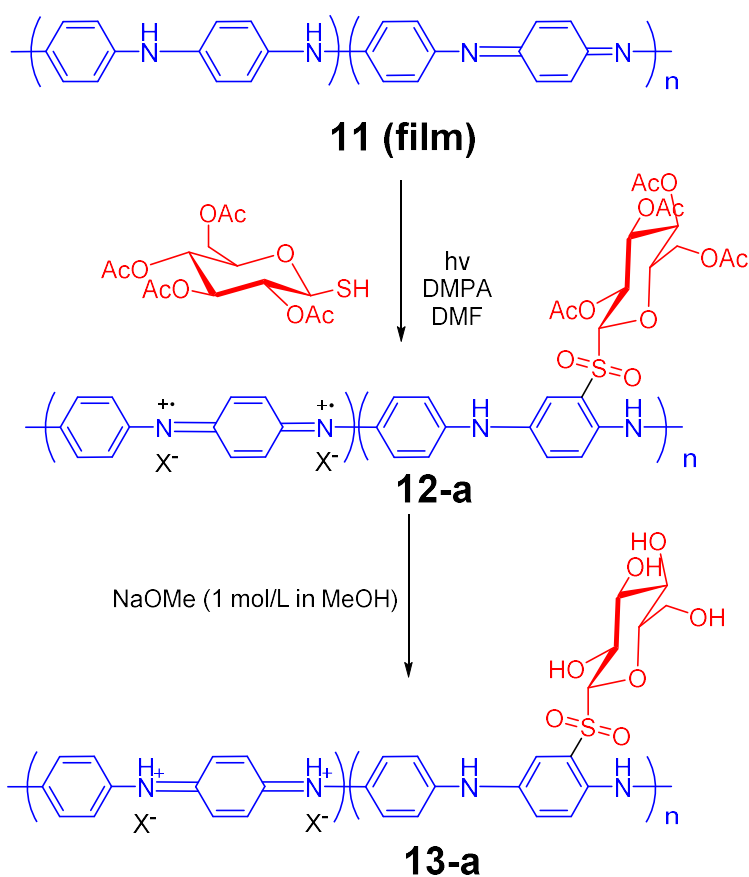


Figure 5.12: The reaction scheme resulting in the formation of glucose functionalized PANI film **13-a** from experimental evidence.

The N 1s core level scan of **13** was deconvoluted into two approximately equal concentration nitrogen environments. These two peaks were assigned to amine, -NH-, nitrogen and also a charged nitrogen species.

5.3.6. Concanavalin A adhesion study

Upon attachment of the glucose moiety to the PANI backbone a glycopolymeric film is formed. The aim of synthesising a glycopolymer in this thesis is to provide biological attachment to the polymer and to investigate the effects of the binding on the resulting bactericidal potency. It is therefore important to analyse the attachment and interaction of a biological entity with glucose functionalized PANI film **13**. The specificity provided to the polymer by the attached carbohydrate can be utilised in several ways, whether a sensor for certain molecules is being produced or to interact with certain microorganisms for bactericidal action. This has been demonstrated in chapter 3 where interaction with ConA showed aggregation and precipitation of a solid out of a solution when a polymer containing mannose ligands was added. A new method was developed in house for the qualitative analysis of binding of a fluorescently labelled ConA lectin to the polymer.

The method used in this chapter to observe the biological interaction of glucose functionalized PANI **13** was devised to show binding of the ConA to the surface of the PANI glycopolymer film. The hypothesised results from a theoretically perfect film with surface bound carbohydrates would be a large amount of fluorescence seen after initial attachment. By attempting to remove the ConA, by a simple solvent/mechanical rinse cycle, it would be expected that for polymer films without carbohydrate functionality fluorescence would not be observed. However, binding of the ConA to glucose functionalized PANI film **13** would be strong enough that rinsing the film with a solvent wouldn't remove the surface bound ConA, with the film retaining the fluorescently labelled lectin. Fluorescence would then be completely quenched by washing with a solution containing a stronger competitor ligand, in this case methyl- α -D-mannopyranoside, to show the specific binding of the films surface.

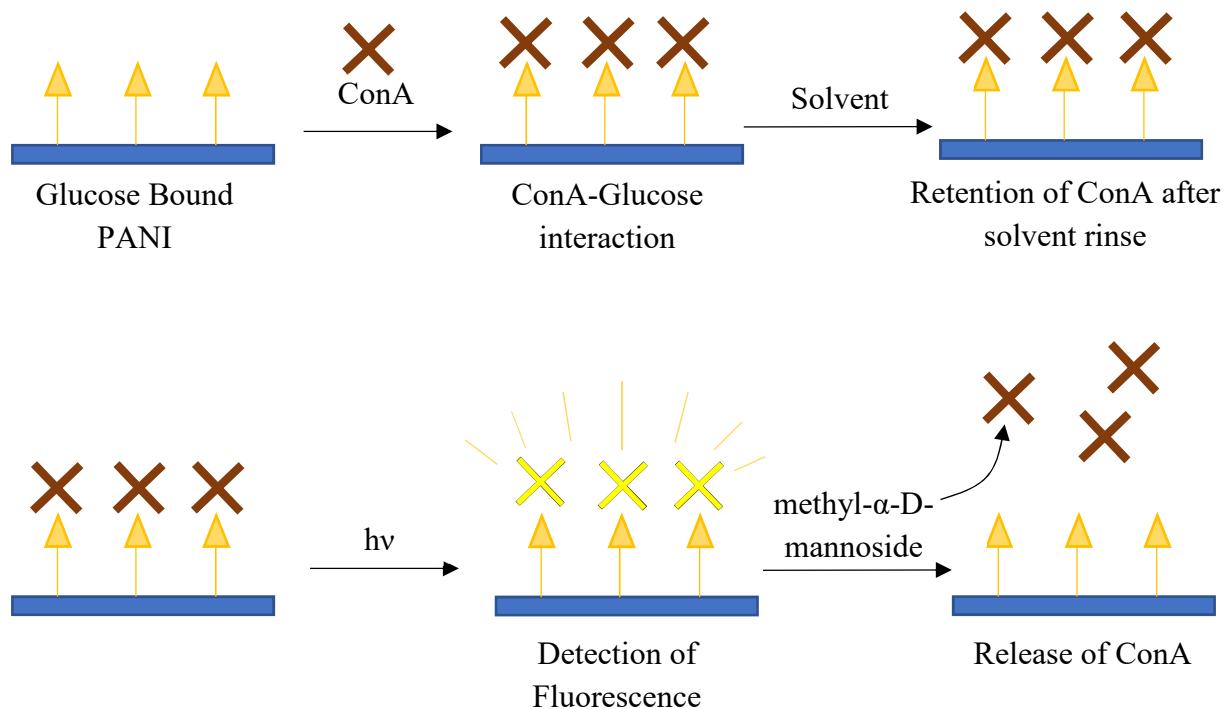


Figure 5.13: Diagram depicting the process for the attachment of Texas Red labelled ConA to glucose functionalized PANI film **13**.

Figure 5.14 shows the lectin binding assay on the control sample. The control sample shows no interaction between the surface and ConA as expected. After initial application of ConA to the surface strong fluorescence is easily observable due to the high concentration of ConA-Texas Red conjugate. This fluorescence is completely removed, however, after a single rinse with buffer solution demonstrating that there is no binding between ConA and the substrate surface.

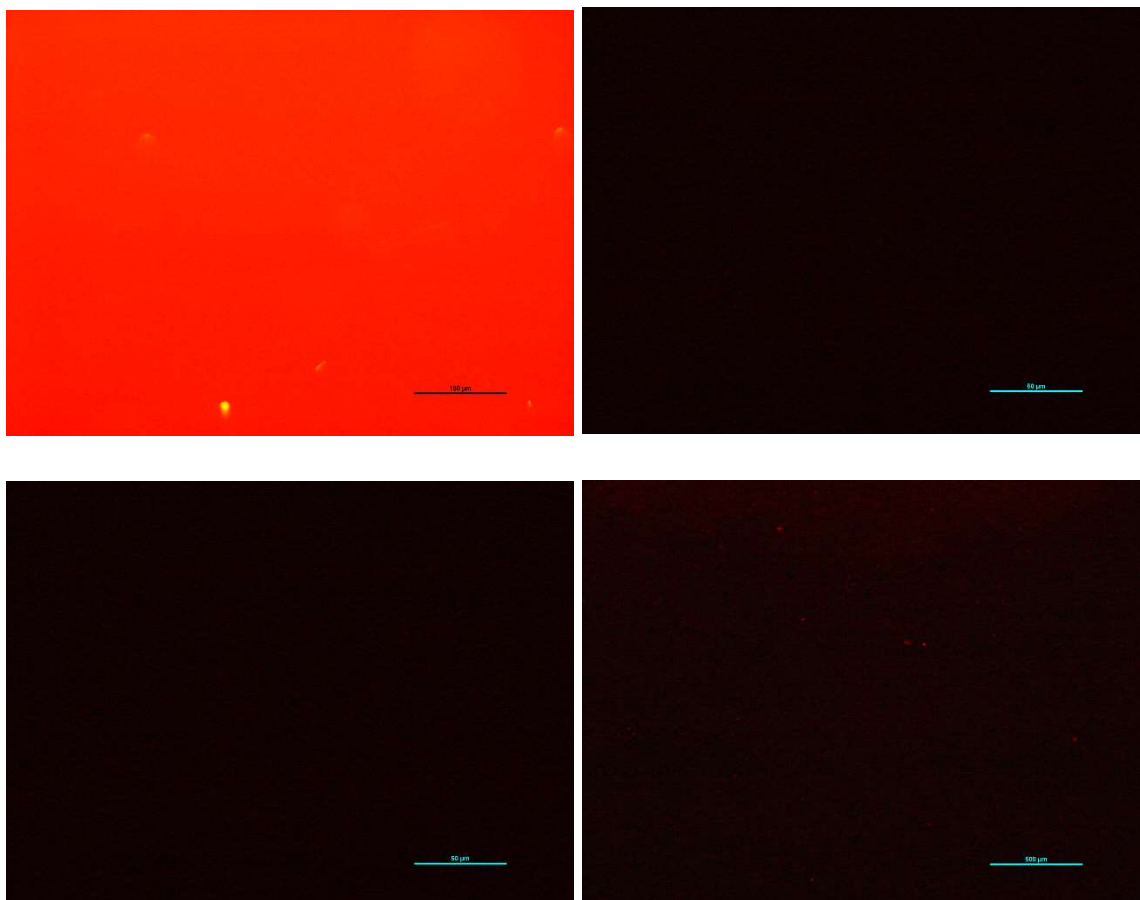


Figure 5.14: Control samples with no wash (top left), 1 wash (top right), 3 washes (bottom left) and after methyl- α -D-mannopyranoside wash (bottom right).

PANI EB film **11** was then analysed using the same experimental procedure and the results of the binding experiment are shown in Figure 5.15. PANI EB film **11** is also expected to show little to no binding between ConA and the films surface due to the lack of carbohydrates or specific binding moieties. However, after one and three washes it can be observed that some fluorescence is observed and that therefore ConA is retained on the surface of the film. After addition of methyl- α -D-mannopyranoside, nearly complete quashing of the fluorescence is observed.

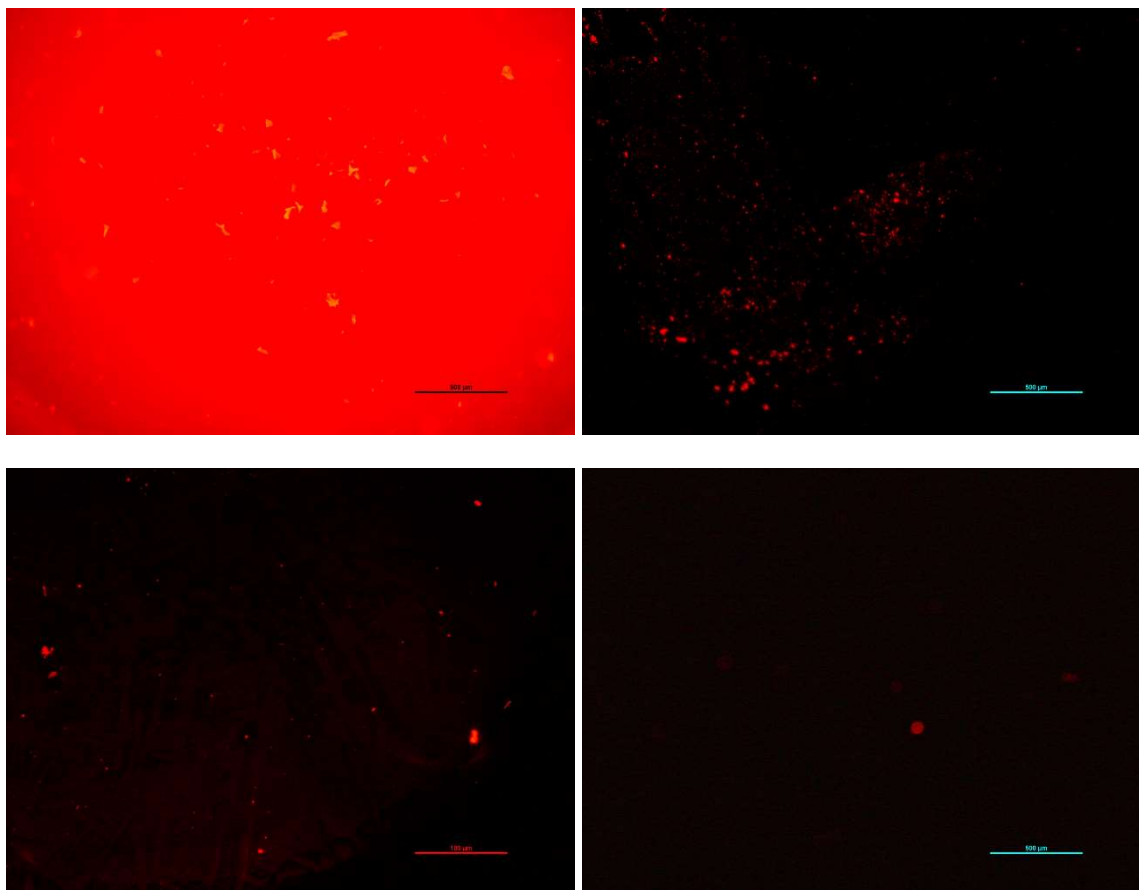


Figure 5.15: PANI EB film **11** with no wash (top left), 1 wash (top right), 3 washes (bottom left) and after methyl- α -D-mannopyranoside wash (bottom right).

Significantly higher fluorescence is observed after a single rinse step in comparison with both the control and PANI EB samples as shown in Figure 5.16. This high concentration of fluorescence remains observable even after three rinse steps, after which it had significantly dropped for PANI EB film **11** and was non-existent for the control sample. This leads to the conclusion that there is stronger attachment of the ConA lectin to the surface of glucose functionalized PANI film **13** compared with PANI EB film **11** and the control. Complete removal of the fluorescently labelled ConA is achieved by addition of methyl- α -D-mannopyranoside which results in complete nullification of the observed fluorescence due to the strong competition provided by the mannoside ligand.

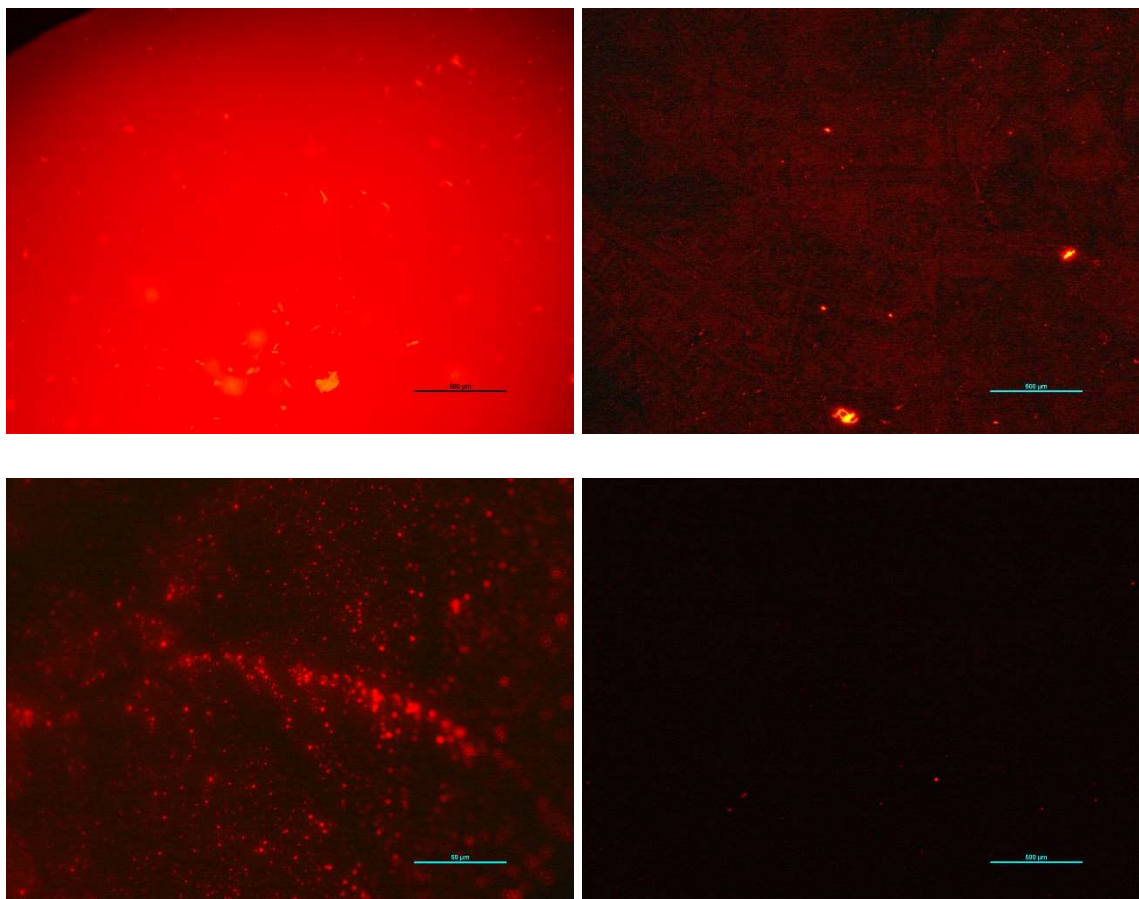


Figure 5.16: Glucose functionalized PANI film **13** with no wash (top left), 1 wash (top right), 3 washes (bottom left) and after methyl- α -D-mannopyranoside wash (bottom right).

It is recognised that the above results are not fully conclusive, however, indicates that this method may be useful for the qualitative analysis of ConA binding to glycopolymer films. Correlation of the intensity of the fluorescence may potentially be used to compare the improved binding shown for **13**. Based on the above results it can be suggested that the addition of the glucose moiety to the PANI structure has resulted in a net increase in the lectin binding ability of glucose functionalized PANI film **13** in comparison with native PANI EB film **11**.

5.3.7. MBC of synthesized glucose functionalized PANI films

The method utilised to determine the MBC of the synthesised films measures the difference between the optical density (at 600 nm) between 0 and 16 hours post rescue of the cells and is plotted to investigate the viability of the cells after being challenged by an antimicrobial surface. 10^4 cells are used as an experimental inoculum and added to the surface of the film to be tested in this experiment. Should any of the cells survive the challenge by the surface their incubation they will begin to grow and an increase in the optical density will be observed (greater concentration of cells results in increased turbidity and therefore increased optical density). However, if the films challenge is successful and the cells are eradicated growth will not occur

which which will be shown by no change in the optical density between 0 and 16 hours. This method is not highly sensitive as even a small survival population of viable cells will result in max optical density being reached.¹⁶⁸

PANI EB film **11** and glucose functionalized PANI film **13** were compared to a control sample and tested against *E coli* and *S aureus* to investigate the MBC. Plating of the samples (which was not utilised in this experiment) is a very slow process as each replicate sample requires plating along with the two time points. By analysing the difference in OD₆₀₀ to determine the effectiveness of the antimicrobial agents results in a much higher throughput method.

Figure 5.17 shows the effect of PANI EB film **11** and glucose functionalized PANI film **13** against *S aureus*, a commonly used gram positive bacteria. The graph shows that a similar increase in optical density was found for all the samples 16 hours post rescue. The increase in the optical density is due to the growth of bacterial cells after removal from the polymer surface and incubation with nutrients. There was a slightly lower optical density difference for PANI EB film **11** and glucose functionalized PANI film **13** in comparison with the control which may represent a knockdown to the total number of viable bacterial cells. The Kruskal-Wallis non-parametric test (followed by Dunn's post hoc test) was used to determine whether this difference was significant (P value <0.05) and represented a knockdown in cells or if the observed lower optical density was a result of randomness (P value >0.05). The calculated P value showed that the difference between the control and **11**, and the control and **13**, were not significant (P value >0.05) and that therefore there was no difference in the antimicrobial ability of **11** and **13** in comparison to the control against 10⁴ CFU of *S aureus* after 24 hour inoculation.

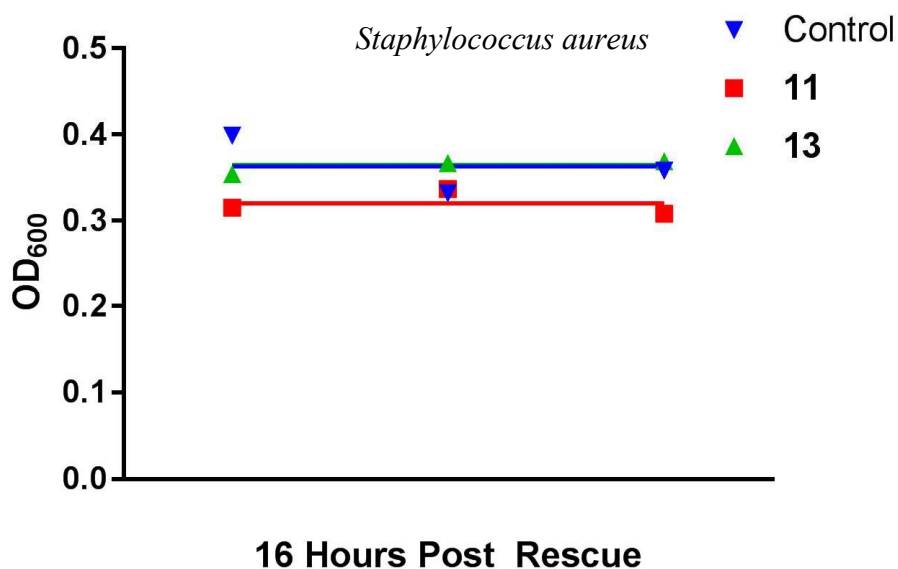


Figure 5.17: Difference in OD₆₀₀ over three replicates post rescue of *S aureus* and 16 hour incubation on control, PANI EB film **11** and glucose functionalised PANI film **13** surfaces. Each point represents a technical replicate with the line representing the mean of the replicates. The standard deviation for each treatment is as follows; control 0.03378, PANI EB film **11** 0.1513 and glucose functionalised PANI film **13** 0.00815.

Figure 5.18 shows the effects on *E coli* (mean and standard deviation over three replicates plotted) after being exposed to films of PANI EB film **11**, glucose functionalized PANI film **13** and a control. The recorded optical density of all the samples 16 hours post rescue was similar to the test against *S aureus* indicating that growth of the bacteria has occurred after rescue. The slightly reduced optical densities for **11** and **13** may represent a slight knockdown in the viable cells after the challenge by the polymer surfaces. To determine whether there was a significant difference between these results and the control a Kruskal-Wallis non-parametric test (followed by Dunn's post hoc test) was utilised. The test showed that the difference between the control and **11**, and the control and **13**, was not significant (P value >0.05) and that therefore there was no difference in the antimicrobial ability of **11** and **13** in comparison to the control against 10⁴ CFU of *E coli* after 24 hours of exposure to the film surface.

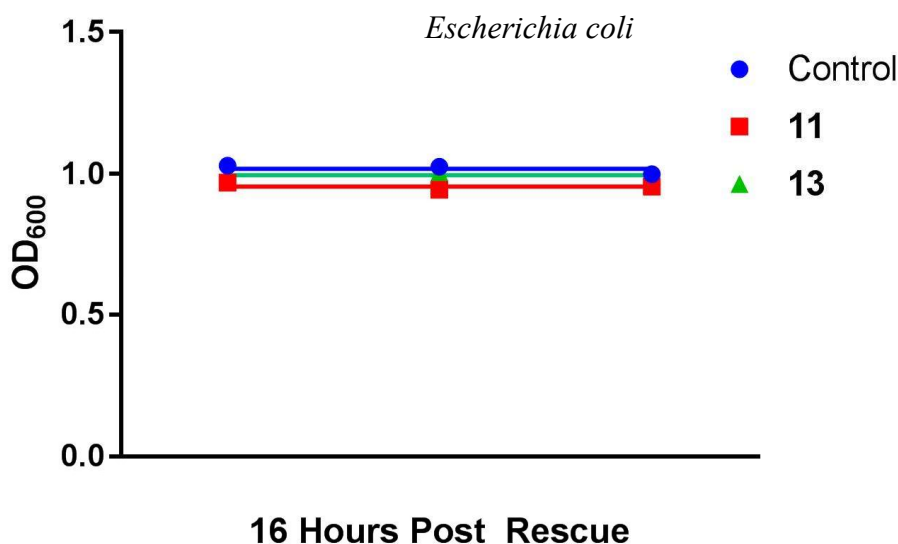


Figure 5.18: Mean difference and standard deviation in OD₆₀₀ over three replicates post rescue of *E coli* and 16 hour incubation on control, PANI EB film **11** and glucose modified PANI film **13** surfaces. Each point represents a technical replicate with the line representing the mean of the replicates. The standard deviation for each treatment is as follows; control 0.01652, PANI EB film **11** 0.01253 and glucose functionalised PANI film **13** 0.00985.

5.4. Conclusion

An experiment developed in house was used to qualitatively observe the strength of binding between glucose functionalized PANI film **13** and a carbohydrate binding lectin. ConA was described in chapter 3 as a carbohydrate binding lectin which was specific to the Man/Glc specificity group which showed enhanced binding to these carbohydrates and their glycosides. In this chapter it was shown that Texas Red labelled ConA displayed stronger binding to **13** in comparison with both a control and PANI EB film **11**. Attempted removal of the ConA, by rinsing with buffer solution, was enough to nearly completely remove the observed fluorescence from the control and PANI EB film **11** samples, however, **13** retained its fluorescence through three of these solvent rinse cycles and could only be completely removed by addition of methyl- α -D-mannopyranoside.

While there was definite enhanced binding observed from carbohydrate binding lectins, the antimicrobial ability of **13** was also experimentally determined with comparison to PANI EB and a negative control surface against both *S aureus* and *E coli*. Overall, the sample showed no improved ability to kill either gram positive or gram negative bacteria. The synthesis of the salt form of **13** was attempted utilising several different doping solvents at various concentrations, however, all the experiments resulted in disintegration of the polymer film.

Chapter 6. Polyaniline thin films incorporating Silver nanoparticles and Glucose

6.1. Introduction

The promising results from chapter 5 showed that a carbohydrate functionalized with a thiol may interact and bind to PANI in an unusual thiol-ene reaction involving the PANI aromatic ring structure resulting in a novel glycopolymeric material. One of the major objectives at the initiation of this work was to synthesise an antimicrobial PANI, however, the previous synthetic products showed no antimicrobial properties. Previous chapters have demonstrated that the inclusion of mannose and glucose enhances the interaction between PANI and various lectins through various binding experiments the functionalized PANI's themselves have shown no demonstratable antimicrobial ability. Therefore, to form an antimicrobial PANI film while still retaining the increased biological interaction an additional biocidal compound was added in the form of silver nanoparticles.

Silver nanoparticles are efficient biocidal agents and have been shown to be easily formed on the surface of PANI in the literature (chapter 1.3). The reduction of silver nitrate to produce silver nanoparticles on the surface of PANI EB powder was first conducted to determine optimal reaction conditions. Subsequently PANI EB films were utilised as surfaces to produce silver nanoparticles and two different experimental routes were analysed with the inclusion of 1-thio- β -D-glucose tetraacetate forming a biocidal PANI glycopolymer. The order of the reagent reactions was altered in the two synthetic routes to investigate if any effect on the properties of the final product was apparent.

6.2. Experimental

6.2.1. Chemicals

Aniline, ammonium persulfate, 1-thio- β -D-glucose tetraacetate, NaOMe and NMP were purchased from Sigma Aldrich and used as received. Concentrated HCl was purchased from Macron and used as received. Silver nitrate was used as received from ECP labchem. Glass microscope slides were rinsed with methanol and wiped with dust free wipes prior to use. The teflon and polypropylene substrates were donated by the Centre for Advanced Composite Materials from the University of Auckland.

6.2.2. Synthesis of PANI EB film 11

The synthetic procedure for producing PANI thin films will be the same as that of chapter 5. Freestanding films were prepared using a Teflon substrate as per 5.1.2. They were then dried in an oven at 100 °C for 12 hours and further at 210 °C for 2 hours.

6.2.3. Synthetic Route 1

Synthetic route 1 involves the binding of silver nanoparticles to the surface of PANI EB followed by the attachment of 1-thio- β -D-glucose tetraacetate through a thiol-ene click reaction. Final deprotection of the acetylated glucose affords the final glucose modified PANI with surface bound silver nanoparticles.

6.2.3.1. Synthesis of PANI EB powder containing silver nanoparticles

A silver nitrate solution was prepared at various concentrations (0.001-0.05 mol/L) in milli-q water (15 mL). PANI EB prepared using the same method found in chapter 4.2.2 was added to this solution and left for 24 hours. After 24 hours the powder was collected via vacuum filtration and washed with milli-q water (50 mL x 3).

6.2.3.2. Synthesis of PANI films with surface bound silver nanoparticles (14)

As prepared PANI thin films were briefly washed with methanol and wiped with dust free wipes to remove any accumulated dust or debris from the surface. A solution of silver nitrate at various concentrations (0.1, 0.5, 1.0 and 5.0 mmol/L) was prepared in milli-q water in separate beakers. The volume of the water was such that it allowed complete submersion of the PANI on the glass slide and complete wetting of the PANI film. Slides were placed in the beaker and left for 6 hours with a watch glass on top. The slides were then rinsed with milli-q water (3 x 50 mL) to remove any unreacted reagent and dried in an oven at 100 °C.

6.2.3.3. Synthesis of 1-thio- β -D-glucose tetraacetate modified PANI films containing silver nanoparticles (15)

1-thio- β -D-glucose tetraacetate (0.200 g, 0.550 mmol) was fully dissolved in DMF (1 mL). Just prior to reaction DMPA (0.015 g, 0.055 mmol) was added. To this solution PANI EB films were added and irradiated with UV light (365 nm). The reaction was left for 24 hours. After the reaction is completed the film is removed from the solution and washed with DMF (3 mL x 3) and methanol (5 mL x 3) and then air dried.

6.2.3.4. Synthesis of glucose modified PANI films containing silver nanoparticles (16)

A solution of NaOMe (1.0 mol/L) in methanol was prepared. To this solution 1-thio- β -D-glucose tetraacetate functionalized PANI films were added. After 60 minutes the films were rinsed using methanol (100 mL x 3). The films were left to dry in the fumehood.

6.2.4. Synthetic Route 2

Synthetic route 2 involves the initial thiol-ene click reaction of 1-thio- β -D-glucose tetraacetate to the surface of PANI EB as per chapter 5. To this silver nanoparticles are formed on the surface of the PANI with final removal of the acetyl groups on the glucose.

6.2.4.1. Synthesis of surface bound silver nanoparticles on acetyl protected glucose modified PANI films (17)

Glucose modified PANI film **12** was briefly washed with methanol and wiped with dust free wipes to remove any accumulated dust or debris from the surface. A solution of silver nitrate at various concentrations (0.1, 0.5, 1.0 and 5.0 mmol/L) was prepared in milli-q water in separate beakers. The volume of the water was such that it allowed complete submersion of the PANI on the glass slide and complete wetting of the PANI film. Slides were placed in the beaker and left for 6 hours with a watch glass on top. The slides were then rinsed with milli-q water (3 x 50 mL) to remove any unreacted reagent and dried in an oven at 100 °C.

6.2.4.2. Synthesis of surface bound silver nanoparticles on glucose modified PANI films (18)

A solution of NaOMe (1 mol/L) in MeOH was prepared. To this solution silver nanoparticle modified glucose functionalized PANI film **17** was added. After an hour the films were washed using methanol (100 mL x 3). The films were left to dry in the fumehood.

6.3. Results and Discussion

Two synthetic pathways were investigated and are shown in Figures 6.1 and 6.2. Figure 6.1 shows the hypothesised route for the initial reaction of silver nitrate with PANI EB film **11**, resulting in the formation of silver nanoparticles on the surface with the subsequent attachment of glucose forming silver nanoparticle modified acetyl protected glucose functionalized PANI film **15**. Removal of the acetyl groups on the glucose moieties resulted in the final product silver nanoparticle modified glucose functionalized PANI film **16**.

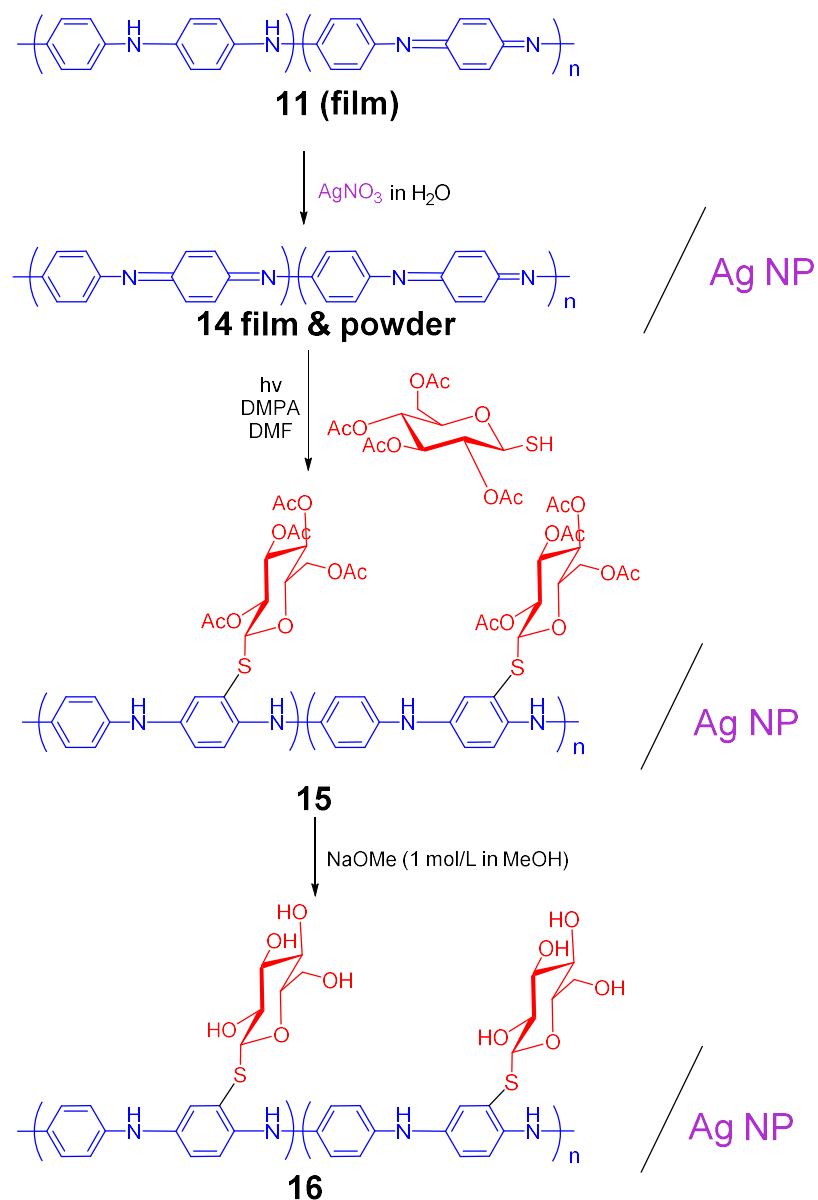


Figure 6.1: Proposed synthetic procedure of synthetic route 1 for the synthesis of silver nanoparticle modified glucose functionalized PANI film **16**.

Alternatively, for route 2, PANI EB film **11** was initially reacted with 1-thio- β -D-glucose tetraacetate as per chapter 5 with subsequent inclusion of the silver nanoparticles producing silver nanoparticle modified acetyl protected glucose functionalized PANI film **17** with deprotection of the glucose to form silver nanoparticle modified glucose functionalized PANI film **18**. The order of reaction was completed to analyse if the attachment of either group altered the chemistry and reactivity of the resulting polymer. Both **16** and **18** were expected to show increased antimicrobial activity due to the surface bound silver nanoparticles in comparison to previously synthesised materials.

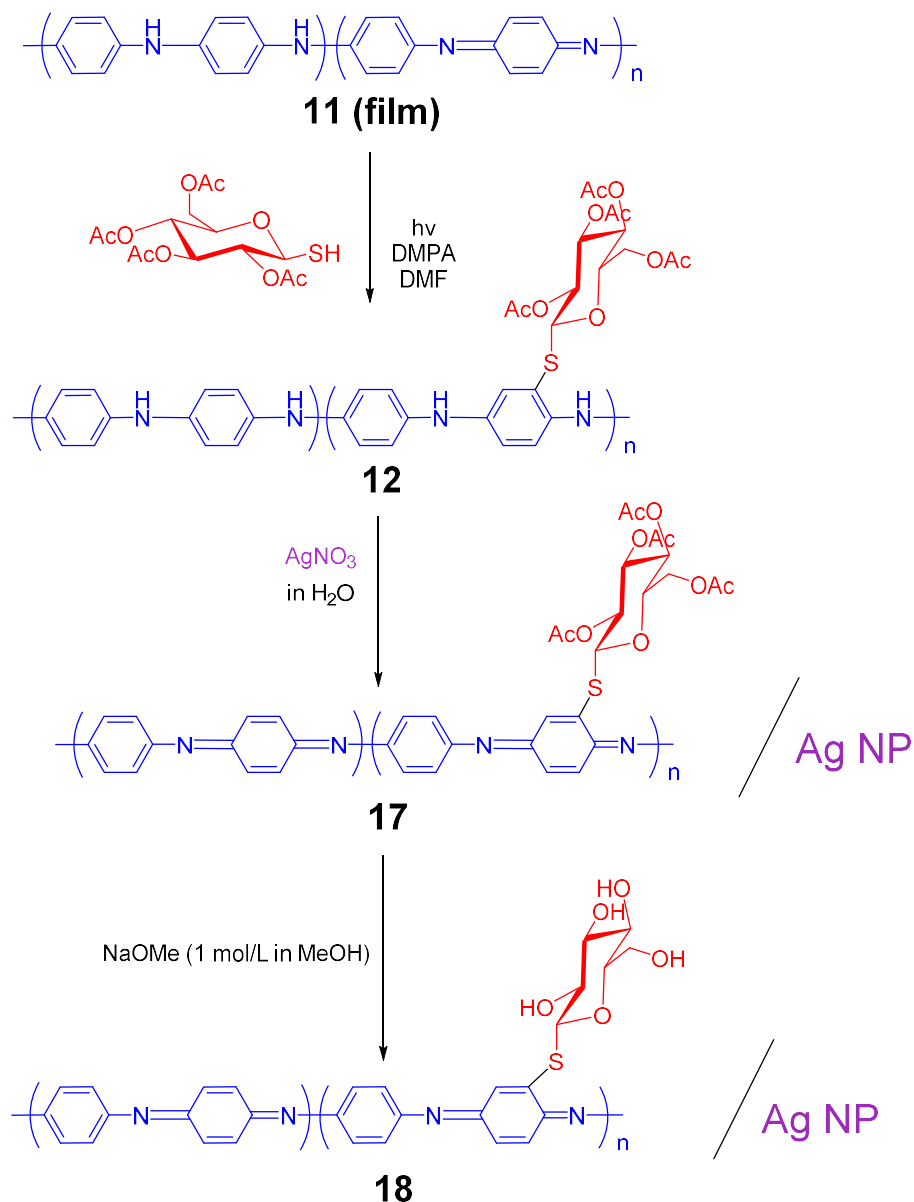


Figure 6.2: Proposed synthetic procedure of synthetic route 2 for the synthesis of silver nanoparticle modified glucose functionalized PANI film **18**.

6.3.1. Scanning Electron Microscopy (SEM)

SEM is a useful technique for probing the surface characteristics and morphologies of materials. The investigation of the surface of the functionalized films is very important due to the application of surface based chemistry, not only in qualitatively confirming the successful deposition of silver nanoparticles but also the particle size, distribution and shape of the nanoparticles which can be observed and are important to the antimicrobial ability of the silver.⁶⁶ Analysis of the effect of the silver nitrate concentration on the resulting nanoparticles onto silver nanoparticle modified PANI EB film **14** was undertaken by varying the silver nitrate concentration between 0.1-5.0 mmol/L.

The SEM scans shown below shows the size of the deposited silver nanoparticles on the surface of the polymer. The diameter of the silver nanoparticles was found to be the same across all the silver nitrate concentrations used in the reaction syntheses, thus indicating that the nanoparticle growth appears to be controlled via reaction time rather than the concentration of silver nitrate when utilising these experimental parameters. It was found that with long reaction times (12 hours +) a macroscopic metallic silver coating formed on the films surface. By limiting the reaction time to 6 hours, even with increased silver nitrate loading, it appeared that the reaction left silver nanoparticles of comparable size. Figure 6.3 shows the SEM scan at 100000x magnification of the sample using 0.1 mmol/L silver nitrate and shows the particle size of the silver nanoparticles to be in the range of 100-200 nm. Marakova et al. conducted similar experiments and found that non-uniform silver nanoparticles in the range of 50-500 nm were formed and often produced clusters like what was found in the present research.⁴¹

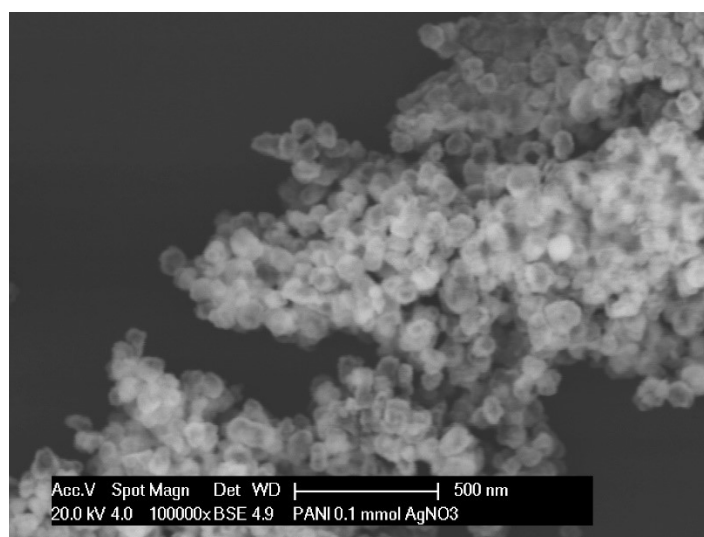


Figure 6.3: SEM scan of 0.1 mmol/L silver nitrate deposited on silver nanoparticle adsorbed Silver nanoparticle modified PANI EB film **14**.

Figure 6.4 shows the SEM scan of the film surfaces produced in the reaction method of silver nanoparticle modified PANI EB film **14**, using differing concentrations of silver nitrate at 10000x magnification. The size and distribution of the silver nanoparticles on the surfaces of the films are very similar across all the samples produced, with variation of the silver nitrate loading having an insignificant effect on the size and morphology of the formed nanoparticles after reaction times of 6 hours.

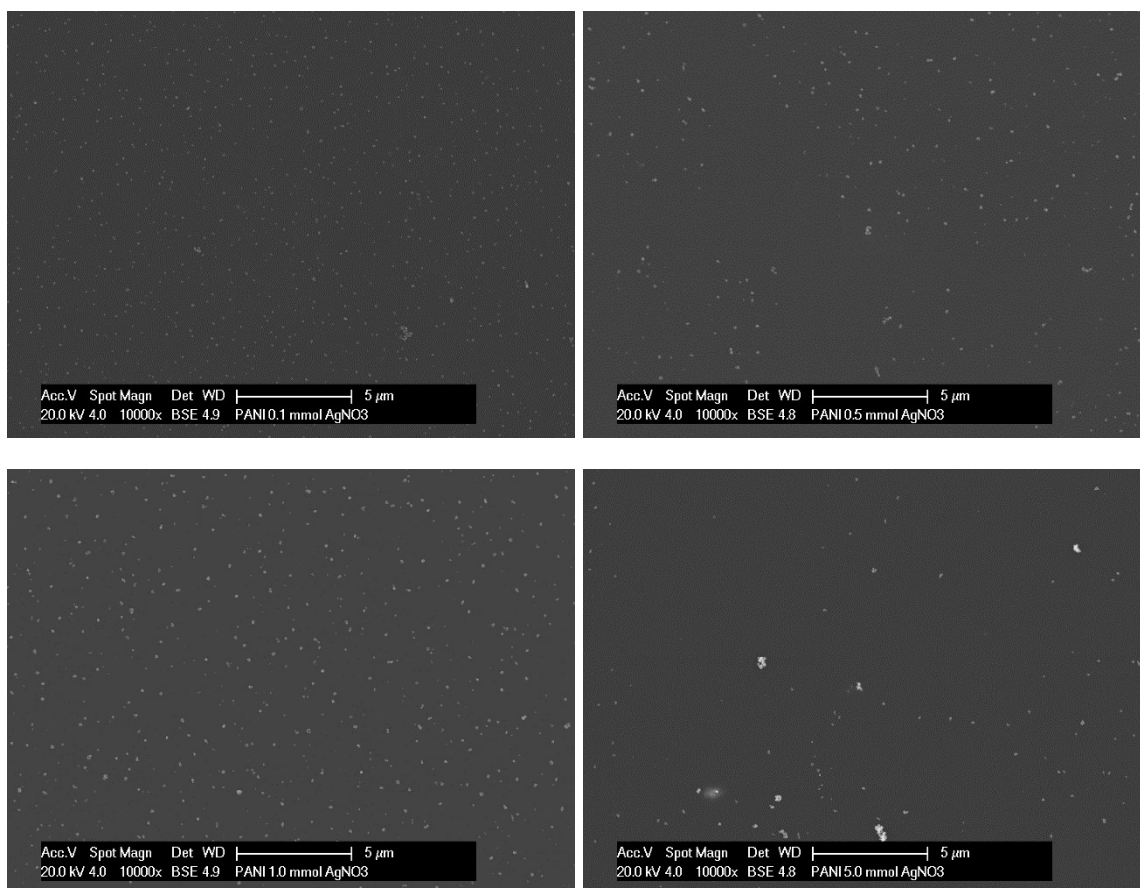


Figure 6.4: SEM scans of silver nanoparticle modified PANI film **14** at 0.1 (top left), 0.5 (top right), 1.0 (bottom left) and 5.0 (bottom right) mmol/L silver nitrate concentrations

6.3.2. Energy Dispersive X-ray Spectroscopy (EDX)

Figure 6.5 and 6.6 shows the EDX spectrum with an inset image showing the precise region that was analysed for the samples with different silver nitrate concentrations. The silver $L\alpha$ peak is found at ~ 2.9 keV in all the samples analysed. This analysis was not quantitative due to the variation in the distribution in the silver nanoparticles in the analysis zone. It can, however, be qualitatively concluded that silver nanoparticles have formed on the surface of the PANI film.

Carbon has the highest elemental concentration found in all the spectra which is a result of the PANI backbone and the glucose moiety. The nitrogen peak is also observed, however, due to the high concentration of carbon in the sample it exists as a shoulder on the higher energy side. The sulfur K peak indicates the presence of 1-thio- β -D-glucose. Around 2.10 keV, platinum is found due to its use as the sputter coating material which ensures a good conducting surface and prevent charging of the sample which distorts the image.

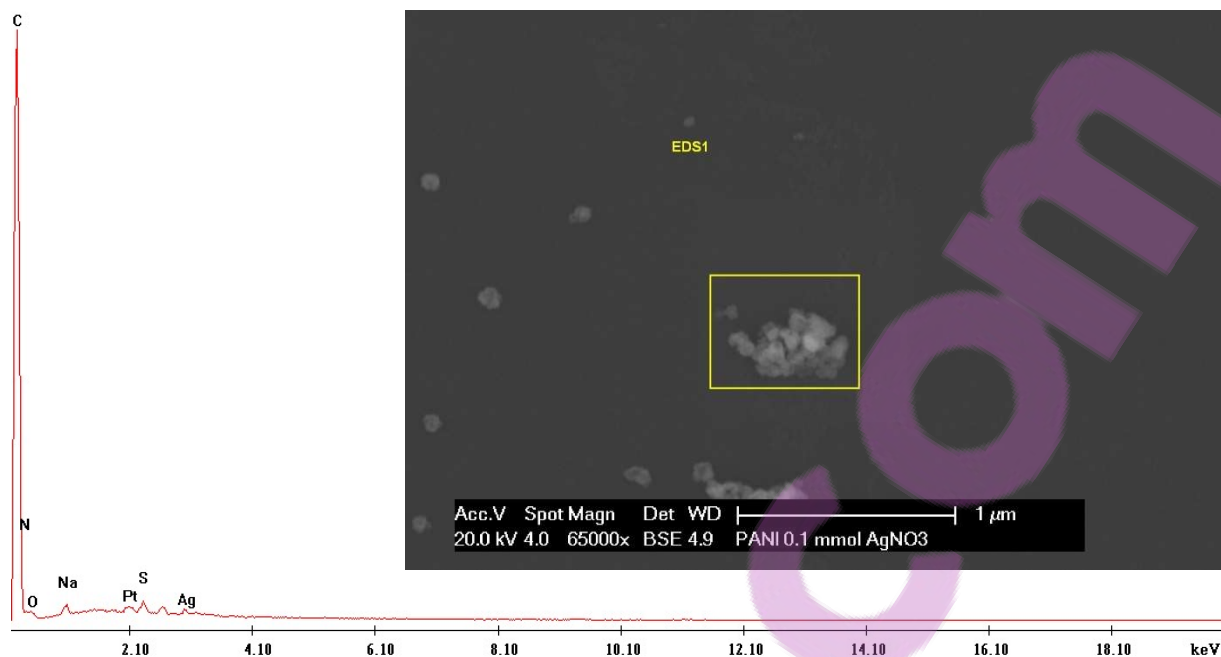


Figure 6.5: Attachment of silver nanoparticles with 0.1 mmol/L AgNO₃ on silver nanoparticle modified glucose functionalized PANI film 16.

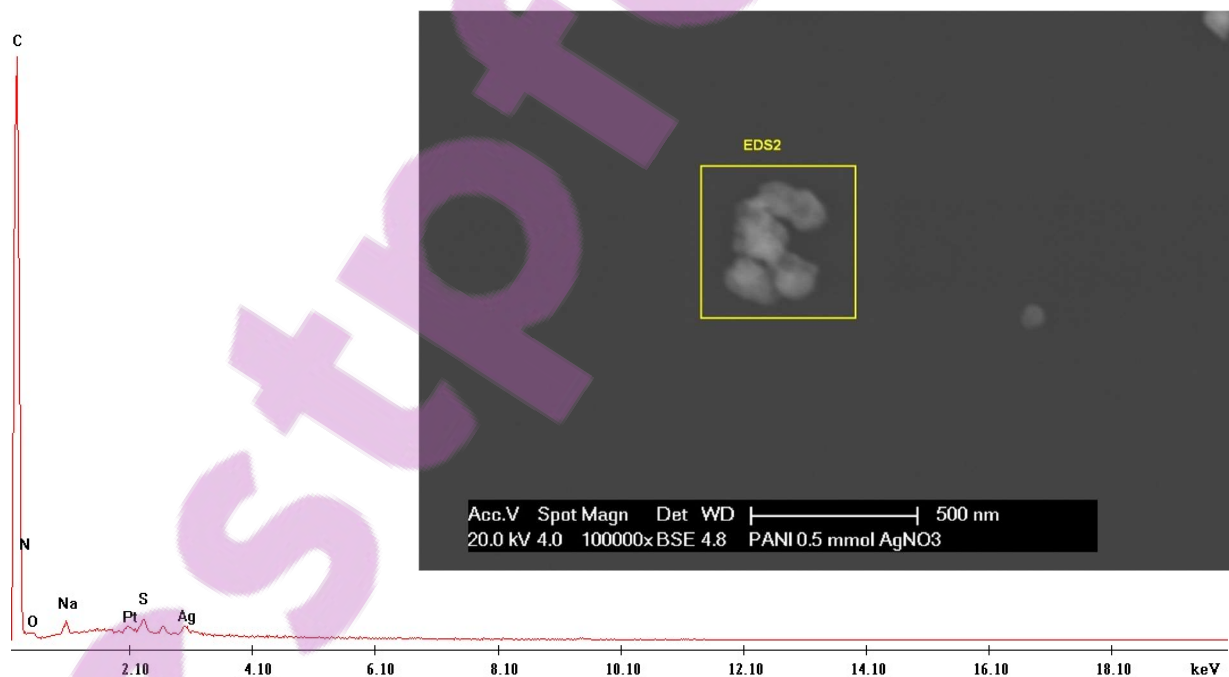


Figure 6.6: Attachment of silver nanoparticles with 0.5 mmol/L AgNO₃ on silver nanoparticle modified glucose functionalized PANI film 16.

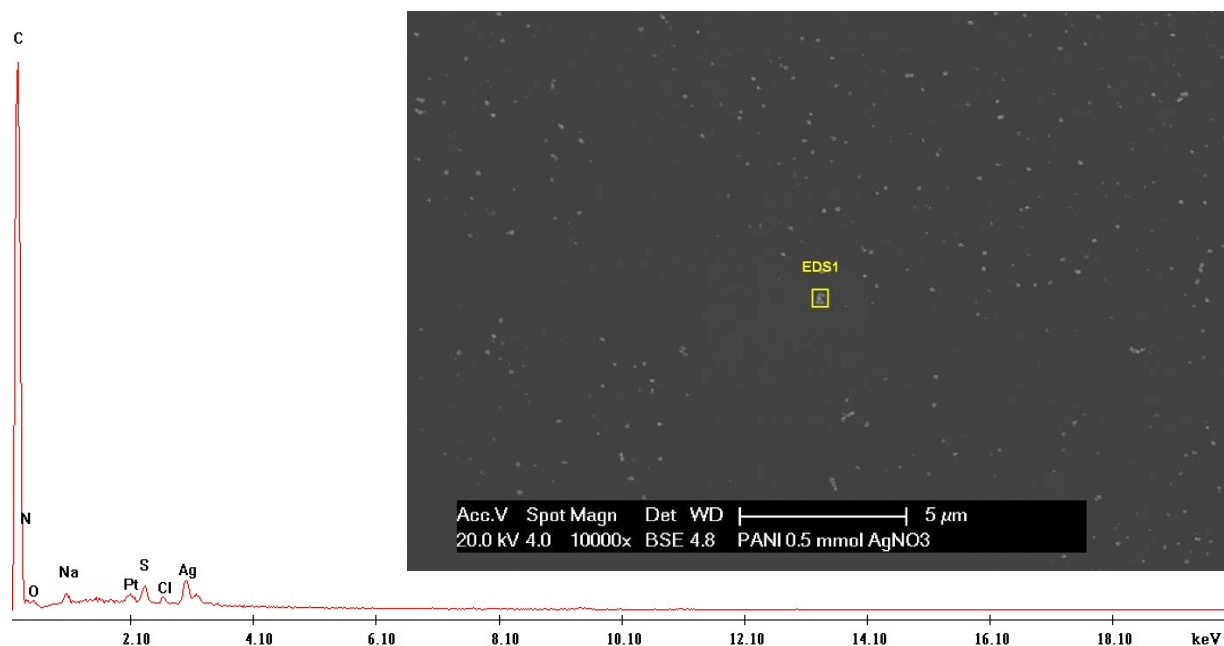


Figure 6.7: Attachment of silver nanoparticles with 1.0 mmol/L AgNO_3 on silver nanoparticle modified glucose functionalized PANI film **16**.

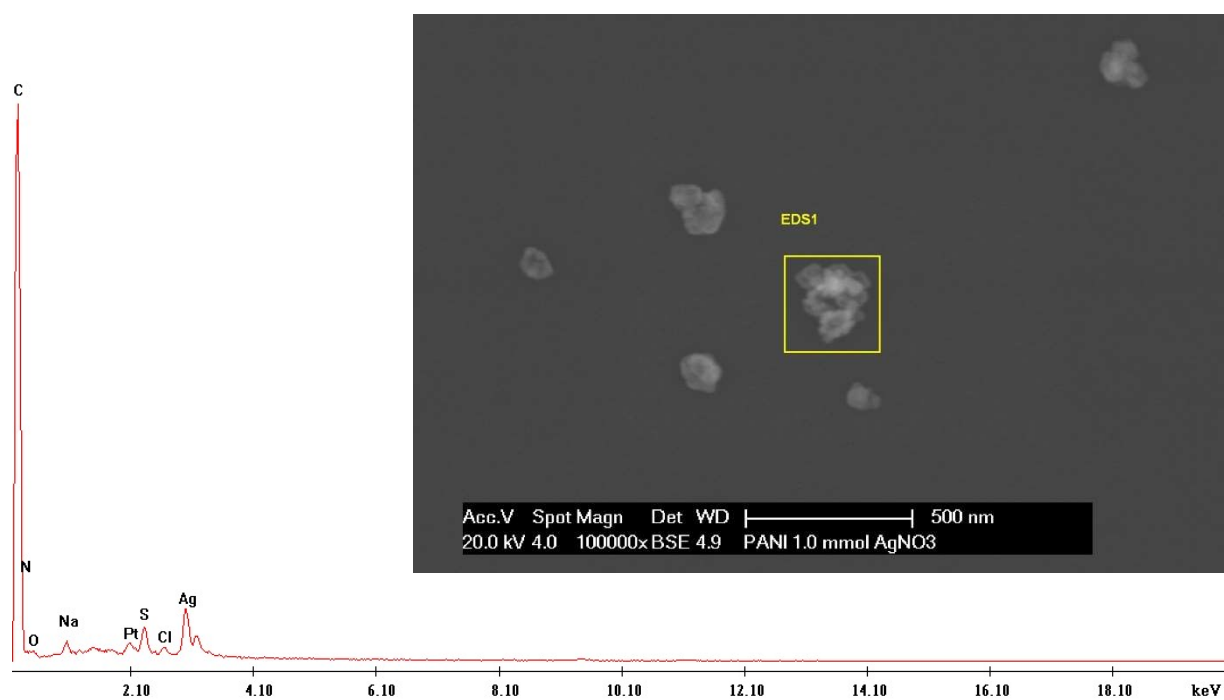


Figure 6.8: Attachment of silver nanoparticles with 5.0 mmol/L AgNO_3 on silver nanoparticle modified glucose functionalized PANI film **16**.

6.3.3. X-ray Photoelectron Spectroscopy

The survey scan of the XPS experiment examines the entire binding energy scale and is useful for determining the qualitative existence of elements within a sample. Elements pertaining to the PANI backbone (C, N), 1-thio- β -D-glucose (C, O, S) and silver nanoparticles (Ag) were all found in the survey of silver nanoparticle modified glucose functionalized PANI film **16** as shown in Figure 6.9 and agreed with the EDX spectrum displayed previously.

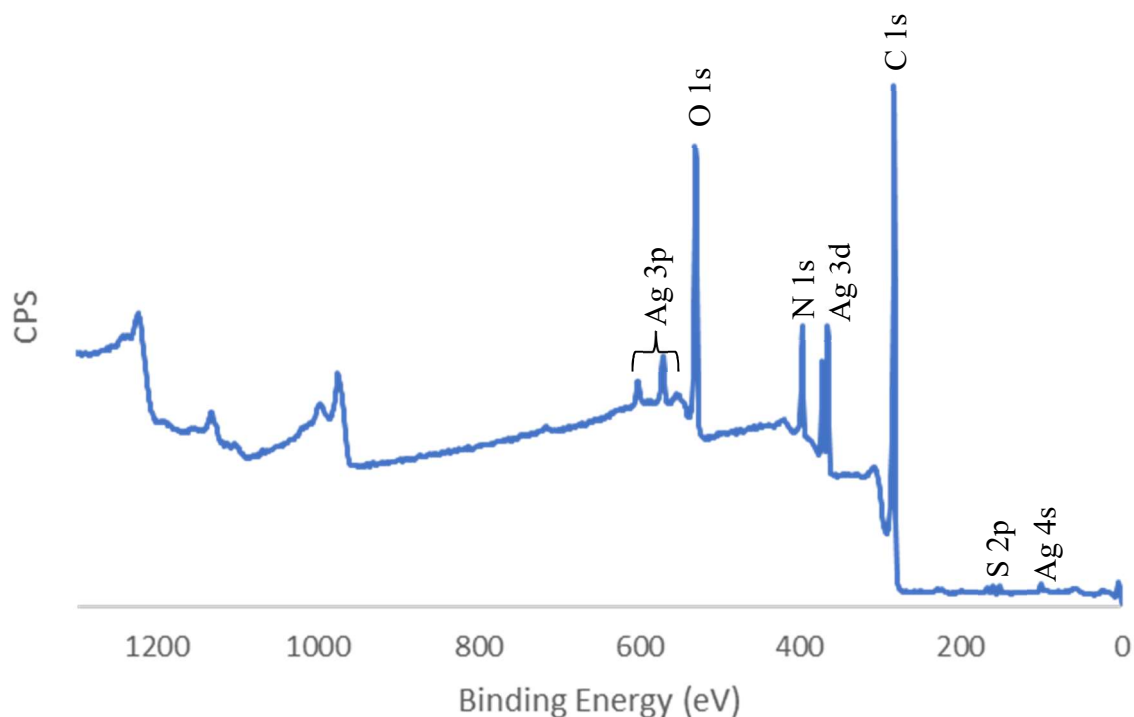


Figure 6.9: Survey scan of silver nanoparticle modified glucose functionalized PANI film **16**.

The C 1s core level spectrum of silver nanoparticle modified glucose functionalized PANI film **16** and **18** is shown in Figure 6.10. The scan for both **16** and **18** is deconvoluted into 4 separate peaks with similar peak assignments. The lowest binding energy peak was used to calibrate the spectra at 285.0 nm and is assigned as saturated carbon species and is used as a common charge reference.^{141,142} This peak also contains the aliphatic C-H and C-C functionality found from **16** and **18**. Carbon bound to nitrogen is observed at 285.5 eV, with this peak encompassing both the singly and doubly bond C-N, C=N bonds resulting from the amine and imine nitrogen species in the PANI backbone but may also contain the C-S functionality of 1- β -D-glucose tetraacetate bound to PANI. The two peaks found at higher binding energy result in the C 1s peak having an asymmetric peak shape. The deconvoluted peak found at 286.5 eV is a result of C-O and C=O bonds. Attachment of glucose to the PANI would impart a high concentration of

these bonds due to C-O-H and C-O-C. The final peak at the high energy tail end of the C 1s peak is typical of PANI and conducting polymer samples as it results from π - π^* satellite structures. The satellites occur due to excitation of valence electrons when a core hole is created, with the extent of conjugation of the aromatic system having a significant effect on the position and strength of the peak.¹⁶⁹

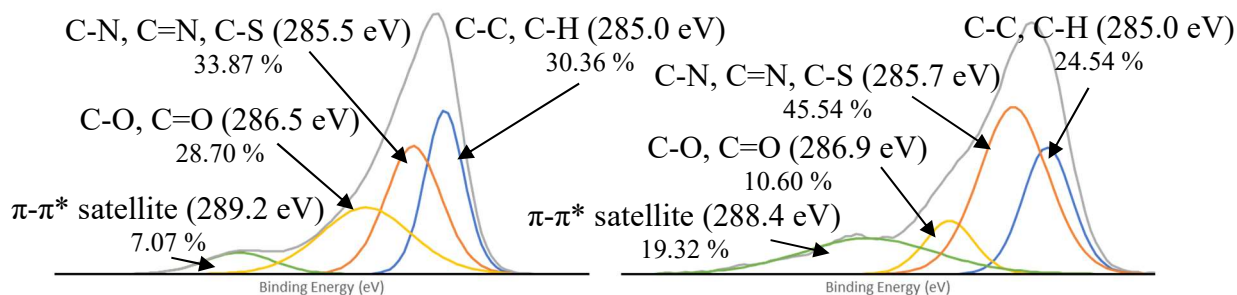


Figure 6.10: C 1s core level scan of silver nanoparticle modified glucose functionalized PANI film **16** (left) and silver nanoparticle modified glucose functionalized PANI film **18** (right).

Shown in Figure 6.11 is the N 1s core level spectrum for **16** and **18**. The N 1s spectrum of **16** is deconvoluted into three peaks, two small peaks either side of a large central peak. These peaks are found at 398.7, 400.2 and 402.8 eV. The peak at 400.2 eV, which is the largest peak found, has been assigned to the amine nitrogen, -N=, and results from a reduced PANI chain. Upon reduction of the silver nitrate salt to the metallic silver found in the nanoparticles the PANI backbone should become oxidised which would correspond to an increase in imine nitrogen's and the peak situated at *ca* 398.8 eV. However, route 1 (resulting in **16**) involves the subsequent attachment of 1-thio- β -D-glucose tetraacetate after the formation of the silver nanoparticles. This reaction, as previously explained in chapter 5, results in the reduction of the PANI chain with the attachment of the thiol. The initial oxidation of the PANI chain through the thiol-ene reaction results in a greater concentration of quinoidal rings which are subsequently able to be reduced in the thiol-ene reaction potentially maximising the attachment of the thiolated glucose. **16** showed a peak at a very high binding energy (402.8 eV) which results from the formation of charged nitrogen species, however, it was in relatively low concentration (2.7 %) in comparison with the amine nitrogen's (87.8 %). Das et al. synthesised folic acid-PANI hydrogel hybrids with attached silver nanoparticles for energy storage applications and reported similar results, a higher concentration of amine in comparison with imine nitrogen's along with the formation of charged nitrogen species.⁷⁷ Bhattarai et al. showed in their synthesis of PANI coated polystyrene nanoparticles an observed reduction in the amine peak with a non-proportional increase in the imine nitrogen peak as would be theoretically expected.¹⁷⁰ The excess nitrogen's were found to

form charged nitrogen species which they concluded were due to the chelation of the silver ions to the imine nitrogen's.

Silver nanoparticle modified glucose functionalized PANI film **18** showed a similar N 1s core level scan to that of **16**, however, no charged nitrogen species were found. A high concentration of the amine peak is observed (86.98 %) with the remaining nitrogen's being found as imine (13.02 %).

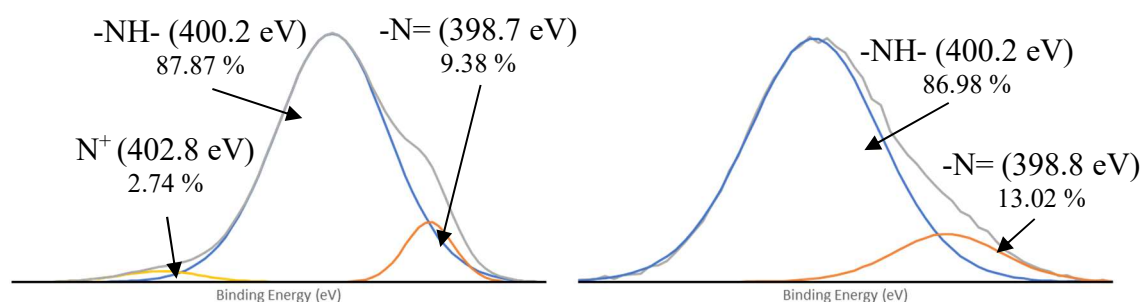


Figure 6.11: N 1s core level scan of silver nanoparticle modified glucose functionalized PANI film **16** (left) and silver nanoparticle modified glucose functionalized PANI film **18** (right).

The O 1s core level spectrum of **16** and **18** has been deconvoluted into three peaks each. As previously stated the O 1s spectra can be difficult to deconvolute unambiguously as many compounds and species have O 1s binding peaks in a very narrow range. Peaks also result from several impurities including adventitious hydrocarbons, water/moisture and oxidation. It is, however, very similar to the previous O 1s spectrum analysed in chapter 5. The inclusion of silver nanoparticles has not altered the O 1s core level scan at all and therefore the peak assignments have not changed. The lower energy peak is assigned as C-O resulting from both the glucose moiety and adventitious hydrocarbon impurities. The peak at 532.6 eV, while shifted to a higher binding energy peak by approximately 2 eV in comparison with the two previous chapters, is still assigned as the C=O peak, mainly from impurities due to atmospheric contaminants. Finally, the peak at 5324.1 eV is a result of S=O binding due to formation of R-SO₂-R' from the thiol found on glucose.

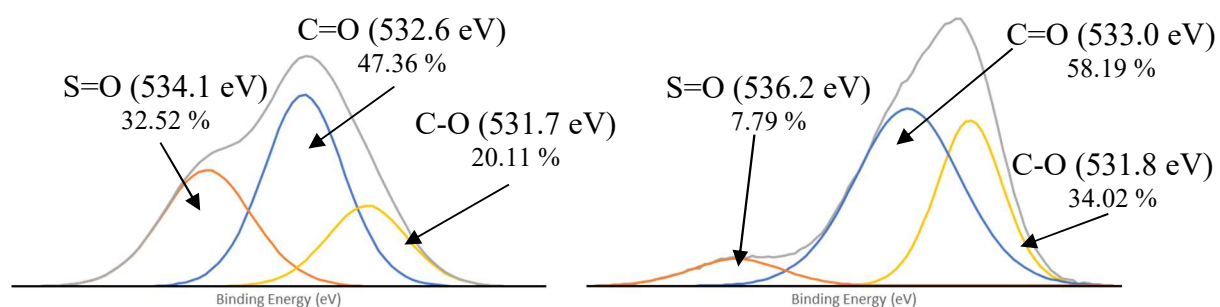


Figure 6.12: O 1s core level scan of silver nanoparticle modified glucose functionalized PANI film **16** (left) and silver nanoparticle modified glucose functionalized PANI film **18** (right).

In the current work sulfur has been found in two different environments for **16**, as is evident by two well defined doublets with the S 2p 3/2 peaks centred at 168.3 and 161.8 eV shown in Figure 6.13. Both doublets have a binding energy split of approximately 1.22 eV. The higher energy peak in the S 2p spectrum is nearly identical in binding energy to the S 2p peak found in 5.2.3. As mentioned in chapter 5 this is hypothesised to be a result of oxidation of the thio/thioether resulting in a sulfone, $-C-S(=O_2)-C-$. This sulfone acts as the bridge between the PANI substrate and the 1-thio- β -D-Glucose tetraacetate. The lower binding energy peak is found at 161.8 eV and is assigned as Ag-S-R. Battocchio et al. investigated the local chemistry and chemical structure of silver nanoparticles stabilised with thiols and found three S 2p peaks. The important correlation is that the S 2p peak found in the current work is observed at 161.8 eV and Battocchio et al. found it to be at 161.9 eV indicating that 1-thio- β -D-glucose has bound itself to the silver nanoparticle surface in **16**.^{171,172} Therefore, upon reaction of silver nanoparticle modified PANI film **14** with 1-thio- β -D-glucose tetraacetate, two different reactions occur resulting in the two different sulfur environments. Some of the thiolated glucose reacts with the surface of the silver nanoparticles resulting in an Ag-S-R bond while other thiolated glucose molecules react with the PANI surface resulting in a sulfonyl $-C-S(=O_2)-C-$ bond.

The S 2p spectrum resulting for silver nanoparticle modified glucose functionalized PANI film **18** shown in Figure 6.13 is different to that of **16** described above. While a similar S 2p 3/2 peak is found at 168.8 eV (168.3 eV for **16**) and has been assigned as the same functional group, the sulfone, the lower energy peak is observed at a different binding energy. This peak is found at 164.2 eV which is significantly higher than the peak resulting from sulfur bound to silver shown in Figure 6.13 leading to the conclusion that this route leads to no glucose bound to the silver surface, as formation of the nanoparticles has been conducted after the attachment of the glucose. This peak is assigned as a thioether R-S-R' which is the typical result of a thiol-ene reaction. The reasoning for this assignment is that if 1-thio- β -D-glucose tetraacetate remained

and was not covalently attached to the PANI surface, upon formation of the silver nanoparticles any unbound thiol would be expected to react with the silver. Because the Ag-S-R peak isn't observed it can be deduced that there is no unbound thiol after the thiol-ene reaction and that therefore the glucose moieties are bound covalently to the PANI surface. Therefore, for **18** both the thioether and sulfone bridges are found which has not been observed previously.

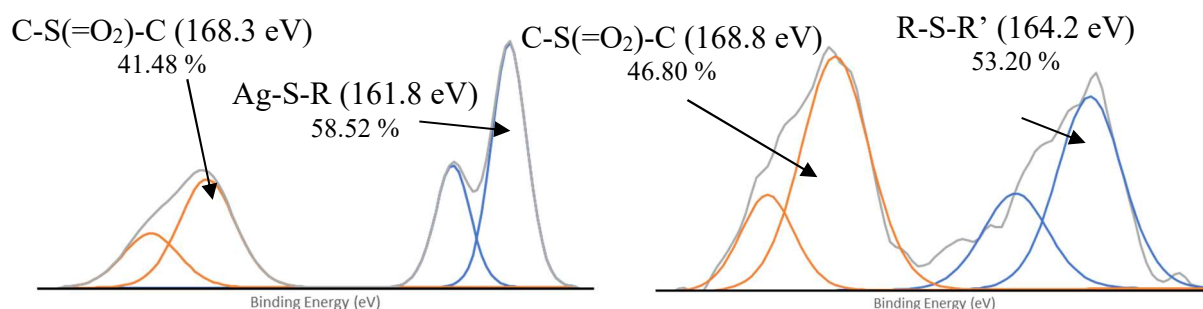


Figure 6.13: S 2p core level scan of silver nanoparticle modified glucose functionalized PANI film **16** (left) and silver nanoparticle modified glucose functionalized PANI film **18** (right).

The Ag 3d spectrum shown in Figure 6.14 indicates that the silver in **16** is found in two separate environments, with a definitive major and minor component. Ag 3d XPS spectra have spin orbit splitting similar to sulfur and result in a 3d 5/2 and 3d 3/2 with separation of 6.0 eV. The silver environment found in higher concentration has a 3d 5/2 binding energy of 368.7 eV whereas the 3d 5/2 binding energy of the minor component is 369.5 eV. Metallic ground state silver has been assigned to the peak located at 368.7 eV and has an energy split of 6.01 eV.¹⁷³⁻¹⁷⁵ The higher concentration for this peak (80 %) indicates that the silver in **16** is primarily in the ground state as expected for the synthesis of silver nanoparticles.

The Ag 3d 5/2 peak found at 369.5 eV is much lower in concentration than the ground state silver peaks (20 %). The S 2p core level scan shown previously concluded that some sulfur has reacted with the surface of the silver nanoparticle resulting in an Ag-S-R bond. It is therefore expected that this bonding arrangement would also be represented in the Ag 3d core level scan. Thakur et al. utilised XPS to analyse the Ag 3d core level of Ag-CdS nanoparticles and their spectral deconvolutions suggested that their peak was a result of binding between silver and sulfur which is the same conclusion that has been drawn through the present results.¹⁷⁶

The Ag 3d spectrum from the formation of **18** shows a single doublet peak as opposed to the two Ag 3d doublet peaks found from **16**. This peak is found at 368.9 eV and is in an identical position to the lower binding energy peak for **16**, which was assigned as metallic silver from the

silver nanoparticles. Therefore, the silver found in **18** occurs entirely as metallic silver from the silver nanoparticles and no glucose is found bound to the nanoparticles surface.

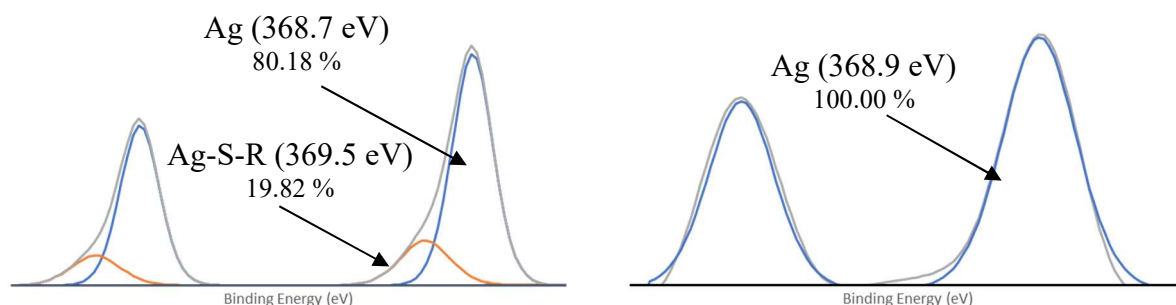


Figure 6.14: Ag 3d core level scan of silver nanoparticle modified glucose functionalized PANI film **16** (left) and silver nanoparticle modified glucose functionalized PANI film **18** (right).

The S 2p and Ag 3d core level spectra of **16** (Figures 6.13 and 6.14) suggest that 1-thio- β -D-glucose tetraacetate has reacted with both the PANI backbone, resulting in -C-(=SO₂)-C- bonds, as well as the silver nanoparticles resulting in an Ag-S-R peak in the S 2p spectrum and the Ag-S peak in the Ag 3d spectrum.

6.3.4. Conclusion on the Characterization of PANI containing silver nanoparticles and glucose

The reduction of silver (I) to silver (0) on the surface of PANI EB powder was initially used for the synthetic procedure to explore the potential of the reaction and produced silver nanoparticle modified PANI powder **14**. It was obvious that the redox reaction occurred as the longer reaction times utilised resulted in an obvious formation of silver nanoparticles on the surface of PANI powder **14**. Figure 6.15 shows how the formation of silver on the surface is easily observable.

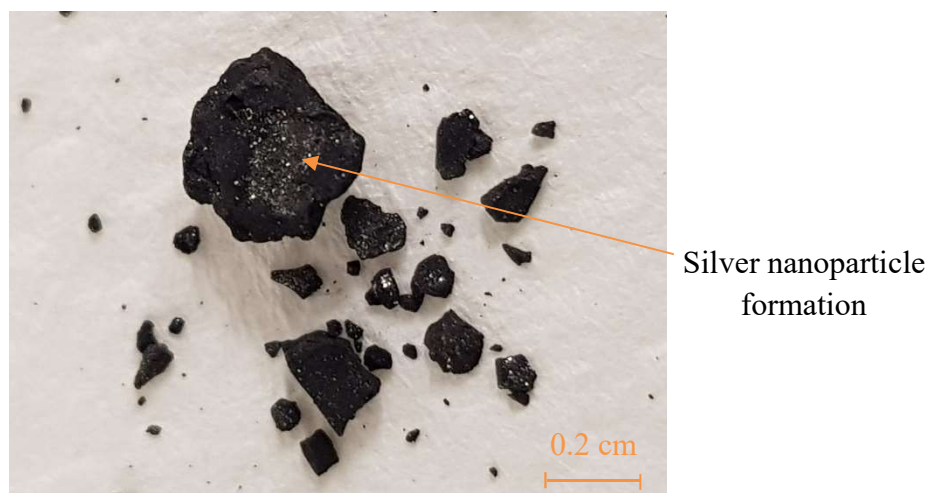


Figure 6.15: Photograph depicting the formation of silver particles on the surface of silver nanoparticle modified PANI **14** (powder).

After the proof of concept reaction was completed it was conducted on PANI EB films via two slightly different synthetic methods resulting in silver functionalized glycopolymers. Route 1 involved the reaction of PANI EB films with silver nitrate and subsequent thiol-ene reaction to attach the glucose unit resulting in silver nanoparticle modified glucose functionalized PANI film **16**. Route 2 reversed the order of silver and glucose attachment, so the PANI EB film was initially reacted with 1-thio- β -D-glucose tetraacetate and then subsequently silver nanoparticles were formed to the polymer surface forming silver nanoparticle modified glucose functionalized PANI film **18**.

In the reaction of silver nitrate with PANI, the silver gets reduced from Ag^+ to Ag^0 with oxidation of the PANI chain, theoretically resulting in more pernigraniline character. This would be expected to be shown in the N 1s core level XPS scan with an increase in the CPS of the peak corresponding to the imine nitrogens. However, it was observed in the N 1s core level scan of the products from both routes that majority of the nitrogens were in fact amines. This is expected for route 1 because the thiol-ene reaction as shown in chapter 5 would result in reduction of the PANI chain resulting in the increased amine nitrogen concentration observed. However, for route 2 this is unexpected because the silver reduction reaction occurs after the thiol-ene click reaction and the silver reaction results in oxidation of the PANI chain. Perhaps after the thiol-ene reaction, the attached glucose carbohydrate prevents access of the silver nitrate to the amines surface, preventing the oxidation of the PANI backbone. If this was the case, however, it would be expected that a lower concentration of silver nanoparticles would be formed on the surface of **18** in comparison with **16** which may result in a lower antimicrobial efficacy of the film.

The synthesis of the silver nanoparticles was conducted by soaking a PANI film in a solution of silver nitrate for 6 hours. It was found that by utilising this time that silver nanoparticles of approximately 100-200 nm could be prepared. Greater reaction times resulted in a metallic silver film forming as a coating over the PANI film, as per Figure 6.16.



Figure 6.16: Photograph of a PANI film with metallic silver film after reaction of silver nitrate for >6 hours. The PANI to silver transition occurs due to the experimental set up, the PANI films were placed vertically in a beaker and the level of the solution is depicted by the transition.

The S 2p and Ag 3d core level scans for route 1 showed that the subsequent reaction with 1-thio- β -D-glucose tetraacetate resulted in the thiol reacting with both the PANI and silver nanoparticles surface. Interestingly the comparison of the reaction products of route 1 and route 2 shows that the reaction of PANI EB with 1-thio- β -D-glucose tetraacetate results in the glucose becoming bound to the PANI surface, with the thiol undergoing the reaction. This conclusion is drawn because if 1-thio- β -D-glucose tetraacetate was simply adsorbed onto the surface of PANI and had not reacted and formed a covalent bond, A) it should have been removed in the solvent washing step and B) formation of the silver nanoparticles would result in the unbound thiol reacting with the silver surface which is observed for route 1 but not route 2. The XPS results showed that for route 2 there was only a single environment for metallic ground state silver. Route 1 showed two peaks in the Ag 3d scan representing both the metallic silver and Ag-S bond. Therefore, it was concluded that 1-thio- β -D-glucose tetraacetate reacts and is covalently bound to the PANI surface. Figures 6.17 and 6.18 show the experimentally derived reaction schemes for the synthesis of silver nanoparticle modified glucose functionalized PANI film **16-a** and silver nanoparticle modified glucose functionalized PANI film **18-a**.

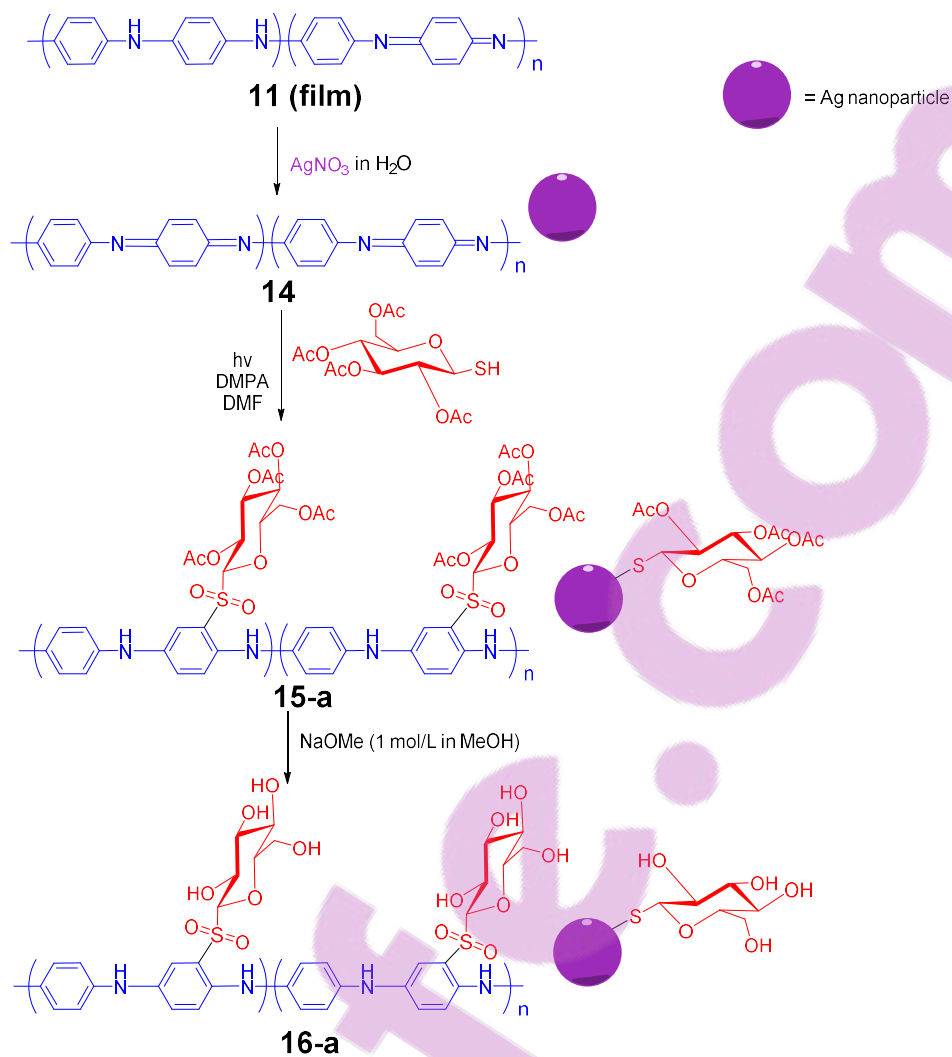


Figure 6.17: Empirical reaction pathway deduced for route 1, the synthesis of silver nanoparticle modified glucose functionalized PANI film **16-a**.

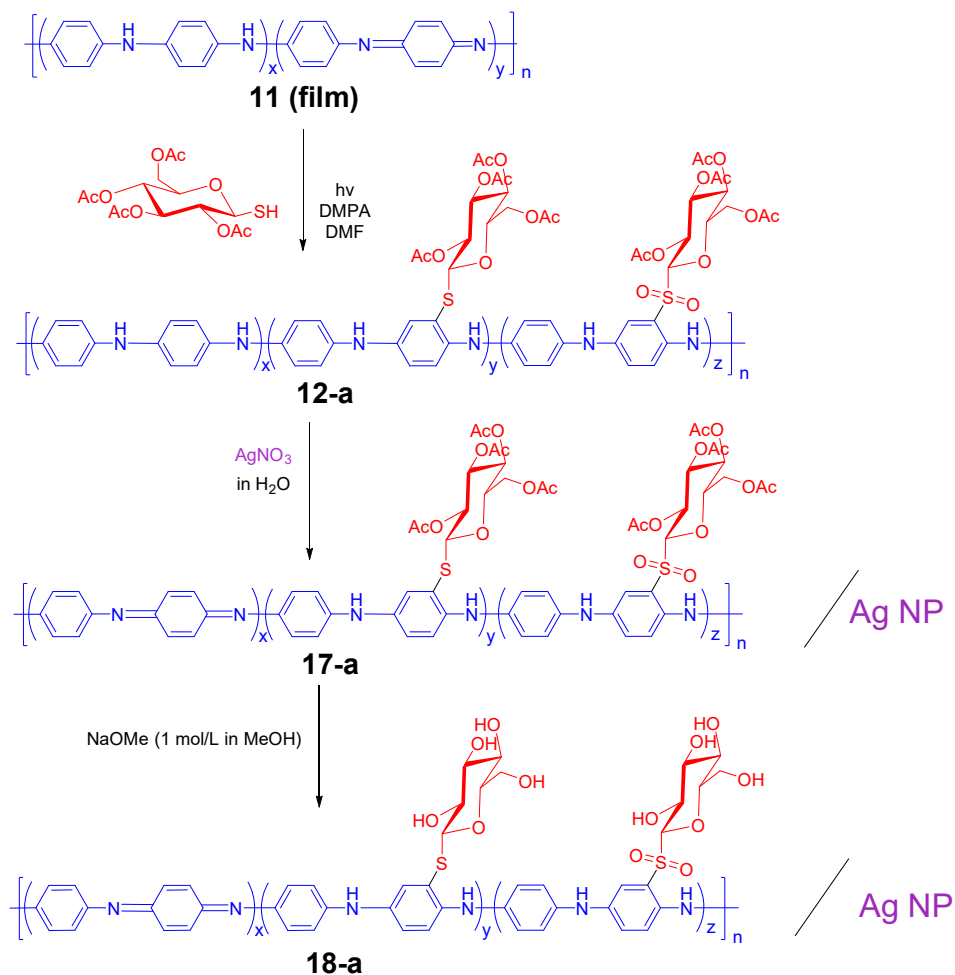


Figure 6.18: Empirical reaction pathway deduced for route 1, the synthesis silver nanoparticle modified glucose functionalized PANI film **18-a**.

6.3.5. Antimicrobial Ability of the Silver Nanoparticle Functionalized PANI Powders and Films

Silver functionalized PANI powder **14**, silver nanoparticle modified glucose functionalized PANI film **16** and silver nanoparticle modified glucose functionalized PANI film **18** were all analysed for their ability to eradicate bacterial cells. Powder **14** utilised the same method shown in chapters 3 and 4 whereas **16** and **18** utilised the method shown in chapter 5 due to the differences in morphologies.

6.3.5.1. Minimum Lethal Concentration of Silver Nanoparticle Functionalized Powders

The MLC is defined as the lowest concentration required to kill a microorganism after a period of incubation. The MLC of silver nanoparticle functionalized PANI powder **14** was studied to investigate the effect of the silver nanoparticles on the surface of PANI EB without the added

glucose. Figure 6.19 shows the MLC of silver nanoparticle functionalized PANI **14** (powder) against *S aureus* and *E coli* with the results tabulated in table 6.1.

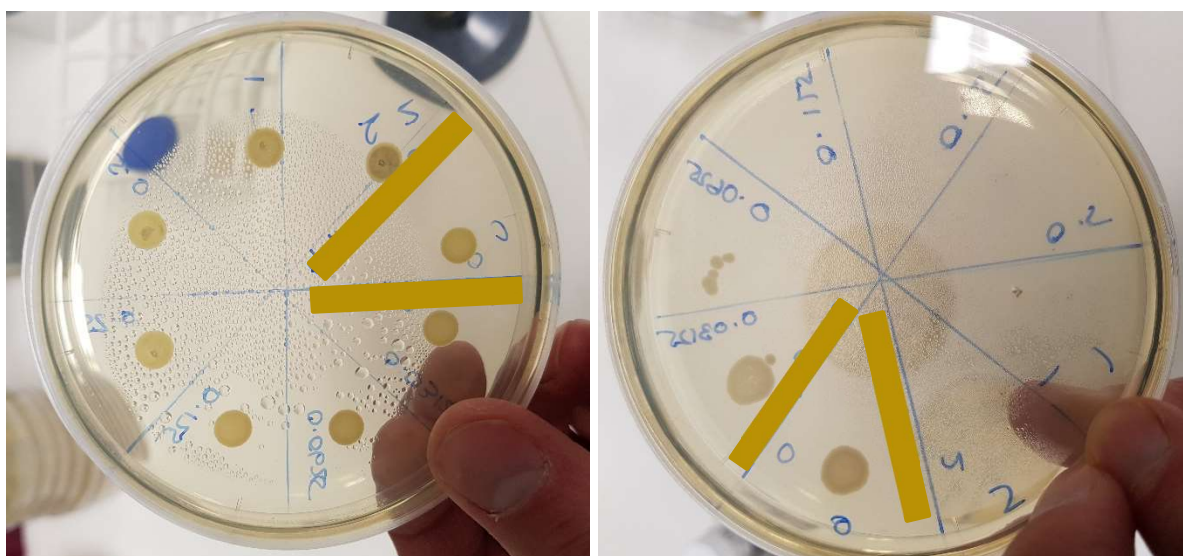


Figure 6.19: Photographs showing the results of the MLC analysis of silver nanoparticle modified PANI powder **14** against *S aureus* (left) and *E coli* (right) after 4 hours.

An aliquot of culture exposed to the test samples was taken after 4 and 24 hours and incubated after spotting on TSA to determine if any bacteria survived the challenge, with the lowest concentration resulting in no growth being described as the MLC. Silver nanoparticle adsorbed PANI **14** (powder) had a profound effect against *E coli* after only 4 hours of exposure, with a concentration of 0.125 wt % being enough to prevent any growth of the bacteria when the aliquot was spread on an agar plate. After 24 hours exposure, a concentration of 0.0625 wt % was enough to kill the bacterial inoculum. Interestingly, when comparing against gram positive bacteria *S aureus*, **14** (powder) had a much weaker biocidal effect. Exposure for 4 hours proved ineffective against this bacterium, resulting in confluent growth at all the concentrations analysed. Inoculating for 24 hours did allow **14** (powder) to show a biocidal effect against *S aureus* with 0.5 wt % resulting in significant knock down of the cells. 1 wt % of **14** (powder) after 24 hours eradicated all the cells and prevented any growth of *S aureus*. These results showed that the inclusion of silver nanoparticles onto **14** (powder) had a positive effect on the antimicrobial efficacy of PANI EB.

	Minimum Lethal Concentration (wt %)			
	4 hour inoculation		24 hour inoculation	
Bacterial Strain	PANI EB (powder)	silver nanoparticle modified PANI 14	PANI EB (powder)	silver nanoparticle modified PANI 14
<i>Staphylococcus aureus</i> 6538	> 1	> 1	> 1	0.5
<i>Escherichia coli</i> 25922	> 1	0.125	> 1	0.0625

Table 6.1: Mean MLC of silver nanoparticle modified PANI **14** (powder) over three triplicates against both *S aureus* and *E coli* after 4 and 24 hours. Note that the maximum polymer concentration analysed was 1 wt %.

6.3.5.2. Minimum Bactericidal Concentration of PANI/Ag NP/Glucose Functionalized Films

The MBC of an antimicrobial agent is the lowest concentration required to kill the bacteria, which is observed by prevention of cellular growth after removal of the antimicrobial agent from the inoculum. The method utilised to determine the MBC of the synthesised films measured the difference between the optical density (at 600 nm) after 0 and 16 hours post rescue and is plotted to investigate the viability of the cells after being challenged by an antimicrobial surface. If bacteria in the inoculum survived the challenge of the antimicrobial film, when they are placed in a nutrient rich medium and incubated they will begin to grow and multiply and an increase in the optical density will be observed. If they have been killed, however, no growth will occur after incubation. In this experiment the concentration of the antimicrobial surface is constant and the experiment simply determined whether the film was bactericidal against a certain concentration of inoculated bacteria.

Figure 6.20 shows the results of the challenge by **16**, **18** and PANI EB film **11** against *E coli*, in comparison with a control sample. The control sample had the highest recorded optical density from the three treatments, however, all three responded with an increase in detected cells after 16 hours revealing that these treatments were ineffective against *E coli* at the tested concentrations. **16** showed the lowest increase in OD₆₀₀ over 16 hours indicating that it potentially eradicated some of the cells in the inoculum and resulted in a low knockdown.

Kruskal-Wallis' non-parametric test (followed by Dunn's post hoc test) indicates that treatment of the bacterial cells with **16** is significantly different from that of the control sample (P value <0.05), however, treatment with **18** and PANI EB film **11** resulted in a non-significant difference in comparison with the control (P value >0.05). Low levels of cell knockdown have therefore been concluded to have occurred for the *E coli* cells inoculated on **16**.

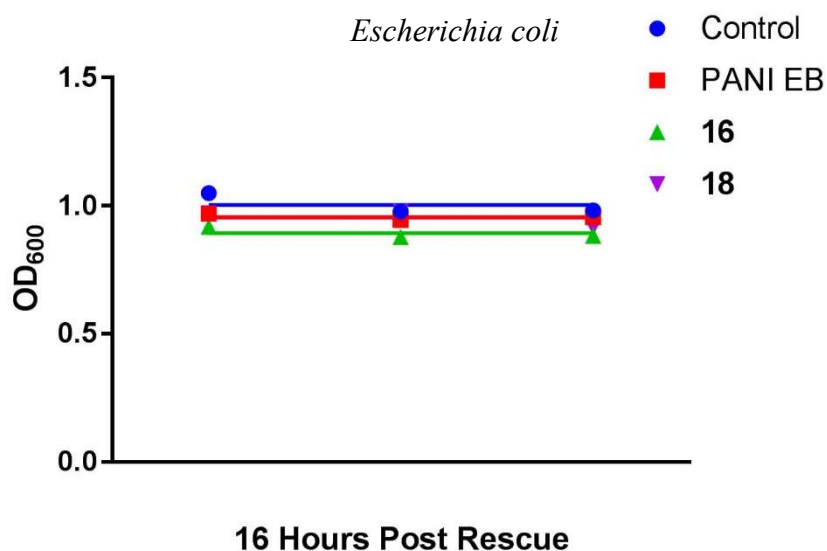


Figure 6.20: Difference in OD₆₀₀ over three replicates post rescue of *E coli* on control, PANI EB film **11**, silver nanoparticle modified glucose functionalized PANI film **16** and silver nanoparticle modified glucose functionalized PANI film **18** surfaces. Each point represents a biological replicate with the line representing the mean of the replicates. The standard deviation for each treatment is as follows; control 0.03989, PANI EB film 0.01253, silver nanoparticle modified glucose functionalized PANI film **16** 0.02179 and silver nanoparticle modified glucose functionalized PANI film **18** 0.03396.

Figure 6.21 shows the same test against *S aureus*, a gram-positive bacterial strain. The difference in OD₆₀₀ at 0 and 16 hours of PANI EB film **11** and the control both increased, indicating that the number of viable cells was not reduced and were therefore able to begin growing once transferred to a nutrient rich medium. These treatments were ineffective against *S aureus* as the Kruskal-Wallis non-parametric test (followed by Dunn's post hoc test) determined that the PANI EB film **11** result was not significantly different from that of the control sample (P value >0.05). Glucose functionalized silver nanoparticle modified PANI films **16** and **18**, however, exhibited nearly no increase in OD₆₀₀ after 16 hours, indicating that these treatments were effective at eradicating the cells on the film surface. As can be expected, the difference between the results of **16** and the control and **18** and the control, as determined by the Kruskal-Wallis

non-parametric test with Dunn's post hoc test, is indeed significantly different proving that they are an effective antimicrobial surface against *S aureus*. The glucose that occurs bound to the silver nanoparticles in the synthesis of silver modified acetyl protected glucose functionalised PANI film **16** appears to have not hindered the antimicrobial efficacy of the silver nanoparticles towards *S aureus*, however, it cannot be concluded to have increased this ability due to the complete eradication of the cells for both treatments.

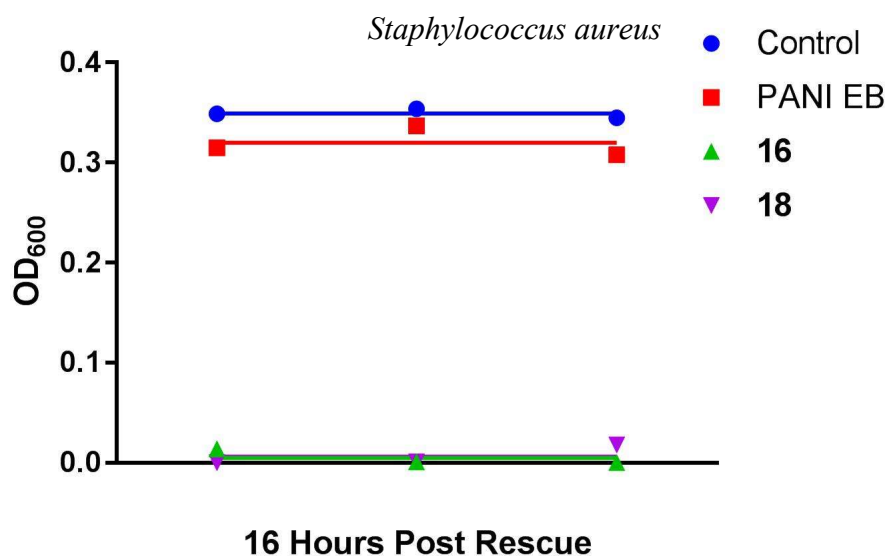


Figure 6.21: Difference in OD₆₀₀ over three replicates post rescue of *S aureus* on control, PANI EB film **11**, silver nanoparticle modified glucose functionalized PANI film **16** and silver nanoparticle modified glucose functionalized PANI film **18** surfaces. Each point represents a biological replicate with the line representing the mean of the replicates. The standard deviation for each treatment is as follows; control 0.00451, PANI EB film 0.01513, silver nanoparticle modified glucose functionalized PANI film **16** 0.00781 and silver nanoparticle modified glucose functionalized PANI film **18** 0.01012.

Silver nanoparticles adhered to PANI films with glucose showed greater effectiveness against *S aureus* than *E coli*, however, a significant difference was found for both cell cultures in comparison with a control for *S aureus*. The antimicrobial action of these films is shown to be completely due to the silver nanoparticles as PANI EB film **11** and glucose functionalized PANI film **13** (chapter 5.3.7), which was also tested showed no activity against either bacterial strain with no significant difference (P values >0.05).

The activity of silver nanoparticles is dependent on several factors including size and shape. The size of the nanoparticles is important, as the high surface area to volume ratio allows better interaction of the silver nanoparticle with the bacterial cell wall, so therefore a smaller

nanoparticle which has higher surface areas would be more antimicrobial than a larger nanoparticle. As analysed the nanoparticles synthesised in this work were in the range of 100-200 nm. Morones et al. found that nanoparticles in the range of 1-10 nm were effective against *E coli* potentially indicating that the larger size of the nanoparticles in the present research hindered antimicrobial effectiveness.¹⁷⁷ Adjustment of the reaction time to less than 6 hours may promote the formation of smaller nanoparticles. Gomaa studied the inhibition of *S aureus* and *E coli* as models for the inhibition of gram-positive and negative bacteria by silver nanoparticles, and while the strains were different to those used in the present research, came to some interesting conclusions.¹⁷⁸ The size of the silver nanoparticles were hypothesised to have a significant affect and their average diameter of 17 nm was significantly smaller than the particles synthesised in the current research. Samples inoculated with silver nanoparticles showed increased leakage of proteins and reducing sugars along with formation of reactive oxygen species in comparison with the control samples. It was found that only after incubation for four to six hours with silver nanoparticles was a considerable increase in membrane leakage observed. It was noted that in all cases that *S aureus* was much more sensitive to treatment in comparison with *E coli* which confirms the results found presently but also the general theme that gram-negative bacteria are more resistant to antimicrobial treatment than gram-positive.

6.4. Conclusion

PANI surfaces (both powders and films) were successfully functionalized with silver nanoparticles. Films containing surface bound glucose along with the silver nanoparticles were successfully synthesised by utilising thiol-ene chemistry and a redox reaction of PANI with silver nitrate. Two different synthetic routes were analysed to determine the optimal path to a highly antimicrobial polymer film surface while also investigating any effects the difference in reaction order may impose. Synthetic route 1 involved the reduction of silver nitrate to silver nanoparticles on the surface of PANI EB films. Subsequent thiol-ene reaction with 1-thio- β -D-glucose tetraacetate resulted in the thiol group interacting with both the PANI chain and the surface of the silver nanoparticles which was confirmed via XPS of both the sulfur 2p and silver 3d core level scans. Synthetic route 2 involved the initial thiol-ene reaction of 1-thio- β -D-glucose tetraacetate as per chapter 5 with subsequent formation of the silver nanoparticles on the surface of the PANI film. This synthetic route removed the interaction of the thiolated glucose with the silver nanoparticles which was evident by the shift of one of the peaks in the sulfur 2p core level scan and complete removal of one of the peaks in the silver 3d core level scan.

For both routes it was found control of the size of the nanoparticles in the reaction involving the reduction of silver in silver nitrate to silver nanoparticles could be controlled via reaction time as opposed to other conditions such as reagent concentration. Redox reactions that were conducted for 12 hours resulted in a film of metallic silver forming over the surface as opposed to the desired nanoparticle morphology. When the reaction times were reduced to 6 hours, however, silver nanoparticles in the range of 100-200 nm were produced. This result was consistent across a range of silver nitrate concentrations indicating that under these conditions the reaction time is more important than the concentration of the silver nitrate. Potentially smaller, more biocidal nanoparticles could be formed with further reduced reaction times.

The films produced from both synthetic routes had very similar antimicrobial properties against both gram-positive and gram-negative bacteria. They proved effective at killing 10^4 CFU/mL of the gram-positive bacteria *S aureus*, however, proved ineffective at completely killing the *E coli* cells. This shows that the attachment of the glucose onto the surface of the silver nanoparticles as per synthetic route 1 did not alter the antimicrobial properties of the resulting polymer film. Further work in this area should look at the nanoparticle size as a simple means to attempt to increase the bactericidal effect against gram-negative bacteria as it is shown in the literature that nanoparticles <100 nm are significantly more potent. Salem et al. conducted a similar reaction method to synthesise silver nanoparticles on PANI but showed that a reaction time of 3 hours under shaking produced nanoparticles in the range of 5-15 nm.⁷⁵ Comparison of the effect of the attached glucose should also be further explored to deduce the effect glucose has on the overall bactericidal ability of the polymer film. Finally, looking into the ability of the glucose to retain its structure after doping or investigation of alternative doping reagents may result in a significant increase in its bactericidal ability as the ES form is much more potent than the EB form.

Chapter 7. Conclusion

The hypothesis of this work was to enhance the antimicrobial ability of PANI and increase its potency by attachment of carbohydrates to form a PANI glycopolymer. The increase in antimicrobial ability was anticipated to be increased due to a synergistic and interactive effect created by the carbohydrate, as many species of bacteria show selective binding to carbohydrates. The initial chapter investigated the synthesis of a carbohydrate functionalized aniline monomer, with subsequent attempted polymerization of the functionalized aniline. Successful formation of mannose functionalised aniline **2** was shown by ^1H and ^{13}C NMR along with HRMS. Polymerization of **2** resulted in the successful formation of mannose functionalised PANI **4** although in relatively low yields compared with typical neat PANI syntheses. FTIR and UV-Vis both contained absorptions and excitations resulting from both the PANI and mannose structures while the confirmed retention of the C:N ratio of 6:1 was observed for neat PANI and **4**. GPC showed two peaks indicating a dimeric by-product along with the polymer which confirmed a lot of the earlier characterization techniques which were also displaying dimeric structures. The dimerization was hypothesised to be a result of head-to-head polymerization due to the large mannose structure imparting a steric effect during the reaction. Biological activity of **4** was investigated via a ConA binding assay. As mentioned previously ConA is a lectin that is highly specific towards mannose and glucose, although glucose is less attractive to it. The ConA binding study showed that **4** successfully interacted and bound ConA resulting in precipitation of the ConA-**4** complex. The ConA-**4** precipitate was also successfully dissolved by addition of methyl- α -D-mannoside showing that the interaction was due to the mannose structure on **4**. The antimicrobial ability of the polymer was also investigated against *E coli* and *S aureus* which unfortunately showed that **4** had no antimicrobial ability against either or the mentioned bacteria up to 1 wt %. Methods to improve the bactericidal ability of **4** were hypothesised such as improved/altered dopant ions which may also improve the molecular weight and reduce the likelihood of by-products via a templating type scheme.

Due to the limitations of the first reaction surrounding low molecular weight and the formation of by-products, a second route to counteract these issues was explored. Synthesis of a functionalised PANI which could take part in a click reaction, rather than aniline was expected to bypass both the primary issues found earlier as there would be no steric effects during the polymerization reaction. However, it was recognised that by utilising this method it would be difficult to achieve 100 % attachment of carbohydrate to the backbone as PANI is difficult to process. The chemical synthesis involved sulfonation of the PANI backbone, which has been shown previously in the literature, and reduction of the sulfonic acid to a thiol to allow the PANI

to take part in a thiol-ene click reaction. The reduction of sulfonic acid to thiol on PANI had not been shown to any extent in the literature and had primarily been shown on aromatic groups utilising a PPh_3/I_2 system. By utilising the reported reaction conditions it resulted in thiolated PANI **8-a**, which contained both thiol and unconverted sulfonic acid. Self-doping of the nitrogen rings occurred with the sulfonic acid moieties on both **8-a** and **10-a** as shown by the N 1s core level scans displaying charged nitrogen states. S 2p scans showed that the reduction of the sulfonic acid was incomplete, however, some conversion to thiol did occur. Also required was allylic mannose **9** which would be the corresponding unsaturated compound to click to thiolated PANI and was successfully synthesised according to the literature. The click reaction was completed, and presence of the mannose structure was observed in the FTIR and XPS spectra confirming attachment to the thiol groups. Finally, the antimicrobial ability of **10-a** was examined using the same method as for **4** with similar results showing that **10-a** was not effective up to 1 wt % against either *S aureus* or *E coli*.

The synthesis of PANI films were an interesting method towards forming antimicrobial surfaces. PANI films were shown to be possible through the literature and the formation of brilliant blue coloured films was successful. Also interesting was the reports noting that PANI could potentially directly take part in the thiol-ene reaction, as the unsaturated “ene” group which is unusual as aromatic groups are not unsaturated in the typical sense due to their resonance structures. However, the potential for PANI to directly take part in the thiol-ene reaction was promising and a PANI glycopolymer was attempted via thiol-ene reaction with 1-thio- β -D-glucose tetraacetate. Successful reaction resulted in the inclusion of 1-thio- β -D-glucose tetraacetate onto the surface of glucose functionalized PANI film **13** which was confirmed through concurrent peaks for both the PANI in the FTIR and the presence of elevated sulfur in the EDX. The S 2p core level scan showed the sulfur peak at a high binding energy, 168.4 eV, whereas R-S-R' was expected to be at approximately 162-164 eV. Therefore, it was hypothesised that the sulfur has oxidised resulting in an R-SO₂-R' type bond which would be expected at this binding energy. While sulfonic acids were shown in chapter 4 to be found at 168 eV as well, due to the inability to remove the glucose it was therefore concluded to be covalently bound to the PANI and therefore exist as a sulfone. The conclusion of the characterization showed the unusual ability of the aromatic PANI backbone to act as an “ene”. A different experiment was utilised for the analysis of the bactericidal effect of the films surface. Bacteria were introduced to the films surface for a period and then were rescued and placed in nutrient rich media. If they survived the surface challenge they would therefore grow which could be detected via an increase in optical density. The experiment showed that glucose

functionalised PANI film **13** was not antimicrobial as it offered no reduction in cell viability in comparison with a pure PANI EB film and a negative control.

Finally, due to the promising results from the previous chapter involving PANI films and the ability of PANI to be a direct player as the “ene” in the thiol-ene reaction, improvement of the bacterial efficacy by attaching silver nanoparticles was explored. The power of PANI has been recognised via all these reactions shown previously, however, to further add to its repertoire it was shown that it can also successfully reduce the silver ions found in silver nitrate to silver metal, resulting in silver nanoparticles. The reaction of PANI films with and without glucose with silver nitrate resulted in silver nanoparticle modified glucose functionalized PANI film **16** and **18**. The XPS results indicated that the reaction order had a large effect on the final product as **16** resulted in a sulfone bond between the glucose and PANI post thiol-ene reaction but also some of the thiol had become bound to the silver nanoparticles surface. **18** showed a mixture of thioether and sulfone bonds, however, the silver nanoparticles were pure and had no thiol attachment. The nanoparticles formed on **16** and **18** were observed by SEM and found to be in the range of 100-200 nm in diameter. Silver nanoparticle modified PANI **14** (powder) was initially synthesised to observe the ability of PANI to reduce silver nitrate and was also tested for its MLC against *S aureus* and *E coli*. **14** showed effective antimicrobial ability against *E coli* with 0.125 wt % being able to prevent any growth after 4 hours incubation and 0.0625 wt % being effective after 24 hours inoculation. **14**'s efficacy against *S aureus* was weaker with 4 hours inoculation being ineffective up to 1 wt %, however, 0.5 wt % was effective after 24 hours inoculation. The analysis of MBC of **16** and **18** showed that even though there were variations in their structures, they both behaved the same against *S aureus* and *E coli*. They both were ineffective against 10^4 CFU of *E coli* showing no improvement relative to PANI EB film **11** or the control. However, against *S aureus* the two films showed complete eradication of the microbial cells.

7.1. Future Work

The functionalized aniline molecule synthesised in chapter 3 was a promising premise, however, due to the large triazole and carbohydrate, the polymerization wasn't as simple or robust as hoped. While a polymer did form, an unwanted side reaction resulting in a dimeric by-product also occurred. While the difficulty arose from the relatively large pendant groups on aniline, potential templating methods such as using alternative doping reagents (toluenesulfonic acid etc) may be able to overcome the steric hindrance, forcing the polymerization to occur in a head-to-tail fashion and increasing the chain length. Another important avenue to analyse, which may

prove beneficial for the antimicrobial ability of PANI glycopolymers, is to investigate the choice of acid dopant and concentration. While hydrochloric acid was chosen due to its historical use in the syntheses of PANI it appears to not be the optimal choice when dealing with carbohydrates. Milder dopants which still result in the ES form, the stronger antimicrobial form, may be beneficial in increasing the biocidal potency. However due to the limited amounts of the precious monomer, the full analysis of varying dopants was restricted. Copolymerization is also a very promising option to overcome the present challenges resulting from the inclusion of the carbohydrate moiety. By copolymerizing the functionalized aniline monomer with aniline, the aniline will be able to act as a spacer group increasing the distance between the carbohydrates and hopefully promoting coupling of the molecules in the *para* position, where it is favoured during reactions of PANI. By the inclusion of aniline as a comonomer this will also allow control of the carbohydrate density, which can allow investigation of the effects on binding at different carbohydrate loadings.

By using the extremely hazardous fuming sulfuric acid, sulfonated PANI was produced as per the literature. The reduction of the sulfonic acid group on PANI was promising theoretically, however, did not result in 100 % conversion from the sulfonic acid to the thiol. By altering the reagent concentrations potential increases in the thiol concentration may be found. Other reagent systems such as more powerful reducing agents (e.g. lithium based reductants) may also improve the overall reaction. There is massive potential in being able to reduce sulfonic acids to thiol not just in the synthesis of functionalized PANI but in other important areas where the thiol-ene click reactions can be utilised to form PANI's with different end goals.

PANI films are shown to be capable of forming on a large variety of substrates. The ability to form these films quickly and easily could produce unique surfaces for many applications. The ability of polyaniline to take part in the thiol-ene reaction, as the alkene unit, is very interesting because the aromaticity of the rings is not considered a typical alkene. Further investigation into this reaction, along with potential analyses to improve the attachment rate, could result in this reaction becoming a wide spread method of synthesising libraries of PANI via simple attachment of different thiolated molecules. The ability of the thiol-ene reaction to be conducted on electrochemically synthesised films may also be beneficial due to the control exerted on the PANI product in utilising the electrochemical method.

Finally, chapter 6 showed the surface attachment of silver nanoparticles to polyaniline films. The ease at which these nanoparticles were formed, with control on their size being shown through reaction time rather than concentration, could demonstrate several uses in quickly forming antimicrobial surfaces. One conclusion drawn was that the size of the nanoparticles are

very important in their biocidal ability, with nanoparticles with sizes <100 nm being highly potent agents when comparing the products synthesised in chapter 6 with the literature. The current research synthesised particles in the range of 100-200 nm therefore production of silver nanoparticles of smaller size, perhaps by further reducing reaction time, should increase the potency of these PANI films.

References

1. Shirakawa, H.; Louis, E.; MacDiarmid, A. G.; Chiang, C. K.; Heeger, A. J. Synthesis of Electrically Conducting Organic Polymers: Halogen Derivatives of Polyacetylene, $(\text{CH})_x$. *J. C. S. Chem. Comm* **1977**, 578.
2. Xia, L.; Wei, Z.; Wan, M. Conducting polymer nanostructures and their application in biosensors. *Journal of Colloid and Interface Science* **2010**, 341, 1.
3. Bhadra, S.; Khastgir, D.; Singha, N. K.; Lee, J. H. Progress in preparation, processing and applications of polyaniline. *Progress in Polymer Science* **2009**, 34, 783.
4. Kaneto, K.; Kaneko, M.; Min, Y.; MacDiarmid, A. G. "Artificial muscle": Electromechanical actuators using polyaniline films. *Synthetic Metals* **1995**, 71, 2211.
5. Chen, X.; Liu, J.; Qian, K.; Wang, J. Ternary composites of Ni-polyaniline-graphene as counter electrodes for dye-sensitized solar cells. *RSC Advances* **2018**, 8, 10948.
6. Latonen, R.; Maattanen, A.; Ihalainen, P.; Xu, W.; Pesonen, M.; Nurmi, M.; Xu, C. Conducting ink based on cellulose nanocrystals and polyaniline for flexographical printing. *Journal of Materials Chemistry C* **2017**, 5, 12172.
7. Wang, J.; Zhang, D. One-Dimensional Nanostructured Polyaniline: Syntheses, Morphology Controlling, Formation Mechanisms, New Features, and Applications. *Advances in Polymer Technology* **2013**, 32, E323.
8. Yin, Z.; Zheng, Q. Controlled Synthesis and Energy Applications of One-Dimensional Conducting Polymer Nanostructures: An Overview. *Advanced Energy Materials* **2012**, 2, 179.
9. Yu, P.; Cardona, M. *Fundamentals of Semiconductors*; Springer Berlin Heidelberg: 2010; , pp 775.
10. MacDiarmid, A. G.; Epstein, A. J. The concept of secondary doping as applied to polyaniline. *Synthetic Metals* **1994**, 65, 103.
11. Letheby, H. On the production of a blue substance by the electrolysis of sulphate of aniline. *Journal of the Chemical Society, Transactions* **1862**, 15, 161.
12. Tran, H. D.; D'Arcy, J. M.; Wang, Y.; Beltramo, P. J.; Strong, V. A.; Kaner, R. B. The oxidation of aniline to produce "polyaniline": a process yielding many different nanoscale structures. *Journal of Materials Chemistry* **2011**, 21, 3534.
13. Thanpicha, T.; Sirivat, A.; Jamieson, A.; Rujiravanit, R. Preparation and characterization of polyaniline/chitosan blend film. *Carbohydrate Polymers* **2006**, 64, 560-568.
14. D'Aprano, G.; Leclerc, M.; Zotti, G. Stabilization and Characterization of Pernigraniline Salt: The "Acid-Doped" Form of Fully Oxidized Polyanilines. *Macromolecules* **1992**, 25, 2145.
15. MacDiarmid, A.; Chiang, J.; Richter, A. Polyaniline: A New Concept in Conducting Polymers. *Synthetic Metals* **1987**, 18, 285.

16. Sinn, H.; Kaminsky, W. Ziegler-Natta Catalysis. *Advances in Organometallic Chemistry* **1980**, *18*, 99.
17. Stejskal, J.; Gilbert, R. Polyaniline. Preparation of a Conducting Polymer. *International Union of Pure and Applied Chemistry* **2002**, *74*, 857-867.
18. MacDiarmid, A. G.; Jones, W. E.; Norris, I. D.; Gao, J.; Johnson, A. T.; Pinto, N. J.; Hone, J.; Han, B.; Ko, F. K.; Okuzaki, H.; Llaguno, M. Electrostatically-generated nanofibers of electronic polymers. *Synthetic Metals* **2001**, *119*, 27.
19. Cao, Y.; Andreatta, A.; Heeger, A. J.; Smith, P. Influence of chemical polymerization conditions on the properties of polyaniline. *Polymer* **1989**, *30*, 2305.
20. Pruneanu, S.; Veress, E.; Marian, I.; Oniciu, L. Characterization of polyaniline by cyclic voltammetry and UV-Vis absorption spectroscopy. *Journal of Materials Science* **1999**, *34*, 2733-2739.
21. Ciric-Marjanovic, G.; Konyushenko, E. N.; Trchova, M.; Stejskal, J. Chemical oxidative polymerization of anilinium sulfate versus aniline: Theory and experiment. *Synthetic Metals* **2008**, *158*, 200.
22. Genies, E. M.; Boyle, A.; Lapkowski, M.; Tsintavis, C. Polyaniline: A Historical Survey. *Synthetic Metals* **1990**, *36*, 139.
23. Pron, A.; Genoud, F.; Mendardo, C.; Nechtschein, M. The Effect of the Oxidation Conditions on the Chemical Polymerization of Polyaniline. *Synthetic Metals* **1988**, *24*, 193.
24. Blinova, N. V.; Stejskal, J.; Trchova, M.; Prokes, J.; Omastova, M. Polyaniline and polypyrrole: A comparative study of the preparation. *European Polymer Journal* **2007**, *43*, 2331.
25. Wudl, F.; Angus Jr, R. O.; Lu, F. L.; Allemand, P. M.; Vachon, D. J.; Nowak, M.; Liu, X. Z.; Heeger, A. J. I. Poly(*p*-phenyleneamineimine): Synthesis and Comparison to Polyaniline. *Journal of the American Chemical Society* **1987**, *109*, 3677.
26. Stejskal, J.; Sapurina, I.; Trchova, M. Polyaniline nanostructures and the role of aniline oligomers in their formation. *Progress in Polymer Science* **2010**, *35*, 1420-1481.
27. Zujovic, Z. D.; Laslau, C.; Bowmaker, G. A.; Kilmartin, P. A.; Webber, A. L.; Brown, S. P.; Travas-Sejdic, J. Role of Aniline Oligomeric Nanosheets in the Formation of Polyaniline Nanotubes. *Macromolecules* **2010**, *43*, 662.
28. Stejskal, J.; Trchova, M. Aniline oligomers versus polyaniline. *Polymer International* **2012**, *61*, 240-251.
29. Trchova, M.; Sedenkova, I.; Konyushenko, E. N.; Stejskal, J.; Hollder, P.; Ciric-Marjanovic, G. Evolution of Polyaniline Nanotubes: The Oxidation of Aniline in Water. *Journal of Physical Chemistry B* **2006**, *110*, 9461.
30. Sinha, S.; Bhadra, S.; Khastgir, D. Effect of Dopant Type on the Properties of Polyaniline. *Journal of Applied Polymer Science* **2009**, *112*, 3135.

31. Bhadra, J.; Madi, N. K.; Al-Thani, N. J.; Al-Maadeed, M. A. Polyaniline/polyvinyl alcohol blends: Effect of sulfonic acid dopants on microstructural, optical, thermal and electrical properties. *Synthetic Metals* **2014**, *191*, 126.
32. Scotto, J.; Ines Florit, M.; Posadas, D. Redox commuting properties of polyaniline in hydrochloric, sulphuric and perchloric acid solutions. *Journal of Electroanalytical Chemistry* **2018**, *817*, 160.
33. Camalet, J. L.; Lacroix, J. C.; Aeiyaich, S.; Lacaze, P. C. Characterization of polyaniline films electrodeposited on mild steel in aqueous *p*-toluenesulfonic acid solution. *Journal of Electroanalytical Chemistry* **1998**, *445*, 117.
34. Gospodinova, N.; Terlemezyan, L. Conducting polymers prepared by oxidative polymerization: Polyaniline. *Progress in Polymer Science* **1998**, *23*, 1443.
35. Wei, Y.; Jang, G.; Chan, C.; Hsueh, K.; Hariharan, R.; Patel, S.; Whitecar, C. Polymerization of Aniline and Alkyl Ring-Substituted Anilines in the Presence of Aromatic Additives. *The Journal of Physical Chemistry* **1990**, *94*, 7716.
36. Bhadra, S.; Singha, N.; Khastgir, D. Effect of aromatic substitution in aniline on the properties of polyaniline. *European Polymer Journal* **2008**, *44*, 1763-1770.
37. Stejskal, J.; Sapurina, I. Polyaniline: Thin Films and Colloidal Dispersions. *Pure Appl. Chem* **2005**, *77*, 815.
38. Rajapakse, R. M. G.; Chandani, A. D. L.; Lankeshawara, L. P. P.; Kumarasiri, N. L. W. L. Retention of polyaniline on glass functionalized with aniline. *Synthetic Metals* **1996**, *83*, 73.
39. Tan, S.; Laforgue, A.; Belanger, D. Characterization of a Cation-Exchange/Polyaniline Composite Membrane. *Langmuir* **2003**, *19*, 744.
40. Avlyanov, J. K.; Josefowicz, J. Y.; MacDiarmid, A. G. Atomic force microscopy surface morphology studies of 'in situ' deposited polyaniline thin films. *Synthetic Metals* **1995**, *73*, 205.
41. Marakova, N.; Humpolicek, P.; Kasparkova, V.; Capakova, Z.; Martinkova, L.; Bober, P.; Trchova, M.; Stejskal, J. Antimicrobial activity and cytotoxicity of cotton fabric coated with conducting polymers, polyaniline or polypyrrole, and with deposited silver nanoparticles. *Applied Surface Science* **2017**, *396*, 169.
42. Mehdizadeh, M.; Khorasanian, M.; Baghal, S. Direct electroplating of nickel on ABS plastic using polyaniline-silver surface composite synthesized using different acids. *Journal of Coatings Technology and Research* **2018**, *1*.
43. Chen, Y.; Kang, E. T.; Neoh, K. G. Electroless polymerization of aniline on platinum and palladium surfaces. *Applied Surface Science* **2002**, *185*, 267.
44. Shi, N.; Guo, X.; Jing, H.; Gong, J.; Sun, C.; Yang, K. Antibacterial Effect of the Conducting Polyaniline. *Journal of Materials Science and Technology* **2006**, *22*, 289-290.

45. Robertson, J.; Gizdavic-Nikolaidis, M.; Nieuweouft, M.; Swift, S. The antimicrobial action of polyaniline involves production of oxidative stress while functionalisation of polyaniline introduces additional mechanisms. *PeerJ* **2018**, *6*, e5135.
46. Gizdavic-Nikolaidis, M.; Bennett, J.; Swift, S.; Eastal, A.; Ambrose, M. Broad spectrum antimicrobial activity of functionalized polyanilines. *Acta Biomaterialia* **2011**, *7*, 4204-4209.
47. Guo, Y.; Gao, Z.; Wang, X.; Sun, L.; Yan, X.; Yan, S.; Long, Y.; Han, W. A highly stretchable humidity sensor based on spandex covered yarns and nanostructured polyaniline. *RSC Advances* **2018**, *8*, 1078.
48. Zhang, L.; Dong, S. The electrocatalytic oxidation of ascorbic acid on polyaniline film synthesized in the presence of camphorsulfonic acid. *Journal of Electroanalytical Chemistry* **2004**, *568*, 189.
49. Liu, Y.; Su, Z.; Zhang, Y.; Chen, L.; Gu, T.; Huang, S.; Liu, Y.; Sun, L.; Xie, Q.; Yao, S. Amperometric determination of ascorbic acid using multiwalled carbon nanotube-thiolated polyaniline composite modified glassy carbon electrode. *Journal of Electroanalytical Chemistry* **2013**, *709*, 19.
50. Kolb, H.; Finn, M.; Sharpless, B. Click Chemistry: Diverse Chemical Function from a Few Good Reactions. *Angewandte Chemie International Edition* **2001**, *40*, 2004-2021.
51. Finn, M. G.; Fokin, V. V. Click chemistry: function follows form. *Chemical Society Reviews* **2010**, *39*, 1231.
52. V, R.; Green, L.; V, F.; Sharpless, B. A Stepwise Huisgen Cycloaddition Process: Copper(I)-Catalyzed Regioselective "Ligation" of Azides and Terminal Alkynes. *Angewandte Chemie International Edition* **2002**, *41*, 2596-2599.
53. Tornøe, C.; Christensen, C.; Meldal, M. Peptidotriazoles on Solid Phase: [1,2,3]-Triazoles by Regiospecific Copper (I)-Catalyzed 1,3-Dipolar Cycloadditions of Terminal Alkynes to Azides. *Journal of Organic Chemistry* **2002**, *67*, 3057-3064.
54. Hein, J. E.; Fokin, V. V. Copper-catalyzed azide-alkyne cycloaddition (CuAAC) and beyond: new reactivity of copper(I) acetylides. *Chemical Society Reviews* **2010**, *39*, 1302.
55. Bock, V. D.; Hiemstra, H.; van Maarseveen, J. H. Cu^I-Catalyzed Alkyne-Azide "Click" Cycloadditions from a Mechanistic and Synthetic Perspective. *European Journal of Organic Chemistry* **2005**, 51.
56. Posner, T. Beiträge zur Kenntniss der ungesättigten Verbindungen II. Ueber die Addition von Mercaptanen an ungesättigte Kohlenwasserstoff. *Berichte der deutschen chemischen Gesellschaft* **1905**, *38*, 646.
57. Hoyle, C. E.; Bowman, C. N. Thiol-Ene Click Chemistry. *Angewandte Chemie International Edition* **2010**, *49*, 1540.
58. Lowe, A. Thiol-ene "click" reactions and recent applications in polymer and materials synthesis. *Polymer Chemistry* **2010**, *1*, 17-36.

59. Morgan, C. R.; Magnotta, F.; Ketley, A. D. Thiol/Ene Photocurable Polymers. *Journal of Polymer Science Part A: Polymer Chemistry* **1977**, *15*, 627.
60. Uygun, M.; Tasdelen, M. A.; Yagci, Y. Influence of Type of Initiation on Thiol-Ene "Click" Chemistry. *Macromolecular Chemistry and Physics* **2010**, *211*, 103.
61. Hoyle, C. E.; Lee, T. Y.; Roper, T. Thiol-Enes: Chemistry of the Past with Promise for the Future. *Journal of Polymer Science Part A: Polymer Chemistry* **2004**, *42*, 5301.
62. Huynh, V. T.; Chen, G.; de Souza, P.; Stenzel, M. H. Thiol-yne and Thiol-ene "Click" Chemistry as a Tool for a Variety of Platinum Drug Delivery Carriers, from Statistical Copolymers to Crosslinked Micelles. *Biomacromolecules* **2011**, *12*, 1738.
63. Wesley, A. History of the Medical Use of Silver. *Surgical Infections* **2009**, *10*, 289.
64. Ventola, C. L. The Antibiotic Resistance Crisis Part 1: Causes and Threats. *Pharmacy and Therapeutics* **2015**, *40*, 277.
65. Khachatourians, G. G. Agricultural use of antibiotics and the evolution and transfer of antibiotic-resistant bacteria. *Canadian Medical Association Journal* **1998**, *159*, 1129.
66. Rai, M.; Yadav, A.; Gade, A. Silver nanoparticles as a new generation of antimicrobials. *Biotechnology Advances* **2009**, *27*, 76.
67. Lansdown, A. B. G. Silver I: its antibacterial properties and mechanism of action. *Journal of Wound Care* **2002**, *11*, 125.
68. Castellano, J.; Shafii, S.; Ko, F.; Donate, G.; Wright, T.; Mannari, R.; Payne, W.; Smith, D.; Robson, M. Comparative evaluation of silver-containing antimicrobial dressings and drugs. *International Wound Journal* **2007**, *4*, 114.
69. Dos Santos, C. A.; Seckler, M. M.; Ingle, A.; Gupta, I.; Galdiero, S.; Galdiero, M.; Gade, A.; Rai, M. Silver Nanoparticles: Therapeutical Uses, Toxicity, and Safety Issues. *Journal of Pharmaceutical Sciences* **2014**, *103*, 1931.
70. Pareek, V.; Gupta, R.; Panwar, J. Do physico-chemical properties of silver nanoparticles decide their interaction with biological media and bactericidal action? A review. *Materials Science & Engineering C* **2018**.
71. Amaya, T.; Isaji, T.; Abe, M.; Hirao, T. Synthesis of Polyaniline and Transition Metal Nanoparticles Hybrids. *Journal of Inorganic and Organometallic Polymers and Materials* **2015**, *25*, 145.
72. Tian, G.; Wang, W.; Mu, B.; Kang, Y.; Wang, A. Ag(I)-triggered one-pot synthesis of Ag nanoparticles onto natural nanorods as a multifunctional nanocomposite for efficient catalysis and adsorption. *Journal of Colloid and Interface Science* **2016**, *473*, 84.
73. Tian, J.; Peng, D.; Wu, X.; Li, W.; Deng, H.; Liu, S. Electrodeposition of Ag nanoparticles on conductive polyaniline/cellulose aerogels with increased synergistic effect for energy storage. *Carbohydrate Polymers* **2017**, *156*, 19.

74. Youssef, A. M.; Mohamed, S. A.; Abdel-Aziz, M. S.; Abdel-Aziz, M. E.; Turkey, G.; Kamel, S. Biological studies and electrical conductivity of paper sheet based on PANI/PS/Ag-NPs nanocomposite. *Carbohydrate Polymers* **2016**, *147*, 333.
75. Salem, M.; Elsharkawy, R.; Hablas, M. Adsorption of brilliant green dye by polyaniline/silver nanocomposite: Kinetic, equilibrium, and thermodynamic studies. *European Polymer Journal* **2016**, *75*, 577.
76. Khesuoe, M. P.; Okumu, F. O.; Matoetoe, M. C. Development of a silver functionalised polyaniline electrochemical immunosensor for polychlorinated biphenyls. *Analytical Methods* **2016**, *8*, 7087.
77. Das, S.; Chakraborty, P.; Mondal, S.; Shit, A.; Nandi, A. Enhancement of Energy Storage and Photoresponce Properties of Folic Acid-Polyaniline Hydrid Hydrogel by in Situ Growth of Ag Nanoparticles. *ACS Applied Materials & Interfaces* **2016**, *8*, 28055.
78. Goldstein, I. J.; Hughes, R. C.; Monsigny, M.; Osawa, T.; Sharon, N. What should be called a lectin? *Nature* **1980**, *285*, 66.
79. Spain, S.; Cameron, N. A spoonful of sugar: the application of glycopolymers in therapeutics. *Polymer Chemistry* **2011**, *2*, 60-68.
80. Aronson, M.; Medalia, O.; Schori, L.; Mirelman, D.; Sharon, N.; Ofek, I. Prevention of colonization of the urinary tract of mice with *Escherichia coli* by blocking of bacterial adherence with methyl α -D-mannopyranoside. *The Journal of Infectious Diseases* **1979**, *139*, 329.
81. Sharon, N.; Lis, H. History of lectins: from hemagglutinins to biological recognition molecules. *Glycobiology* **2004**, *13*, 53R.
82. Sharon, N. *Lectins*; Dordrecht : Springer Netherlands. 2007: 2007; .
83. Bouckaert, J.; Mackenzie, J.; de Paz, J.; Chipwaza, B.; Choudhury, D.; Zavialov, A.; Mannerstedt, K.; Anderson, J.; Pierard, D.; Wyns, L.; Seeberger, P.; Oscarson, S.; De Greve, H.; Knight, S. The affinity of the FimH fimbrial adhesin is receptor-driven and quasi-independent of *Escherichia coli* pathotypes. *Molecular Microbiology* **2006**, *61*, 1556.
84. Martinez, J.; Mulvey, M.; Schilling, J.; Pinkner, J.; Hultgren, S. Type 1 pilus-mediated bacterial invasion of bladder epithelial cells. *The Embo Journal* **2000**, *19*, 2803.
85. Korhonen, T.; Leffler, H.; Eden, C. Binding Specificity of Piliated Strains of *Escherichia coli* and *Salmonella typhimurium* to Epithelial Cells, *Saccharomyces cerevisiae* Cells, and Erythrocytes. *Infection and Immunity* **1981**, *32*, 796.
86. Cusumano, C.; Pinkner, J.; Han, Z.; Greene, S.; Ford, B.; Crowley, J.; Henderson, J.; Jenetka, J.; Hultgren, S. Treatment and Prevention of Urinary Tract Infection with Orally Active FimH Inhibitors. *Science Translational Medicine* **2011**, *3*, 1-10.
87. Abgottsson, D.; Rolli, G.; Hosch, L.; Steinhuber, A.; Jiang, X.; Schwarzt, O.; Cutting, B.; Smiesko, M.; Jenal, U.; Ernst, B.; Trampuz, A. Development of an aggregation assay to screen FimH antagonists. *Journal of Microbiological Methods* **2010**, *82*, 249.

88. Cohen, S.; Gerding, D.; Johnson, S.; Kelly, C.; Loo, V.; McDonald, C.; Pepin, J.; Wilcox, M. Clinical Practice Guidelines for *Clostridium difficile* Infection in Adults: 2010 Update by the Society for Healthcare Epidemiology of America (SHEA) and the Infectious Diseases Society of America (IDSA). *Infection Control and Hospital Epidemiology* **2010**, *31*, 431.
89. Cairo, C.; Gestwicki, J.; Kanai, M.; Kiessling, L. Control of Multivalent Interactions by Binding Epitope Density. *Journal of the American Chemical Society* **2001**, *124*, 2002.
90. Wiegand, I.; Hilpert, K.; Hancock, R. E. Agar and broth dilution methods to determine the minimal inhibitory concentration (MIC) of antimicrobial substances. *Nature Protocols* **2008**, *3*, 163.
91. Boyle, J. V.; Fancher, M. E.; Ross, Jr, R. W. Rapid, Modified Kirby-Bauer Susceptibility Test with Single, High Concentration Antimicrobial Disks. *Antimicrobial Agents and Chemotherapy* **1973**, *3*, 418.
92. Connolly, P.; Bloomfield, S. F.; Denyer, S. P. The use of impedance for preservative efficacy testing of pharmaceuticals and cosmetic products. *Journal of Applied Bacteriology* **1994**, *76*, 68.
93. Ug, A.; Ceylan, O. Occurance of Resistance to Antibiotics, Metals, and Plasmids in Clinical Strains of *Staphylococcus* spp. *Archives of Medical Research* **2003**, *34*, 130.
94. Jorgenson, J.; Ferraro, M. J. Antimicrobial Susceptibility Testing: A Review of General Principles and Contemporary Practices. *Medical Microbiology* **2009**, *49*, 1749.
95. Robertson, J. Understanding the Antimicrobial Mechanism for Applications of Polyaniline and Functionalised Polyanilines, the University of Auckland, The University of Auckland, 2016.
96. Lundquist, J.; Toone, E. The Cluster Glycoside Effect. *Chemical Reviews* **2002**, *102*, 555-578.
97. Beignet, J.; Tiernan, J.; Woo, C.; Kariuki, B.; Cox, L. Stereoselective Synthesis of Allyl-C-Mannosyl Compounds: Use of a Temporary Silicon Connection in Intramolecular Allylation Strategies with Allylsilanes. *Journal of Organic Chemistry* **2004**, *69*, 6341-6356.
98. Geng, J.; Mantovani, G.; Tao, L.; Nicolas, J.; Gaojian, C.; Wallis, R.; Mitchell, D.; Johnson, B.; Evans, S.; Haddleton, D. Site-Directed Conjugation of "Clicked" Glycopolymers To Form Glycoprotein Mimics: Binding to Mammalian Lectin and Induction of Immunological Function. *Journal of the American Chemical Society* **2007**, *129*, 15156-15163.
99. Yu, K.; Kizhakkedathu, J. Synthesis of Functional Polymer Brushes Containing Carbohydrate Residues in the Pyranose Form and Their Specific and Nonspecific Interactions with Proteins. *Biomacromolecules* **2010**, *11*, 3073-3085.
100. Vinson, N.; Gou, Y.; Becer, R.; Haddleton, D.; Gibson, M. Optimised 'click' synthesis of glycopolymers with mono/di- and trisaccharides. *The Royal Society of Chemistry* **2011**, *2*, 107-113.

101. Ruggieri, M. R.; Hanno, P. M.; Levin, R. M. Mannose Inhibition of *Escherichia coli* Adherence to Urinary Bladder Epithelium: Comparison with Yeast Agglutination. *Urological Research* **1985**, *13*, 79-84.
102. Zanello, P. Basic Equipment for Electrochemical Measurements. In *Inorganic Electrochemistry: Theory, Practice and Applications* Royal Society of Chemistry: 2003; pp 149-139-159.
103. Miras, M.; Barbero, C.; Haas, O. Preparation of Polyaniline by Electrochemical Polymerization of Aniline in Acetonitrile Solution. *Synthetic Metals* **1991**, *41*, 3081.
104. Saraswat, A.; Sharma, L.; Srivastava, M.; Siddiqui, I.; Singh, R. A Novel Electro-Organic Synthesis of Aniline-Based Copolymers at Platinum Electrodes. *Journal of Applied Polymer Science* **2012**, *123*, 1479.
105. Baba, A.; Tian, S.; Stefani, F.; Xia, C.; Wang, Z.; Advincula, R.; Johannsmann, D.; Knoll, W. Electropolymerization and doping/dedoping properties of polyaniline thin films as studied by electrochemical-surface plasmon spectroscopy and by the quartz crystal microbalance. *Journal of Electroanalytical Chemistry* **2004**, *562*, 95-103.
106. Kilmartin, P.; Wright, G. Photoelectrochemistry and spectroscopy of substituted polyanilines. *Synthetic Metals* **1999**, *104*, 145-156.
107. Genies, E. M.; Lapkowski, M.; Penneau, J. F. Cyclic Voltammetry of Polyaniline: Interpretation of the Middle Peak. *Journal of Electroanalytical Chemistry* **1988**, *249*, 97-107.
108. Genies, E. M.; Tsintavis, C. Redox mechanism and electrochemical behaviour of polyaniline deposits. *Journal of Electroanalytical Chemistry* **1985**, *195*, 109.
109. Inzelt, G.; Puskas, Z. Adsorption and precipitation during the redox transformations of phenazine. *Electrochimica Acta* **2004**, *49*, 1969.
110. Trchova, M.; Stejskal, J. Polyaniline: The infrared spectroscopy of conducting polymer nanotubes (IUPAC Technical Report). *Pure Appl. Chem* **2011**, *83*, 1803-1817; 1803.
111. Wolkers, W. F.; Oliver, A. E.; Tablin, F.; Crowe, J. H. A Fourier-transform infrared spectroscopy study of sugar glasses. *Carbohydrate Research* **2004**, *339*, 1077.
112. Kanou, M.; Nakanishi, K.; Hashimoto, A.; Kameoka, T. Influences of Monosaccharides and Its Glycosidic Linkage on Infrared Spectral Characteristics of Disaccharides in Aqueous Solutions. *Applied Spectroscopy* **2005**, *59*, 885-892.
113. Sun, S.; Wu, P. Mechanistic Insights into Cu(I)-Catalyzed Azide-Alkyne "Click" Cycloaddition Monitored by Real Time Infrared Spectroscopy. *Journal of Physical Chemistry A* **2010**, *114*, 8331-8336.
114. E, Y.; Wan, L.; Zhou, X.; Huang, F.; Du, L. Synthesis and properties of novel polytriazoleimides derived from 1,2,3-triazole - containing diamines and aromatic dianhydrides. *Polymers Advanced Technologies* **2012**, *23*, 1092-1100.

115. Stejskal, J.; Kratochvil, P.; Radhakrishnana, N. Polyaniline Dispersions 2. UV-Vis absorption spectra. *Synthetic Metals* **1993**, *61*, 225-231.
116. Schweinfurth, D.; Pattacini, R.; Strobel, S.; Sarkar, B. New 1,2,3-triazole ligands through click reactions and their palladium and platinum complexes. *Dalton Transactions* **2009**, 9291-9297.
117. Emam, S.; El-Tabl, A.; Ahmed, H.; Emad, E. Synthesis, structural characterization, electrochemical and biological studies on divalent metal chelates of a new ligand derived from pharmaceutical preservative, dehydroacetic acid, with 1,4-diaminobenzene. *Arabian Journal of Chemistry* **2017**, *10*, 3816.
118. Jian, F.; Zhao, P.; Guo, H.; Li, Y. Synthesis, characterization, crystal structure and DFT studies on 1-acetyl-3-(2,4-dichloro-5-fluoro-phenyl)-5-phenyl-pyrazoline. *Spectrochimica Acta Part A* **2008**, *69*, 647.
119. Malinauskas, A.; Holze, R. *In situ* UV-Vis Spectroelectrochemical Study of Polyaniline Degradation. *Journal of Applied Polymer Science* **1998**, *73*, 287-294.
120. Albuquerque, J. E.; Mattoso, L. H. C.; Balogh, D. T.; Faria, R. M.; Masters, J. G.; MacDiarmid, A. G. A simple method to estimate the oxidation state of polyanilines. *Synthetic Metals* **2000**, *113*, 19.
121. Yang, D.; Adams, P.; Goering, A.; Mattes, B. New Methods for Determining the Molecular Weight of Polyaniline by Size Exclusion Chromatography. *Synthetic Metals* **2003**, *135*, 293.
122. Kang, E.; Neoh, K.; Tan, K. Polyaniline: A polymer with many interesting intrinsic redox states. *Progress in Polymer Science* **1998**, *23*, 277-324.
123. Golczak, S.; Kancierzewska, A.; Fahlman, M.; Langer, K.; Langer, J. Comparative XPS Surface Study of Polyaniline Thin Films. *Solid State Ionics* **2008**, *179*, 2234-2239.
124. Barr, T. L.; Seal, S. Nature of the use of adventitious carbon as a binding energy standard. *Journal of Vacuum Science & Technology A: Vacuum, Surfaces, and Films* **1995**, *13*, 1239.
125. Milton, A. J.; Monkman, A. P. A comparative study of polyaniline films using thermal analyses and IR spectroscopy. *Journal of Physics D: Applied Physics* **1993**, *26*, 1468.
126. Sharon, N.; Lis, H. *Lectins*; Kluwer Academic Publishers: Netherlands, 2003; , pp 454.
127. Sharon, N.; Lis, H. Specificity and Affinity. In *Lectins* Dordrecht Springer: 2007; pp 63-63-103.
128. Charville, H.; Jin, J.; Evans, C.; Brimble, M.; Williams, D. The Synthesis and Lectin-Binding Properties of Novel Mannose-Functionalised Polymers. *RSC Advances* **2013**.
129. Munoz-Bonilla, A.; Fernandez-Garcia, M. Polymeric materials with antimicrobial activity. *Progress in Polymer Science* **2012**, *37*, 281-339.

130. Timofeeva, L.; Kleshcheva, N. Antimicrobial polymers: mechanism of action, factors of activity, and applications. *Applied Microbiology and Biotechnology* **2010**, *89*, 475.
131. Boomi, P.; Prabu, H. G. Synthesis, characterization and antibacterial analysis of polyaniline/Au-Pd nanocomposite. *Colloids and Surfaces A: Physicochemical and Engineering Aspects* **2013**, *429*, 51.
132. Shaban, M.; Rabia, M.; Fathallah, W.; El-Mawgoud, N. A.; Mahmoud, A.; Hussein, H.; Said, O. Preparation and Characterization of Polyaniline and Ag/Polyaniline Composite Nanoporous Particles and Their Antimicrobial Activities. *Journal of Polymers and the Environment* **2018**, *26*, 434.
133. Broxton, P.; Woodcock, P. M.; Gilbert, P. A study of the antibacterial activity of some polyhexamethylene biguanides towards *Escherichia coli* ATCC 8739. *Journal of Applied Bacteriology* **1983**, *54*, 345.
134. Ikeda, T.; Hirayama, H.; Yamaguchi, H.; Tazuke, S.; Watanabe, M. Polycationic Biocides with Pendant Active Groups: Molecular Weight Dependence of Antibacterial Activity. *Antimicrobial Agents and Chemotherapy* **1986**, *30*, 132.
135. Wei, X.; Epstein, A. Synthesis of highly sulfonated polyaniline. *Synthetic Metals* **1995**, *74*, 123-125.
136. Fujimori, K.; Togo, H.; Oae, S. Iodine Catalyzed Reduction of Arenesulfonic Acid to the Arenethiol with Triphenylphosphine. *Tetrahedron Letters* **1980**, *21*, 4921-4924.
137. Hartmann, M.; Betz, P.; Sun, Y.; Gorb, S.; Lindhorst, T.; Krueger, A. Saccharide - Modified Nanodiamond Conjugates for the Efficient Detection and Removal of Pathogenic Bacteria. *Chem. Eur. J* **2012**, *18*, 6485-6492.
138. Blyholder, G.; Bowen, D. O. Infrared Spectra of Sulfur Compounds Adsorbed on Silica-Supported Nickel. *Journal of Physical Chemistry* **1962**, *66*, 1288.
139. Li, X.; Chen, G.; Duan, M.; Yang, W.; Tang, S.; Cao, Y.; Luo, Y. Branched Hydroxyl Modification of SBS Using Thiol-Ene Reaction and Its Subsequent Application in Modified Asphalt. *Industrial & Engineering Chemistry Research* **2017**, *56*, 10354.
140. Gruger, A.; Novak, A.; Regis, A.; Colomban, P. Infrared and Raman study of polyaniline Part II: Influence of ortho substituents on hydrogen bonding and UV/Vis-near-IR electron charge transfer. *Journal of Molecular Structure* **1994**, 328.
141. Metson, J. B. Charge Compensation and Binding Energy Referencing in XPS Analysis. *Surface and Interface Analysis* **1999**, *27*, 1069.
142. Wagner, C. D. Chemical Shifts of Auger Lines, and the Auger Parameter. *Faraday Discussions of the Chemical Society* **1976**, *60*, 291.
143. Chen, W.; Wen, T.; Gopalan, A. Negative capacitance for polyaniline: an analysis via electrochemical impedance spectroscopy. *Synthetic Metals* **2002**, *128*, 179.
144. Yue, J.; Epstein, A. J. XPS Study of Self-Doped Conducting Polyaniline and Parent Systems. *Macromolecules* **1991**, *24*, 4441.

145. Tan, K. L.; Tan, B. T. G.; Kang, E. T.; Neoh, K. G. X-ray photoelectron spectroscopy studies of the chemical structure of polyaniline. *Physical Review B* **1989**, *39*, 8070.
146. Wagner, C. D. *Handbook of X-ray Photoelectron Spectroscopy*; Physical Electronics Division, Perkin-Elmer Corporation: 1979; , pp 190.
147. Yue, J.; Wang, Z. H.; Cromack, K. R.; Epstein, A. J.; MacDiarmid, A. Effect of sulfonic acid group on polyaniline backbone. *Journal of the American Chemical Society* **1991**, *113*, 2665-2671.
148. Gonzalez, M. D.; Salagre, P.; Taboada, E.; Llorca, J.; Molins, E.; Cesteros, Y. Sulfonic acid-functionalized aerogels as high resistant to deactivation catalysts for the etherification of glycerol with isobutene. *Applied Catalysis B: Environmental* **2013**, *136-137*, 287.
149. Brunetti, B.; De Giglio, E.; Cafagna, D.; Desimoni, E. XPS analysis of glassy carbon electrodes chemically modified with 8-hydroxyquinoline-5-sulphonic acid. *Surface and Interface Analysis* **2011**, *44*, 491.
150. Su, Z.; Liu, Y.; Zhang, Y.; Xie, Q.; Chen, L.; Huang, Y.; Fu, Y.; Meng, Y.; Li, X.; Ma, M.; Yao, S. Thiol-ene chemistry guided preparation of thiolated polymeric nanocomposite for anodic stripping voltammetry analysis of Cd²⁺ and Pb²⁺. *Analyst* **2013**, *138*, 1180-1186.
151. Chen, L.; Su, Z.; He, X.; Liu, Y.; Qin, C.; Zhou, Y.; Li, Z.; Wang, L.; Xie, Q.; Yao, S. Square wave anodic stripping voltammetric determination of Cd and Pb ions at a Bi/Nafion/thiolated polyaniline/glassy carbon electrode. *Electrochemistry Communications* **2012**, *15*, 34.
152. Molino, P.; Wallace, G.; Hanks, T. Hydrophobic conducting polymer films from post deposition thiol exposure. *Synthetic Metals* **2012**, *162*, 1464.
153. Bergman, B.; Hanks, T. W. Spectroscopic, Microscopic, and Surface Analysis of Alkanethiol- and Fluoroalkane-thiol-Modified Conducting Polymer Thin Films. *Macromolecules* **2000**, *33*, 8035.
154. Su, Z.; Liu, Y.; Xie, Q.; Chen, L.; Zhang, Y.; Meng, Y.; Li, Y.; Fu, Y.; Ma, M.; Yao, S. Preparation of thiolated polymeric nanocomposite for sensitive electroanalysis of dopamine. *Biosensors and Bioelectronics* **2012**, *36*, 154.
155. Wang, Z.; Sun, C.; Vegesna, G.; Liu, H.; Liu, Y.; Li, J.; Zeng, X. Glycosylated aniline polymer sensor: Amine to imine conversion on protein - carbohydrate binding. *Biosensors and Bioelectronics* **2013**, *46*, 183-189.
156. Huan, T. N.; Ganesh, T.; Han, S.; Yoon, M.; Chung, H. Sensitive detection of an Anthrax biomarker using a glassy carbon electrode with a consecutively immobilized layer of polyaniline/carbon nanotube/peptide. *Biosensors and Bioelectronics* **2011**, *26*, 4227.
157. Halliwell, C.; Simon, E.; Toh, C.; Bartlett, P.; Cass, A. Immobilisation of lactate dehydrogenase on poly(aniline)-poly(acrylate) and poly(aniline)-poly(vinyl sulphonate) films for use in a lactate biosensor. *Analytica Chimica Acta* **2002**, *453*, 191.

158. Monkman, A. P.; Adams, P. Optical and electronic properties of stretch-oriented solution-cast polyaniline films. *Synthetic Metals* **1991**, *40*, 87.
159. Lamouri, S.; Bendahgane, S.; Oudia, A. The Preparation and Analytical Study of Conducting Polyaniline Thin Films. *J Pet Environ Biotechnol* **2014**, *5*.
160. Kumar, S. N.; Gaillard, F.; Bouyssoux, G.; Sartre, A. High-resolution XPS studies of electrochemically synthesized conducting polyaniline films. *Synthetic Metals* **1990**, *36*, 111.
161. Aldissi, M.; Armes, S. P. X-ray Photoelectron Spectroscopy Study of Bulk and Colloidal Polyaniline. *Macromolecules* **1992**, *25*, 2963.
162. Blazevska-Gilev, J.; Bastl, Z.; Subrt, J.; Stopka, P.; Pola, J. IR laser ablative degradation of poly(phenylene ether-sulfone): Deposition of films containing ether, sulfone, sulfoxide and sulfide groups. *Polymer Degradation and Stability* **2009**, *94*, 196.
163. Grzybek, T.; Pietrzak, R.; Wachowska, H. The Comparison of Oxygen and Sulfur Species Formed by Coal Oxidation with O₂/Na₂CO₃ or Peroxyacetic Acid Solution. XPS Studies. *Energy and Fuels* **2004**, *18*, 804.
164. Guerrero-Corella, A.; Martinez-Gualda, A. M.; Ahmadi, F.; Ming, E.; Fraile, A.; Aleman, J. Thiol-ene/oxidation tandem reaction under visible light photocatalysis: synthesis of alkyl sulfoxides. *Chemical Communications* **2017**, *53*, 10463.
165. Li, Z.; Liu, J.; Li, J.; Kang, F.; Gao, F. Graphite cathode and anode becoming graphene structures after cycling based on graphite-based dual ion battery using PP₁₄NTF₂. *Carbon* **2018**, *138*, 52.
166. Schick, G. A.; Ziqi, S. Spectroscopic Characterization of Sulfonyl Chloride Immobilization on Silica. *Langmuir* **1994**, *10*, 3105.
167. Lee, H.; Lee, D. J.; Lee, J.; Song, J.; Lee, Y.; Ryou, M.; Park, J.; Lee, Y. M. Chemical aspect of oxygen dissolved in a dimethyl sulfoxide-based electrolyte on lithium metal. *Electrochimica Acta* **2014**, *123*, 419.
168. Robertson, J.; Gizdavic-Nikolaidis, M.; Swift, S. Investigation of Polyaniline and a Functionalised Derivative as Antimicrobial Additives to Create Contamination Resistant Surfaces. *Materials (Basel)* **2018**, *11*.
169. Scholl, A.; Zou, Y.; Jung, M.; Schmidt, T.; Fink, R.; Umbach, E. Line shapes and satellites in high-resolution x-ray photoelectron spectra of large π -conjugated organic molecules. *Journal of Chemical Physics* **2004**, *121*, 10260.
170. Bhattarai, S.; Kim, J. S.; Yun, Y.; Lee, Y. Preparation of polyaniline-coated polystyrene nanoparticles for the sorption of silver ions. *Reactive and Functional Polymers* **2016**, *105*, 52.
171. Battocchio, C.; Meneghini, C.; Fratoddi, I.; Venditti, I.; Russo, M. V.; Aquilanti, G.; Maurizio, C.; Bondino, F.; Matassa, R.; Rossi, M.; Mobilio, S.; Polzonetti, G. Silver Nanoparticles Stabilized with Thiol: A Close Look at the Local Chemistry and Chemical Structure. *The Journal of Physical Chemistry C* **2012**, *116*, 19571.

172. Laiho, T.; Leiro, J. A.; Heinonen, M. H.; Mattila, S. S.; Lukkari, J. Photoelectron spectroscopy study of irradiation damage and metal-sulfur bonds of thiol on silver and copper surfaces. *Journal of Electron Spectroscopy and Related Phenomena* **2005**, *142*, 105.
173. Zou, X.; Bao, H.; Guo, H.; Zhang, L.; Qi, L.; Jiang, J.; Niu, L.; Dong, S. Mercaptoethane sulfonate protected, water-soluble gold and silver nanoparticles: Syntheses, characterization and their building multilayer films with polyaniline via ion-dipole interactions. *Journal of Colloid and Interface Science* **2005**, *295*, 401.
174. Dong, T.; Chen, W.; Wang, C.; Chen, C.; Chen, C.; Lin, M.; Song, J.; Chen, I.; Kao, T. One-step synthesis of uniform silver nanoparticles capped by saturated decanoate: direct spray printing ink to form metallic silver films. *Physical Chemistry Chemical Physics* **2009**, *11*, 6269.
175. Krutyakov, Y. A.; Kudrinsky, A. A.; Olenin, A. Y.; Lisichkin, G. V. Synthesis of highly stable silver colloids stabilized with water soluble sulfonated polyaniline. *Applied Surface Science* **2010**, *256*, 7037.
176. Thakur, P.; Joshi, S. S.; Patil, K. R. Investigations of CdS and Ag-CdS nanoparticles by X-ray photoelectron spectroscopy. *Applied Surface Science* **2010**, *257*, 1390.
177. Morones, J. R.; Elechiguerra, J. L.; Camacho, A.; Holt, K.; Kouri, J. B.; Ramirez, J. T.; Yacaman, M., Jose. The bactericidal effect of silver nanoparticles. *Nanotechnology* **2005**, *16*, 2346.
178. Gomaa, E. Silver nanoparticles as an antimicrobial agent: a case study on *Staphylococcus aureus* and *Escherichia coli* as models for gram-positive and gram-negative bacteria. *Journal of General and Applied Microbiology* **2017**, *63*, 36.